UNIVERSIDAD COMPLUTENSE DE MADRID
FACULTAD DE CIENCIAS QUIMICAS

TESIS DOCTORAL

El papel de la mitofagia en la neurogénesis y la neurodegeneración

The role of mitophagy in neurogenesis and neurodegeneration

MEMORIA PARA OPTAR AL GRADO DE DOCTOR

PRESENTADA POR

Petra Teresak

Directora

Patricia Boya

Madrid

UNIVERSIDAD COMPLUTENSE DE MADRID
FACULTAD DE CIENCIAS QUÍMICAS

TESIS DOCTORAL

EL PAPEL DE LA MITOFAGIA EN LA NEUROGÉNESIS Y LA NEURODEGENERACIÓN

THE ROLE OF MITOPHAGY IN NEUROGENESIS AND NEURODEGENERATION

MEMORIA PARA OPTAR AL GRADO DE DOCTORA

PRESENTADA POR

PETRA TERESAK

DIRECTORA

PATRICIA BOYA

UNIVERSIDAD COMPLUTENSE DE MADRID

Doctorado de Bioquímica, Biología Molecular y Biomedicina-
Facultad de Ciencias Químicas

CONSEJO SUPERIOR DE INVESTIGACIONES CIENTÍFICAS
Centro de Investigaciones Biológicas Margarita Salas

EL PAPEL DE LA MITOFAGIA EN LA NEUROGÉNESIS Y LA NEURODEGENERACIÓN

THE ROLE OF MITOPHAGY IN NEUROGENESIS AND NEURODEGENERATION

Memoria presentada por Petra Teresak para optar al grado de Doctora en Bioquímica, Biología Molecular y Biomedicina por la Universidad Complutense de Madrid

VºBº de la Directora de la Tesis

Patricia Boya, PhD

VºBº del Tutor

Cristina Sanchez, PhD

PETRA TERESAK
2022

Acknowledgements

It takes a long time to write a PhD thesis, especially if you're doing it in the midst of a global pandemic. I'd want to take this opportunity to thank everyone who has been very helpful to me throughout the time it has taken me to complete my thesis.

First and foremost, I am deeply grateful to Professor Patricia Boya, who in a distant 2018 had a Skype call with me and decided to accept becoming my supervisor. I am extremely grateful for her invaluable advice, continuous support, and patience during my PhD study. Her immense knowledge and plentiful experience have encouraged me in all the time of my academic research and daily life. I would also like to thank Elena for her technical support on my study and for teaching me all the necessary skills to conduct my thesis. I would like to thank all the members of the DRIVE ITN. I am grateful for the funding from Marie Skłodowska-Curie ITN grant under the European Union's Horizon 2020 Research and Innovation Programme (Grant Agreement No 765912 DRIVE). I'd like to express my gratitude to Prof. Anne Simonsen and her whole group for their kind welcome and assistance. Thank you for making me feel at ease and for assisting me in learning and progressing with my thesis.

A good support system is important to surviving and staying sane during a PhD. I was lucky to have Inés, Iñaqui and Bea. These three formed the core of my research time in the Boya group. I couldn't have survived without them. We've all been there for one another and have taught ourselves and each other many tools and issues of mitophagy. I know that I could always ask them for advice and opinions on lab related issues. Inés is a wonderful and generous friend who will go out of her way in order to help, I appreciate her positive outlook and her ability to smile despite the situation. I admire her diligence and persistence. Iñaqui is the one to look out for in the future, can't wait to read all your Nature papers 😊 He cares about and will look out for everyone. I know I can count on Bea to always provide helpful suggestions and help with instrumentation and general lab questions. It is their kind help and support that have made my study and life in Spain a wonderful time.

To my friends Ivana, Una, Sonja, Dora, Mia, Taz, Luka – thank you for your continued friendship, support, hugs, chats, laughs and cups of tea (gin tonic) along the way. Una, thank you for taking the time to proofread this thesis, your input was invaluable. And Ivana, thank you for all the support and encouragement you give me, and the patience and unwavering faith you have in me. You believe in me even when I don't believe in myself. For that I am eternally grateful. Thank you, Taz and Luka, for all the conversations, philosophical debates and inspirational conversations. I am truly lucky to count you amongst my friends. Love, always

I especially thank my mom, aunt, Stjepko and Saša. Some special words of gratitude go to my mom who has always been a major source of support when things would get a bit discouraging. She has sacrificed everything for my brother and myself and provided unconditional love and care. I love her so much, and I would not have made it this far without her. My aunt has been my rock all my life and I love her dearly and thank her for all her advice and support. I know I always have my family to count on when times are rough. Without their tremendous understanding and encouragement in the past few years, it would be impossible for me to complete my study. Finally, I'd want to thank coffee for always changing my mood and lifting my spirits. I'm not sure how I would have survived the last three years of my PhD without you. Thank you for ensuring that I begin each day at my best. I'd be a grumpy, dysfunctional mess if it weren't for you. But, with your help, I am always prepared to face any challenge that comes my way.

Contents

Resumen

La retina neural de los vertebrados es una estructura formada por seis tipos neuronales y un tipo de célula glial, que surgen de un conjunto de progenitores multipotentes. Hemos demostrado previamente que la mitofagia es necesaria para el desarrollo de la retina, ya que los animales deficientes de NIX (proteína reguladora de mitofagia), muestran un número menor de células ganglionares tanto en la retina embrionaria como en la adulta. En la presente tesis doctoral queremos estudiar más a fondo el papel de la autofagia y la mitofagia durante el desarrollo de la retina y comprender los niveles de mitofagia en las diferentes etapas de su desarrollo. Para ello hemos utilizado los ratones reporteros de mitofagia MitoQC. El reportero MitoQC contiene una proteína de fusión en tándem (mCherryGFP) que está unida a FIS1, situada en la membrana mitocondrial externa. En condiciones normales, todas las mitocondrias emiten fluorescencia tanto en verde como en rojo. Sin embargo, durante la mitofagia, cuando las mitocondrias son transportadas al lisosoma, la fluorescencia de GFP se extingue por el pH ácido del lisosoma por lo que esa mitocondria se marca en rojo. Nuestros datos muestran que muchos tipos celulares de la retina muestran puntos rojos indicativos de mitofagia durante las diferentes etapas del desarrollo embrionario. Además, también demostramos que podemos inducir mitofagia farmacológicamente a diferentes edades.

La enfermedad de Parkinson (EP) es la segunda enfermedad neurológica más prevalente después del Alzheimer. La etiología de la enfermedad de Parkinson es compleja y desconocida, aunque las alteraciones mitocondriales y lisosomales juegan un importante papel. La mitofagia, está alterada en pacientes y modelos con enfermedad de Parkinson. PINK1 y Parkin son dos proteínas mutadas en algunos pacientes con la EP que tienen un papel en el control de la mitofagia. Nuestros datos utilizando los animales MitoQC inyectados con 6-OHDA muestran cómo se ve disminuida la mitofagia en las neuronas dopaminergicas mientras que los astrocitos presentan niveles aumentados de mitofagia.

Abstract

The vertebrate neural retina is a structure made up of six neuronal and one glial cell type, which arise from a pool of multipotent progenitor cells. We have previously shown that mitophagy is necessary for retinal development, since animals deficient in the protein that regulates mitophagy, NIX, show reduced numbers of retinal ganglion cells (RGC) in both the embryonic and adult retinas. In this doctoral thesis we want to further study the role of autophagy and mitophagy during retinal development, understand mitophagy levels at different stages of retinal development using MitoQC mitophagy reporter mice. The MitoQC reporter contains a tandem fusion protein (mCherryGFP) that targets the outer mitochondrial membrane (OMM). Under normal conditions, all mitochondria fluoresce in both green and red. During mitophagy, when mitochondria are transported to the lysosome, the GFP fluorescence is quenched by the acidic pH of the lysosome resulting in mitochondria marked red. Our data show that in the retina, many cell types show red dots indicative of mitophagy during different stages of embryonic development. In addition, we also show that we can induce mitophagy at different ages using pharmacological tools.

Parkinson's disease (PD) is the second most prevalent neurological disease after Alzheimer's. The aetiology of Parkinson's disease is complex and unknown, although mitochondrial and lysosomal alterations play an important role. Mitophagy is impaired in patients and models with Parkinson's disease. PINK1 and Parkin are two proteins mutated in some PD patients that have a role in the control of mitophagy. Our data using the MitoQC animals injected with 6-OHDA show how mitophagy is decreased in dopaminergic neurons while the astrocytes present high levels of mitophagy.

Abbreviations

3-MA	3-Methyladenine
AKT	Protein kinase B
Ambra1	Activating Molecule of Beclin-1 Regulated Autophagy
AMPK	Protein kinase activated by AMP
Atg	Autophagy Related Gene
ATP	Adenosine triphosphate
AZD	AZD8055
Bak	Bcl-2 homologous antagonist killer
Bax	Bcl-2 associated x protein
Becn1	Beclin1 gene
Boc	Boc-D-FMK. Caspase inhibitor
Brn3a	Transcription factor Brain3a
BSA	Bovine serum albumin
Casp3a	Caspase-3 active
CCCP	Carbonylcyanide-m-chlorophenylhydrazone
cDNA	Complementary DNA
CMA	Chaperone mediated autophagy
CNS	Central nervous system
COX	Cytochrome oxidase
DABCO	1,4-diazabicyclo- (2, 2,2) -octane
DAn	Dopaminergic neurons
DAPI	1,4-diamino-2-phenylindole
DFP	Deferiprone
dpf	Days post fertilization
DMEM	Dulbecco's Modified Eagle's Medium
DNA	Deoxyribonucleic Acid
DNase	Enzyme that digests DNA

dNTP	Deoxynucleotide-triphosphate
E	Embryonic day
EBSS	Earl's Balanced Salt Solution
ER	Endoplasmic reticulum
FBS	Fetal bovin serum. Fetal bovine serum
FCCP	Fluoro-carbonyl cyanide phenylhydrazone
FOXO3	Forkhead box O family transcription factor
GAPDH	Glyceraldehyde phosphate dehydrogenase
RGCL	Retinal ganglion cell layer
GFP	Green fluorescent protein
HCQ	Hydroxychloroquine
HK	Hexokinase
HIF1α	Hypoxia Inducible Factor 1 Subunit Alpha
hpf	Hours post fertilization
Hsc70	Heat shock cognate protein of 70kDa
IP	Intraperitoneal injection
IMM	Inner mitochondrial membrane
INL	Inner nucler layer
INbL	Inner neuroblast layer
IPL	Inner plexiform layer
KO	Knock-out
LAMP-2A	Lysosome-associated membrane glycoprotein type 2
LC3	Microtubule-associated protein 1 light chain 3
LKB	Kinase B from liver
MMP	Permeabilization of the mitochondrial membrane
mPTP	Mitochondrial permeability transition pore
mRNA	Messenger RNA
mtDNA	Mitochondrial DNA

MTDR	Mitotracker deep red
Mtf	Mitofusin
mTOR	Target of rapamycin
MUL1	Mitochondrial E3 ubiquitin protein ligase 1
NbL	Neuroblast layer
NGS	Normal Goat Serum
NRF1	Nuclear respiratory factor 1
OCR	Oxygen consumption rate
OMM	Outer mitochondrial memmbrane
ONL	Outer nuclear layer
ONbL	Outer neuroblast layer
OPL	Outer plexiform layer
OXPHOS	Oxidative phosphorylation
P	Postnatal
Prkn	Gene of Parkin
PBS	Phosphate buffered saline
PCNA	Proliferating cell nuclear antigen
PCR	Polymerase chain reaction
PD	Parkinson’s disease
PE	Phosphatidylethanolamine
PFA	Paraformaldehyde
PI3K	Phospho-Inositide-3 kinase. Phosphatidyl-inositol-3 kinase
PINK1	Protein kinase 1 induced by PTEN
PK	Pyruvate kinase
PQ	Paraquat
PS	Phosphatidyl-serine
qPCR	Quantitative polymerase chain reaction
Rapa	Rapamycin

RGC	Retinal ganglion cells
GCL	Ganglion cell layer
ROS	Reactive oxygen species
SDS	Sodium dodecyl sulfate
Sirt1	Sirtuin 1
TdT	Terminal Deoxynucleotidyl Transferase
TF	Transcription factor
TFEB	Transcription factor EB
TH	Tyrosine hydroxylase
TNT	tunnelling nanotubes
TUNEL	dT-mediated dUTP Nick End Labeling
VDAC	Voltage-gated anion channel
Wt	Wildtype, wild genotype
α-syn	Alpha synuclein
+ / +	Homozygous genotype for wild type allele
ΔΨm	Mitochondrial membrane potential

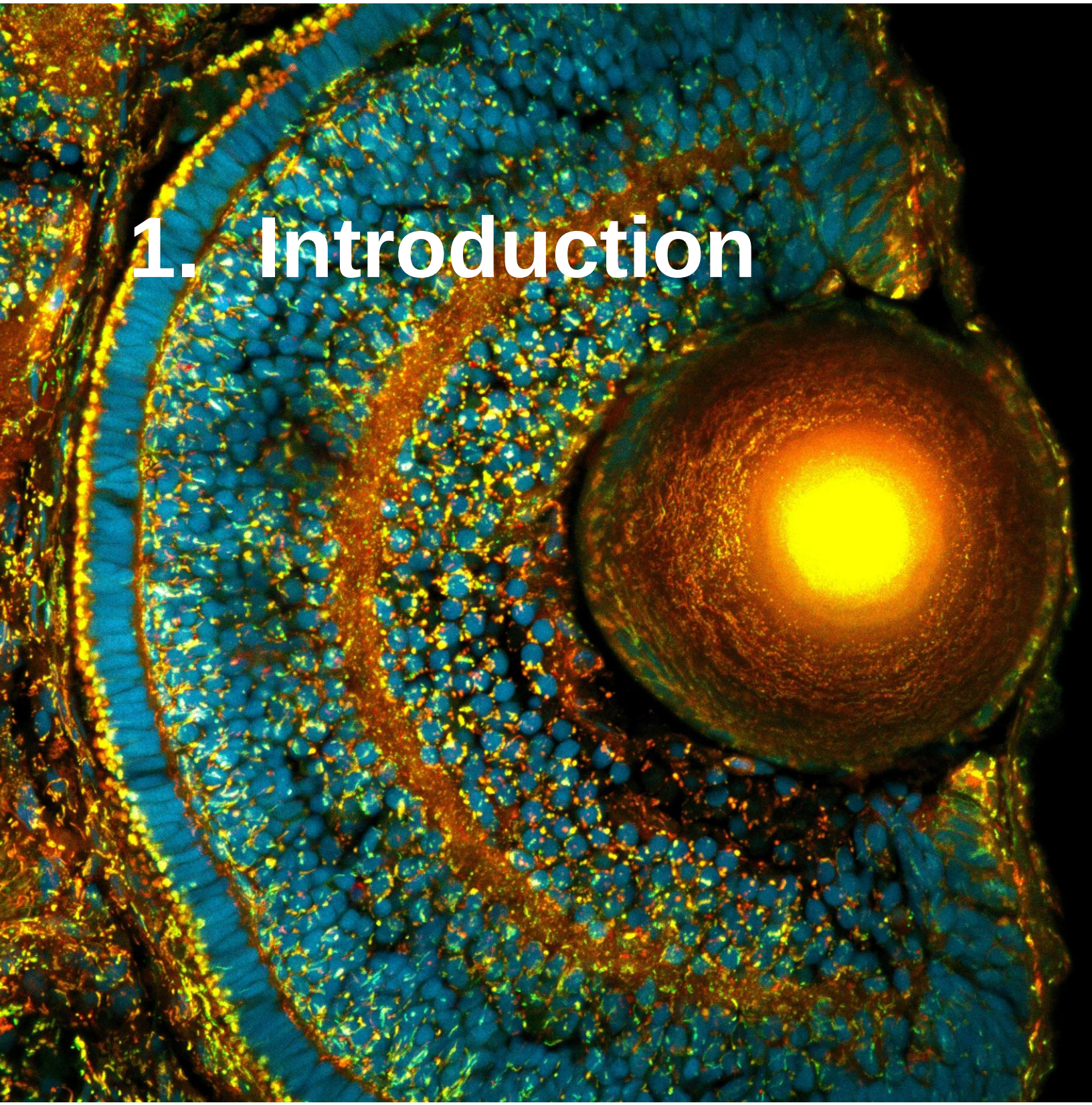

1. Introduction

1. Introduction

1.1. Autophagy pathways

The term autophagy was first used by Christian de Duve at the CIBA Foundation Symposium on Lysosomes in 1963. It originates from the Ancient Greek autóphagos, meaning "self-devouring" and κύτος kýtos, meaning "hollow", and it is a cell regulated mechanism allows the orderly degradation and recycling of cellular components. In the 1960's autophagy was largely based on the observed degradation of mitochondria and other intracellular structures within lysosomes of rat liver perfused with the pancreatic hormone, glucagon (Deter and Duve, 1967). In the upcoming years the scientific world has grown a better understanding for autophagy, with major contributions to our molecular knowledge and appreciation of the physiological significance of this process coming from numerous laboratories (Nakatogawa et al., 2009; Levine and Kroemer, 2008), Ohsumi's research the late 1980s, identified the genes that regulate the and has opened the path to understanding the fundamental importance of autophagy in many physiological processes, such as in the adaptation to starvation or response to infection. Other discoveries have also shown that mutations in autophagy genes can cause disease, and the autophagic process is involved in several conditions including cancer and neurological disease (Tsukada and Ohsumi, 1993; Mizushima et al., 1998; Ichimura et al., 2000). Although the importance of autophagy is well recognized in mammalian systems, a great number of the mechanistic breakthroughs in understanding the regulation of autophagy on the molecular level have been made in yeast (Saccharomyces cerevisiae) (Nakatogawa et al, 2009; Levine and Kroemer, 2008; Mizushima 2007; Xie and Klionsky, 2007; Klionsky, 2007). Currently, close to 40 different autophagy-related genes (Atg) have been identified, many of these genes are conserved throughout the phylogeny, which shows the importance of the autophagic process.

There are three defined types of autophagy depending on how the material is delivered to the lysosome: macro-autophagy, micro-autophagy, and chaperone-mediated autophagy, all of them promote proteolytic degradation of cytosolic components at the lysosome (Figure 1.1.). In macroautophagy, bulk cytoplasm and dysfunctional organelles are sequestered by the expanding phagophore, leading to the formation of the

autophagosome. The autophagosome then fuses with the lyososome, releasing the engulfmed material into the lyososmal lumen. Eventually, the sequestered cargos are degraded or processed by lyosomal enzymes (Figure 1.1.).

In chaperone-mediated autophagy (CMA), targeted proteins are translocated across the lysosomal membrane in a complex with chaperone proteins (such as Hsc-70) that are recognized by the lysosomal membrane receptor lysosomal-associated membrane protein 2A (LAMP-2A), resulting in their unfolding and degradation (Saftig et al., 2008). The characteristic of all CMA substrates is a pentapeptide targeting motif biochemically related to KFERQ (Cuervo and Dice, 1996). CMA degrades a wide range of substrate proteins, including certain glycolytic enzymes, transcription factors and their inhibitors, calcium and lipid binding proteins, proteasome subunits, and proteins involved in vesicular trafficking (Arias and Cuervo, 2011).

Microautophagy, a third autophagic mechanism, has been reported in yeast but has not yet been well studied in eukaryotic cells. Internalization of cytosolic cargo occurs through lysosomal membrane invaginations that mirrors the development of endosomal multivesicular bodies (Mizushima et al., 2007). In mammals, the molecular mechanisms that mediate microautophagy-like transfer of cytosolic cargo to lysosomes are unclear.

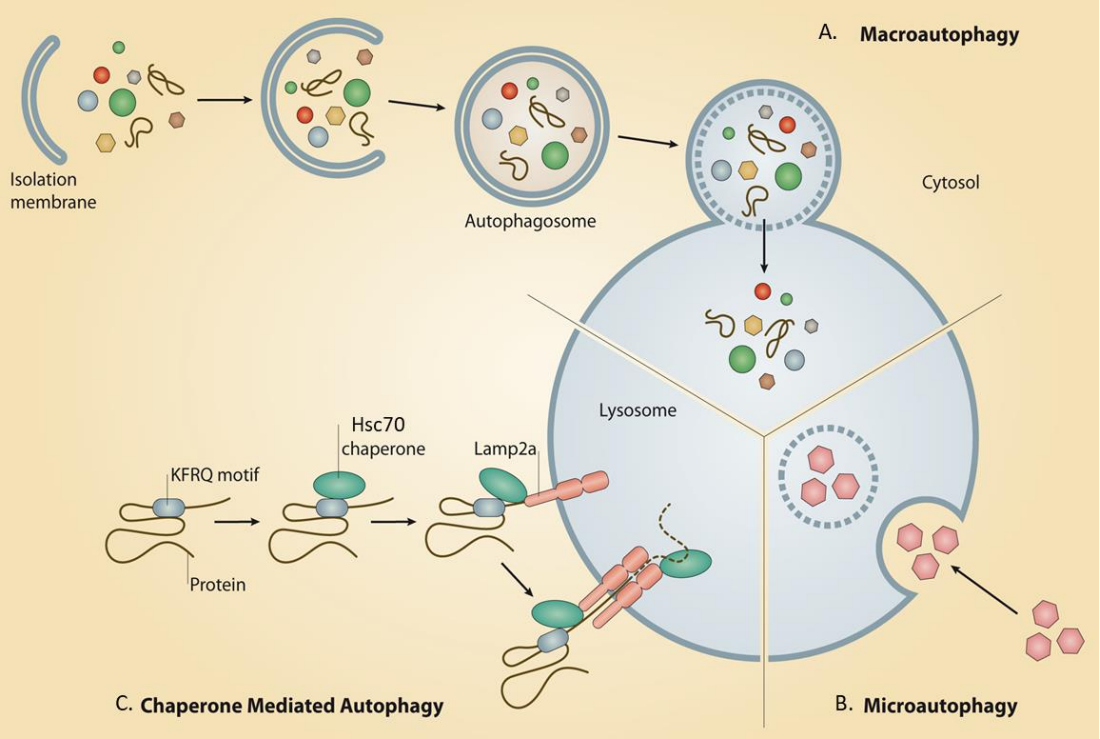

Figure 1.1. Three main types of autophagy. (A) Macroautophagy, (B) Microautophagy, and (C) Chaperone-mediated autophagy (CMA).

1.1.1. Macroautophagy

As mentioned above, the most distinguishing feature of macroautophagy, and what makes it different from microautophagy and CMA, is the formation of the double-membrane bound autophagosome. The origin of the membrane cistern forming new autophagosomes has been the subject of numerous studies, but still this issue is unresolved in mammalian cells. Many older ultrastructural studies suggested that smooth endoplasmic reticulum (ER) cisternae are the source of autophagosome membranes, (Dunn ,1994) but evidence against this interpretation has also been published (Hamasaki et al., 2013) and many other sources come from the plasma membrane and endosomes. In mammalian cells, the phagophore formation remains one the most fundamental unanswered questions in the understanding of the autophagy pathway. Over the last few years, a lot of effort has been put in resolving this matter, and numerous studies have indicated several different organelles as potential membrane sources. These include the plasma membrane, the Golgi apparatus (Orsi et al., 2010), the ER (Hayashi-Nishino et

al., 2009) and the mitochondria (Hailey et al. 2010). In a study in Nature, Hamasaki et al. (2013) shows that autophagosomes form at ER-mitochondria interfaces in mammalian cells.

After initiation, the membrane begins to expand (Figure 1.2.). At this stage, it is called a phagophore, which is the primary double-membrane sequestering compartment (He and Klionsky, 2009). As the phagophore expands, the membrane bends to finally create a spherical autophagosome. The elements that manage curvature of the membrane during macroautophagy are not known. As far as selective macroautophagy is concerned, the autophagosomal membrane wraps around the cargo, which ultimately adjusts to fit the specific target (Mijaljica et al., 2012). The phagophore expands through the acquisition of lipids and ultimately seals, thus completing the formation process and generating an autophagosome (Figure 1.2.). The size of the autophagosome varies based on organism and cargo type. The diameter of autophagosomes ranges from ~0.4 to 0.9 μm in yeast, and 0.5 to 1.5 μm in mammals (Mizushima and Klionsky, 2007). Once formed, the autophagosome carrying a cytosolic cargo will fuse with the lysosome, causing its contents to degrade releasing it's components in the cytosol to be recycled. The lysosome can then be regenerated to restart the process (Figure 1.2.) (Mijaljica et al., 2012).

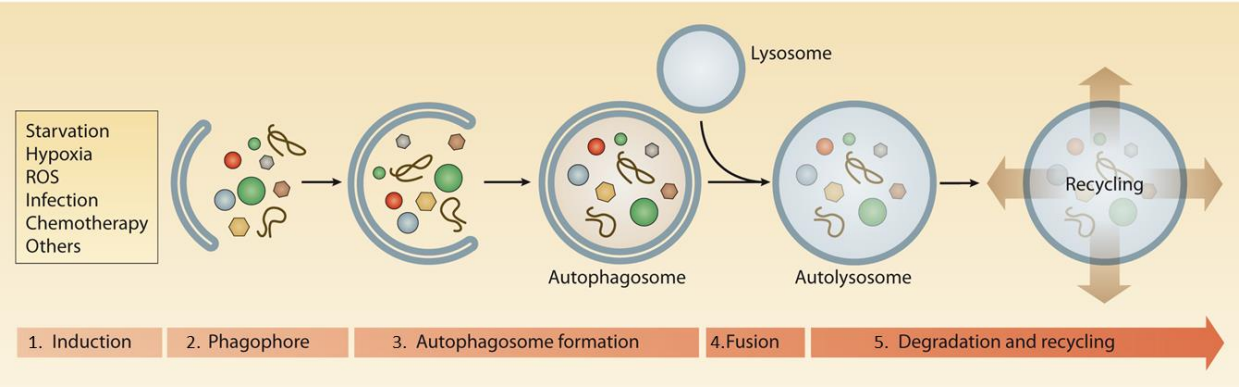

Figure 1.2. The macroautophagy process. There are five steps in the macroautophagy process: (1) Autophagy can be induced by several stress (2) The formation of the phagophore (or isolation membrane) begins during the nucleation stage regulated by a protein complex comprising VPS34, a class III PtdIns3K. (3) Phagophore elongation requires two «ubiquitin-like» conjugation systems: Atg12-Atg15 and Atg8-PE, both of which are essential for autophagosome formation. (4) The autophagosome bearing cytosolic cargo will fuse with the lysosome, causing (5) the degradation of the engulfemd material that will recycled back to the cystoplasm.

1.1.1.1. Signalling pathways that regulate autophagy

Autophagy is active at basal levels in most cell types where it is involved in a housekeeping function in maintaining the wholeness of intracellular organelles and proteins (Klionsky, 2007). Autophagy is induced by starvation and is a key part of the adaptive response of cells and organisms to nutrient deprivation that promotes survival until nutrients become available again. In both yeast and mammalian cells, two well-characterized signalling cascades that sense nutrient levels, activate cell division and growth, and negatively regulate autophagy are the TOR and Ras-cAMP-PKA pathways. TOR was initially identified as the target of rapamycin, which is a macrolide antifungal agent with structural similarity to FK506. Inactivation of TORC1 by rapamycin promotes autophagy in the presence of nutrients, indicating that TOR downregulates autophagy (Diaz-Troya et al., 2008).

The Ras/cAMP-dependent protein kinase A (PKA) signalling pathway plays an important role in glucose sensing from yeast to mammals. The small GTPases Ras1 and Ras2 are active and generate cAMP production by the adenylyl cyclase in nutrient-rich conditions. Enhanced cAMP binds to Bcy1 and translates its inhibitory effect on PKA. Constitutive activation of the Ras/PKA pathway suppresses autophagy induced by TOR inhibition in yeast (Budovskaya et al., 2004; Schmelzle et al., 2004), indicating that the Ras-PKA pathway downregulates autophagy.

The removal of growth factors from the extracellular space induces autophagy and is essential for maintaining cellular functions and energy production (Lum et al., 2005). In Drosophila and mammalian cells the pathways through which hormones regulate autophagy are distinct from those of nutrients, but both pathways utilize TOR. Insulin and insulin-like growth factors regulate mTOR through the class I PtdIns3K. When insulin binds to the insulin receptor, autophosphorylation of tyrosine residues results in the recruitment and phosphorylation of IRS1 and IRS2 (insulin receptor substrate 1 and 2). This generates a docking scaffold that allows binding of adaptor proteins, including subunits of the class I PtdIns3K such as p85. Generation of PIP3 (phosphatidylinositol (3,4,5)-trisphosphate) by the class I PtdIns3K increases membrane recruitment of both protein kinase B (PKB)/Akt and its activator PDK1 (phosphoinositide-dependent protein

kinase 1), leading to phosphorylation and activation of PKB/Akt by PDK1 (Diaz-Troya et al., 2008). The 3′-phosphoinositide phosphatase PTEN overturns PIP3 production, decreases the downstream PKB/Akt signalling and thus induces autophagy (Diaz-Troya et al., 2008).

During intracellular metabolic stress, activation of autophagy is essential for cell viability, and the underlying pathways are well understood. In mammalian cells, a decreased cellular energy (ATP) level is recognized by AMPK (5′-AMP-activated protein kinase). AMPK is activated by a decreased ATP/AMP ratio across the upstream LKB1. Active AMPK initiates phosphorylation and activation of the TSC1/2 complex, which reduces mTOR activity via Rheb (Inoki et al., 2003), ultimately resulting in elevated ATP production through recycling nutrients.

1.1.1.2. Autophagy: machinery and regulation

The molecular properties of phagophore formation in yeast are broadly known, but the finer details of how they function and when they act in the early formation stages in mammalian systems are not yet understood and it is likely to lead to many important findings.

However, the function of class III PI-3 kinases, Vps34 (vesicular protein sorting 34) in particular, and its binding partner Atg6/Beclin-1, in phagophore formation and autophagy is well studied in mammalian systems (Figure 1.3.). Vps34 is involved in various membrane-sorting processes in the cell but is selectively involved in autophagy when complexed to Beclin-1 and other regulatory proteins (Backer, 2008). Vps34 is particular in the group of PI3-kinases in using phosphatidylinositol (PI) as substrate to generate phosphatidyl inositol triphosphate (PI3P), which is crucial for phagophore elongation and recruitment of other Atg proteins to the phagophore (Xie and Klionsky, 2007). The interaction between Beclin-1 and Vps34 triggers its catalytic activity and increases levels of PI3P (Figure 1.3.).

Other proteins that bind with Vps34 and Beclin-1 to either promote autophagy, such as UVRAG, BIF-1, Atg14L and Ambra or to inhibit autophagy, such as Rubicon and Bcl-2 (Kang et al., 2011). One well-characterized regulatory event is the interaction of

Beclin-1 with Bcl-2, which disrupts the interaction of Beclin-1 with Vps34 (Pattingre et al. 2005; Maiuri et al. 2007). Bcl-2 serves a double purpose in regulating cell viability based on its subcellular localization: a pro-survival function at mitochondria inhibiting cytochrome c release, ultimately blocking apoptosis; and an autophagy-inhibitory activity at the ER, mediated by interaction with Beclin1 that can lead to non-apoptotic cell death (Pattingre et al. 2005). How the balance between autophagy and apoptosis is controlled in the cellular response to specific stresses is a research area of extreme interest given its relevance for disease progression and treatment, but again is an area that is not resolved (Maiuri et al., 2007).

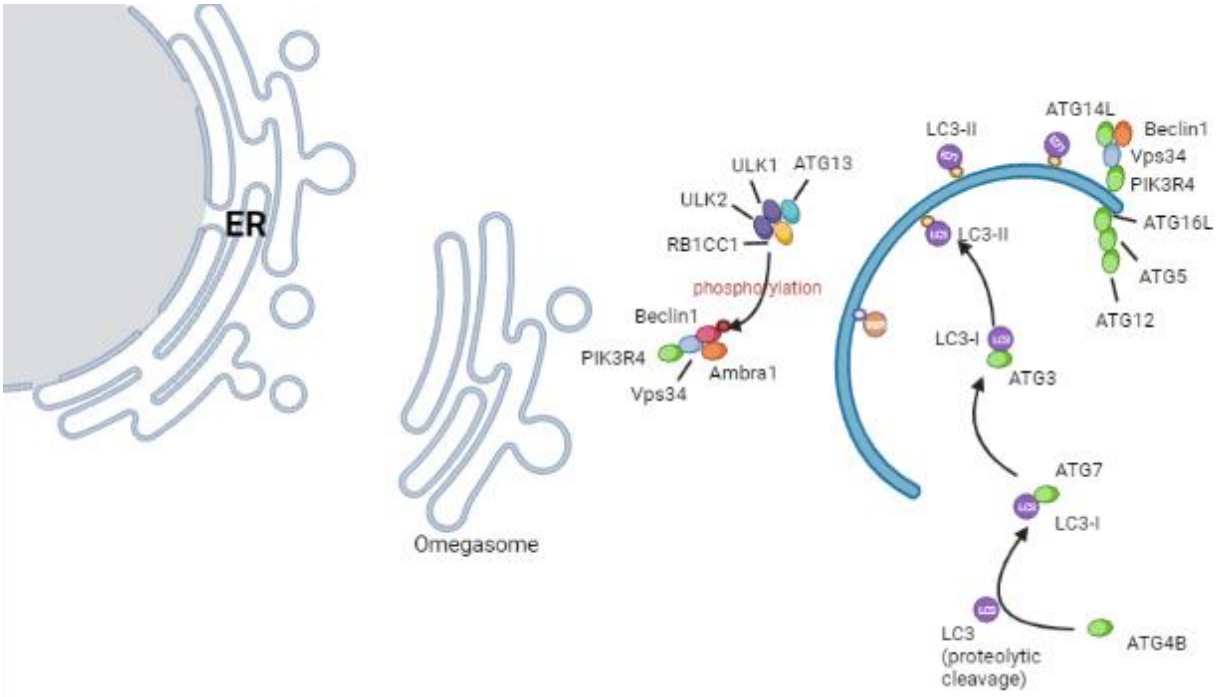

Figure 1.3. Phagophore formation. Autophagy is initiated by the formation of phosphatidylinositol 3-phosphate [PI(3)P]-rich areas of the endoplasmic reticulum (ER), which are referred to as omegasomes according to their structure. PI(3)P is produced by hVps34, the Beclin 1 complex's catalytic subunit, and is essential for the recruitment of downstream autophagy components such as WIPI1/2 and DFCP1. Autophagy is also initiated by the ULK1/2 kinase complex, which includes ULK1, ULK2, ATG13, and RB1CC1. It indirectly controls the Beclin 1 complex by phosphorylating Beclin 1 and activating hVps34. Furthermore, LC3 is transformed in two phases to LC3-II, which is often employed as an autophagy marker. ATG4B first cleaves LC3 to create LC3-I. The ubiquitin-activating (E1)-like enzyme ATG7 conjugates LC3-I to phosphatidylethanolamine (PE) to create LC3-II. WIPI1/2 and the ATG16L-ATG5-ATG12 Ubiquitin-like complex are PI(3)P effector proteins that positively control LC3-II production. LC3-II binds cargo, through several adaptor proteins.

In autophagy there are two crucial ubiquitin-like systems that function at the Atg5–Atg12 conjugation step and at the LC3 processing step (Mizushima, 2007; Kirkin et al., 2009). In the first of these systems the C-terminal carboxyl group of Atg12 is activated by the E1 enzyme Atg7 with consumption of ATP to form a thioester bond with its catalytic cysteine residue, then transferred to the catalytic cysteine residue of the E2 enzyme Atg10, and eventually attached to the amino group of the lysine residue in Atg5 via an isopeptide bond (Mizushima, 2007). Conjugated Atg5–Atg12 complex pairs with Atg16L dimers to form a multimeric Atg5–Atg12–Atg16L complex that connects with the growing phagophore. The association of Atg5–Atg12–Atg16L complexes is thought to induce curvature into the phagophore through asymmetric recruitment of processed LC3B-II (Mizushima, 2007). The activation of autophagy does not determine Atg5–Atg12 conjugation, and Atg5–Atg12–Atg16L dissociates from the membrane once the autophagosome is formed, this makes conjugated Atg5–Atg12 a poor marker of autophagy (Barth et al., 2010).

The second ubiquitin-like system involved in autophagosome formation is the processing of microtubule-associated protein light chain 3 (LC3B). Most cells express LC3B as a full-length cytosolic protein that, upon induction of autophagy, is proteolytically cleaved by Atg4, a cysteine protease, to expose the glycine residue essential for subsequent reactions and to generate LC3B-I (Kirisako et al., 2000). The conjugation reaction of LC3B-I is catalysed by Atg7 (Atg12 and LC3B-I share the same E1 enzyme) (Ichimura et al., 2000). Activated LC3B-I is then passed on to Atg3, a different E2-like carrier protein, which catalyses the conjugation of phosphatidylethanolamine (PE) to the carboxyl glycine to generate processed LC3B-II, thereby making LC3B-II anchored to membranes. Recruitment and integration of LC3B-II into the expanding phagophore is dependent on Atg5–Atg12. LC3B-II has a function in both hemifusion of membranes and in selecting cargo for degradation (Noda et al., 2008). The synthesis and processing of LC3 is increased during autophagy which makes it a crucial marker for levels of autophagy (Barth et al., 2010).

When the autophagosome completes fusion of the expanding ends of the phagophore membrane, the next crucial step in macroautophagy is the autophagosome

acquiring degradative enzymes by fusing with the lysosome. The high energy barrier of membrane fusion is overcome by the formation of a complex consisting of SNARE (soluble N-ethylmaleimide-sensitive factor attachment protein receptor) proteins embedded on either of the two membranes (Han et al., 2017). The cytoskeleton also plays a role in autolysosome formation, since agents such as nocadazole, which are microtubule poisons, block fusion of the autophagosome with the lysosome (Webb et al., *2004*). The efficiency of autophagosome-lysosome fusion is also sensitive to the types and levels of particular phosphatidylinositol (PI) phosphates in the autophagosomal and lysosomal membranes. So far shown to be important are the reduction of PI(3,5)P2, production of PI4P, and suppression of PI(4,5)P2 appearance on either or both membranes (Hasegawa et al. 2016). Lysosomal membrane proteins, LAMP1 and LAMP2, are also critical for autophagy to function, as evidenced by the inhibitory effect of targeted deletion of these proteins in mice on autolysosome maturation (Tanaka et al., 2000).

1.2. Selective autophagy

Autophagy can be either non-selective or selective. In selective autophagy, autophagy receptors bind to cargoes and result in their degradation within lysosomes. The typical characteristic of selective autophagy receptors is that they contain an Atg8-interacting motif (AIM)/LC3-interacting region (LIR) (Zaffagnini and Martens, 2016 Rogov et al., 2017). The AIMs or LIRs are responsible for selective binding to Atg8/LC3/GABARAP protein family. The AIMs or LIRs are characterized by [W/F/Y] XX[L/V/I] sequences, where X represents any amino acid. Isoleucine or leucine is typically observed as the third residue downstream of tryptophan (Noda et al 2008). The Atg8/LC3/GABARAP protein family functions as a bridge between the cargo and the core autophagic machinery, ensuring efficient recognition and sequestration of the cargo within autophagosomes (Johansen and Lamark, 2011).

Pathways for selective removal of mitochondria (mitophagy), proteasomes (proteaphagy), ribosomes (ribophagy), peroxisomes (pexophagy), ER (ER-phagy), lysosomes (lysophagy), LDs (lipophagy) and nuclei (nucleophagy) exist (Figure 1.4.) (Gatica et al., 2018).

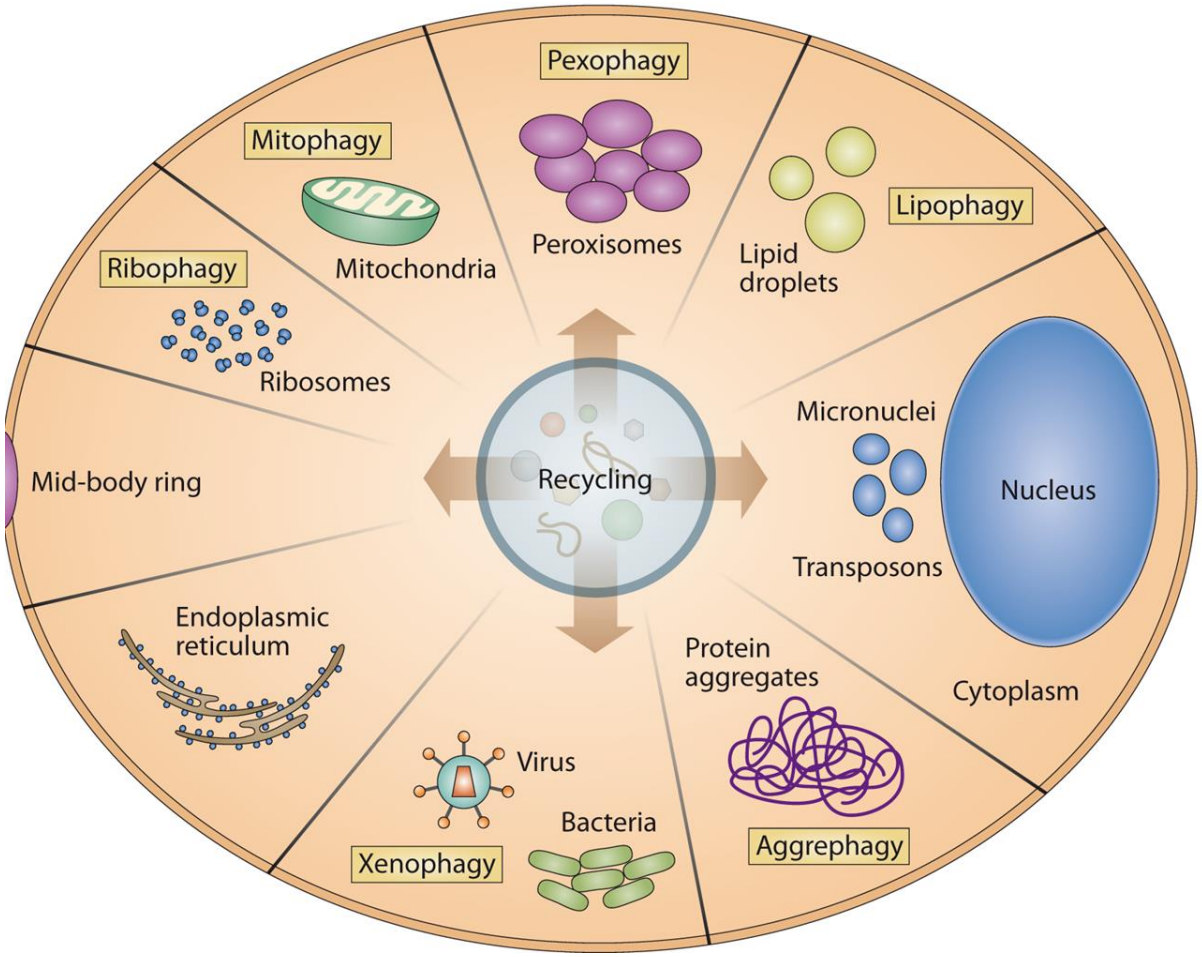

Figure 1.4. Types of selective autophagy. Numerous organelles have been discovered to be selectively turned over by autophagy, and cargo-specific names have been assigned to the various selective pathways, including the ER (reticulophagy or ERphagy), peroxisomes (pexophagy), mitochondria (mitophagy), lipid droplets (lipophagy), secretory granules (zymophagy), and even portions of the nucleus (nucleophagy). Additionally, autophagy targets pathogens (xenophagy), ribosomes (ribophagy), and aggregate-prone proteins (aggrephagy) for breakdown.

1.2.1. Mitophagy: the selective removal of whole mitochondria

Mitochondria are organelles that act as signalling platforms and generate most of the chemical energy needed to power the cell's biochemical reactions They are involved in a multitude of essential cellular processes such as ATP production through oxidative phosphorylation (OXPHOS), fatty acid oxidation, calcium buffering, phospholipid synthesis, reactive oxygen species (ROS) generation and maintenance, iron-sulfur cluster biosynthesis, and innate immune signalling (Spinelli and Haigis, 2018). Numerous quality control mechanisms have evolved to minimize mitochondrial damage that can

occur as a result of external factors such as nutrient deprivation, hypoxia, and OXPHOS uncoupling, or as a consequence of abnormal mitochondrial proteostasis. The mechanisms consist of protein quality control checkpoints such as mitochondrial-associated degradation (MAD) and other processes linked to the ubiquitin (Ub)-proteasome system (UPS). Mitochondrial proteases (mitoproteases) are in charge of regulating the condition of imported proteins and mtDNA-encoded gene products inside the mitochondria. Mitochondrial quality control checkpoints involve removal and turnover of mitochondrial fragments in mitochondrial-derived vesicles (MDVs) or entire organelles (mitophagy) and nuclear transcriptional responses (unfolded protein response of the mitochondria (UPRmt)).

Quality control at the organelle level can be achieved by selective autophagy of mitochondria, in a process commonly referred to as mitophagy (Lemasters, 2005). Mitophagy is essential for the maintenance of the quality of the mitochondrial pool and for regulation of mitochondrial abundance in response to external factors like hypoxia (Quinsay et al., 2010; Tracy et al., 2007), erythroid cell maturation, the glycolytic switch during cell differentiation and stem cell pluripotency (Takano-Ohmuro et al., 2000; Diwan et al., 2007; Esteban-Martínez et al., 2016). Mitophagy shares the core molecular machinery with general macroautophagy (Levine and Kroemer, 2019). In the process of mitophagy, autophagosomes engulf whole mitochondria via specific receptor proteins that link mitochondria to the autophagy membrane (Dikic and Elazar, 2018). The receptors can either interact with ubiquitin molecules conjugated to proteins on the mitochondrial surface or themselves be integrated into the OMM but have the ability to bind to ATG8 homolog proteins of the LC3 and GABARAP subfamilies in the autophagy membrane via a specific LC3 interacting region (LIR) (Johansen and Lamark, 2020). Mitophagy can be separated into two functionally different groups, which depend on the use of the kinase PINK1 and the Ub E3 ligase Parkin termed PINK1/Parkin-dependent and PINK1/Parkin-independent mitophagy.

1.2.2. Mitophagy pathways

1.2.2.1. PINK1-Parkin dependent mitophagy

In normal conditions PINK1 is continuously translocated into the mitochondria where it is cleaved by the mitochondrial processing peptidases MPP (Greene et al., 2012) and PARL (Jin et al., 2010) in the matrix and subsequently retro-translocated to the cytosol to be degraded by the N-end rule pathway. Once the mitochondria are damaged the mitochondrial membrane potential is depolarized and PINK1 accumulates on the OMM establishing a TOM-PINK1 complex that promotes the recruitment of the Parkin ubiquitin ligase (Figure 1.5.) (Lazarou et al., 2012), which mediates the ubiquitylation of a series of outer mitochondrial membrane proteins. MITOL/MARCH5 catalyses the ubiquitylation of OMM proteins to form the "seeding" Ub chains for Parkin recruitment (Koyano et al., 2019). Subsequently, PINK1 phosphorylates Ub chains to accelerate the mitochondrial recruitment of Parkin and promote its E3 Ub ligase activity (Figure 1.5.) (Wauer et al., 2015). The generation of phosphorylated poly-Ub chains on OMM proteins triggers the recruitment of autophagy receptors that contain Ub-binding domains to the mitochondrial surface, like the OPTN and NDP52 (also known as CALCOCO2) (Wong and Holzbaur, 2014; Lazarou et al., 2015). Furthermore, in a recent study mitochondrial matrix proteins 4-Nitrophenylphosphatase domain and non-neuronal SNAP25-like protein homolog 1 (NIPSNAP1) and 2 (NIPSNAP2) were proven to be necessary for PINK1/Parkin-dependent mitophagy in both mammalian cell lines and in zebrafish by facilitating mitochondrial recruitment of the SLRs, the autophagy-linked FYVE protein (ALFY) and ATG8 proteins (Princely Abudu et al., 2019). NIPSNAP1/2 accumulate on the OMM upon mitochondria depolarization, functioning as activating signal for mitophagy by interacting with mitophagy receptors to stimulate PINK1/Parkin mitophagy (Princely Abudu et al., 2019).

Our understanding of the importance of PINK1/Parkin-dependent mitophagy *in vivo* is debatable, due to differences seen across species, tissues, and cell lines. Depletion of *PINK1* and *Parkin* does not affect basal mitophagy in *Drosophila* or mice (Kim et al., 2019, McWilliams et al., 2018). On top of that, PINK1 is not essential for Parkin activation upon mitochondrial depolarization in cardiac myocytes from mice (Kubli et al., 2015) nor is it required in acute exercise-induced mitophagy in mice (Drake et al.,

2019). In contrast, PINK1 and Parkin are necessary for hypoxia-induced mitophagy in the wing discs of L3 larvae (Kim et al., 2019), as well as in *in vivo* to remove damaged mitochondria and to regulate innate immunity highlighting potential tissue- or organism-specific influences on mitophagy. To conclude, all this evidence confirms the probability of alternative mechanisms, acting in parallel to the PINK1/Parkin-dependent mitophagy pathway in whole organisms.

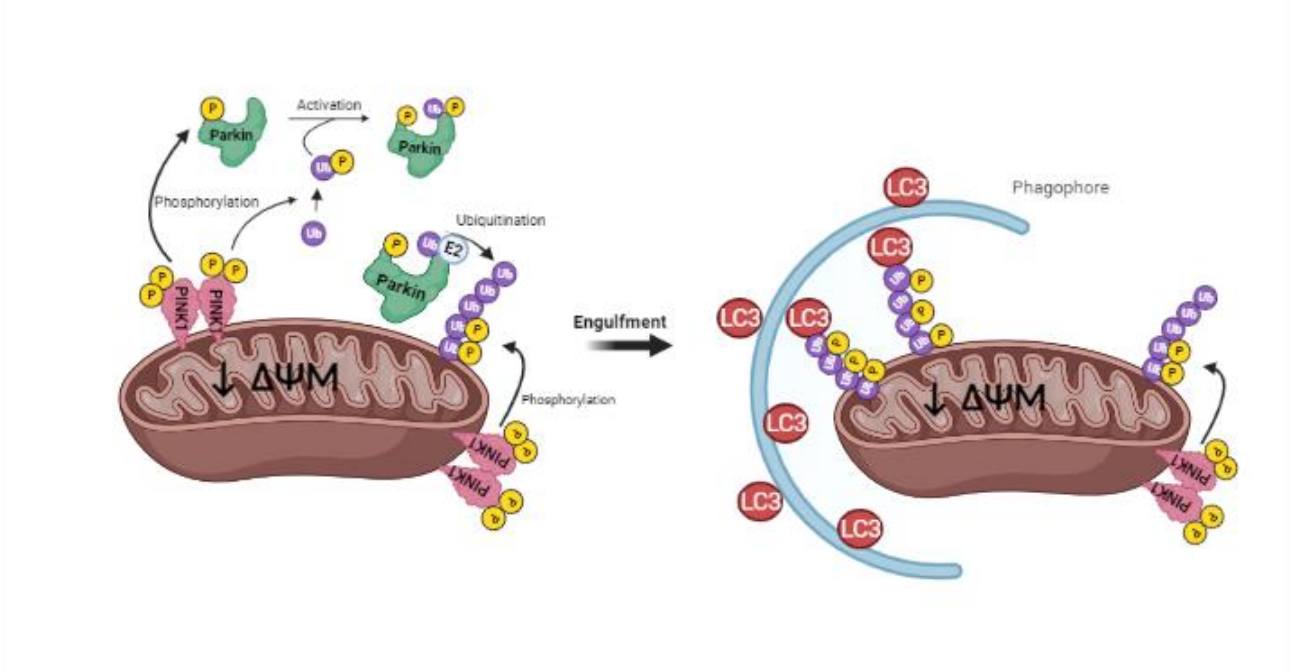

Figure 1.5. PINK1/Parkin-mediated mitophagy. When mitochondria are damaged and lose their mitochondrial membrane potential (ΔΨm), PINK1 degradation is inhibited, resulting in a build-up of full-length PINK1 on the outer mitochondrial membrane (OMM). PINK1 phosphorylates ubiquitin, which causes Parkin to be recruited to mitochondria and its E3 ligase function to be activated. At the same time, phospho-ubiquitin engages autophagy receptors to start the creation of autophagosomes. Parkin contributes to this signalling by ubiquitinating mitochondrial proteins further. Parkin acts as an enhancer of this signaling through further ubiquitination of mitochondrial proteins.

1.2.2.2. Parkin independent mitophagy

At any step along the PINK1/Parkin pathway, from Parkin translocation through autophagosome formation, alternative mitophagy pathways can branch into or parallel the PINK1/Parkin pathway. The majority of investigations, however, have focused on one of two steps: ubiquitination of OMM proteins by E3 ubiquitin ligases other than Parkin, or participation of OMM mitophagy receptors that direct mitochondria to autophagosomes without Parkin-induced ubiquitination (Teresak et al., 2021.).

(1) RECEPTOR MEDIATED MITOPHAGY: These receptors have a unique binding motif, the LC3-interacting region, that interacts directly with LC3-II and GABARAP, two components of the autophagosomal membrane (LIR). FKBP8, a member of the FK506-binding protein family, recruits LC3A to damaged mitochondria in response to depolarization (Figure 1.6.(1)) (Bhujabal et al., 2017), BNIP3 and NIX, pro-apoptotic Bcl2-family members, and FUNDC1, which target mitochondria to autophagosomes by interacting directly with LC3B and GABARAP in response to hypoxia or receptor phosphorylation (Figure 1.7.(1)) (Georgakopoulos et al., 2017; Terešak et al., 2022).

BCL2 (adenovirus E1B 19 kDa that interacts with protein 3) and its homologue Bnip3L / Nix are atypical members of the pro-apoptotic protein subfamily Bcl-2 (Chinnadurai et al., 2008), with 56 percent amino acid sequence similarity. Both enter into the MME through their C-terminal transmembrane domains, with the N-terminus towards the cytoplasm, following expression (Ray et al., 2000). The BH3 domains of Bnip3 expression (Ray et al., 2000) and Nix (Imazu et al., 1999) inhibit the activity of antiapoptotic Bcl-2 proteins in mitochondria. Bnip3 has been shown to activate autophagy (Daido et al., 2004) and mitophagy (Hamacher-Brady et al., 2007) in addition to its apoptotic effects (Figure 1.6.). Basal mitophagy plays an important role throughout retinal development, according to research from our group. Hypoxia and HIF-1 (Hypoxia-Inducible Factor 1), a BNIP3L / NIX target gene, control mitophagy, which stimulates mitochondrial clearance via mitophagy and leads to a metabolic shift toward glycolysis, which is required for retinal development. Similarly, during blood cell formation, Nix mediates mitochondrial clearance (Schweers et al., 2007; Sandoval et al., 2008). Hypoxia activates Bnip3, which then translocates to the OMM through a transmembrane domain (Figure 1.6.). Phosphorylation of serine 17 is required for Bnip3 LIR function, while phosphorylation of serine 24 improves it. The kinase(s) and phosphatase(s) responsible have yet to be discovered. The pro-survival Bcl-xL activation promotes the binding of Bnip3 to LC3. Nix has an analogous SWxxL LIR motif and is regulated similarly by phosphorylation (Hamacher-Brady and Brady, 2016).

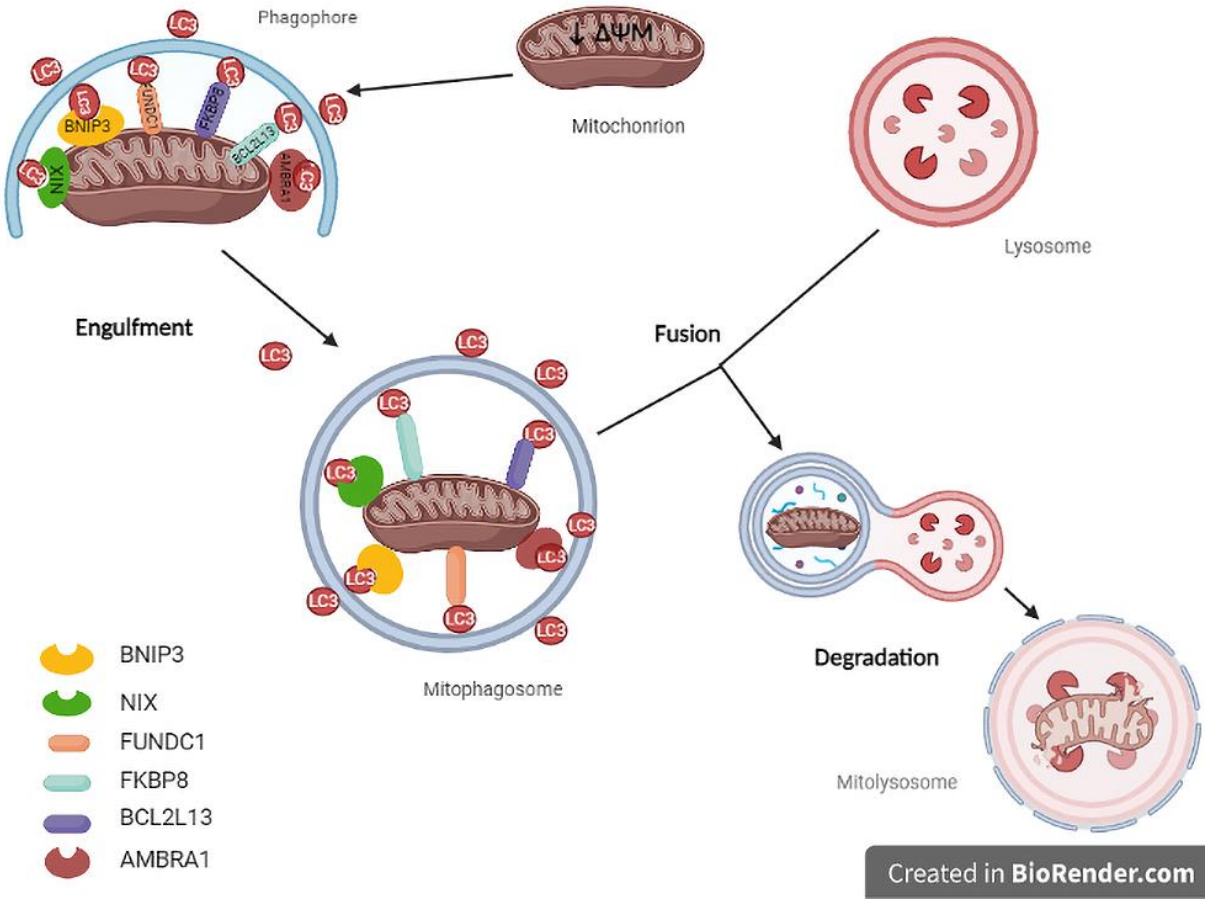

Figure 1.6. Receptor mediated mitophagy: BNIP3, NIX/BNIP3L, FUNDC1, FKBP8, Bcl2L13 are OMM receptors containing an LIR-domain that directly binds to LC3 proteins allowing the recruitment of the phagophore to the damaged mitochondria and leading to its degradation. A pool of AMBRA1, can be localized at the mitochondria, and is also able to bind to LC3 to induce the selective elimination of damaged mitochondria.

(2) LIPID MEDIATED MITOPHAGY: The inner mitochondrial membrane (IMM) phospholipid Cardiolipin (CL), which has an LIR motif, is another non-protein molecule that can bind directly with LC3-II. CL can engage LC3 and induce mitophagy when it is externalized from the IMM to the OMM in response to depolarization, described as lipid mediated mitophagy (Figure 1.7. (2)) (Terešak et al., 2022).CL externalization has been demonstrated to promote mitophagy in primary cortical neurons and in response to PD-inducing toxins (Chu et al., 2013), indicating that this route is important in neuronal survival and death.

(3) OTHER E3 UBIQUITIN LIGASES, including as Gp78, MUL1, and SIAH1, have also been shown to contribute to the ubiquitination of OMM target proteins like Mitofusin, a mitochondrial fusion protein (Mfn). Gp78 ubiquitinates Mfn1 and Mfn2, causing them to be degraded by proteasomes and therefore controlling mitochondrial dynamics, motility, and mitophagy (Fu et al., 2013; Terešak et al., 2022). MUL1 has also been found to ubiquitinate Mfn and control mitophagy in Drosophila (Georgakopoulos et al., 2017). SIAH1 enhances mitophagy in the absence of Parkin by forming a complex with PINK1 and syniphilin-1. Synphilin-1 can be recruited to the mitochondria by PINK1, which then recruits SIAH1, which then ubiquitinates mitochondrial proteins, allowing LC3 to be recruited (Figure 1.7.(3)). Interestingly, PINK1 PD-related mutants do not generate this complex, suggesting that this route may be involved in the illness (Szargel et al., 2016).

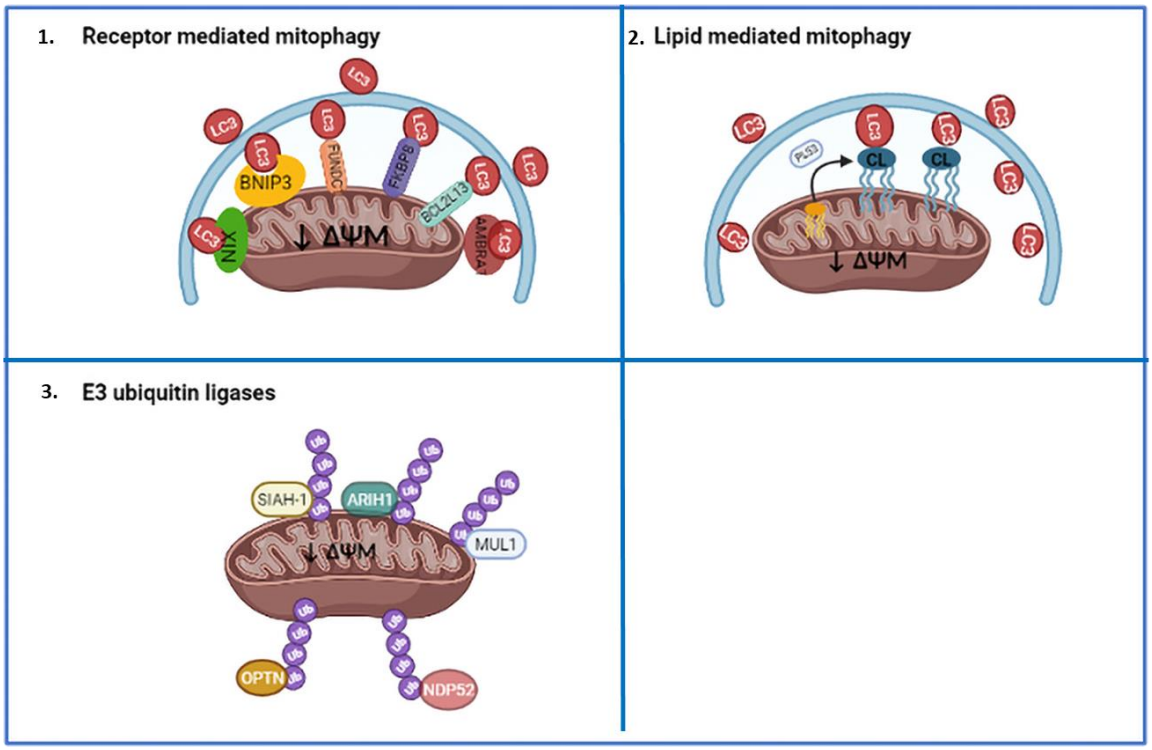

Figure 1.7. Parkin independent mitophagy. 1. Receptor-mediated mitophagy: BNIP3, NIX/BNIP3L, FUNDC1, FKBP8, Ambra1 and Bcl2L13 are OMM receptors with an LIR-domain that directly bind to LC3 proteins, enabling the phagophore to be recruited to the mitochondria 2. Lipid-mediated mitophagy: IMM cardiolipin may be translocated to the OMM through PLS3. Cardiolipin binds to LC3A at the OMM to engage the phagophore formation. 3. E3 ubiquitin ligases: MUL1, ARIH1, and SIAH1 are E3 ligases that found near damaged mitochondria and ubiquitinate OMM proteins, therefore recruiting the phagophore to engulf and breakdown damaged mitochondria. OPTN and NDP52, two autophagy adaptors, can bind to ubiquitinated OMM proteins and promote mitophagy in a parkin-independent way.

1.2.3. Mitophagy modulation

The most utilized mitophagy inducer in cell biology studies is the proton (H+) ionophore. Protonophores are weakly acidic lipophilic compounds that can transport H+ across the inner mitochondrial membrane (IMM), in that way reducing the electrochemical proton gradient and uncoupling oxidative phosphorylation from the electron transport chain (ETC) (Liberman et al.,1969). The phenylhydrazones carbonyl cyanide m-chlorophenyl hydrazone (CCCP) and carbonyl cyanide-p-(trifluoromethoxy) phenylhydrazone (FCCP) have been widely used to investigate the core mechanisms of mitophagy and characterize the biological pathways involved in this process (Figure 1.8.) (Narendra et al., 2008; Gatliff, J. et al., 2014).

Protonophores do have some disadvantages as mitophagy stimulators. Firstly, their effects on mitochondria do not resemble those under naturally occurring conditions, since the effect is damaging and ultimately leading to mitochondrial failure (Wang, et al., 2012). Secondly, they affect the entire mitochondrial population rather than a specific subgroup and can even lead to the complete elimination of mitochondria from cells after longer treatments (Narendra et al., 2008). Protonophores are not specific for mitochondria, which means they have protonophoric activity on other membranes, particularly the plasma and the lyosomal membrane. As a result, they mediate a variety of off-target effects, including disruption of the microtubule cytoskeleton, inhibition of lysosomal activity and activation of ion channels, which leads to relatively high levels of toxicity and a narrow therapeutic window (Park et al., 2002; Maro, et al., 1982; Padman et al., 2013).

In addition to protonophores, a variety of toxins and mitochondrial respiration inhibitors activate PINK1-mediated mitophagy resulting in the disruption of the ΔΨm. A good example is valinomycin, a highly specific potassium (K+) ionophore that transports K+ ions across the IMM by masking their charge through a reversible interaction (Ashrafi and Schwarz, 2013). The electrical potential of the mitochondrion is reduced resulting from the accumulation of K+ in the matrix, this activates the PINK1–Parkin pathway without changing the pH gradient.

A model for the respiration inhibitors is the antibiotic antimycin A, which stimulates a mitochondria-targeted autophagic response by inhibiting the respiratory complex III, consequently leading to elevated levels of ROS (Shen et al., 2014). In contrast to protonophores and mitochondrial toxins, antimycin A causes a limited decrease in ΔΨm that is stabilized quickly by the reverse hydrolysis activity of the F1F0-ATP synthase (McLelland et al.,2014). Hence, it is used in combination with oligomycin, an inhibitor of ATP synthase, whose role of action is to prevent this balancing process by inhibiting the F1Fo-ATP synthase and therefore enables a more intense depolarization (Lazarou et al., 2015). The activation of mitophagy by antimycin A and oligomycin mimics naturally occurring conditions better than before mentioned compounds since both inhibitors are relatively selective for their targets and mediate less toxic effects, causing subtler mitochondrial damage (Narendra et al.,2008).

Paraquat (1,1′-dimethyl-4,4′-bipyridine), a widely used herbicide, is another well-studied mitochondrial toxin, whose role of action is to activate mitophagy through excessive complex-I-dependent superoxide generation (Narendra et al., 2008). Alike other mitochondrial toxins, paraquat induces mitophagy by mitochondrial depolarization and operates via the PINK1–Parkin pathway. Paraquat is known to cause parkinsonian symptoms and is often used to model Parkinson's disease both *in vitro* and *in vivo* due to the production of ROS, oxidative stress, and aggregation of α-synucleins in dopaminergic neurons (Kuter et al., 2007; Kuter et al., 2010.) The mechanism used by paraquat to access dopaminergic neurons is not well understood yet. (Liou et al., 1996.)

Similarly, to paraquat, some of the other parkinsonian toxins include rotenone, MPP+ (1-methyl-4-phenylpyridinium) which promote mitophagy, but through a different mechanism (Dagda et al., 2008; Chu et al., 2013; Zhu et al., 2012). Rotenone triggers moderate mitochondrial depolarization, which is insufficient to induce PINK1-mediated mitophagy in primary neurons or neuroblastoma cells (Chu et al., 2013). It promotes the externalization of cardiolipin and mediates the accumulation of ERK2 (extracellular-signal-regulated protein kinase 2) which leads to sequestration of mitochondria into autophagosomes and enables their degradation (Dagda et al., 2008; Zhu et al., 2012).

Iron loss induced by an iron chelator can also trigger mitophagy PINK1/Parkin independent pathway (Allen et al, 2013) with the underlying mechanisms remaining unknown. In a chemical screen using a tandem mCherry–GFP tag anchored on the OMM, iron chelator deferiprone (DFP) was identified as a novel inducer of mitophagy (Allen et al., 2013). DFP was shown to promote mitochondrial turnover via an iron-depletion-dependent mechanism without causing a ΔΨm collapse (Figure 1.8.). DFP manages to keep its activity even in cells lacking a functional PINK1–Parkin pathway, and this has shown its role as a chemical tool for analysing parkin-independent mitophagy (Kondapalli et al. 2012). A recent study showed that iron loss induced by DFP is associated with HIF1α-SP1 axis-mediated regulation of mitochondrial ferritin (FTMT) expression (Figure 1.8.). The FTMT accumulation across the outer membrane of defective mitochondria leads to induction of mitophagy through the specific interaction between FTMT and nuclear receptor coactivator 4 (NCOA4), autophagic cargo receptor (Hara et al., 2020). This type of mitophagy may have therapeutic potential since iron chelators are clinically used.

1,10′-phenanthroline (Phen) was another compound identified as a 'hit' in a chemical screen for mitophagy activators, but unlike DFP, Phen mediates a collapse of ΔΨm, which further generates a dynamin-1-related protein (Drp1)-dependent mitochondrial fission and induction of mitophagy (Park et al. 2012). It also acts as an iron chelator. However, Phen does not induce the same effects in neuronal-like SH-SY5Y cells, indicating that its mitophagic activity might be cell-type dependent (Mauro-Lizcano et al., 2015).

Nicotinamide (NAM), a precursor of nicotinamide adenine dinucleotide (NAD+), is a vitamin B3 that activates mitophagy by SIRT1 (silent information regulator T1) activation, and in the NAD+/NADH ratio increase (Jang et al., 2012). In addition, it functions as an iron chelator. Importantly, the mitochondria in the NAM-treated cells were marked with high membrane potentials (Δψm). These suggested that NAM treatment may cause SIRT1-mediated activation of mitophagy that is selective for mitochondria that suffer from low Δψm and high levels of ROS generation (Mauro-Lizcano et al., 2015).

Interestingly, other SIRT1 activators, including the natural products resveratrol, fisetin and the synthetic small molecule SRT1720, decrease the mitochondrial network size to a similar extent as NAM, but without increasing the ΔΨm. This proposes that the hyperpolarization induced by NAM is independent of its effects on SIRT1 (Jang et al., 2012; Lee et al., 2008).

The transcription factor nuclear factor E2-related factor 2 (Nrf2; Gene ID: 4780) has been proposed as an attractive target for enhancing mitochondrial function and health. A small molecule that activates Nrf2 was named p62/SQSTM1-mediated mitophagy inducer (PMI), it increases the expression of p62/SQSTM1 and drives mitochondria into autophagy without disrupting the ΔΨm (East et al., 2014). Interestingly, PMI is able to induce mitophagy in cells lacking a functional PINK1–Parkin pathway (PINK1 knockout (KO) or Parkin knockdown (KD)), which highlights its therapeutic potential in conditions associated with impaired PINK1 and Parkin activity.

The most widely used compound for blocking the process of mitophagy relies on the pharmacological inhibition of lysosomal acidification, using the V-ATPase (vacuolar-type H+-ATPase) inhibitor bafilomycin A1 or the lysomotropic agents chloroquine and hydroxychloroquine (Figure 1.8.) (Yang et al, 2013). Furthermore, compounds that suppress general autophagy by inhibiting the formation of autophagosomes have also been used to stop mitophagy, the class III PI3K inhibitor 3-methyladenine to be an example (Figure 1.8.). Although these methods are successful at inhibiting mitophagy, they also affect other autophagic and lysosomal processes and are consequently unspecific.

Additionally, molecular mechanisms underlying cyclosporin A (CsA) induced cytotoxicity are not well elucidated. Cyclosporin A, a cyclic polypeptide, is a specific inhibitor of mitochondrial permeability transition, which inhibits mitochondrial depolarization and mitophagy by interfering with the interaction of cyclophilin D and mitochondrial permeability transition pores (Mishra et al., 2019). It has been shown that CsA inhibits mitophagy (Mauro-Lizcano et al., 2015).

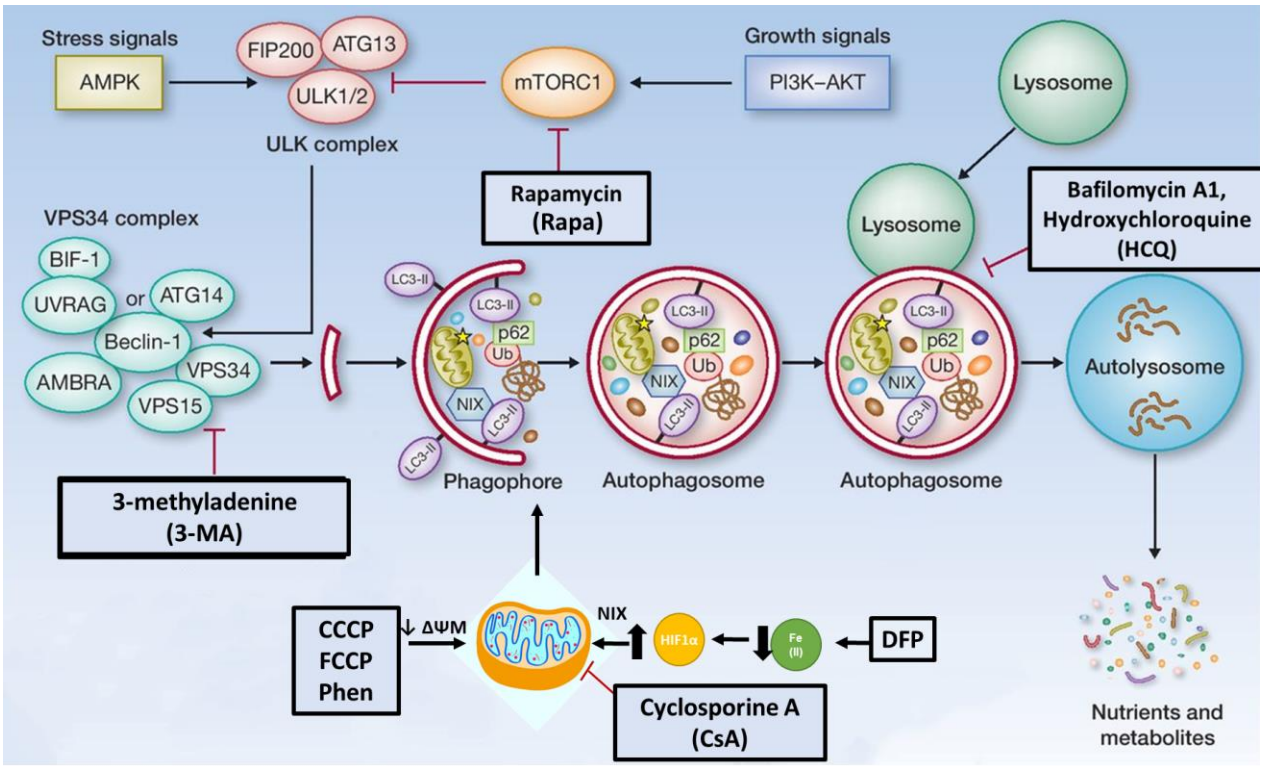

Figure 1.8. Schematic presentation of the effect of different drugs on the various stages of autophagosome formation (Modified from Cicchini et al., 2015).

1.2.4. Mitophagy in development and differentiation

Numerous evidence shows the links between mitophagy and cell differentiation. For example, mitophagy regulated NIX-mediated mitochondrial elimination during erythrocyte maturation (Schweers et al, 2007; Sandoval et al, 2008). Intracellular organelles including mitochondria are removed when reticulocytes differentiate into mature erythrocytes. Mice lacking the autophagy gene Atg7 in the hematopoietic system suffer from severe anaemia, and Atg7-deficient erythrocytes accumulate damaged or dysfunctional mitochondria with altered membrane potential (Mortensen et al, 2010). Furthermore, loss of NIX in mice causes defects in mitochondrial clearance and anaemia (Schweers et al, 2007; Sandoval et al, 2008).

Data from our lab shows that NIX has a key role in mouse retinal ganglion cell (RGC) differentiation (Esteban-Martinez et al, 2017). During RGC differentiation, a shift from oxidative phosphorylation to glycolysis is needed in order to meet the metabolic demands of RGCs. Retinas from NIX-deficient mice show increased mitochondrial mass,

reduced expression of glycolytic enzymes, and inefficient neuronal differentiation (Esteban-Martinez et al, 2017).

Mitophagy is also involved in the maturation of muscle tissue. During myogenesis and muscle regeneration, mitochondrial activity is drastically increased, as a result of a shift in metabolism from glycolysis to oxidative phosphorylation which ultimately increases mitochondrial oxidative stress (Duguez et al, 2002; Sin et al, 2016). Silencing of the autophagy gene Atg5 results in accumulation of abnormal mitochondria and inefficient differentiation into mature muscle tissue (Sin et al, 2016).

Parkin-dependent mitophagy is also linked to cell fate decision of adipocytes. Mice deficient of Parkin have an increase in mitochondrial mass in beige adipocytes and show defects in beige-to-white adipocyte transition (Lu et al, 2018). In general, white adipocytes have a small amount of mitochondria and undertake the role of fat tissue to store energy, beige adipocytes contain a large quantity of mitochondria and act in thermogenesis by uncoupling mitochondrial proton gradient in response to several signals such as chronic cold exposure and exercise (Harms and Seale, 2013). After withdrawal of such stimuli, beige adipocytes start acting like white adipocytes and obtain white adipocyte-like characteristics in a manner dependent on autophagic mitochondrial turnover (Altshuler-Keylin et al, 2016).

1.2.5. Tools and techniques to assess mitophagy in cells and tissues

Various techniques for visualizing mitophagy in mammalian tissues are currently available.

(1) Electron microscopy (EM) has been a vital tool in cell biology since its introduction in the early 1940s. EM is used in cell biology for imaging of stained thin slices of plastic-embedded cells by passing an electron beam through the sample and absorbing and scattering the beam, generating contrast and an image. Because of the electron beam's short wavelength (100,000-fold shorter than photons in visible light), EM may attain subnanometer resolution—well below that of even the highest-resolution light microscopes, which have a resolution of 20 nm (Eskelinen et al., 2011). Because autophagy includes subcellular structures that are beyond the resolution capacity of the

light microscope, the use of EM to investigate the intricacies of autophagy will continue in the foreseeable future (Eskelinen et al., 2011).

(2) Colocalization of mitochondria with autophagosomes or lysosomes using immunofluorescence for mitochondrial and lysosomal proteins. To retain epitopes and allow antibodies to penetrate tissue, sensitive and specific antibody labelling is required, as well as meticulous tissue processing.

(3) Dual-excitation ratiometric fluorescent probes that may be used to measure mitophagy. Mt-keima is a pH-sensitive fluorescent protein that targets the mitochondrial matrix and has been effectively utilized *in vitro* to examine mitophagy (Katayama et al., 2011; Bingol et al., 2014). Mt-Keima is a pH-sensitive, dual-excitation ratiometric fluorescent protein with lysosomal protease resistance. The shorter-wavelength excitation predominates at the physiological pH of the mitochondria (pH 8.0). After mitophagy, mt-Keima gradually shifts to longer-wavelength excitation inside the acidic lysosome (pH 4.5) (Sun et al., 2015). Sun and colleagues (Sun et al., 2015) recently reported the Mt-Keima mouse, which is based on the similar principle, however mt-Keima in tissues has a number of drawbacks. One of the disadvantages of the mt-Keima is that it can only be utilized in live cells due to signal loss during fixation.

Ian Ganley's group developed a fluorescent reporter (Allen et al., 2013) to circumvent these issues. The expression of a mCherry-GFP tandem fused with the sequence of the outer mitochondrial membrane protein FIS1 is employed in this reporter. The mitochondrial network fluoresces in both red and green under normal circumstances; however, during mitophagy, mitochondria inside lysosomes the stable mCherry fluorescence persists but GFP fluorescence is quenched by the acidic microenvironment. As a result, mCherry point foci (in red) are displayed, which can be easily qunatified as a measure of mitophagy (Figure 1.9.). Moreover, they generated a transgenic mouse expressing the MitoQC reporter in all cells under the control of the xxx promoter which is ubitiquitus to determine mitophagy *in vivo* (Figure 1.9.) (McWilliams et al., 2016). Compared to the mt-Keima, the MitoQC has the advantage that the cells can be fixed and that the signal is not lost during the fixation process.

In addition, there are stable transgenic zebrafish (Danio rerio) lines that also express mitophagy reporters such as (cytochrome c oxidase subunit 8A (Cox8A)-GFP-mCherry) with the same principle as the MitoQC (Jung Kim et al., 2008; Princely Abudu et al., 2019). The transparency of transgenic zebrafish embryos allows for real-time and in-vivo monitoring of mitochondrial morphology. Because zebrafish live in fresh water, incubating them in drug-dissolved water proved effective to deliver medications to the zebrafish. Consequently, transgenic zebrafish serve as a study platform for apoptosis and mitochondrial physiology, as well as a screening tool for apoptosis-modulating compounds (Jung Kim et al., 2008).

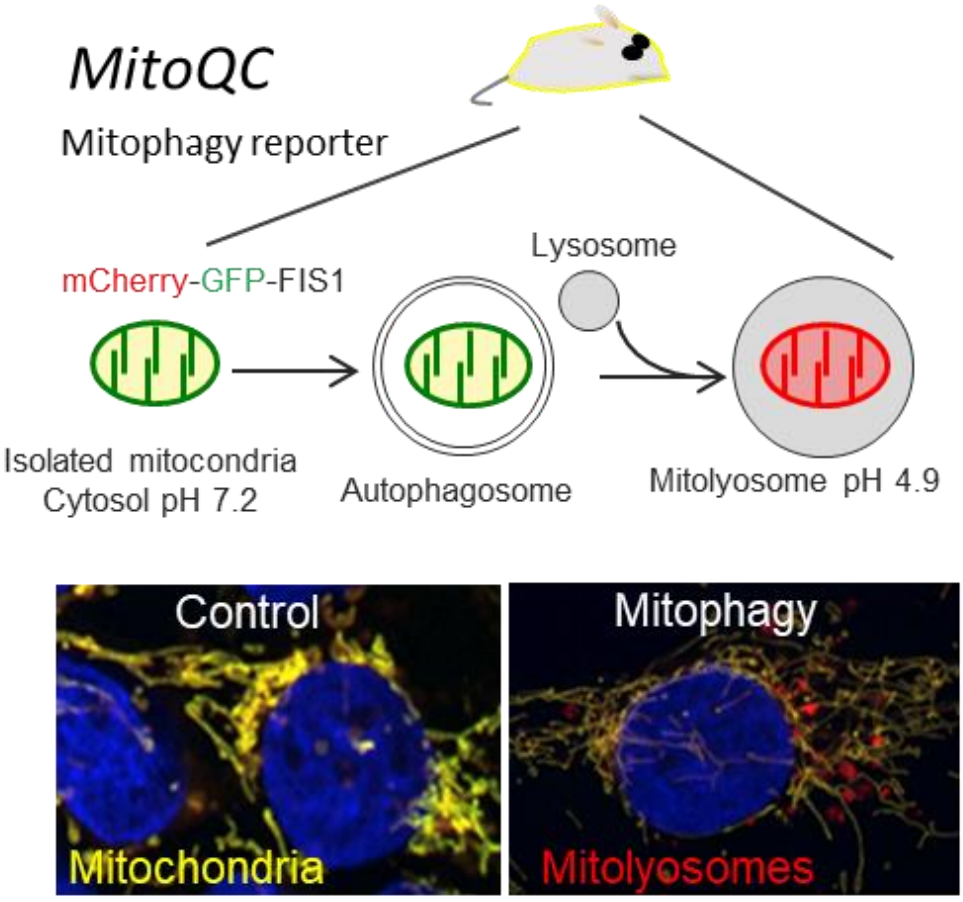

Figure 1.9. The MitoQC mouse model. The MitoQC assay is based on a tandem mCherry-GFP construct. This construct targets mitochondria through the addition of a 51 amino acid mitochondrial targeting sequence derived from the mitochondrial outer membrane protein, FIS1. The resulting construct mCherry-GFP-FIS1 (MitoQC) is observable as a red and green fluorescent signal, which when fused appears yellow. When the mitochondria are enveloped by the phagophore and fuse with the lysosome, forming a mitophagosome, only red mCherry dots appear, due to the acid-labile properties of GFP. This provides easy mitophagy quantifications and allows mitochondrial morphology to be observed *in vitro* and *in vivo*.

1.3. The vertebrate retina

1.3.1. Structure of the adult retina in rodents

The retina is a light-sensitive tissue that processes and transmits visual information. It is positioned on the inner surface of the eye. The mature retina in vertebrates is made up of six neural and one glial cell type organized in a trilaminar structure that includes the retinal ganglion cell layer (RGCL, made up of displaced ganglion and amacrine cells), the inner nuclear layer (INL, made up of bipolar neurons Müller, amacrine, and horizontal), and the outer nuclear layer (ONL, where the photoreceptors are located) (Figure 1.10.) (Hoon et al, 2014). These three layers produce synaptic connections, which are arranged into additional layers termed the inner and outer plexiform layers. The retina also includes the retinal pigmented epithelium (RPE) that separates the retina from the choroidal vasculature. Synapses are separated from cell somas along the depth axis of the retina, which is divided into two major layers: the outer plexiform layer (OPL) and the inner plexiform layer (IPL). The OPL has synapses between rod and cone photoreceptors and bipolar cells, with horizontal cells providing lateral connections (Zhang et al., 2021). Synapses exist between bipolar cells, amacrine cells, and output ganglion cells in the IPL. Furthermore, the OPL is separated into rod and cone synapses, while the IPL is divided into ON (sublamina B) and OFF (sublamina A) bipolar cell axon terminations, which give rise to ON and OFF channels that supposedly react to light increments and decrements, respectively (Zhang et al., 2021).

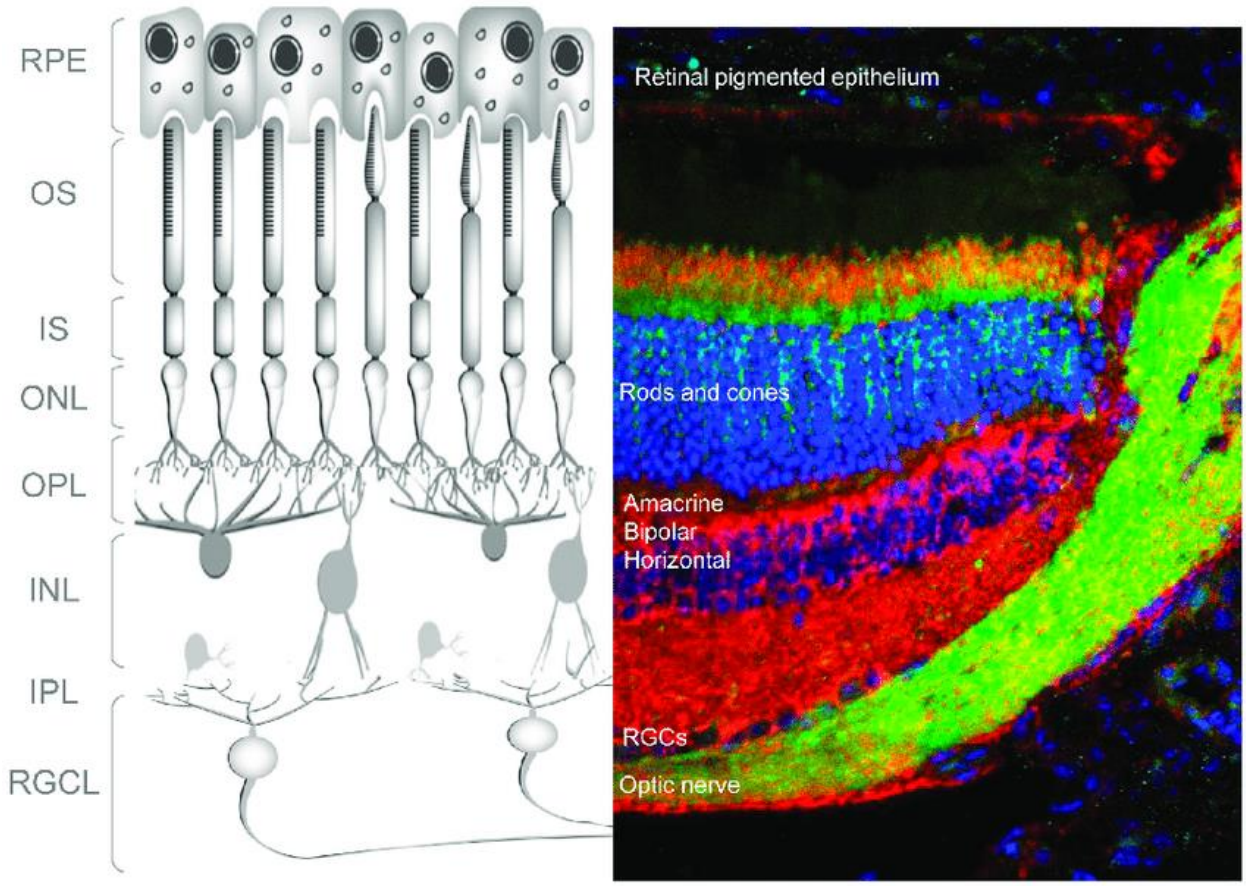

Figure 1.10. Morphology of the adult mouse retina. (Left) Representation of the various cell types in the adult mouse retina; (right) retinal section from an adult GFP-LC3 animal (green) stained with TOMM20 (in red) to detect mitochondria and DAPI (in blue) to stain nuclei. RPE: retinal pigment epithelium; OS: outer segment; IS: inner segment; ONL: outer nuclear layer; OPL: outer plexiform layer; INL: inner nuclear layer; IPL: inner plexiform layer; RGCL: retinal ganglion cell layer.

1.3.2. Retinal development in the mouse

The development of the vertebrate eye is a complex process regulated by intrinsic and extrinsic factors that specify an area of the forebrain as the ocular field and subsequently produce the neural retina (Chow and Lang, 2001). On embryonic day (E) 8.5, optic vesicles appear and evaginate laterally from the forebrain, growing towards the surface of the ectoderm (Schoenwolf, 2009), which later forms the optic cup and lenses. The optic cup is made up of two layers: the RPE and the neuroretina, which develops into the mature three-layered retina (Zagozewski et al, 2014). Neuroretinal development begins on embryonic day 12.5 (E12.5) and neurogenesis does not end until postnatal day 12 (P12). During the early stages of retinal development, the outer neuroblast layer consists

primarily of mitotic progenitor cells, while newly differentiated neurons (primarily ganglion and amacrine cells) are located in the inner neuroblast layer. The different cell types of the mature retina develop from a common set of multipotent progenitors (Zagozewski et al, 2014) through a spatio-temporal dynamic process in the following order: ganglion cells, horizontal cells, cones, amacrine cells during the embryonic development, and bipolar cells, rods and Müllerian glia during postnatal development (Figure 1.11) (Vecino and Acera, 2015; Zagozewski et al, 2014). Photoreceptors, mainly rods, are the most abundant cell type in the retina and have a differentiation peak at P0 (Blackshaw et al, 2004). Finally, at P6 most of the cells of the retina occupy their final destinations, decreasing the expression of characteristic progenitor markers (Blackshaw et al, 2004). Various transcription factors are involved in the organization of the retina, whose cell differentiation follows a central-peripheral pattern (Figure 1.11.) (Zagozewski et al, 2014).

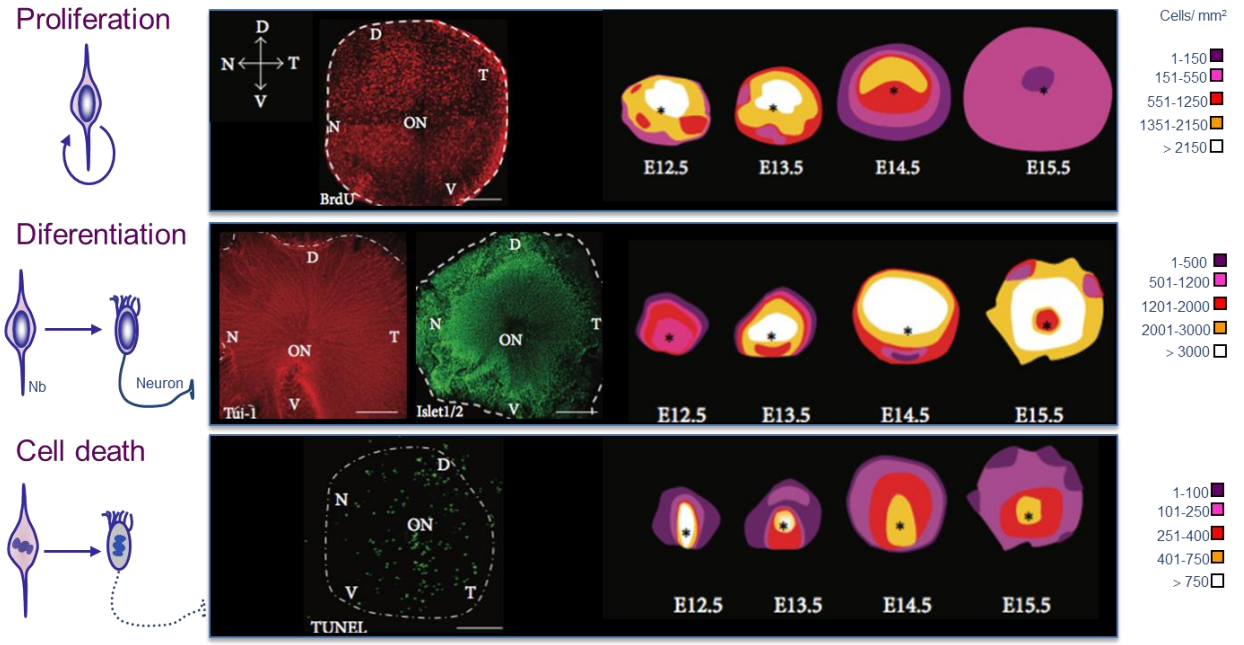

Figure 1.11. Neurogenesis follows a central to peripheral gradient. In mice, first-born RGCs initially form a small patch around the future optic nerve head in the central retina. Thus, RGC differentiation starts in the central retina and then proceeds towards the periphery of the retina.

Among these transcription factors, Pax6 stands out, which is the main regulator of the development of the eye (Figure 1.12.) (Zagozewski et al, 2014) and is essential for the maintenance of multipotency (Marquardt et al., 2001). In addition, Pax6 regulates the

expression of proneural genes of the bHLH family specific for each subpopulation of progenitors that determine the specific cellular destiny (Marquardt et al., 2001). Due to the regionalization of the retina during differentiation, it is likely that progenitors located close to differentiated neurons in the central region are exposed to different signals in comparison to those progenitors located in the periphery far from the differentiated area. Furthermore, there are differences in gene expression between these two regions of the retina (Koso et al, 2007). The progenitor cells of the retina have the ability to generate different cell types of this tissue, their subsequent cell fate is determined by their intrinsic properties and by extrinsic factors (Bassett and Wallace, 2012). Factors of the bHLH family such as Atoh7, Mash1 and Ngn2 are activated in subpopulations of progenitor cells, which makes them have a particular destiny (Figure 1.12.) (Marquardt et al., 2001). In this way, throughout the development of the retina, several families of transcription factors maintain the pluripotency of the progenitors, specify the fate of the cells of the retina and promote their differentiation through a dynamic spatio-temporal process (Figure1.11.).

Importantly, cell cycle exit during early retinogenesis corresponds with the first expression of Atoh7, a progenitor-expressed transcription factor required for the formation of ganglion cells, the retina's first differentiated cell type (Gao et al, 2014). Atoh7 expression begins at E11.5, peaks between E12.5 and E13.5, and progressively declines after E14.5 (Gao et al, 2014; Mu et al, 2005), when it begins to gradually decrease (Figure 1.12.) (Wu et al, 2015).

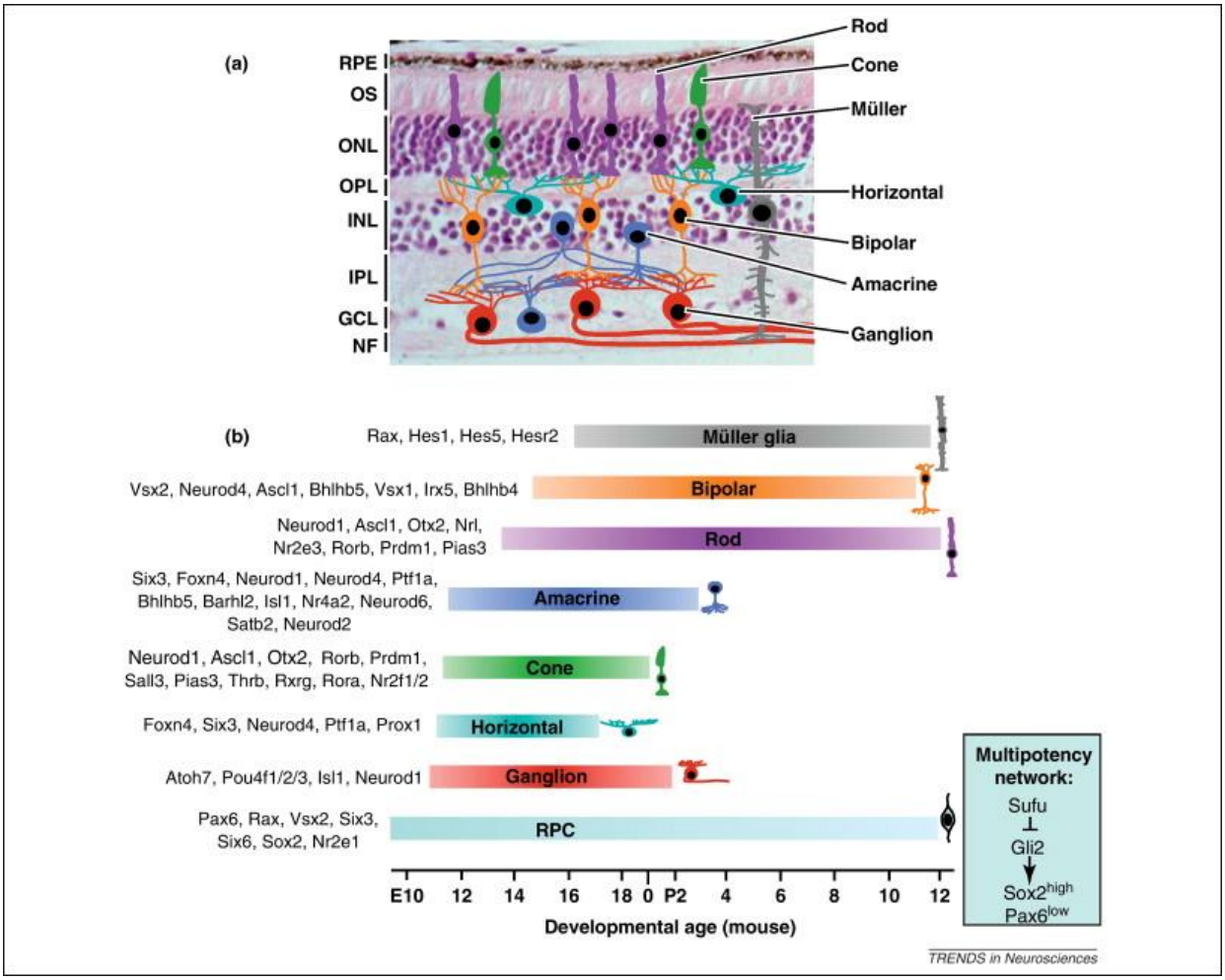

Figure 1.12. The development and structure of the neural retina in vertebrates. a. Histological picture superimposed over a schematic model depicting the adult neural retina structure of a vertebrate, using the mouse retina as an example. While the outer segments of photoreceptors are associated with the retinal pigmented epithelium (RPE), their cell bodies are located in the outer nuclear layer (ONL). In the inner nuclear layer (INL), horizontal, bipolar, and amacrine cells, as well as Müller glia, have their cell bodies. The ganglion cell layer (GCL) is composed of both ganglion and displaced amacrine cells' cell bodies. The outer plexiform layer (OPL) has connections between photoreceptor, bipolar, and horizontal cells, while the inner plexiform layer (IPL) contains synapses between bipolar, ganglion, and amacrine cells (IPL). The nerve fibre (NF) layer is composed of ganglion cell (GC) axons. b. Chronological organization and transcriptional control of the genesis of retinal cells (embryonic and postnatal times based on mouse development). Müller glia are produced last, followed by GCs. A recently described regulatory network involving components of the hedgehog (Hh) pathway and a precise ratio of paired box gene 6 (Pax6) and sex-determining region Y-box containing gene 2 (Sox2) expression maintains the progenitor identity and neurogenic potential of mouse retinal progenitor cells (RPCs) (green box, right). Numerous transcription factors (left) control how each cell type and subtype is specified OS stands for outer segments of photoreceptors (Bassett and Wallace, 2012).

During tissue development, cell death is required for homeostasis. Apoptosis, which is characterized by a decrease in cell size, condensation of chromatin,

phagocytosis, and subsequent degradation of apoptotic bodies after recognition by neighbouring cells (non-professional phagocytes) or microglia (CNS macrophages), is the most common type of death during development (Henson and Hume, 2006). If apoptotic cells are not removed, their plasma membranes can disintegrate, triggering pro-inflammatory responses. A key feature of apoptosis is that it is an active, ATP-dependent cell death that takes place over a long period of time. One of the earliest indications of apoptosis is the appearance of the phospholipid phosphatidyl-serine (PS) on the surface of the apoptotic cell's outer membrane (Fadok et al, 1992), a highly ATP-dependent process that permits dead cells to be recognized and removed from the tissue (Venegas and Zhou, 2007).

Different phases of cell death that affect different cell types such as neural stem cells, proliferative progenitors, undifferentiated neuroblasts, and newly differentiated neurons and glia cells have been identified during the embryonic development of the retina, and whose purpose is to contribute to the correct generation of the retina have been identified (Boya and de la Rosa, 2005; Vecino and Acera, 2015). Three types of retinal death vawes exist, depending on the period of development in which they occur: morphogenetic death, early neuronal death, and neurotrophic death (Valenciano et al, 2009). Morphogenetic death occurs in the optic fissure during the early stages of retinal development (E10.5-E14.5) and is required for retinal reorganization and axon exit from RGCs (Valenciano et al, 2009). Early neural death affects proliferating neuroblasts and newly differentiated ganglion cells in the central retinal area between E13.5 and E16.5 (Boya and de la Rosa, 2005). It's difficult to tell the difference between this sort of death and morphogenetic death in mice (Pequignot et al, 2003). The creation of RGCs happens at the same time as the generation of other subsequent neuronal subtypes, but not the other way around (Chavarria et al, 2007). Finally, neurotrophic death occurs in adult differentiated RGCs owing to a shortage of trophic factors during synaptogenesis with target cells, which is why it occurs in the second half of retinal development (E18.5-P12) (Pequignot et al, 2003). Cell loss happens in the photoreceptor layer as a result of this, which occurs at the same time as the newborn's eye opening (Valenciano et al, 2009). After the RGCs have been generated, both processes take place. Cell death is a genuine

process required for retinal neurogenesis as caspase inhibitors reduce the number of differentiated retinal ganglion cells (Valenciano et al, 2009).

1.3.3. Retinal development and mitophagy

The first *in vivo* comparison of mammalian mitophagy and macroautophagy in the developing and mature eye revealed a significant and very comparable enrichment of both mitolysosomes and autolysosomes in the ONL of MitoQC and autophagy-reporter mice. This suggests that mitophagy is responsible for a considerable portion of the macroautophagy happening in the ONL, making it the location with the greatest level of mitophagy in the eye (McWilliams et al., 2019).

Sections from E16.5 MitoQC eyes were examined to see whether retinal mitophagy is formed throughout development. Mitophagy at E16.5 seemed to be focused in a different area of the retina and was limited to the inner neuroblast layer, in contrast to the adult eye (McWilliams et al., 2019). These results are in line with previous research that suggests retinal ganglion cells, which are present in this location at this time, need controlled mitophagy for development. Macroautophagy was higher in the inner neuroblast layer, although autolysosomes were found throughout the retina, including the outer neuroblast layer, unlike mitophagy (McWilliams et al., 2019). The increasing amount of evidence demonstrating the physiological importance of mitophagy and macroautophagy in mammalian retinal development prompted us to pursue this issue further in this thesis.

1.3.4. Structure of the adult retina in zebrafish

The adult zebrafish retina is made up of three nuclear layers divided by two plexiform layers. The outer nuclear layer contains the photoreceptor rod and cone cell bodies; the inner nuclear layer has the amacrine, horizontal, and Müller glial cell bodies; and the ganglion cell layer contains the ganglion cell bodies. At the plexiform layers, synapsis occurs between these nuclear layers. Cone photoreceptors are nearly exclusively responsible for larval zebrafish vision; zebrafish have blue, UV-sensitive, and red-green double cones, as well as one rod cell type physically organized in a mosaic pattern (Bilotta et al., 2001). Many of the features of retinal development are conseverd in the vertebrate retina although some differences also exist between fish and mammals. By 4 dpf., short

cones are distinguishable, and by 12 dpf, all photoreceptor types are recognizable based on morphological criteria. The human retina, on the other hand, lacks UV-sensitive cones.

1.3.5. The development of the retina in zebrafish

The optic vesicle in zebrafish collapses into two layers at 20 hours post-fertilization (hpf), with the distal portion destined to become the neural retina and the more proximal section destined to become the RPE (Schmitt and Dowling, 1994). At this stage, the future neural retina is a proliferative neuroepithelium that still expresses the eye field transcription factors, which function as positive regulators of proliferation (Hsieh and Yang, 2009). This proliferative neuroepithelium eventually produces the neurons and glia of the retina, demonstrating many retinal neurogenesis principles seen in all vertebrates. Particular types of neurons are produced in waves that are sequential yet overlapping. In the zebrafish, this order is RGCs, then INL cells, then photoreceptor cells (Figure 1.13.) (Hu and Easter, 1999). Other vertebrates have variations on this process, but the “RGCs first, rod photoreceptors second, and Müller glia last” order of neuron production is well-preserved (Bassett and Wallace, 2012; Centanin and Wittbrodt, 2014).

The second principle states that neurons within each cell population are produced in a predictable spatiotemporal manner. Neurogenesis in the zebrafish begins in a "ventral patch" right adjacent to the optic stalk and future site of the optic nerve head, and proceeds nasally, dorsally, and eventually temporally, in a manner similar to the opening of a fan (Figure 1.13.) (Hu and Easter, 1999; Raymond, Barthel, and Curran, 1995). In other vertebrates, such as mice, the spatiotemporal pattern appears as a less complicated central-to-peripheral gradient, with the earliest cells of each cell type produced near the future location of the optic nerve head (Figure 1.13.) (McCabe, Gunther, and Reh, 1999).

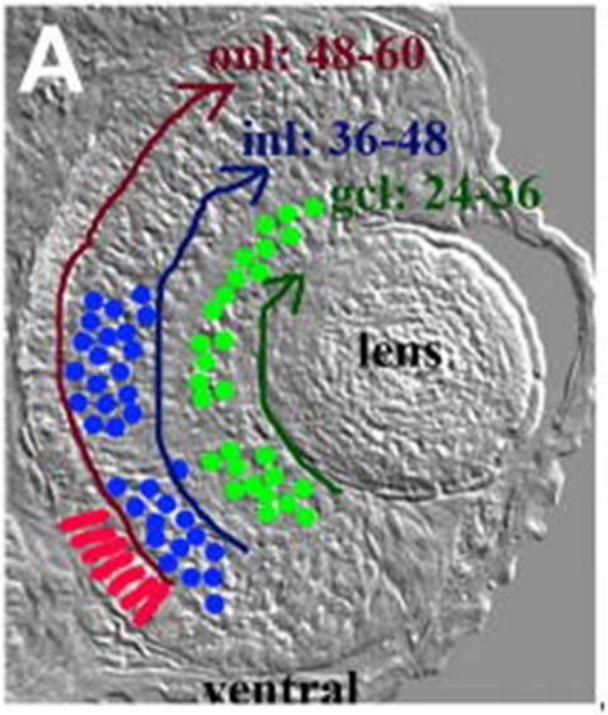

Figure 1.13. Patterns and principles of retinal neurogenesis in zebrafish. Nomarski (DIC) image of a cryosection of the embryonic zebrafish retina, with patterns of neurogenesis of cells of the ganglion cell layer (GCL in green), inner nuclear layer (INL, in blue), and outer nuclear layer (ONL, in red) (Stenkamp, 2015).

Interkinetic nuclear migration is a third basis of retinal neurogenesis that has recently been seen directly in the zebrafish embryo. During most phases of the cell cycle, proliferating progenitor nuclei may be detected at diverse apico-basal sites. However, just before M-phase, nuclei move quickly to the apical side of the neuroepithelium and conduct mitosis there (Baye and Link, 2007). With regard to the retinal hemisphere, the mitotic plane of cleavage might be circumferential or radial. Radial divisions are more likely to form a pair of RGCs that migrate to the proper layer and produce axons as RGCs are produced. Asymmetric destinies are more likely to result from circumferential divides. Because this process has not been explicitly seen in any other vertebrate, it is unknown if it is a conserved mechanism. Factors that establish and maintain apicobasal polarity of retinal progenitors in zebrafish, such as Crumbs, nok, and par (Krock and Perkins, 2014; Zou et al., 2013), are required for normal retinal neurogenesis and cell differentiation in the fish.

The "competence model" was backed by the stereotyped birth order of retinal neurons, which supported a model for the creation of neural variety (Cepko et al., 1996). According to this concept, progenitor cells go through a series of competence stages, each of which allows them to generate a progressively a smaller number of cell types. This model has been further informed by live imaging in the zebrafish embryo, which has revealed that, while birth order biases the destinies of retinal progenitor cells, it does not constrain fates as severely as expected by the model (Poggi et al, 2005).

1.3.6. Mitophagy in zebrafish

The proteins involved in human mitophagy are highly conserved in zebrafish (Wager and Russell, 2013.), making them an excellent model for studying the functional relevance of mitophagy *in vivo*. Although there haven't been many zebrafish mitophagy research, there are various methods for studying mitochondrial dynamics. One research looked for mitophagy sites in zebrafish Rohon Beard neurons where UAS:LC3 was present. In the Isl2b: Gal4 transgenic line, GFP was coinjected with UAS:mitoTagRFP-T. Despite the fact that Lc3 colocalizes with mitochondria, no mitophagy experiments were performed (Mathai et al., 2017). It'd be interesting to see if LC3 disappeared from these contact points over time. As previously stated, a tandem-based method to tagging mitochondrial proteins would aid in the observation of their autophagy degradation rates. It's an exciting time to be investigating zebrafish mitophagy, particularly because there haven't been any previous studies of mitophagy in the zebrafish retina. To further explore this topic, we utilized a stable transgenic zebrafish line expressing a tandem-tagged mitochondria marker (cytochrome c oxidase subunit 8A (Cox8A)-GFP-mCherry, which works in the same way as MitoQC (Jung Kim et al., 2008; Princely Abudu et al., 2019). One important issue is a paucity of antibodies for zebrafish mitochondrial proteins, although with increased academic interest in mitochondrial studies, this is a situation that is expected to change quickly.

1.4. Parkinson's disease

Parkinson's disease (PD) is a common neurodegenerative disorder characterised by loss of dopaminergic neurons in the substantia nigra pars compacta (SNpc). This results in the loss of dopaminergic inputs in the striatum and the characteristic motor symptoms associated with the disease (Postuma et al., 2012). Accumulation of aggregated α-synuclein in Lewy bodies is the pathological hallmark of PD in the SNpc but can also be observed in other affected brain regions (Michel et al., 2016). The typical clinical features involve a movement disorder consisting of bradykinesia, resting tremor, and rigidity, with postural instability occurring at a later stage (Williams-Gray and Worth, 2016).

1.4.1. Mitochondria dysfunction in Parkinson's disease

Mitochondrial dysfunction has been associated with PD for over 30 years. Regardless of that, the role of mitochondrial dysfunction as an initiator, propagator, or bystander is still unknown. The discovery of the role of the PD familial genes PTEN-induced putative kinase 1 (PINK1) and Parkin in mitophagy suggested the importance of this process in PD aetiology (Pickrell and Youle. 2015). Recently, progress has been made in understanding the role of PD-associated genes, such as SNCA, LRRK2, CHCHD2 (PARK22), GCH1, and VPS35 (PARK17) (Figure 1.14.), in mitochondrial dysfunction and their overlap with sporadic PD (sPD), opening opportunities for therapeutically targeting mitochondria in PD (Yue et al., 2015; Funayama et al., 2015). Understanding how these pathways trigger nigral degeneration will reveal mechanisms in both familial and sporadic PD.

Getting a better perception of the influence of PINK1/parkin-mediated mitophagy on basal and stress-induced mitophagy in dopaminergic neurons, in comparison to the PINK1/parkin-independent mechanisms, could help to advance the search of prospective therapeutic activators of this pathway. Also, it is important to understand the role of mitophagy in astrocytes and microglia, in which this pathway seems to be more active, to determine how deficits in mitochondrial quality control in glia contribute to the pathology of PD.

Since several cellular mechanisms are dysfunctional in LRRK2, SNCA, and GBA-related PD, the enhancement of mitophagy and improvement of mitochondrial condition

could moderately rescue dopaminergic cell loss in non-PINK1/Parkin-related diseases. Interestingly, the dysfunction of PD risk genes, particularly LRRK2, is not homogenous across brain regions or cell types, brings up the possibility of an important role for non-neuronal cells in suppressing mitochondrial malfunction through trans-mitochondrial degradation (trans-mitophagy) or by the propagation of mitochondrial damage in either a cell-autonomous manner or through inflammatory processes, such as MITAP or STING-activation. Additionally, the function of CHCHD2 and VPS35 (Figure 1.14.) in mitochondrial dysfunction in dopaminergic neurons and their involvement in the disease is still not fully understood. No matter what the genetic background of patients, the roles of increased LRRK2 kinase activity and α-synuclein aggregation in impairing mitochondria and its impact on mitophagy is probably crucial in identifying the underlying mechanisms in PD (Figure 1.14.).

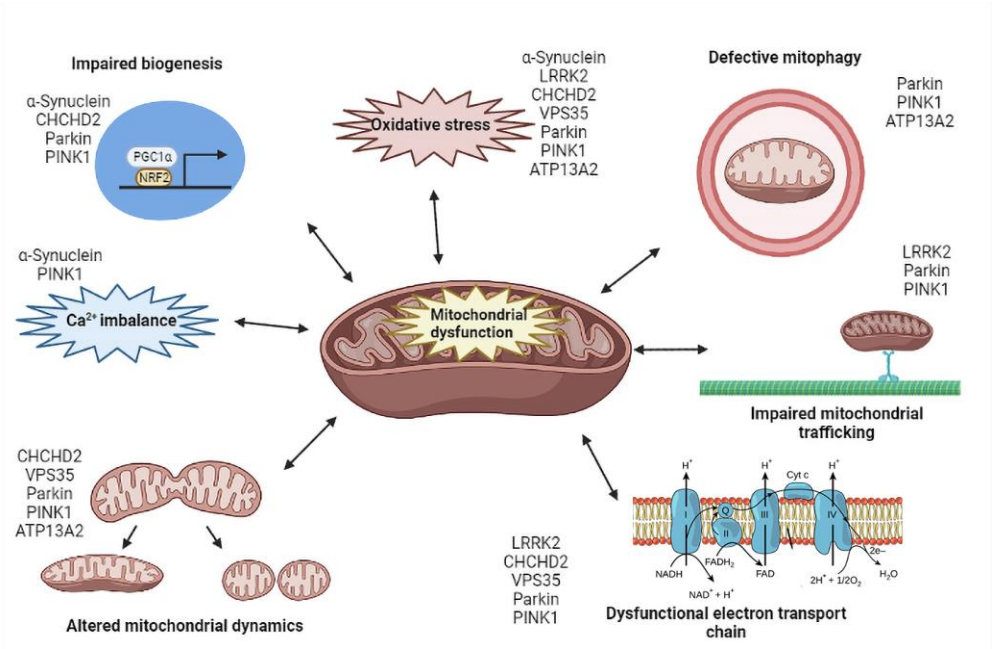

Figure 1.14. Pathways of mitochondrial malfunction implicated in the pathogenesis of Parkinson's disease. Impairment of mitochondrial biogenesis increased reactive oxygen species production, defective mitophagy, compromised trafficking, electron transport chain dysfunction, variations in mitochondrial dynamics, calcium imbalance, or a combination of these factors can cause mitochondrial dysfunction associated with PD pathogenesis. The very intricate interaction of the many activities results in a vicious cycle of increasing cellular failure, which eventually leads to neurodegeneration, which is at the root of PD etiology and development (Modified from Park et al., 2018).

α-synuclein, the primary component of Lewy bodies, has long been linked to mitochondrial dysfunction, but no clear mechanism has been shown. Overexpression of α-synuclein or the addition of exogenous aggregated α-synuclein species, for example, revealed that α-synuclein interacts with many OMM components, including TOM20, (Di Maio et al., 2016, Zambon et al., 2019), VDAC (Jacobs et al., 2019), and F1F0-ATP synthase, resulting in mitochondrial permeability transition pore (MPTP) opening (Ludtmann et al., 2018). Accumulated α-synuclein, as well as dopamine-modified or phospho-mimetic species mimicking pathological forms of the protein, bind to mitochondria, inhibiting mitochondrial protein import and leading to mitochondrial membrane depolarization and impaired cellular respiration (Wang, et al., 2019). Models of α-synuclein aggregates showed decreased levels of MFN-2 and OPA1 levels (Mahul-Mellier, et al., 2020) in accordance with prior findings of how α-synuclein-induced mitochondrial fragmentation and bioenergetic changes in dopaminergic neurons generated from iPSCs (Zambon, et al. 2019). Proteomic studies indicated a substantial recruitment of proteins involved in oxidative phosphorylation into aggregates, which corresponded to respiratory abnormalities (Mahul-Mellier, et al., 2020). Mitochondrial dysfunction and complex I impairments are temporally separated from pS129 production in hippocampal neurons produced by α-synuclein fibrils, indicating that other processes are required for dysfunction beyond the interaction between α-synuclein and the mitochondria (Mahul-Mellier, et al., 2020). In fact, Lewy bodies from Parkinson's disease patients were shown to include fragmented mitochondria packed with lipids and lysosomes as well as -synuclein (Shahmoradian, *et al., 2019*), suggesting that mitochondrial failure, -synuclein aggregation, and Lewy body formation are all inextricably connected.

1.4.2. Therapeutics targeting mitochondrial dysfunction for PD

The loss of mitochondrial quality control may contribute significantly to the increased vulnerability of dopaminergic neurons to neurodegeneration in Parkinson's disease. Latest improvements in our knowledge of mitochondrial homeostasis and damage in Parkinson's disease have led to the identification of many possible treatment pathways to enhance the clearance of old or damaged mitochondria in both PD and other mitochondrial dysfunction-related illnesses.

Small-molecule PINK1 and Parkin activators, as well as inhibitors of the USP30 and pSer65Ub phosphatases, are interesting therapeutic targets for improving mitophagy in Parkinson's disease. Similarly, while less well characterized, USP8, USP14, and USP15 inhibitors are interesting ways to increase mitophagy (Durcan, et al., 2014; Teyra, et al., 2019). Kinetin triphosphate KTP has been shown to activate PINK1 directly (Hertz, et al., 2013), and more bioavailable KTP precursors are being developed (Lambourne and Mehellou, 2018). Furthermore, high-throughput screening revealed two small-molecule PINK1 activators that are structurally different from KTP and have been confirmed in both dopaminergic neurons and PINK1-knockdown Drosophila (Shiba-Fukushima, et al., 2020). Directly expressing recombinant Parkin designed for enhanced solubility and cell permeability has showed potential in shielding cells from both toxin and α-synuclein assault (Chung, et al., 2020).

Direct targeting of proteins affected by autosomal dominant PD mutations might be used to broaden therapy beyond PINK1/Parkin patients. LRRK2 inhibition restored mitochondrial and lysosomal dysfunction in animal models of idiopathic PD (Sanyal, et al., 2020; Rocha, et al., 2020). As a result, LRRK2 inhibitors in clinical trials might hold a lot of promise in terms of addressing mitochondrial dysfunction and mitophagy abnormalities in people who do not have LRRK2 mutations. Furthermore, in iPSC-derived neurons bearing GBA mutations and in Drosophila models, nicotinamide riboside has been shown to repair mitochondrial phenotype. In addition, some small compounds, such as the repositionable medication ursodeoxycholic acid, have been shown to improve mitochondrial complex activity and ATP generation in PD models, most notably in sPD fibroblasts (Carling, et al., 2020).

1.4.3. Astrocytes in PD

A growing body of data shows that astrocytes play a key role in the development of PD (Bantle et al., 2021). Astrocytes make up about 30% of all cells in the central nervous system (CNS) and are the most common cell type in the brain. While early descriptions of these cells referred to them as the "glue of the brain," with a largely passive structural purpose, recent research has revealed that glia have a wide range of activities in the developing and adult brain. Multiple risk alleles implicated in Parkinson's disease

pathogenesis revealed in recent genome-wide association studies and prior candidate gene investigations reveal cellular penetrance in astrocytes (Booth et al., 2017). Astrocytes are dynamic regulators of neuronal synaptic transmission and cerebral blood flow, as well as supporting neuronal homeostasis and participating in the maintenance of the blood–brain barrier (BBB). By secreting glial-derived neurotrophic factor (GDNF), maintaining extracellular ion balance in the CNS, and transporting lactate and glutamine to neurons, they also offer ongoing trophic support and energy metabolism to neurons (Sofroniew and Vinters, 2010). Furthermore, whereas microglia were formerly assumed to be the major inflammatory cell in the CNS, inflammatory activation of astrocytes is typically more persistent than microglia and is expected to play a role in chronic inflammatory activation linked to PD (Bantle et al., 2021).

According to new study, mitochondria influence glutamate modulation, Ca2+ signalling, fatty acid metabolism, transmitophagy, antioxidant synthesis, and neuroinflammatory activation in astrocytes (Ho et al., 2019; Pang et al., 2019; Russo et al., 2019). As a result, one theory is that astrocyte mitochondrial dysfunction affects dopaminergic neuronal health by increasing inflammatory activity while also reducing supporting activities such as trophic and antioxidant support. Astrocytic mitochondrial function preservation may thus offer a disease-modifying strategy for slowing the course of Parkinson's disease.

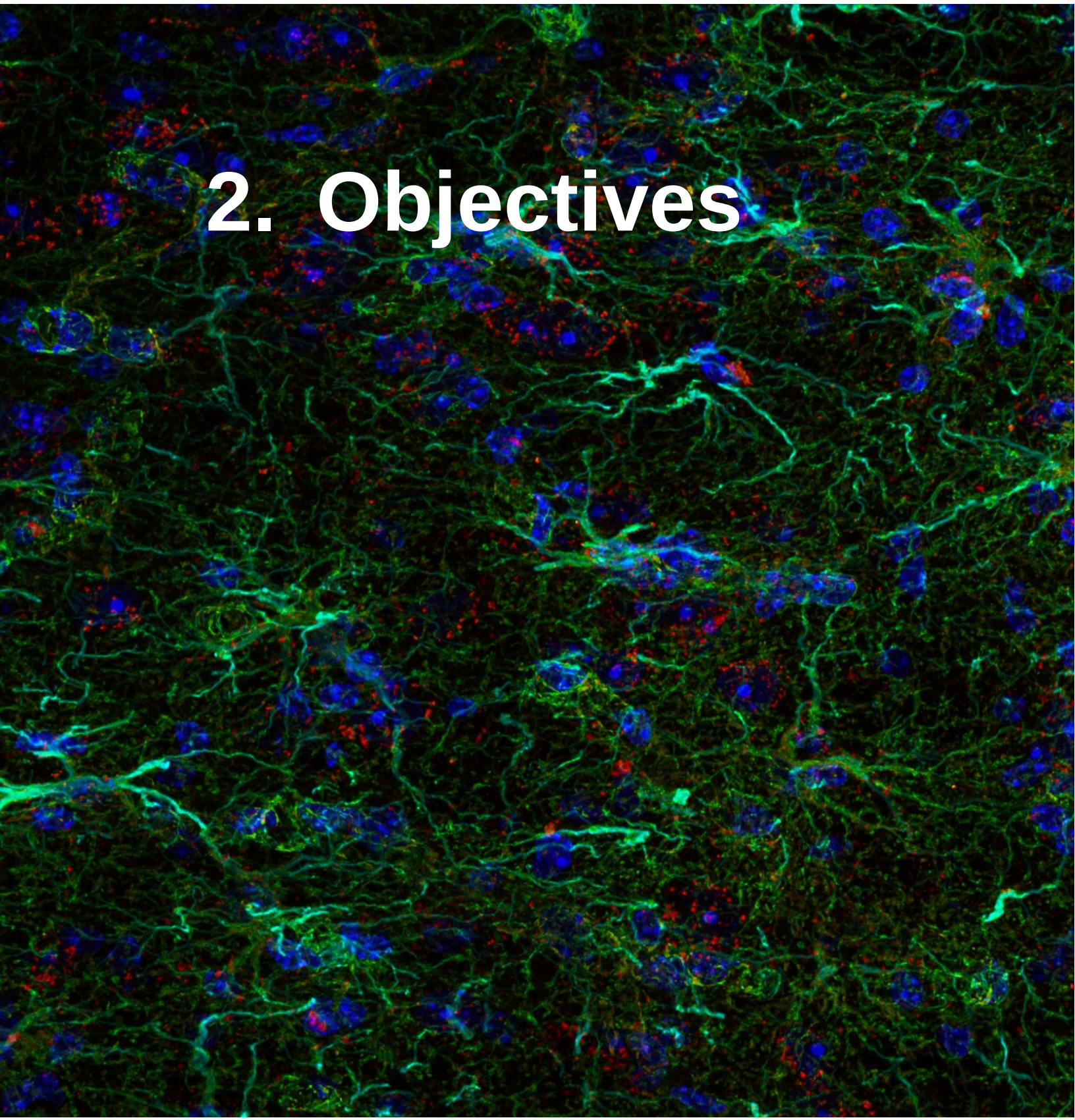

2. Objectives

2. Objectives

Previous data from our laboratory has demonstrated that mitophagy is essential for retinal ganglion cells (RGCs) development at E15.5 as animals deficient in mitophagy have alterations in neurogenesis. The main objective of this Doctoral Thesis is to further expand upon those findings and try to understand the role of mitophagy during retinal development from early embryonic stages to adult using recently developed animal models that allows mitophagy determination *in vivo*.

Mitochondrial alterations are present in many neurodegenerative diseases such as Parkinson's disease but whether mitochondrial dysfunction is due to altered mitophagy is currently unknown. In the second part of this research we will use mitophagy reporter cells and animals to determine mitophagy in several models of Parkinson's disease.

Our main aims are:

1.1. Determine the levels of basal mitophagy during retinal development using mitophagy reporters in mice and zebrafish.

1.2. Manipulate mitophagy pathways pharmacologically throughout retinal development using new and known mitophagy regulators to determine whether mitophagy can be upregulated or inhibited at different developmental stages.

1.3. Unravelling whether mitophagy is altered in Parkinson's disease models.

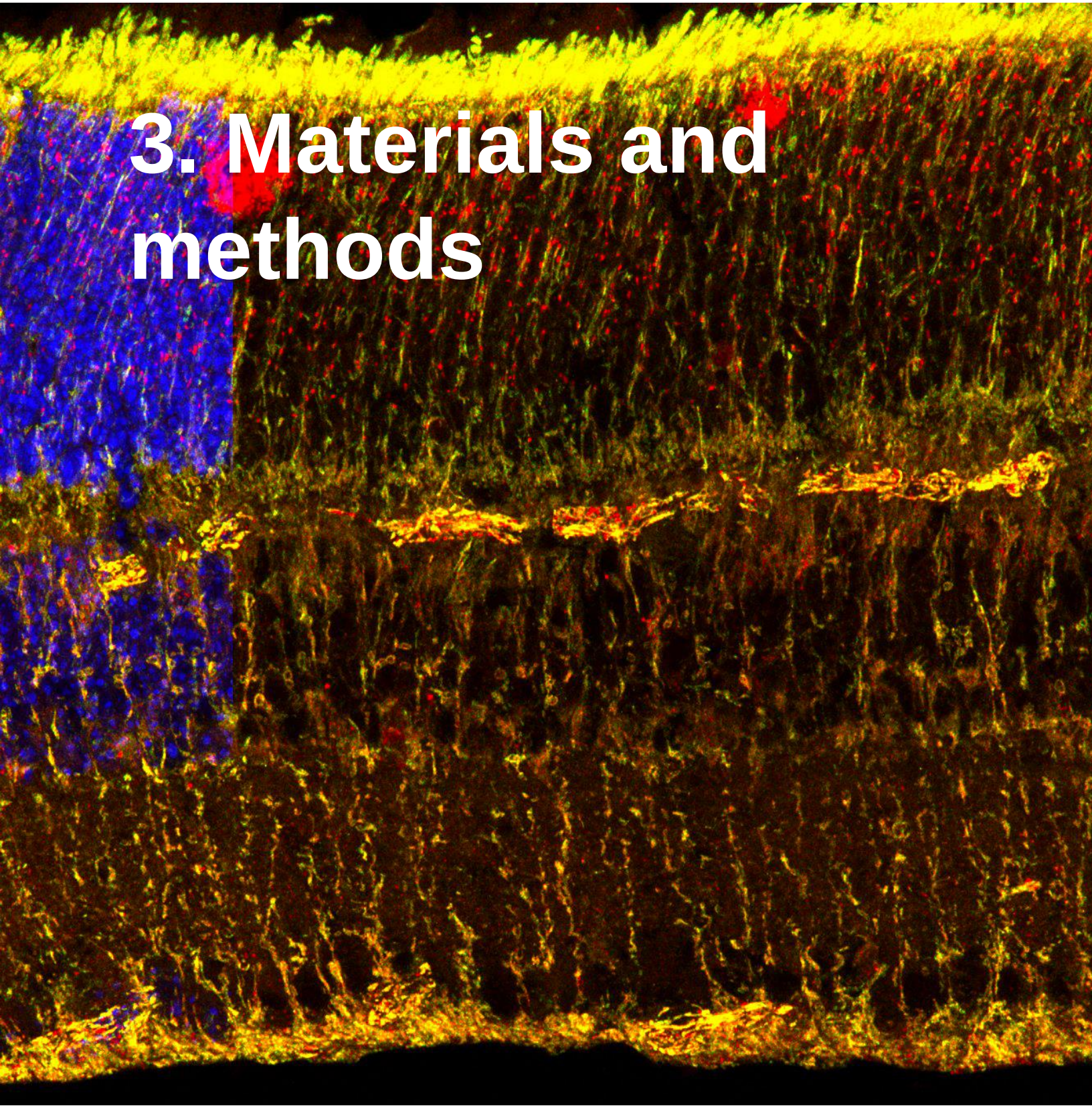

3. Materials and methods

3. Materials and methods

3.1. Animal Procedures

3.1.1. Ethics and Welfare of Laboratory Animals

All the experimental procedures carried out with animals in this Doctoral Thesis have been approved by the local ethical committees for animal experimentation of the CSIC have been carried out following the current regulations of the European Union, and the ARVO statement for the use of animals in ophthalmic research. For the study of postnatal retinas, males and females have been used indistinctly. The animals were kept in cycles of 12:12 hours of light and darkness, at a temperature of 20 ºC, with food and drink ad libitum. To obtain embryos, the animals were crossed and the morning in which the vaginal plug was detected was considered as embryonic day (E) 0.5. All mice were sacrificed by cervical dislocation and embryos were obtained by caesarean section. The embryos were decapitated and placed in a Petri dish with 1x PBS and, with fine forceps under the magnifying glass, the eyes were isolated or the retinas were dissected, separating them from the pigment epithelium, crystalline, vitreous, vessels and other tissue remains. The isolation of the eyes and the retinas of adult mice was carried out in the same way.

Fish (Mito strains) were held at the zebrafish facility at the Centre for Molecular Medicine Norway (AVD.172) using standard practices. Embryos were incubated in egg water (0.06 g/L salt (Red Sea)) or E3 medium (5 mM NaCl, 0.17 mM KCl, 0.33 mM CaCl2, 0.33 mM MgSO4, equilibrated to pH 7.0). From 12 hpf, 0.003% (w/v) 1-phenyl-2-thiourea (Sigma-Aldrich) was used to inhibit pigmentation. Embryos were held at 28 C in an incubator following collection. All use of animals was approved and registered by the Norwegian Animal Research authority. Experimental procedures followed the recommendations of the Norwegian Regulation on Animal Experimentation (‘‘Forskrift om forsøk med dyr’’ fra 15.jan.1996). All experiments conducted on larvae at 7 dpf were approved by Mattilsynet (FDF Saksnr. 16/153907).

3.1.2. Wildtype C57 and CD1 mice

The wild mice used in this work were of the C57BL / 6J and CD1 lineage from Jackson Mice Laboratories (Bar Harbor, ME, USA). These mouse strains were kept in the CIB (CSIC) animal facility.

3.1.3. MitoQC reporter mice

Experiments were performed on MitoQC (mCherry-GFP-Fis1101−152) reporter mice. The MitoQC animals were kindly provided by Dr Ian Ganley (School of Life Sciences, The University of Dundee, Dundee, Scotland). Animals were housed, cared and euthanized in accordance with the European guidelines and experiments were approved by the CIB ethics committee for animal experimentation and the Comunidad de Madrid, codes PROEX 232/17 (approval date 28.1.2018) and PROEX226/16 (approval date 22.9.2016). Briefly, the mice have an introduced CAG promoter cassette with the open reading frame for the mCherry-GFP-FIS1 fusion protein including a Kozak sequence (GCCACC) into the mouse Rosa26 locus in mice with a C57BL/6 background. Genotyping was performed by diagnostic end-point PCR using genomic DNA isolated from tissue biopsy specimens with the following sets of forward and reverse primers: set 1, 50 -CAAAGACCCCAACGAGAAGC-30 and 50 -CCCAAGGCAC ACAAAAAACC-30; and set 2, 50 -CTCTTCCCTCGTGATCTGCAACTCC-30 and 50 -CATGTCTTTA ATCTACCTCGATGG-30.

3.1.4. Zebrafish

Tandem-tag transgenic Mito fish generation and imaging the pME-EGFP no stop vector from the Tol2 kit was cut with NCoI restriction enzyme and then dephosphorylated with calf intestinal phosphatase. This was later phosphorylated with T4 polynucleotide kinase and annealed with mitochondrial localization signal (MLS) of zebrafish COXVIII (Kim et al., 2008). The oligo sequences used for annealing were forward primer (5'cATGTCTGGACTTCTGAGGGGACTAGCTCGCGTCCGCGCCGCTCCGGTTCTGC GGGGATCCACGATCACCCAGCGAGCCAACCTCGTTACGCGAgc3') and reverse primer (5'catggcTCGCGTAACGAGGTTGGCTCGCTGGGTGATCGTGGATCCCCGCAGAACC GGAGCGGCGCGGACGCGAGCTAGTCCCCTCAGAAGTCCAGA3'). Gibson assembly

was used to generate pTol2-CMV-MLS-EGFP-Cherry with linearized pTol2mini and PCR products from the following primers: CMVFw (5'ctgatgcccagtttaatttaaatagatctggccatCGATGTACGGGCCAGATATAC3'), CMVRev (5'cctcagaagtccagacatCCTATAGTGAGTCGTATTAATTTCG3'), MLSGFPFw (5'aatacgactcactataggATGTCTGGACTTCTGAGGG3'), MLSGFPRev (5'ctcctcgcccttgctcacCCTTGAATTCCCAGATCTTC3'), mCherryFw (5'agatctgggaattcaaggGTGAGCAAGGGCGAGGAG3') and mCherryRev (5'aactagagattcttgtttaagcttgatatccatggACGCCTTAAGATACATTGATGAGTTTG3'). Templates for PCR were used from Tol2 Kit. The MLS-EGFP-mCherry was subcloned into iTol2 vector using XhoI and AgeI. 35 pg (final concentration) of iTol2 MLS-EGFP-mCherry vector and 50 pg (final concentration) of in-vitro transcribed transposase mRNA (*in vitro* transcribed from linearized pCS2FA-transposase vector from the Tol2 kit) was injected into the 1 cell stage of control (WT). Injected embryos were raised to adulthood (F0) and out-crossed to wild-type fish to identify transgenic founders. Control (WT) tandem-tagged Mito fish transgenic founders were incrossed respectively. Resulting respective larvae 37 (F1) were fixed in 4% PFA (pH 7.2) overnight at 3dpf and co-stained with 50ug Hoechst reagent for 3-4 h at room temperature. Each larva was mounted on depression slides using low melting point agarose. Confocal images were obtained using an Apochromat 40x/1.2 WC or 60x/1.2 oil DIC objective on an LSM 780 microscope (Zeiss). Red and yellow dots were counted manually for each cell and the ratio of red to yellow dots (per cell) were interpreted as mitophagy.

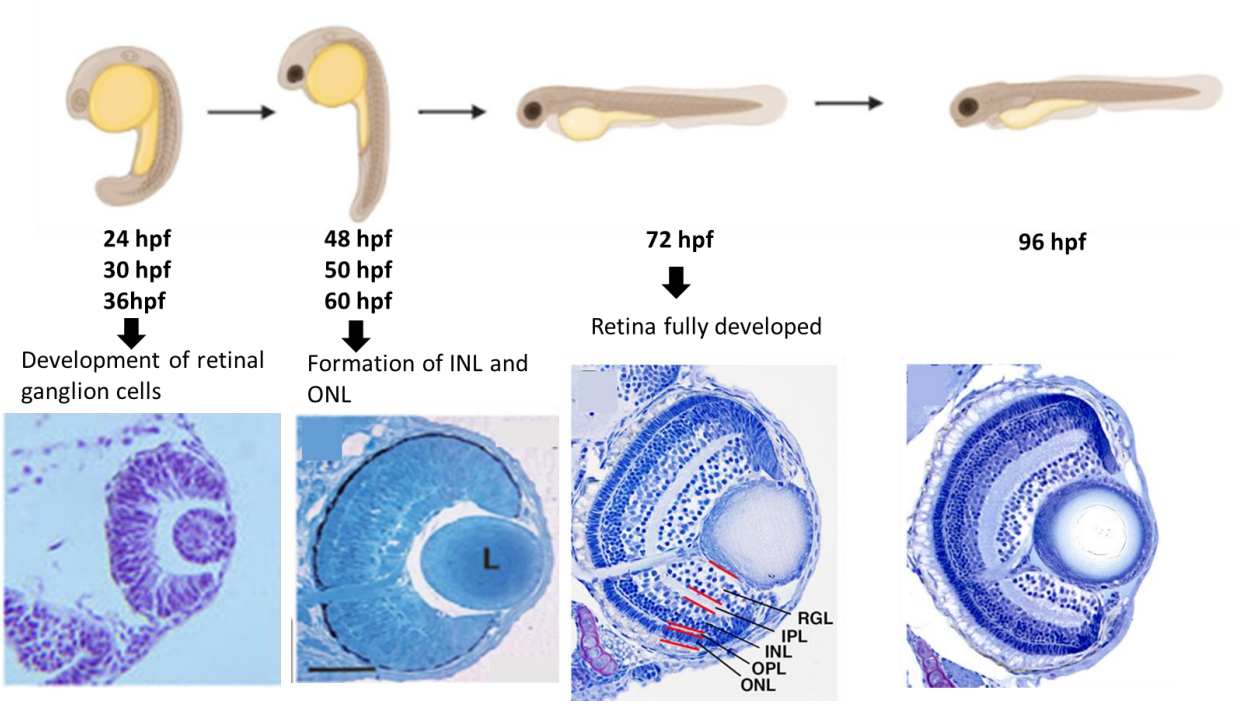

Figure 3.1. Images of cryosections of embryonic zebrafish retinas earlier in neurogenesis. The photos, from left to right, show the embryo at 1-, 2-, 3-, and 4-days post fertilization. In the bottom row, the zebrafish retina is labeled with DAPI and forms several kinds of neuronal cells that assemble into tidy layers. The zebrafish's retinal ganglion cells form a clear channel leaving the eye for their axons to carry messages to the brain. L, lens; RGL, retinal ganglion cell layer; INL, inner nuclear layer; IPL, inner plexiform layer; OPL, outer plexiform layer; ONL, outer nuclear layer.

3.1.5. Surgical procedure for PD model (6-Hydroxidopamine lesion)

A premedication of desipramine (Sigma-Aldrich; D3900-1G, (10 mg/kg/ratón)) was administered to rodents prior to injection of 6-Hydroxydopamine hydrobromide (Sigma-Aldrich; #H116) (6-OHDA) to increase the selectivity and efficacy of 6-OHDA-induced lesions. The noradrenaline / 5HT uptake inhibitor, desipramine decreases 6-OHDA-induced noradrenaline and 5HT depletion. Before the surgical procedure, animals were intraperitoneally anesthetized with ketamine-medetomidine (75 and 0.5 mg/kg, respectively). The scalp was scrubbed with soap, then alcohol then betadine. The head wass placed in a stereotaxic apparatus (Stoelting Co.) for rodents and held in place by ear bars and a nose cone. A midline incision is made on the top of the skull and the skin retracted. The underlying fascia is then pushed away and a hole is drilled through the skull and the skull and dura overlaying the striatum on one side of the brain. A small bur hole is drilled above the injection site using sterile bit. Animals were unilaterally injected

in the right hemisphere with 2 µL of 6-OHDA using a ga 26S/51 mm/pst2 needle Hamilton syringe (Sigma-Aldrich; 28615-u). 6-OHDA was administrated at a rate of 1.0^{-6} L/min at a concentration of 4 µg/µL dissolved in 0.9% NaCl with 0.2 mg/mL of ascorbic acid (A1968; Sigma-Aldrich). The neurotoxin was injected into the striatum (coordinates related to Bregma: AP = +0.4 mm; L = ±2.5 mm, DV = -1.0 mm), according to Paxinos and Watson. After each injection, the needle was raised 2 mm and left there for 2 min to avoid the backflow of the needle tract. During surgery, the eyes of the animals were protected from the light with Vaseline®. After surgery, the surgical region was cleaned with Betadine and sutured with Surgiquick suture. Animals were subcutaneously injected with an antibiotic, analgesic, and anaesthetic antagonist. Then, rats were placed comfortably in a heated cage with food easily available to allow their recovery. Animals were carefully monitored during the following days.

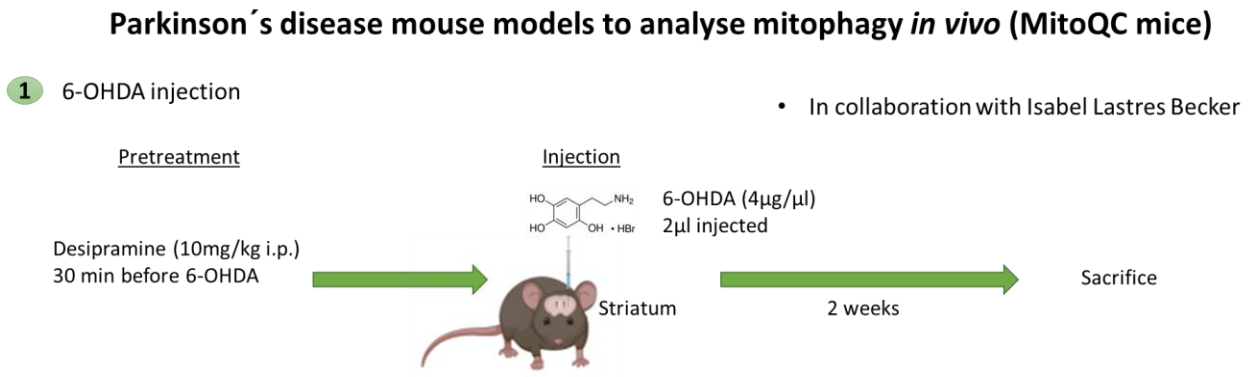

Figure 3.2. Timeline of the experimental design of the Parkinson's disease MitoQC models. Six-month-old MitoQC mice were injected with 6-OHDA. They were sacrificed two weeks following the injection and their brains were fixed and cryopreserved. Following that, the brains were sectioned and the SNpc sections were immunostained.

3.1.6. Whole animal perfusion fixation and brain fixation

After two weeks mice were sacrificed using 150 µL of anaesthesia (1 ml of anaesthesia has 0.5 ml of saline 0,9%, 0.3 ml ketamine, and 0.2 ml xilacine) per mouse. Using the pinch-response method we determined the depth of anaesthesia, since animals must be unresponsive before proceeding with perfusion. An incision was made with a scalpel through the abdomen the length of the diaphragm. Using sharp scissors, we cut through

the connective tissue at the bottom of diaphragm to allow access to rib cage. With large scissors, we cut through ribs just left of the rib cage midline. One center horizontal cut was made through the rib cage to open up thoracic cavity. While holding heart steady with forceps we inserted the needle directly into protrusion of left ventricle to extend straight up about 5 mm. The needle position was secured by clamping in place near the point of entry. Release valve to allow slow, steady flow of around 20 ml/min of 0.9% saline solution. When blood has been cleared from body, we changed to 3.7 % PFA in 200 mM HEPES, pH 7.0 (200-300 ml). Perfusion is almost complete when spontaneous movement (formalin dance) and lightened color of the liver are observed. Then we waited 1 min and finish with the perfusion.

Finally, we excised the brain, placed it in a falcon containing the same fixation (3.7 % PFA in 200 mM HEPES, pH 7.0) and left it to fix overnight at 4 °C. The next day, brains were washed in PBS 1X and put it into sucrose 30% in Phosphate-Buffered Saline (PBS) with 0.01% sodium azide at 4 °C until the brain sinks. After the brains sank, they were sectioned in a microtome (Leica RM2125 RTS) at 30µm thickness and stored in PBS1x + 0.01% sodium azide at 4 °C.

3.2. Cell Culture Techniques

3.2.1. Culture of SH-SY5Y MitoQC and ARPE-19 MitoQC

In-vitro experiments were conducted in either human neuroblastoma SH-SY5Y MitoQC or human RPE ARPE-19 MitoQC cells following American Type Culture collection (ATCC) guidance. Both cell types were generously provided by provided by Dr Ian Ganley (School of Life Sciences, The University of Dundee, Dundee, Scotland). Cells were cultured in 1:1 DMEM: F-12 media (Thermo Scientific; #12634010) supplemented with 10 % (v/v) FBS (Sigma; #F7524), 2 mM l-glutamine (Thermo Scientific; #25030-024), 100 U/ml penicillin, 0.1 mg/ml streptomycin (Thermo Scientific; #15140-122) and were incubated at 37 °C with 5 %. Cells where cultured with 800 µg/mL Hygromycin B (10,453,982, Gibco, Carlsbad, CA, USA) to select only those cells expressing the MitoQC reporter.

3.2.2. Primary astrocyte culture

Newborn mice aged 0–3 days are quickly decapitated, and the prefrontal cortex is taken to a petri plate containing a cold solution of PBS1X+1 % P/S. We checked to see whether

the mice had milk in their stomachs before beginning the culture. We gently removed the cortical meninges under the stereoscope and placed them in a sterile falcon tube with 3 mL of DMEM with 20% or 15% FBS and 1% P/S, ensuring sure the solution was warm. After removing the meninges from the cortex, we gently pressed the tissue with a syringe fitted with a steel cannula under the laminar flow hood. We centrifuged the solution for 15 minutes at 200 g after we had disturbed all of the tissue and ensured there were no agglomerates. After that, we discarded the supernatant and resuspended the cell pellet in 5 mL of fresh medium (DMEM with 20% or 15% FBS and 1% P/S) by pushing the plunger three times up and down to disrupt all the tissue again. The single-cell suspensions were then plated in T-flasks (4 hemispheres/75 cm^2) in DMEM media supplemented with 20% or 15% (v/v) FBS and 1% P/S. Cells were kept at 37 °C in a humidified environment of 7% CO2. The culture media was entirely replaced by the new medium after two days. After one week in culture, when the cells had reached confluence, the cells were divided using a dilution of 12 or 13. The culture's medium was changed twice a week.

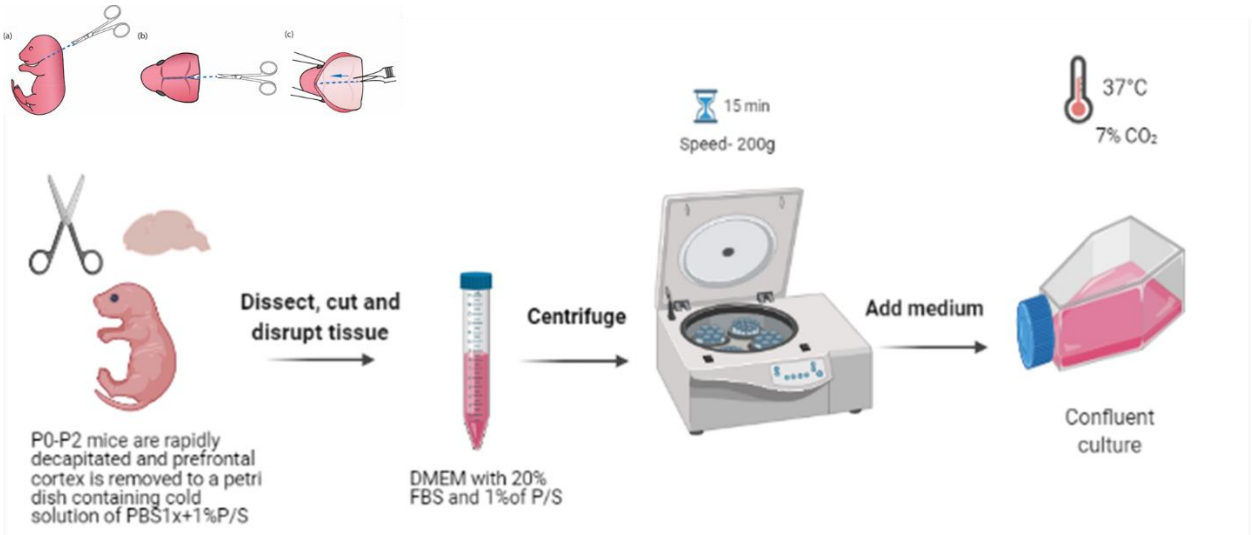

Figure 3.3. Experimental design of the primary astrocyte MitoQC culture. The prefrontal cortex of newborn mice aged 0–3 days is promptly severed and transferred to a petri dish containing a cold solution of PBS1x+1 percent P/S. Extracted the cortical meninges and put them in a sterile falcon tube with 3mL of DMEM containing 20% or 15% FBS and 1% P/S. After dislodging breaking up all tissue and ensuring there were no agglomerates, we centrifuged the solution for 15 minutes at 200g. After that, discard the supernatant and resuspended the cell pellet in 5 mL of new medium (DMEM with 20% or 15% FBS and 1% P/S). Afterwards, the single-cell suspensions were plated in T-flasks (4 hemispheres/75 cm^2) in DMEM medium supplemented with 20% or 15% (v/v) FBS and 1% P/S. Cells were incubated at 37 °C in a humidified 7 percent CO_2 atmosphere. After two days, the new medium had completely supplanted the cultural media.

3.2.3 Cell Culture Treatments

Cells were seeded in 24-well plates at a density of 1.0×10^5 cells/mL. After 24 h of adherent growth, cells were treated for 24 h with different concentrations of 6-OHDA (Sigma-Aldrich; #H116). 6-Hydroxydopamine hydrobromide (6-OHDA; Sigma-Aldrich; #H116) was used as a model treatment for Parkinson's disease.

Iron chelation induced mitophagy with Deferiprone (DFP) (Sigma; #379409) was achieved by treating cells with 1 mM DFP for 24 hours. DFP was dissolved in water before use with a pulse of heat (90 °C), for 1 hour.

Mitophagy inducer carbonyl cyanide m-chlorophenyl hydrazone (CCCP) was also used. Briefly, cells were incubated for 24 h with 25 µM CCCP.

After the treatments cells were fixed with 3.7 % Paraformaldehyde (Electron Microscopy Sciences; #15710) in 200 mM HEPES (Thermo Fisher Scientific; #10453982), pH 7.0 for 20 minutes at room temperature. After two washes with PBS 1X, coverslips were incubated with 1µg/mL of 1, 4-diamino-2-phenylindole (DAPI) for 30 min, washed three times with PBS 1X and mounted onto glass slides with ProLong Diamond Antifade Mountant (Thermo Fisher Scientific; #P36961).

3.2.4. Pharmacological modulation of mitophagy *ex vivo*

Animals were euthanized by cervical dislocation and embryos removed by caesarean section. The embryos were staged and then placed in a Petri dish in 1× phosphate-buffered saline (PBS). Eyes were removed under a dissecting microscope and were processed by immersion fixation in freshly prepared 3.7% formaldehyde (Sigma-Aldrich, P6148) at pH 7.0 in 0.2 M HEPES. For cryosectioning, eyes were cryoprotected in 30% (w:v) sucrose (VWR Chemicals, 27480.360) in PBS at 4°C before sectioning on a cryostat. Vectashield (Vector Laboratories, H-1000) was used to mount tissue sections on slides before sealing with nail polish and a 1.5 glass coverslip. Images were acquired using a Leica TCS SP8 Confocal Laser Scanning Microscope and ×63 objective.

Embryonic eyes or retinas were cultured for 6 h in DMEM: HAM/F12 (42400, Gibco) supplemented with 10 mM sodium bicarbonate (S7561), 1.1 mg/l pyruvate

(P2256), 100 mg/l apotransferrin (T2252), 0.02 mg/ml sodium selenite (S5261), 0.32 mg/l putrescine (P5780), 0.2 mg/l progesterone (P8783), all from Sigma, and 0.05 g/l gentamicin (15710, Gibco), and pH set to 7.14. Before conducting experiments, the medium was supplemented with 2 mM glutamine (25030, Gibco) and 10 nM recombinant human insulin (I2643, Sigma). The eyes were treated by adding the following compounds to the medium, as indicated:

25 µm CCCP (C2750-100 mg, Sigma), 10 mM 3-methyladenine (3-MA; M9281, Sigma), 200 nM rapamycin (R-5000, Euromedex), 5 µM CsA (30024, Sigma), 1 mM DFP (379409, Sigma), 70 mM hydroxychloroquine (HCQ; 880872.4, Laboratorios Rubió S.A.), 50 nM bafilomycin A (B1793-10ug, Sigma), 25 µm VP07 (Maestro et al., 2021), 25 µm IGS2.7 (Ana Martinez Gil; Ankar Pharma), 25 µm JAR1.39 (Maestro et al., 2021).

Table 3.1. List of reagents used in the pharmacological modulation of autophagy.

Compounds	Comercial House	Reference	Concentration	Function
CCCP	Sigma	C2750	10 µm	Mitophagy inducer
DFP	Sigma	379409	1 mM	Mitophagy inducer
Rapamycin (Rapa)	Euromedex	R-5000	200 nM	mTOR inhibitor
Hydroxychloroquine (HCQ)	Laboratorios Rubió	880872.4	30 µg/mL	Lysosomal degradation inhibitor
Cyclosporine A (CsA)	Sigma	30024	5 µM	Mitophagy inhibitor
3-methyladenine (3-MA)	Sigma	M9281	10 mM	PI3K inhibitor
Bafilomycin A1	Sigma	B1793	50 nM	V-ATPase inhibitor
VP07	Ankar Pharma		25 µm	Mitophagy inducer
JAR1.39	Ankar Pharma		25 µm	Mitophagy inducer
IGS 2.7	Ankar Pharma		25 µm	Mitophagy inhibitor

After culturing, the neural retina was mounted under the magnifying glass on a 0.44 µm pore nitrocellulose membrane (Sartorius). The retinas were placed with the ganglion cell layer facing upwards, adhering to the nitrocellulose with the help of fine dissecting forceps. They were subsequently fixed with 3.7 % PFA in 200 mM HEPES, pH 7.0 at least 1 hour at RT in 24-well plates. Finally, they were washed with 1x PBS and kept in 1x PBS with 0.001% sodium azide at 4 ° C until the time of immunofluorescence processing. The whole eye cultures were fixed in 3.7 % PFA in 200 mM HEPES, pH 7.0 for 1 hour at RT and were then washed with 0.1M PBS. Afterward the eyes were immersed in 15% sucrose in PBS with 0.01% sodium azide until they sank. Finally, the

eyes soaked in 30% sucrose in PBS with 0.01% sodium azide prior to embedding them in OCT media.

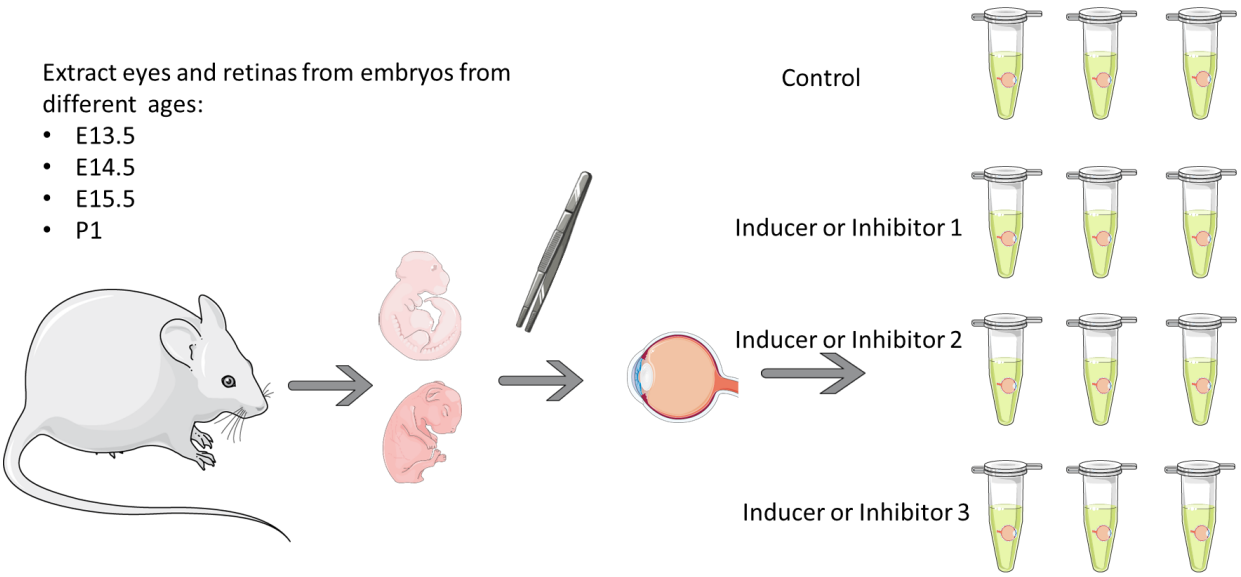

Inducers	Inhibitors	New Compounds
DFP 1 mM	3-MA 10 mM	VP07 25 µM
CCCP 25 µM	HcQ 70 mM	JAR1.39 25 µM
Rapamycin 200 nM	CsA 5 µM	IGS2.7 25 µM
	Bafilomycin 50 nM	

Figure 3.4. Experimental design of the pharmacological modulation of mitophagy *ex vivo* in retinal development. Embryonic eyes (E13.5- E15.5) were treated ex-vivo to check whether mitophagy could be manipulated using different autophagy inducers and inhibitors. The eyes were cultured for 6 h in embryonic culture media. The following compounds were added to the medium to test our theory: 25µm Carbonyl cyanide m-chlorophenylhydrazone (CCCP), 10 mM 3-methyladenine (3-MA), 200 nM rapamycin, 5 µM CsA, 1 mM deferiprone (DFP), 70 mM hydroxychloroquine (HCQ), 50 nM bafilomycin A.

3.2.5. Plasmid DNA transfection

Stable transfected SH-SY5Y MitoQC cells were generated with Lipofectamine 3000 (Invitrogen) using the following constructs: α-syn-WT-EGFP (Addgene; 40822) and α-syn-A53T-EGFP (Addgene; 40823), pHM6- α-synuclein -WT (Addgene; 40824) and pHM6- α-synuclein-A53T (Addgene; 40825) and pHM6 empty vector (Roche).

The day before the transfection 300 000 cells were seeded in a 6 well- plate and were cultured in medium without antibiotics. After reaching 70–90% confluency the cells were transfected by adding 250 µL of DNA-lipid complex (2500 ng DNA, 7.5 µL

Lipofectamine™ 3000 Reagent, 5 µL P3000™ Reagent) per well. Cells were incubated for 2 days at 37°C without changing the media. Finally, cells were fixed with 3.7 % PFA in 200 mM HEPES, pH 7.0 for 20 min at room temperature.

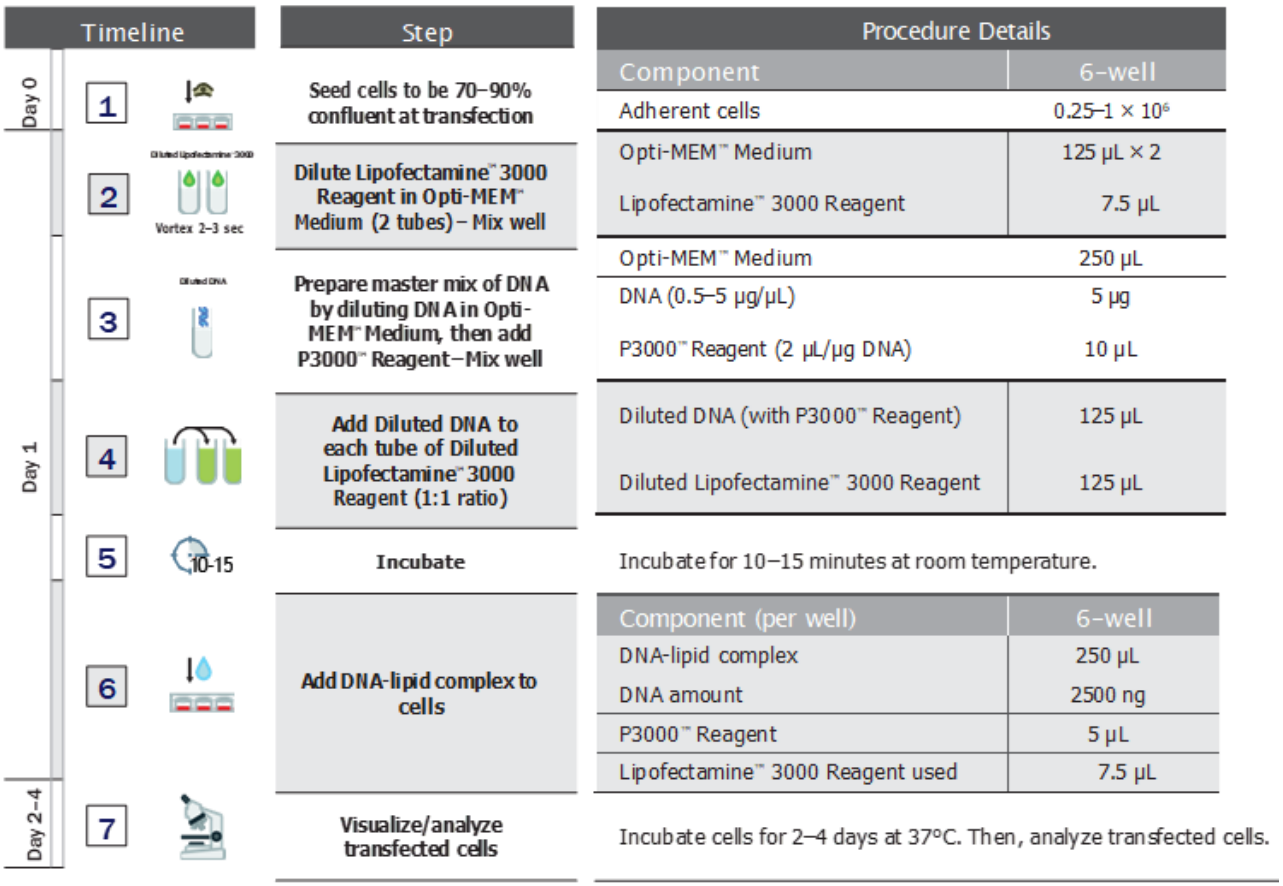

Figure 3.5. Lipofectamine™ 3000 Reagent Protocol. Cells were transfected according to the following table. Using the indicated volume of DNA and P3000™ Reagent with Lipofectamine™ 3000. Each reaction mix volume is for one well and accounts for pipetting variations (modified from thermofisher.com/support).

3.3. Immunofluorescence methods

3.3.1 Cryosections of the embryonic mouse eye

The eyes of embryos *in vivo* or after 6 h culture were fixed for at least 1 hour in 3.7 % PFA in 200 mM HEPES, pH 7.0, washed 3 times with 1x PBS and were embedded in a 15% sucrose solution in 1x PBS (w / v) for at least 12 hours. Subsequently, they were transferred to a 30% sucrose solution in 1x PBS (p / v), where they were kept for a week for their correct cryoprotection and preserved at -80 ºC until use. After that, the eyes were

soaked in OCT (Tissue Tek, Sakura Finetek), inside the lid of a 1.5 mL eppendorf tube. 15 µm sections were made on these samples in a Leica CM 1950 cryostat on treated slides (Superfrost® Plus, Thermo Scientific). The slides were kept at room temperature ON to favour the adhesion of the specimens. After that, they were permeabilized by treating them with 0.5% TritonX for 30 minutes and blocked with BGT for 1 hour, before incubation with the primary and secondary antibodies as described before.

3.3.2. Preparation of zebrafish cryosections

Control tandem-tagged Mito fish transgenic larvae were fixed in 3.7 % PFA for 1 hour at 24 hpf, 30 hpf, 36 hpf, 42 hpf, 50 hpf, 60 hpf, 72 hpf, 96 hpf and 120 hpf, respectively. After a couple of washes with 1X PBS, they were gradually cryopreserved in 15% and subsequently 30% sucrose. After that, the larvae were put in OCT (Tissue Tek, Sakura Finetek), inside the Tissue-Tek® Cryomold® Intermediate, (15 x 15 x 5mm). 16 µm sections were made on these samples in a Leica CM 1950 cryostat on treated slides (Superfrost® Plus, Thermo Scientific). The slides were kept at room temperature ON to favour the adhesion of the specimens.

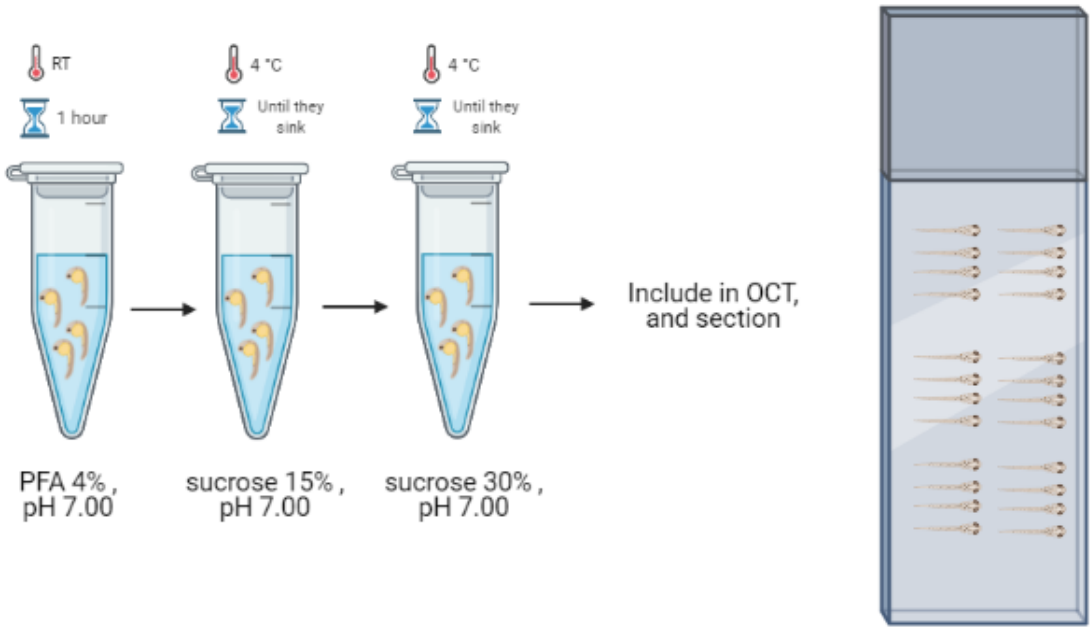

Figure 3.6. Experimental design for cryosections of embryonic zebrafish earlier in neurogenesis. The zebrafish were initially fixed in 4% PFA, then cryopreserved in 15% and 30% sucrose, in that order. The fish were then frozen after being embedded in OCT. Finally, the OCT blocks were sectioned in a cryostat.

3.3.3. Immunofluorescence staining of cell cultures

The immunostaining of SH-SY5Y MitoQC reporter cells with α-synuclein: cells were washed twice with PBS 1X for 5 minutes. Afterwards they were permeabilized with BGT solution (3 mg / mL BSA, 10 mM glycine and 0.25% Triton X-100 in PBS) for 10 min at room temperature. Following permeabilization, coverslips were washed two times with PBS 1X. The α-synuclein primary antibody (Santa Cruz; sc-12767) was diluted at 1:500 in BGT solution, and cells were incubated for 1 hour at room temperature. Then, coverslips were washed with 1 % BSA/PBS four times of 10 min each. The secondary anti-mouse Alexa Fluor 647 nm antibody (Thermo Scientific; #A21236) was incubated at 1:200 in BGT solution for 30 min in the dark at room temperature. Coverslips were washed again four times with PBS1X for 10 min each. At the end cells were then stained with 1µg/mL of 1, 4-diamino-2-phenylindole (DAPI) and mounted on glass slides as described above.

Images with the MitoQC reporter to quantify mitophagy were acquired using a Leica SP8 laser scanning confocal microscope (HC PL APO 63x/1.40 oil CS2). All the images were processed with FIJI v1.52n software (ImageJ, NIH).

3.3.4. Immunofluorescence of embryonic retina

For the detection of nuclear epitopes such as the transcription factor Brn3a, the retinas were treated with citrate buffer at pH 6 for 5 minutes in the microwave, after which it was washed 3 times with 1x PBS. Next, permeabilization was carried out on the flat-mounted retinas, incubating them with Triton 0.5% (w / v) X-100 in 1x PBS (3 times, 15 minutes each time). Triton X-100 traces were removed by washing well with PBS and subsequently incubated with the blocking solution (3 mg / mL BSA, 10 mM glycine and 0.25% Triton X-100 in PBS) for 30 minutes in a humid chamber. The retinas were then incubated with the primary antibodies in a humid chamber at 4 ° C overnight in the blocking solution. Incubation with the corresponding secondary anti-mouse or rabbit antibodies conjugated with Alexa 568 or 647 (1:200, Invitrogen) was carried out for 1 hour at room temperature, in a humid chamber and in the dark, also in blocking solution (BGT). After the corresponding washes with PBS, the retinas were incubated in 1µg / mL of 1, 4-

diamino-2-phenylindole (DAPI) (1:1000) in BGT, to label the nuclei. Vectashield (Vector Laboratories, H-1000) was used to mount tissue sections on slides before sealing with nail polish and a 1.5 glass coverslip.

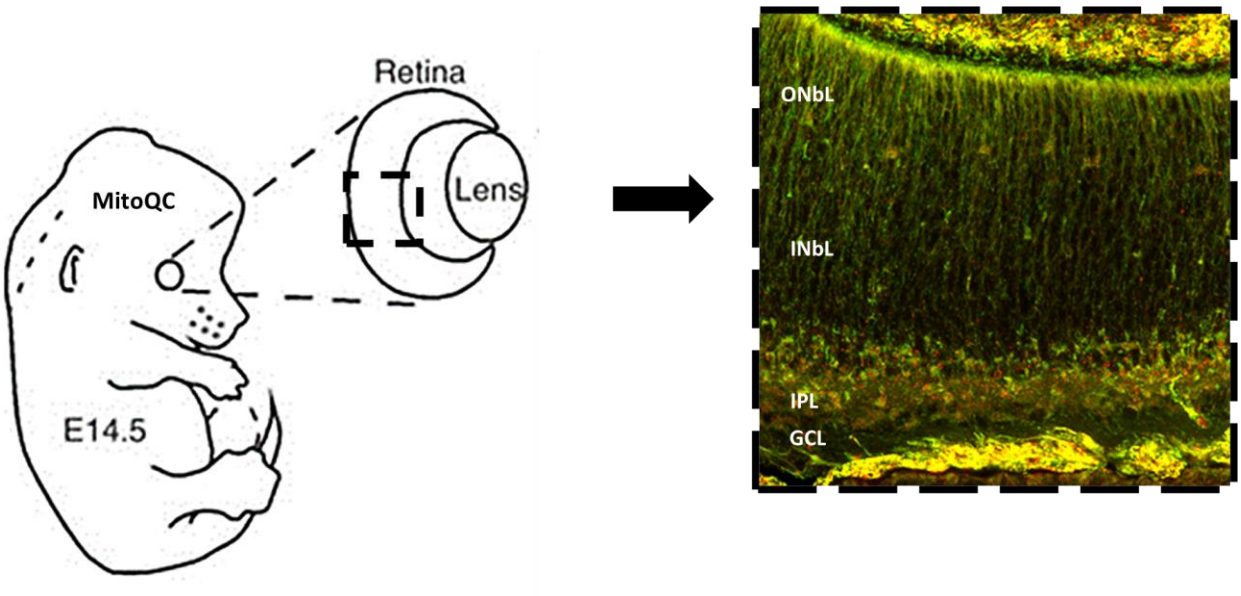

Figure 3.7. Experimental design. Extract the eyes of MitoQC mice during different developmental stages (E13.5 –P15). Eyes were extracted under a dissecting microscope and were processed by immersion fixation in freshly prepared 3.7% formaldehyde at pH 7.0 in 0.2 M HEPES. For cryosectioning, eyes were cryoprotected in 30% sucrose in PBS at 4°C before sectioning on a cryostat. Vectashield was used to mount tissue sections on slides. Images were acquired using a Leica TCS SP5 Confocal Laser Scanning Microscope and ×63 objective. GCL, ganglion cell layer; IPL, inner plexiform layer; ONbL, outer neuroblast layer; INbL, inner neuroblast layer.

3.3.5. Free-floating brain sections immunohistochemistry

The day of the immunohistochemistry, brains were washed three times for 10 minutes at RT in 0.1M PBS with gentle agitation. Afterwards, sections were permeabilized in 0.3% Triton for 30 minutes followed by three washing steps with 0.1M PBS. Then, sections were blocked in BGT solution (3 mg / mL BSA, 10 mM glycine and 0.25% Triton X-100 in PBS) for an hour with gentle agitation. Primary antibody (diluted in BGT solution) was added and incubated for 48 hours at 4°C with gentle agitation, 300 µL per well. After two days, sections were washed (3 x 5 min) in 0.1M PBS. Finally, sections were incubated in secondary antibody 1:200 and DAPI 1:1000 (diluted in BGT solution) for 2 hours at room temperature, 300 µL per well. Sections were washed three times for 5 min in 0.1M PBS.

At the end, we mounted the sections on coverslips using Prolong, letting them air-dry for 24 h at RT in dark. Images were acquired using a Leica TCS SP8 Confocal Laser Scanning Microscope and ×63 objective.

Table 3.2. List of antibodies used in the immunofluorescence technique of PD model brains.

Antibody	Comercial House	Reference	Host species	Target
TH	Milipore	P0878	Rabbit	Dopaminergic neurons
GFAP	Dako	Z0334	Rabbit	Astrocytes
Iba-1	Wako	019-19741	Rabbit	Microglia
α-syn	Santa Cruz	sc-12767	Mouse	α-synuclein

3.3.6. Image acquisition and quantification

Images of both retinas and cells were acquired in the Leica SP8 microscope (Leica Microsystems GmbH) of the Center for Biological Research Margarita Salas (CIB). All the photos shown in this doctoral thesis correspond to the maximum projection of the total thickness of the retina or to sections obtained from the total of 1 µm, in the case of cryosections of the eye, and 2 µm, in the case of mounted retinas. The quantification of the images was carried out with the program ImageJ 1.44 p. using the one of three plugins created by ‘’Ignacio Ramírez Pardo”, it was applied section by section, never in the maximum projection. The three applied plugins were: one specific for flat-mounted retinas, another specific for cryosections and another for cells. The plugins are based on a colocalization measurement (GFP-mCherry) and on a measurement of the population of mCherry (Mitophagy), selecting the populations with the different active fluorophores using the ScatterPlot tool.

3.4 Cell viability and cell death determinations

3.4.1. Crystal Violet Staining and Quantification

The crystal violet staining assay was used to analyse cell viability. Briefly, after compound incubation of cells in 96-well plates, the medium was discarded, and cells were washed once with PBS and fixed with 4% PFA. Cells were incubated with 50 µL of crystal violet staining solution (Sigma; #C3886; 0.5% crystal violet in 80% water and 20% methanol) and rocked gently for 30 min. The staining solution was removed, and cells were washed thoroughly with distilled water. Stained cells were left to dry for ≥4 h on the laboratory

bench or within the chemical hood. The crystal violet staining solution was eluted by the addition of 100 µL of 10% acetic acid (Merck; #1.00063.1000) for 30 min with gentle rocking. Plates were sealed with parafilm to mitigate evaporation. Absorbances were read and quantified in the colorimetric reader (VarioSkan;377) Absorbance was measured at 590 nm and values were averaged between replicate measurements.

3.4.2. Measurement of cell death by TUNEL reaction

Detection was carried out by different methods, such as active caspase 3 immunofluorescence, TUNEL reaction. In addition, DAPI staining allowed corroborating and differentiating the condensed nuclei typical of the apoptotic process.

In the TUNEL technique (TdT-mediated dUTP Nick End Labelling), the enzyme terminal transferase (TdT) adds nucleotides (dUTP) labelled with fluorescein to the free 3'OH ends of the DNA, which allows to detect the fragmentation of the DNA that is produced during programmed cell death. The TUNEL kit used was DeadEnd ™ Fluorometric TUNEL System (Promega, G3250). The TUNEL reaction was always carried out in combination with immunofluorescence for the detection of proteins, so the processing of the retinas was the same as in section 5, applying the reaction after incubation with the primary antibodies after washing with 1x PBS to eliminate the antibody residues. Previously, an incubation was carried out with the kit solution for 30 minutes at room temperature. The reaction mixture was prepared according to the manufacturer's instructions: 88% TUNEL buffer, 9.8% FITC-labelled dNTPs and 1.9% TdT and applied for 1 hour at 37 ° C in the dark. Subsequently, the reaction was stopped with the SSC solution for 10 minutes at room temperature, after which the retinas were washed with 1x PBS and incubation proceeded with the secondary antibodies.

Table 3.3. List of reagents used in the TUNEL technique.

Reagent	Concentration
TUNEL buffer	88%
dNTPs with FITC	9.80%
Terminal Deoxynucleotidyl Transferase (TdT)	1.90%

3.5. Reverse transcription PCR (RT-PCR) and Quantitative PCR (qPCR)

Gene expression analysis in the SNpC of the injected and control brains was carried out by qRT-PCR study. RNA extraction was carried out using the Trizol © reagent (Fisher, 15596-018). The samples analysed were the following: five samples of control SNpC (α-SYN #3.SN-L, α-SYN #4.SN-L, α-SYN #5.SN-L, α-SYN #14.SN-L, α-SYN #15.SN-L), five samples of AAV9-h-α-SYN-A53T injected (α-SYN #3.SN-R, α-SYN #4.SN-R , α-SYN #5.SN-R , α-SYN #14.SN-R, α-SYN #15.SN-R), four samples of control SNpC (6-OHDA #2.SN-L, 6-OHDA #3.SN-L, 6-OHDA #4.SN-L, 6-OHDA #12.SN-L) and four samples of 6-OHDA injected SNpC (6-OHDA #2.SN-R, 6-OHDA #3.SN-R, 6-OHDA #4.SN-R, 6-OHDA #12.SN-R).

The mRNA reverse transcription (RT) reaction was carried out from 1 µg of total RNA using the High-Capacity cDNA Reverse Transcription Kit (Applied Biosystems, Waltham, MA, USA) in a total volume of 13.2 µL, according to the manufacturer's instructions. 6.8 µL of the mixture of the following kit reagents were added to each RT reaction: 2 µL of 10x buffer, 2 µL of 10x Random Primers, 0.8 µL of 25x dNTP Mix (100mM), 1 µL MultiScribe® Reverse Transcriptase (50 U / µL) and 1 µL of RNAse inhibitor (20 U / µL). The mixture was pipetted well, and the reaction was carried out in a thermal cycler with the following schedule: 25 ° C for 10 minutes, 37 ° C for 120 minutes, 85 ° C for 5 minutes, and 4 ° C as a final step.

The real-time PCR reaction was carried out in the Light Cycler® 480 Instrument thermal cycler (Roche, Mannheim, Germany) using Taq polymerase (Taqman Universal PCR Master Mix (Life Technologies, Carlsbad, CA, USA)). The amplification of L2A was used in the Universal Human Probe Roche library (Roche Diagnostics). The assays were performed in duplicates and the results were normalized to the expression of 18S RNA levels. The results were expressed using the ΔΔCT (cycle threshold) quantification method.

Table 3.4. List of probes and references used for qRT-PCR.

Gene	Species	Crossreact	Ref Taqman	Role	Name
18S	Mouse	Human	Hs99999901_s1	reference	BCL2/adenovirus E1B interacting protein 3
Mfn2	Mouse	Human	Mm00500120_m1	mitocondrial fusion	mitofusin 2
Ppargc1a	Mouse	Human	Mm01208835_m1	mitocondrial biogenesis	peroxisome proliferative activated receptor, gamma, coactivator 1 alpha
Bnip3	Human		Hs00969291_m1	autophagy/mitophagy	BCL2/adenovirus E1B interacting protein 3
Bnip3l	Human		Hs00188949_m1	autophagy/mitophagy	BCL2 interacting protein 3 like
COX IV	Human		Hs00971639_m1	mitochondria	cytochrome c oxidase subunit 4I1
Lamp1	Human		Hs00931467_g1	autophagy	lysosomal associated membrane protein 1
TH	Mouse	Human	Mm00447557_m1	dopaminergic neurons	Tyrosine hydroxylase
Park2	Human		Hs01038318_m1	autophagy	parkin RBR E3 ubiquitin protein ligase
Tfam	Human		Hs00273372_s1	autophagy	transcription factor A, mitochondrial
α-synuclein	Human		Hs00240906_m1	neuronal protein	Alpha-Synuclein
TOMM40	Human		Hs06627834_g1	mitochondria	translocase of outer mitochondrial membrane 40
Tfeb	Human		Hs00292981_m1	mitocondrial biogenesis	transcription factor EB
Pink1	Human		Hs00260868_m1	mitophagy	PTEN-induced kinase 1
DNM1L	Mouse	Human	Mm01342903_m1	mitophagy (fision)	dynamin 1-like

3.6. Statistical and data analysis

Descriptive and analytical statistics were generated in Prism 7.0 (GraphPad Software). If the D'Agostino-Pearson test indicated that the normality and homoscedasticity were met, the analysis used to compare different treatments was the T-Student analysis or the analysis of variance (ANOVA). When the populations did not have a normal distribution, the nonparametric Mann-Whitney U-test was performed. Significance was considered significant at $p < 0.05$. Data are presented as the means of each population ± Standard Error of the Mean (SEM).

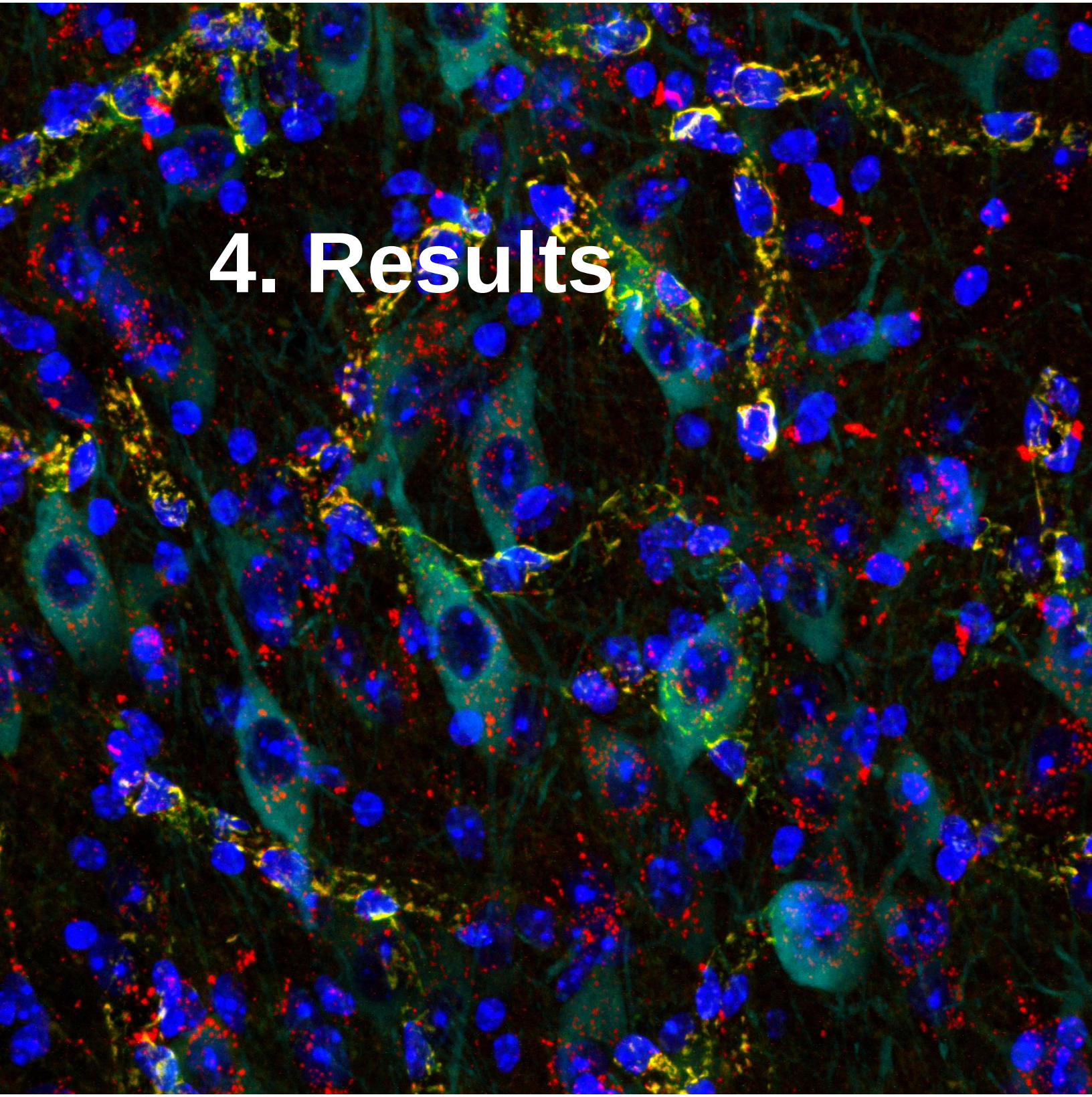

4. Results

4. Results

4.1. Study of mitophagy in the mouse retina

To determine if mitophagy occurs during retinal development, we analysed developmental mitophagy events during gestation from embryonic to adult. In particular we analysed embryonic day E13.5, E14.5, E15.5, E16.5, E18.5 and after birth from postnatal day P1, P9, P15 MitoQC eye sections. We found that there is no basal mitophagy at the embryonic day E13.5 (Figure 4.1). At later stages in E14.5, we saw some red puncta at the RGCL-NbL border, and the amount of mitophagy in the same region rose in E15.5, with noticeable mitophagy in the RGCL as well. In the ONbL, only a few red dots can be seen. This was also visible at the embryonic day E16.5, a lot of red dots on the border of RGCL and NbL, but also red dots in the RGCL and ONbL (Figure 4.1). The last embryonic day *in utero,* E18.5, red dots can be seen in the IPL (on the border of RGCL and INbL) but also some dots in the NbL (Figure 4.1).

After birth, on postnatal day P1 mitophagy levels are increased in all five layers (ONbL, INbL, NbL IPL and RGCL), and mitophagy levels decrease the following P9. Red dots are visible in all layers, also big accumulations of red dots can be seen in the INL and IPL (Figure 4.1). Coincident with the final stages of neuronal differentiation and retinal vascular development, the mice open their eyes, and vision is initiated at approximately P15. At P15, we observed that the ONL has the highest levels of mitophagy in comparison to the other layers. In conclusion our data show that three peaks in mitophagy levels can be seen across the entire retina. The first peak occurs at embryonic day E15.5, the second at postnatal day P1, and the third at P15 (Figure 4.2.).

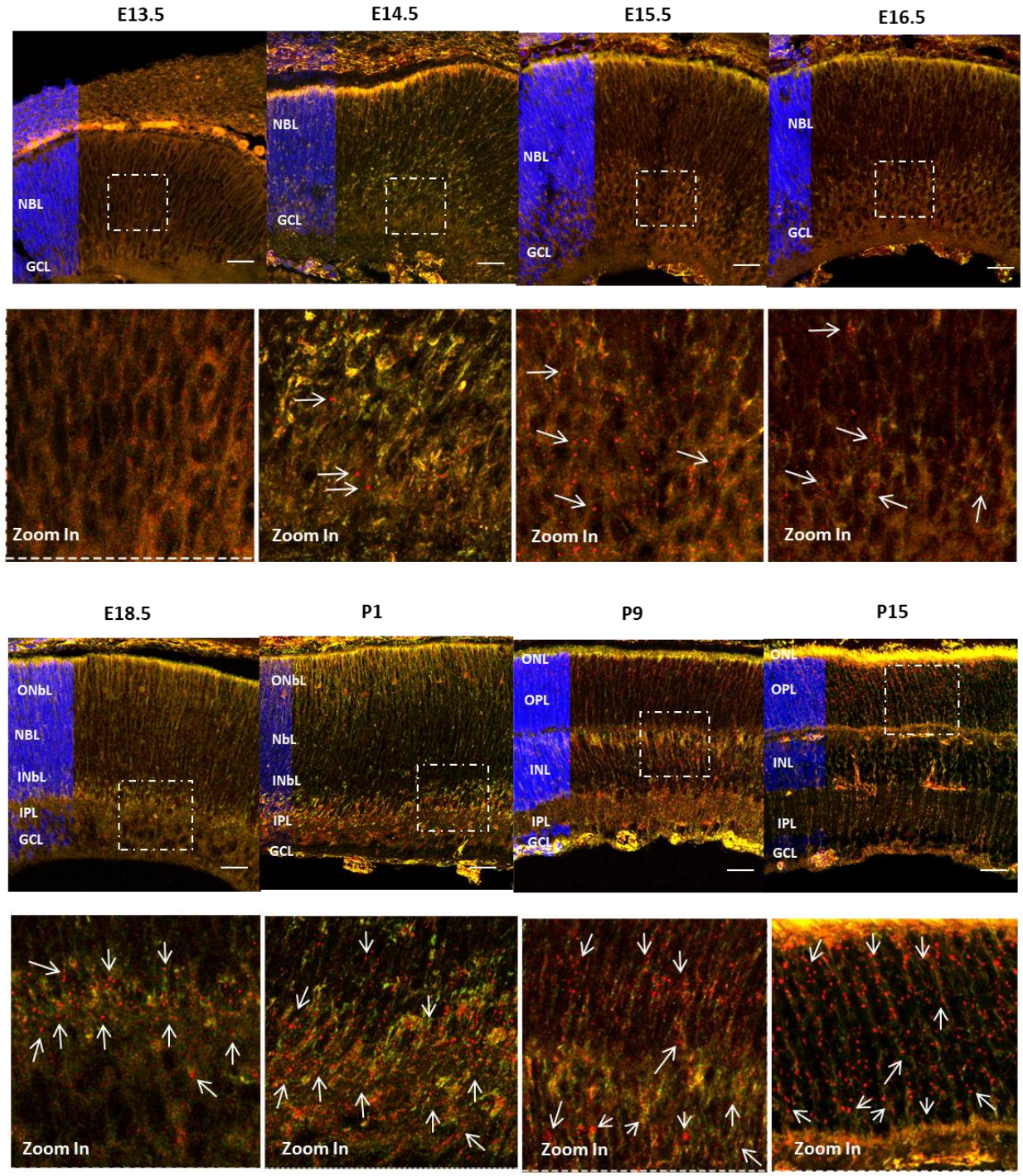

Figure 4.1. Mitophagy determination during retinogenesis in retinas from the MitoQC reporter. Representative eye sections from various stages of the development of the MitoQC mice, red mitolysosomes are indicated with a white arrow. GCL, ganglion cell layer; NbL, neuroblast layer; ONbL, outer neuroblast layer; INbL, inner neuroblast layer; INL, inner nuclear layer; IPL, inner plexiform layer; OPL, outer plexiform layer; ONL, outer nuclear layer. The square in the image above indicates the area of the picture that has been magnified in the image below. Scale bars 25 μm.

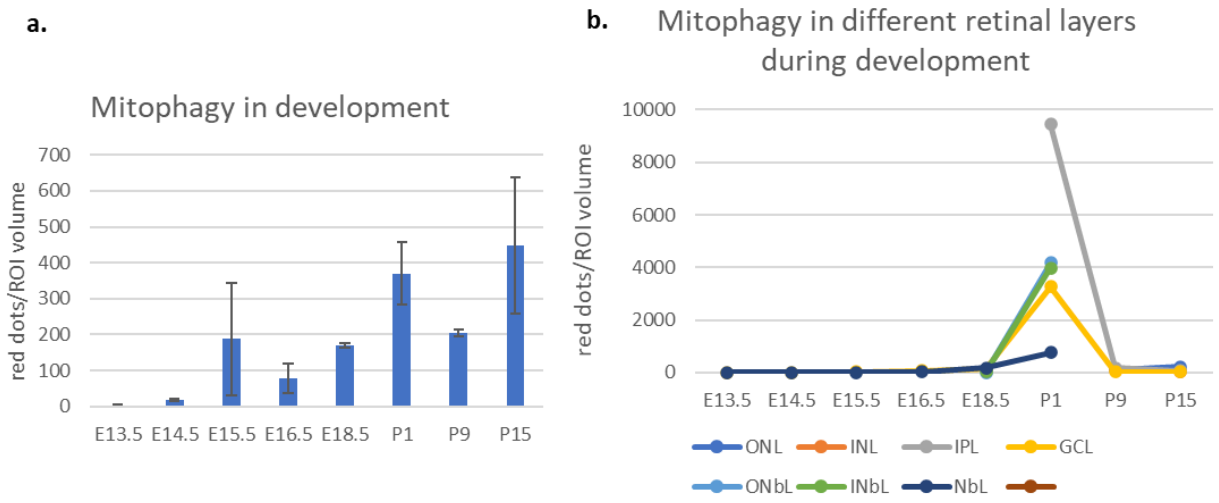

Figure 4.2. Graphical representation of the number of mitolysosomes in the whole retina throughout neurogenesis a. Quantification of mCherry-only puncta from MitoQC (mitophagy) in the entire retina. Three peaks in the proportion of mitophagy can be observed, the first one at E15.5, second at P1 and finally at P15.5 (mean + SEM) **b.** Mitophagy in different layers of the retina during the retinogenesis. (n=4).

To further test if newly differentiated cells exhibit mitophagy, we stained the P9 MitoQC retina with AP-2α antibody, which labels all amacrine cells, and with Brn3a, an RGCL marker (Figure 4.3). We settled on this age since it coincides with the maturation of both types of cells. Both amacrine and retinal ganglion cells have red punctae (Figure 4.3), which confirms that the cells that are newly developed have higher levels of mitophagy.

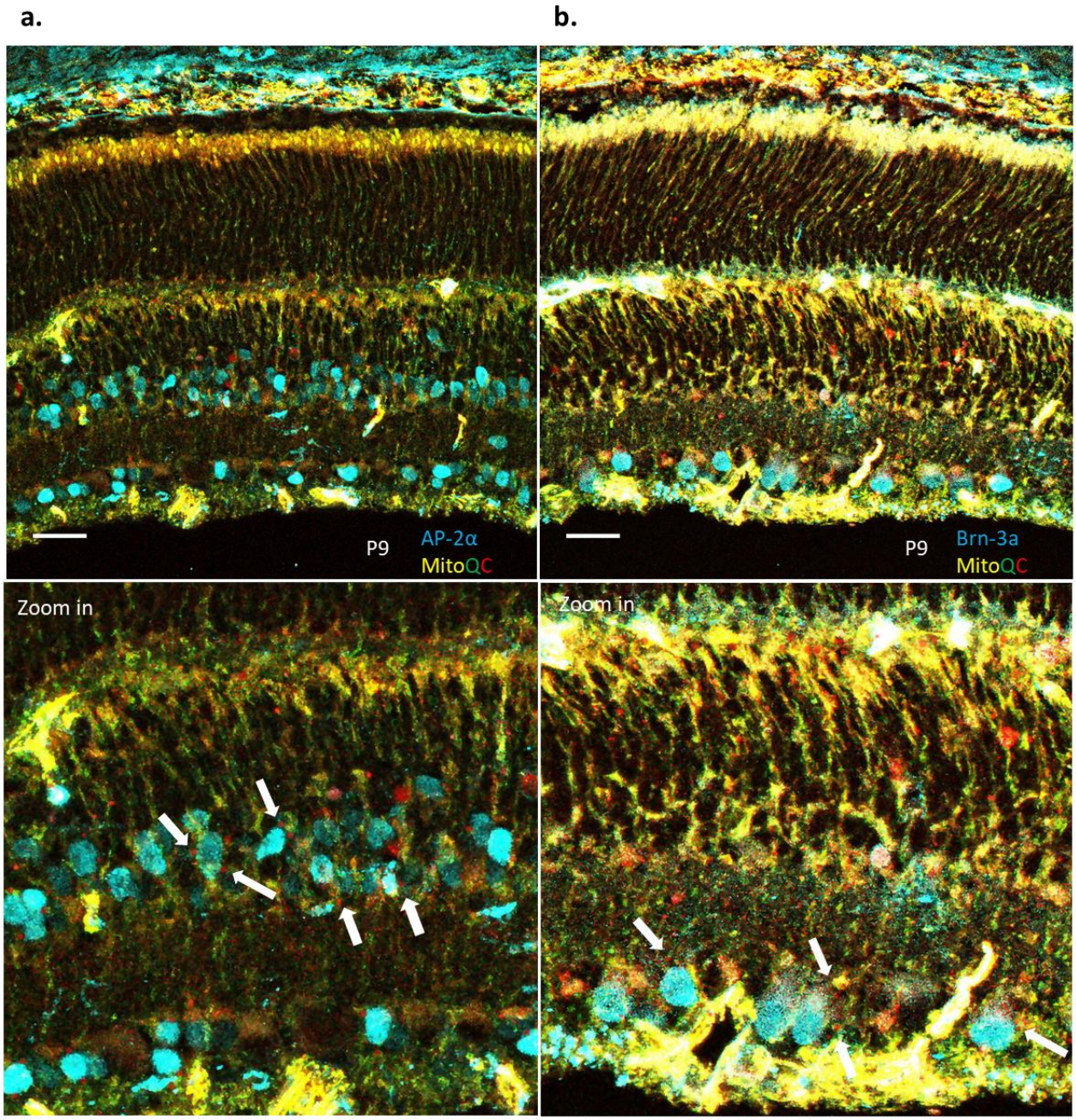

Figure 4.3. Representative immunofluorescence of P9 MitoQC retinal sections stained with a. AP-2α antibody and **b.** Brn3a antibody. Arrows show amacrine cells and retinal ganglion cells exibiting mitophagy. Scale bars 25 μm.

4.2. Pharmacological modulation of mitophagy in MitoQC retinal explants

The second aim of the study is to manipulate the pathways of either autophagy or mitophagy with pharmacological approaches to test whether mitophagy can be induced

or inhibited at differente developmental stages and validate de use of novel mitophagy modulators.

4.2.1. Pharmacological modulation of mitophagy in E13.5

E13.5 MitoQC retinas were treated with the following, well known, mitophagy inducers. CCCP which is a protonophore capable of increasing membrane proton conductance by several orders of magnitude, thereby causing mitochondrial depolarization and uncoupling of respiration (Chen et al., 2014; Liu et al., 2013; Narendra et al., 2008). This has been shown to induce a potent mitophagy response. Rapamycin is an allosteric inhibitor of mTORC1 and has been extensively used to study tumour cell growth, proliferation, and autophagy (Dumont and Su,1996). And finally, DFP, a mitophagy inducer, shown to promote mitochondrial turnover via an iron depletion-dependent mechanism without causing a ΔΨm collapse (Allen et al., 2013). It is also important to mention that iron depletion specifically triggers mitophagy in a PINK1/Parkin independent manner (Allen et al., 2013).

In collaboration with the group Dr. Ana Martinez Gil's and Anne Simonsen at the University of Oslo in the frame of a collaboration in a ITN network DRIVE we have found several mitophagy-modulating compouds. We were looking for compounds that induce mitophagy from the in-house MBC chemical library (Sebastián-Pérez et al., 2017). The compounds we added were shown to induce or inhibit mitophagy in the High-Throughput Screening at the University of Oslo, so we decided to test whether some of the hits affect mitophagy in the retinal explants from the MitoQC animals (Maestro et al., 2021).

The compounds used were JAR1.39, VP07 and IGS2.7 (Table 3.1.). JAR1.39 and VP07 are known as glycogen synthase kinase 3 β (GSK-3β) inhibitors and have the potential for the treatment of chronic diseases (Palomo et al., 2017). Whereas IGS2.7, a benzothiazole-based CK-1δ inhibitor, has shown promising results as a novel strategy for the treatment of frontotemporal dementia (Alquezar et al.,2016), as well as neuroprotective properties and the preservation of motor neurons, owing to its ability to reduce TDP-43 phosphorylation (Martinez-González et al., 2020) (Table 4.1.).

We isolated retinas from the MitoQC mice. They were cultured with the mentioned treatments inducing or inhibiting either autophagy or mitophagy regarding the stage of

development. Our study could tell us which is the relationship of autophagy/mitophagy regarding the retinal development.

Table 4.1. Chemical structure of VP07, JAR1.39 and IGS2.7 and their IC50 values on CK-1. The % inhibition of CK-1δ activity was determined *in vitro* in presence of a fixed concentration of 10 μM of the compounds. IC50: half maximal concentration of both compounds inhibiting CK-1δ activity. BBB prediction. Compounds were classified as CNS+ when they present a permeability >3.74 × 10−6 cm · s−1 [20]. Values shown are the mean ± SD.

Compound	**GSK3beta IC_{50} (μM)**	**Structure**	**BBB prediction**
VP0.7	2.8	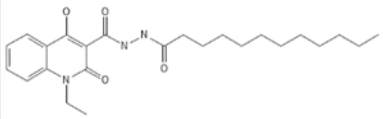	CNS+
JAR1.39	2.01	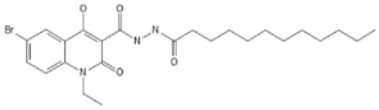	CNS+
Compound	**CK-1 IC_{50} (nM)**	**Structure**	**BBB prediction**
IGS2.7	23 ± 2	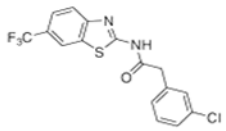	CNS+

DFP induced mitophagy at E13.5 which means that mitophagy can be induced at this age via Parkin independent pathway (Figure 4.4). Interestingly, the compound JAR1.39 also managed to significantly induce mitophagy in the retina (Figure 4.5), although we still do not know what the mechanism of action of this compound is. Both CCCP and VP07 also induced mitophagy levels, although not as effectively as DFP and JAR1.39. JAR1.39 and VP07 were found to induce mitophagy in U2OS-iMLS-Parkin cells; moreover, VP07-induced mitophagy was identified exclusively in Parkin-expressing cells (Maestro et al., 2021).

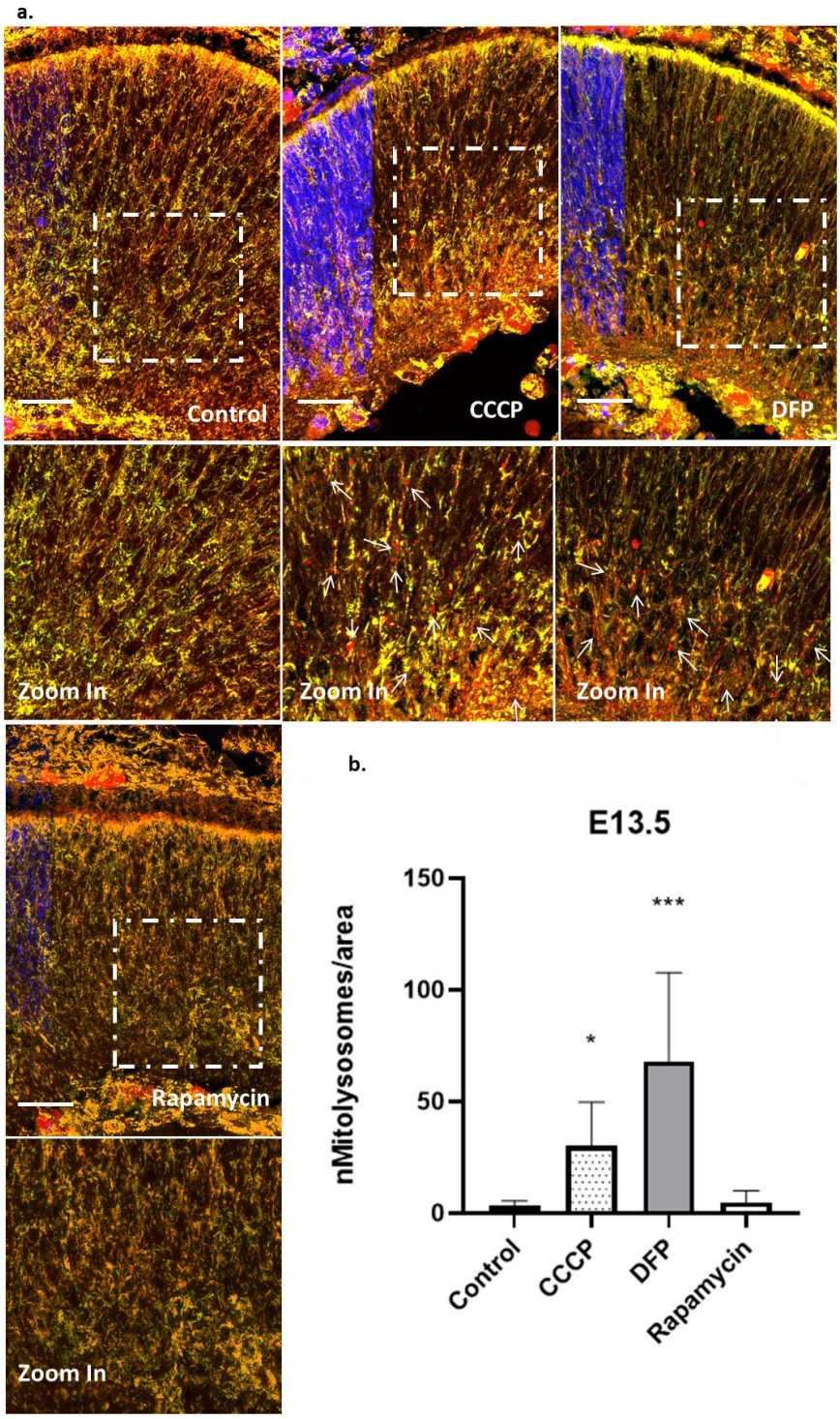

Figure 4.4. Pharmacological modulation of mitophagy with inducers in E13.5 MitoQC retinal explants. a. The formation of red dots representative of mitophagy was analysed by microscopy in the E13.5 retina section of MitoQC mice treated with the indicated treatments for 6 hours ex-vivo. The square in the image above indicates the area of the picture that has been magnified in the image below. The picture below shows the zoomed-in portion of the image above. **b.** Graphical representation of the quantifications of the number of mitolysosomes in the whole retina (mean ± SEM). Ordinary one-way ANOVA statistical tests. Scale bar 25 µm. (n=5).

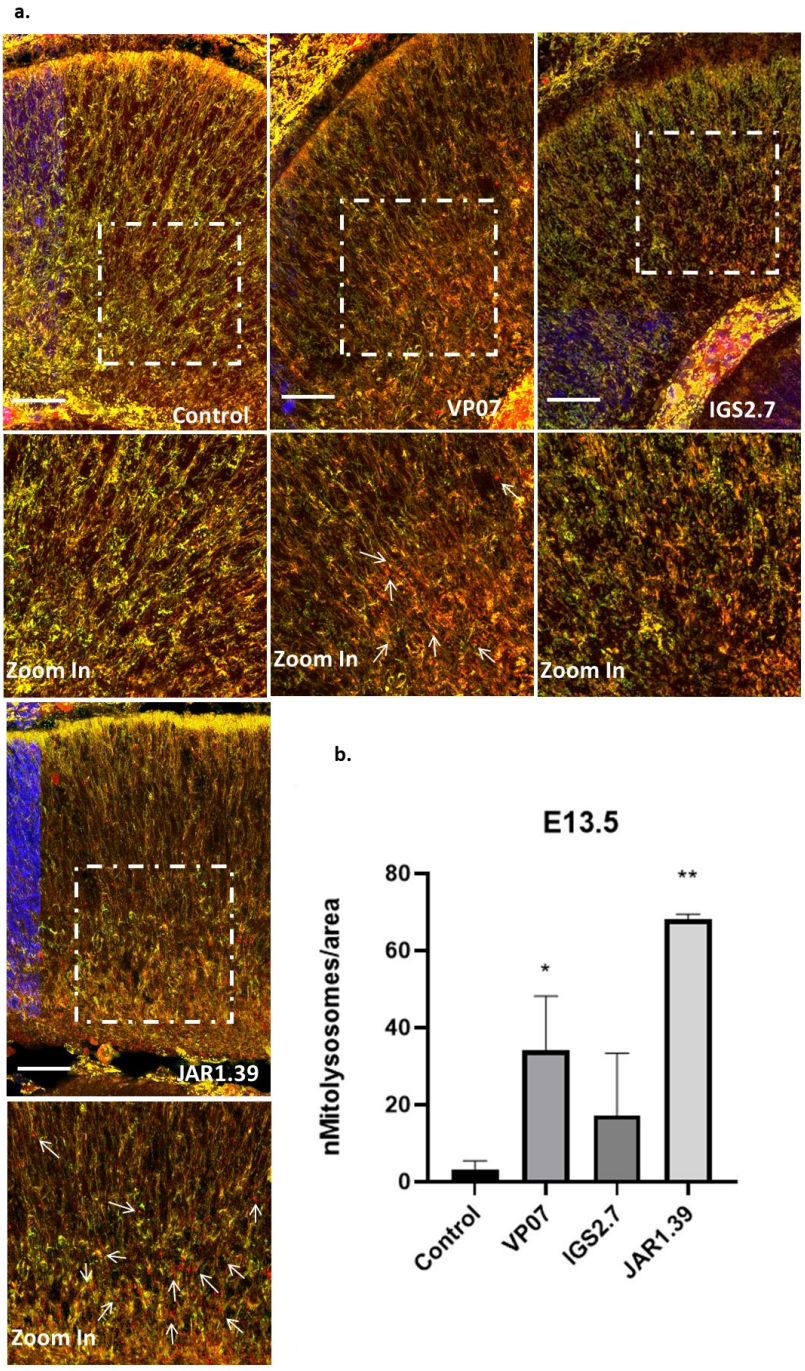

Figure 4.5. Pharmacological modulation of mitophagy with compounds from MBC chemical library in E13.5 MitoQC retinal explants. a. The formation of red dots representative of mitophagy was analysed by microscopy in the E13.5 retina section of MitoQC mice treated with three different treatments (JAR1.39, IGS2.7, VP07) for 6 hours ex-vivo. The picture below shows the zoomed-in portion of the image above. **b.** Graphical representation of the quantifications of the number of mitolysosomes in the whole retina (mean ± SEM). Ordinary one-way ANOVA statistical tests. Scale bar 25 μm. (n=5).

As our previous data show a key role of mitohgay for RGC neurogenesis we quantified mitophagy in the RGCL (Figure 4.6.a). Compounds DFP, JAR1.39, CCCP, and VP07 have a significant influence on mitophagy levels in the MitoQC retina's RGCL (Figure 4.6.b). In this layer, DFP and JAR1.39 had the biggest effect on mitophagy levels.

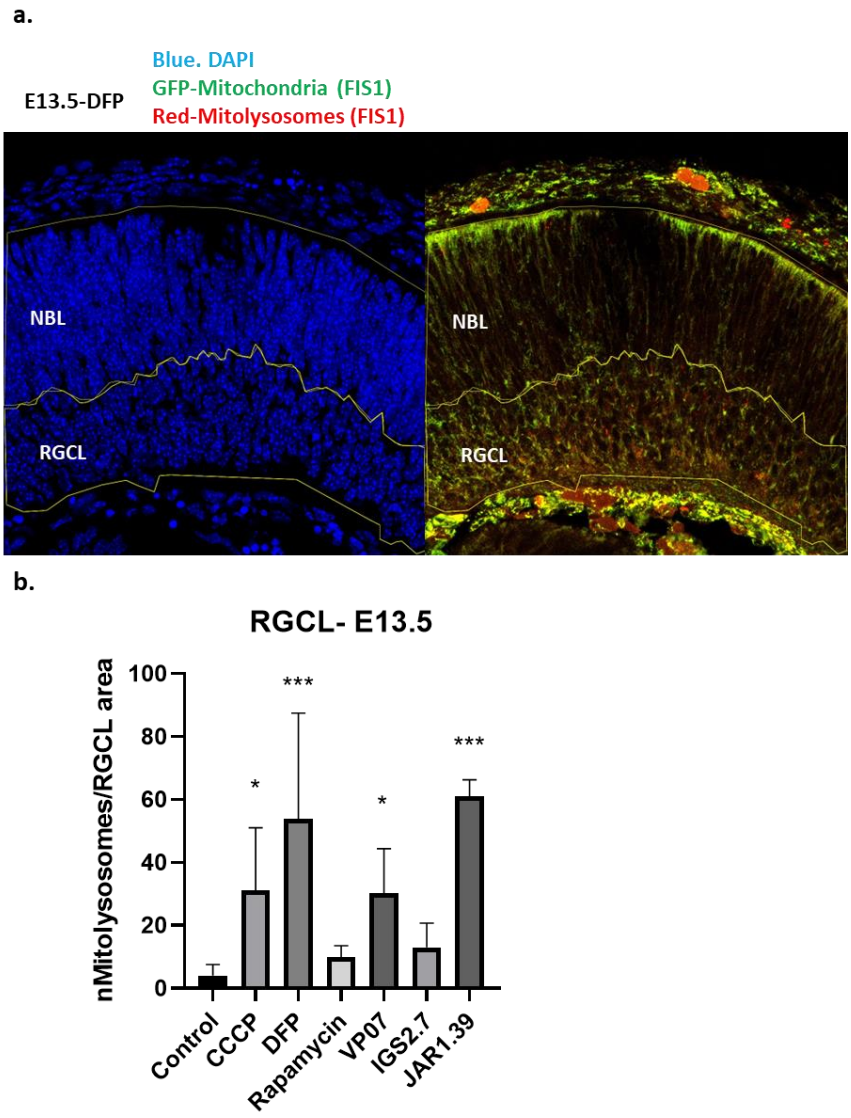

Figure 4.6. Pharmacological modulation of mitophagy in RGCL of E13.5 MitoQC retinal explant sections a. The image shows a demonstration of the selected region of interest (ROI) for pharmacological modulation of mitophagy using DFP in E13.5 MitoQC retinal explants. The first image shows DAPI-stained nuclei to explain how the ROI was selected. DAPI was used to select the ROI of RGCL due to different morphology in the nuclei of RGCL and NbL (image on the left). The right image shows the ROI with the MitoQC fluorophores. RGCL, retinal ganglion cell layer; NbL, neuroblast layer. **b.** Graphical representation of the quantifications of the number of mitolysosomes in the RGCL solely (mean ± SEM). Ordinary one-way ANOVA statistical tests.

In the RGCL both DFP and JAR1.39 exhibited a substantial impact on mitophagy levels (Figure 4.7. and Figure 4.8.). Interestingly, only DFP had a significant effect on the mitophagy in the NbL, whereas the other compounds had little or no impact (Figure 4.9. and Figure 4.10.). Thus, stimulating mitophagy with DFP is completely plausible at this time, given the highly hypoxic environment of the developing retina, and it also corresponds with increased levels of ROS in recently differentiated cells.

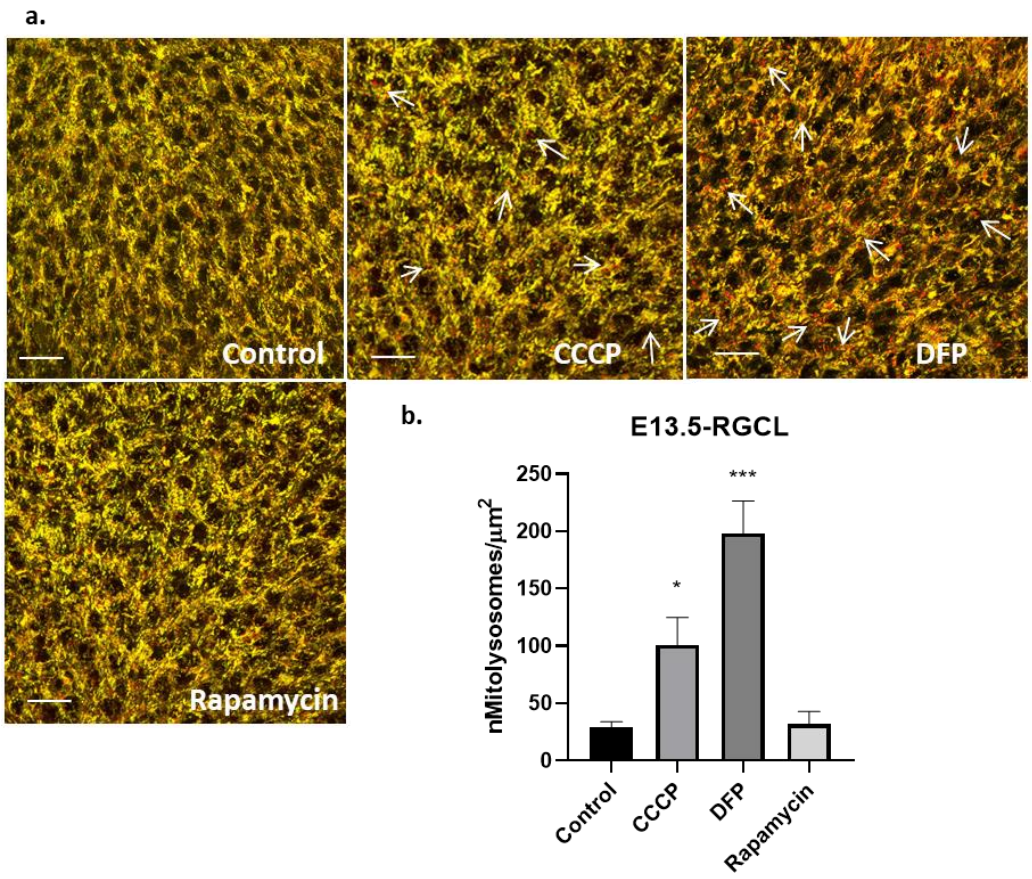

Figure 4.7. Pharmacological modulation of mitophagy in E13.5 MitoQC retinal explants with mitophagy inducers. a. The formation of red dots representative of mitophagy was analysed by microscopy in the RGCL of E13.5 retina flatmount of MitoQC mice treated with the indicated treatments for 6 hours ex-vivo. **b.** Graphical representation of the quantifications of the number of mitolysosomes in the RGCL of the E13.5 retina (mean ± SEM). Ordinary one-way ANOVA statistical tests. Scale bars 25 µm. (n=3).

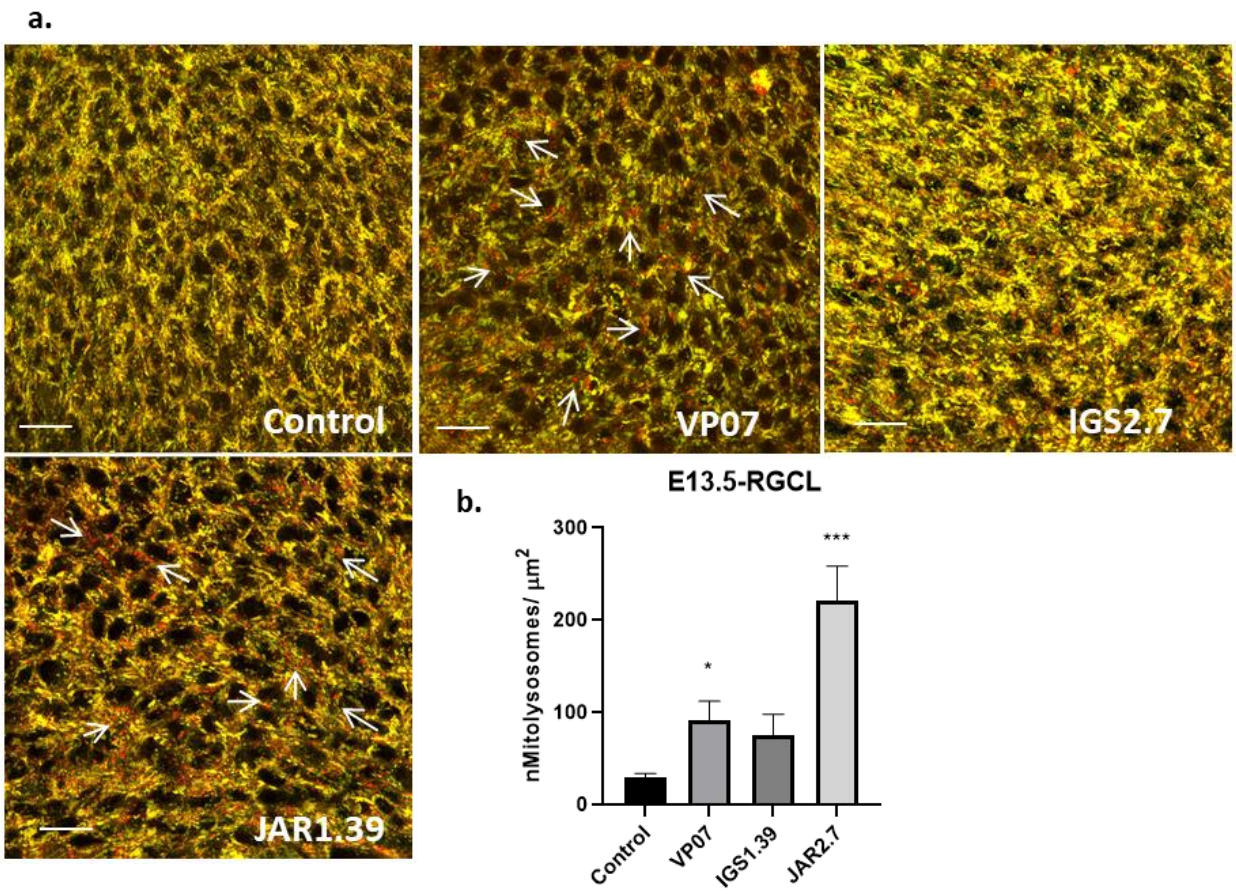

Figure 4.8. Pharmacological modulation of mitophagy in E13.5 MitoQC retinal explants with compounds from MBC chemical library. a. The formation of red dots representative of mitophagy was analysed by microscopy in the RGCL of E13.5 retina flatmount of MitoQC mice treated with the indicated treatments for 6 hours ex-vivo. **b.** Graphical representation of the quantifications of the number of mitolysosomes in the RGCL of the E13.5 retina (mean ± SEM). Ordinary one-way ANOVA statistical tests. Scale bars 25 µm. (n=3).

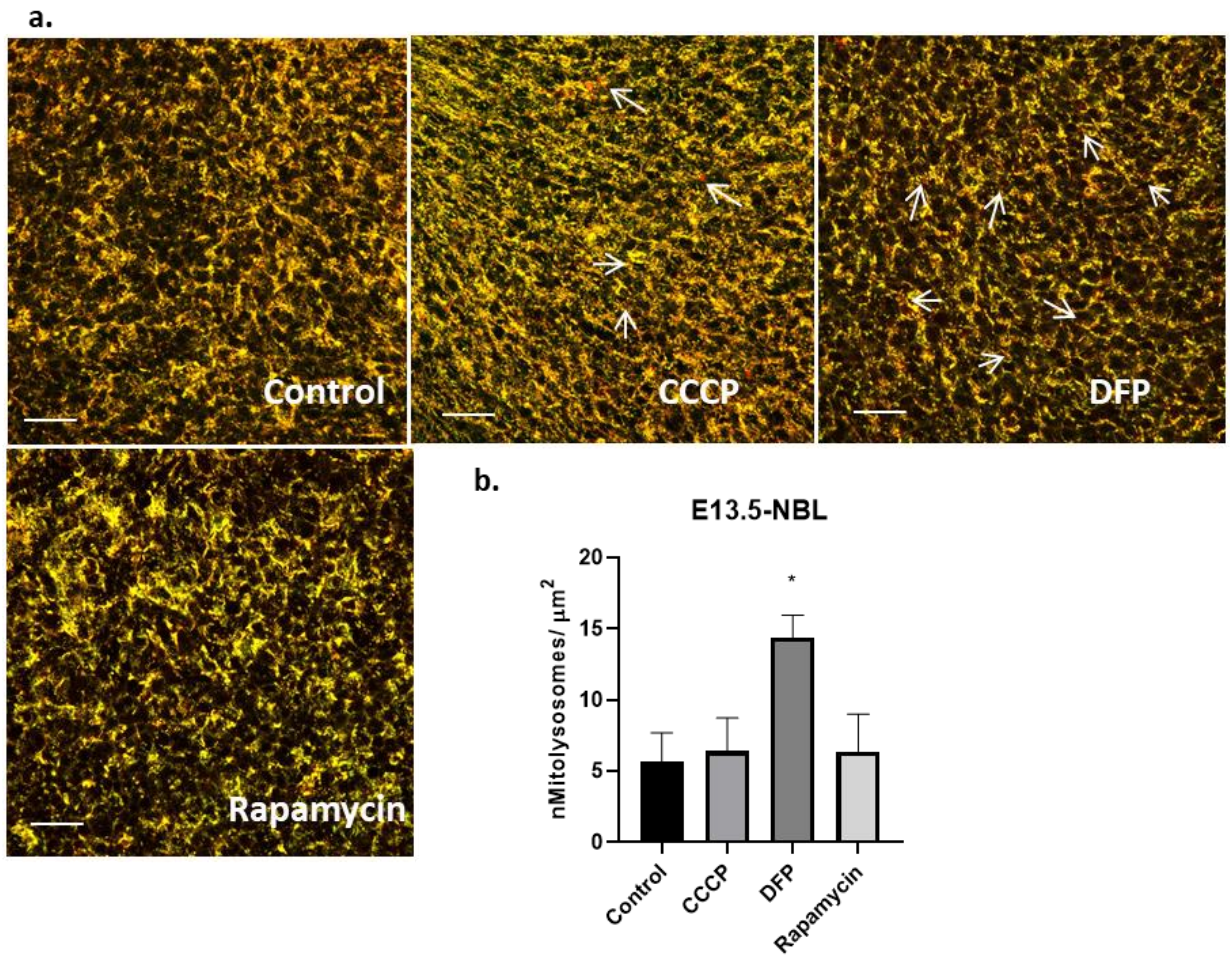

Figure 4.9. Pharmacological modulation of mitophagy in E13.5 MitoQC retinal explants. a. The formation of red dots representative of mitophagy was analysed by microscopy in the NbL of E13.5 retina flatmount of MitoQC mice treated with the indicated treatments for 6 hours ex-vivo. Images showing the levels of red dots, which are indicative of mitophagy, in the NbL of E13.5 retina flatmount MitoQC mice treated with six different treatments for six hours ex-vivo. **b.** Quantifications of the number of mitolysosomes in the NbL of the E13.5 retina are shown graphically (mean ± SEM). Ordinary one-way ANOVA statistical tests. Scale bars 25 µm. (n=3).

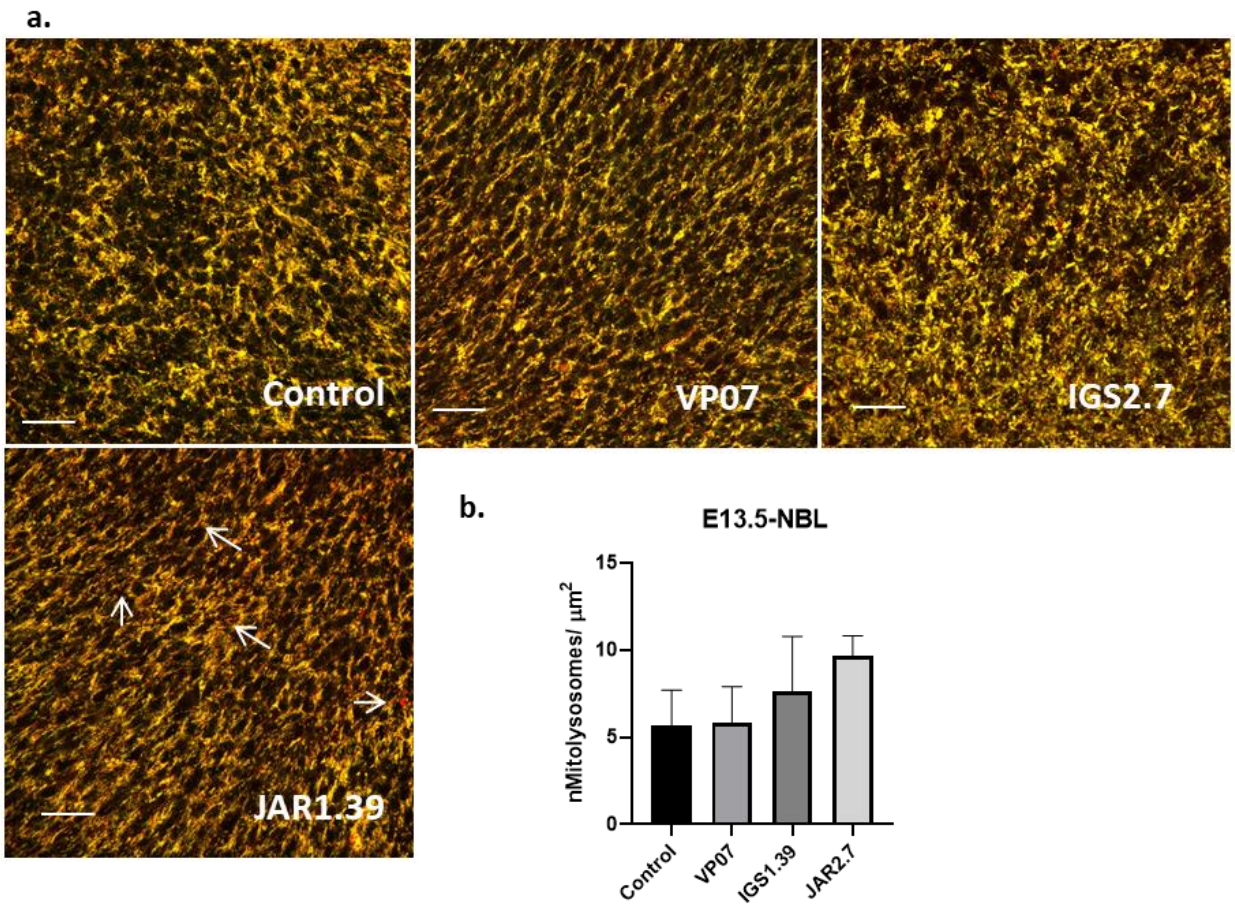

Figure 4.10. Pharmacological modulation of mitophagy in E13.5 MitoQC retinal explants. a. The formation of red dots representative of mitophagy was analysed by microscopy in the NbL of E13.5 retina flatmount of MitoQC mice treated with the indicated treatments for 6 hours ex-vivo. Images showing the levels of red dots, which are indicative of mitophagy, in the NbL of E13.5 retina flatmount MitoQC mice treated with six different treatments for six hours ex-vivo. **b.** Quantifications of the number of mitolysosomes in the NbL of the E13.5 retina are shown graphically (mean ± SEM). Ordinary one-way ANOVA statistical tests. Scale bars 25 µm. (n=3).

4.2.2. Pharmacological modulation of mitophagy in E14.5

To get a better understanding about the mechanism of the mitophagy pathway during development, we sought to investigate if there was a difference in the amount of mitophagy induction when the retinas were treated with the same mitophagy inducers on successive days of development. So, we performed the experiment using embryonic day E14.5. Interestingly, CCCP was able to significantly induce mitophagy at the embryonic day E14.5, as opposed to E13.5 where the induction wasn't so dramatic (Figure 4.11.). Furthermore, contrary at E13.5, when JAR1.39 was the most efficient inducer, VP07 was demonstrated to promote mitophagy levels at E14.5 with the highest efficacy (Figure 4.12.). This demonstrates that there is a change in mitochondria condition, and therefore distinct pathways are triggered, because different compounds have opposite effects on two consecutive days of development. Rapamycin, however, did not have any effect on the level of mitophagy, as did IGS2.7. DFP was able to promote mitophagy, although only to a small extent.

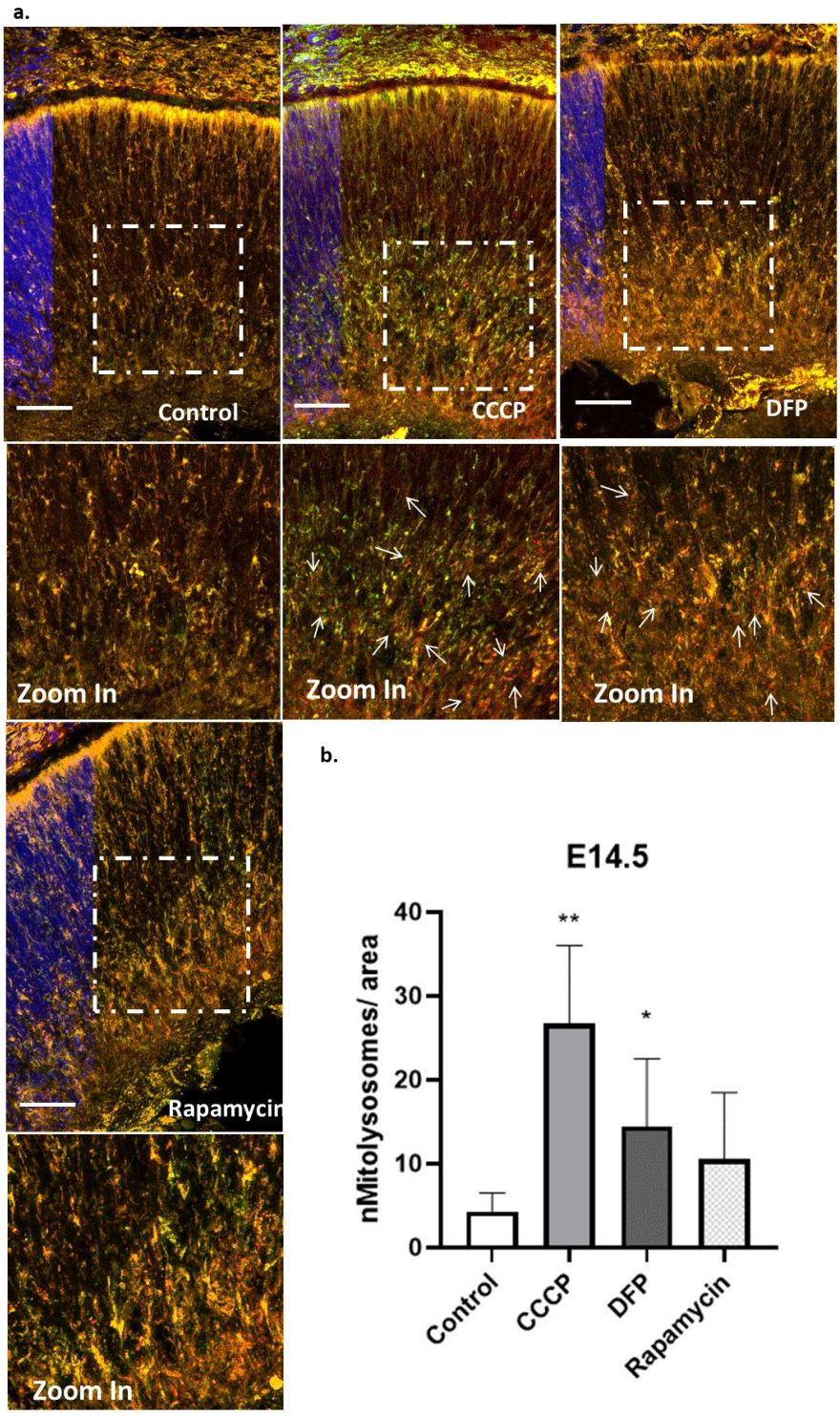

Figure 4.11. Pharmacological modulation of mitophagy with known autophagy inducers in E14.5 MitoQC retinal explants. a. The formation of red dots representative of mitophagy was analysed by microscopy in the E14.5 retina section of MitoQC mice treated with three different treatments for 6 hours ex-vivo. The picture below shows the zoomed-in portion of the image above. **b.** Graphical representation of the quantifications of the number of mitolysosomes in the whole retina. CCCP and DFP increased mitophagy levels (mean ± SEM). Ordinary one-way ANOVA statistical tests. Scale bars 25 μm. (n=5).

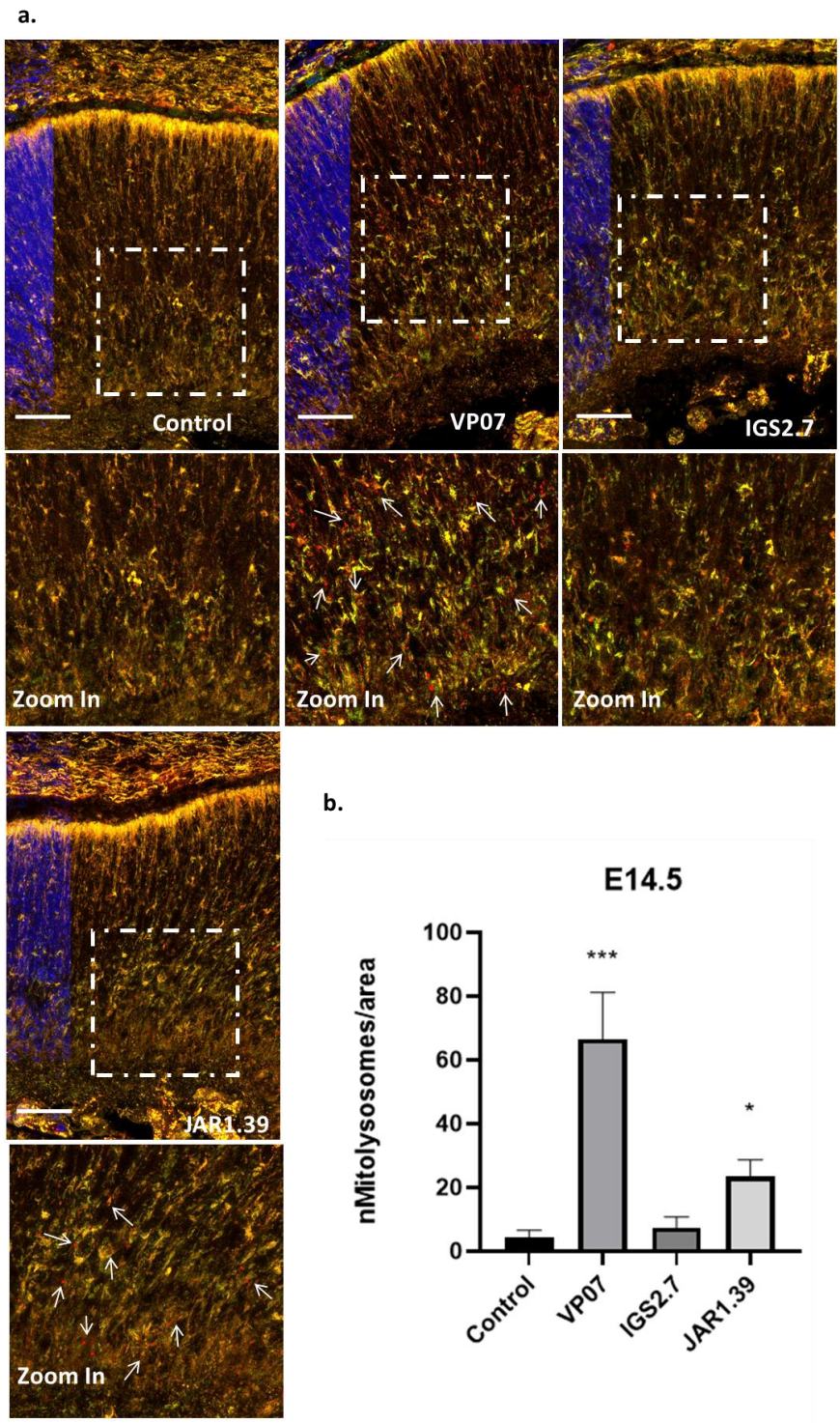

Figure 4.12. Pharmacological modulation of mitophagy with compounds from MBC chemical library in E14.5 MitoQC retinal explants. a. The formation of red dots representative of mitophagy was analysed by microscopy in the E14.5 retina section of MitoQC mice treated with three different treatments for 6 hours ex-vivo. The picture below shows the zoomed-in portion of the image above. **b.** Graphical representation of the quantifications of the number of mitolysosomes in the whole retina. VP07 and JAR1.39 significantly increased mitophagy levels (mean ± SEM). Ordinary one-way ANOVA statistical tests. Scale bars 25 μm. (n=5).

4.2.3. Pharmacological modulation of mitophagy in E15.5

Previous findings from the lab demonstrate high levels of basal mitophagy in the whole retina at E15.5, as well as an increase of mitochondrial mass amount in Atg5-deficient retinas, when autophagy is inhibited with 3-MA and mitophagy is inhibited with CsA. Furthermore, mitophagy in E15.5 retinas promotes a metabolic shift toward glycolysis, which is required for appropriate differentiation of retinal ganglion cells indicating that this is an important developmental stage of the retina (Esteban-Martinez et al, 2017).

Due to higher basal levels of mitophagy at this stage we wanted to explore if mitophagy could be suppressed and how the three novel chemicals affected the retina. 3-MA is a compound that suppresses general autophagy by inhibiting the formation of autophagosomes and that has also been used to halt mitophagy, with the class III PI3K inhibitor 3-methyladenine (Heckmann et al., 2013). Next, we used hydroxychloroquine (HCQ), a potent autophagy inhibitor which prevents lysosomal acidification, thereby interfering with the last step in the autophagic process (Boya et al., 2005). Cyclosporin A, an inhibitor of MPT through interaction with cyclophilin D, blocks mitophagy during mitochondrial permeability transition (Rodriguez-Enriquez et al., 2009) and also mitophagy (Esteban-Martínez et al., 2017). And finally, Bafilomycin A1, a potent inhibitor of the Vacuolar H+ATPase which controls pH in the lysosome (V-ATPase). Through this mechanism bafilomycin inhibits autophagic flux by preventing the acidification of endosomes and lysosomes. The inhibitors that were shown to be most effective at this age were 3-MA and Bafilomycin (Figure 4.13.).

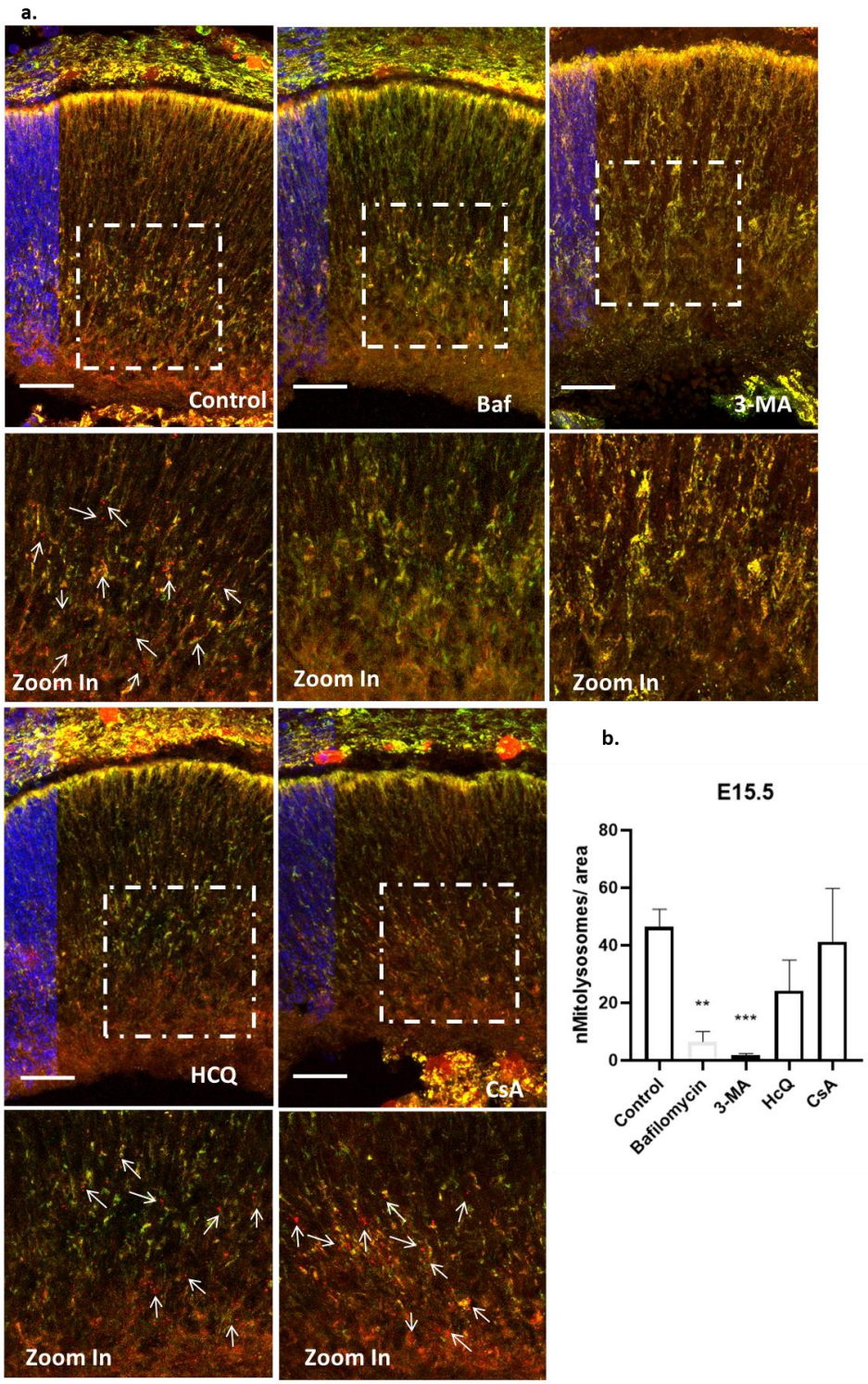

Figure 4.13. Modulation of mitophagy with autophagy inhibiting pharmacological agents in E15.5 MitoQC retinal explants. a. Microscopy was used to determine the amount of red dots indicative of mitophagy in the E15.5 retina section of MitoQC mice treated with four different treatments for six hours *ex vivo*. **b.** Graphical depiction of the counts of mitolysosomes in the whole retina where Bafilomycin and 3-MA have significant effect on mitophagy levels. (mean ± SEM). Ordinary one-way ANOVA statistical tests. Scale bars 25 μm. (n=5).

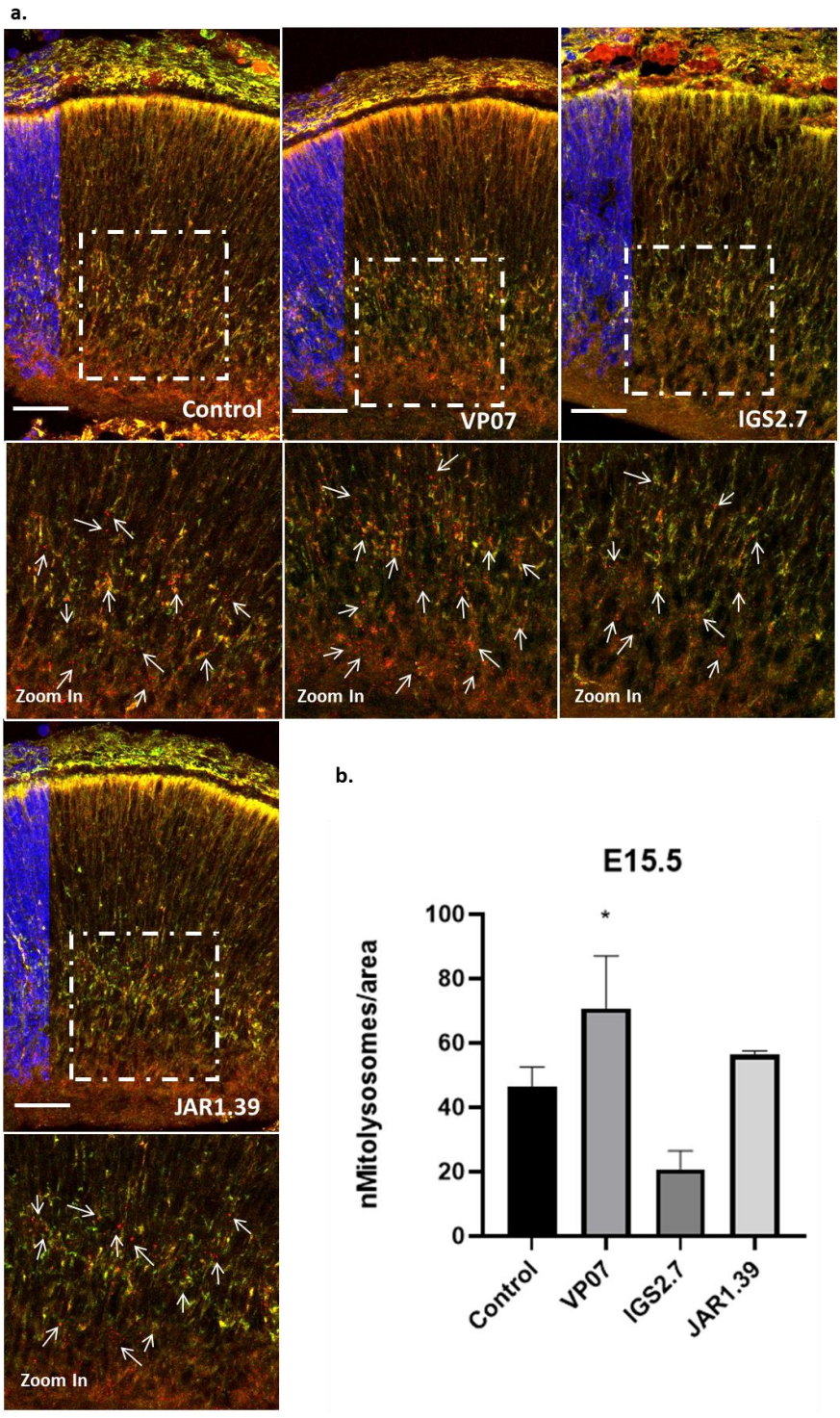

Figure 4.14. Modulation of mitophagy with autophagy modulation using compounds from the MBC chemical library in E15.5 MitoQC retinal explants. a. Microscopy was used to determine the amount of red dots indicative of mitophagy in the E15.5 retina section of MitoQC mice treated with four different treatments for six hours *ex vivo*. The picture below shows the zoomed-in area of the image above. **b.** Graphical depiction of the counts of mitolysosomes in the whole retina (mean ± SEM). Ordinary one-way ANOVA statistical tests. Scale bars 25 μm. (n=5).

Surprisingly, the compound VP07 significantly increased the level of mitophagy at E15.5. HCQ and CsA, on the other hand, had no impact on the degree of mitophagy, as did JAR1.39 and IGS2.7 (Figure 4.14.).

To better quantify the number of red dots per layer we repeated the experiment using MitoQC retinal flatmounts. Specifically, we were interested in determining how the compounds affected mitophagy in various layers of the retina. Bafilomycin, 3-MA, and HCQ all reduced the amount of mitophagy in the RGCL of E15.5 retinal flatmounts, while CsA, JAR1.39, and IGS2.7 had no impact (Figure 4.15.; Figure 4.16.). Surprisingly, VP07 increased the level of mitophagy in the RGCL. In contrast, no chemical altered the rate of mitophagy in the NbL of the E15.5 MitoQC retina (Figure 4.17.; Figure 4.18.). This may indicate that the ganglion cells are more susceptible to the compounds' effect at this stage of development.

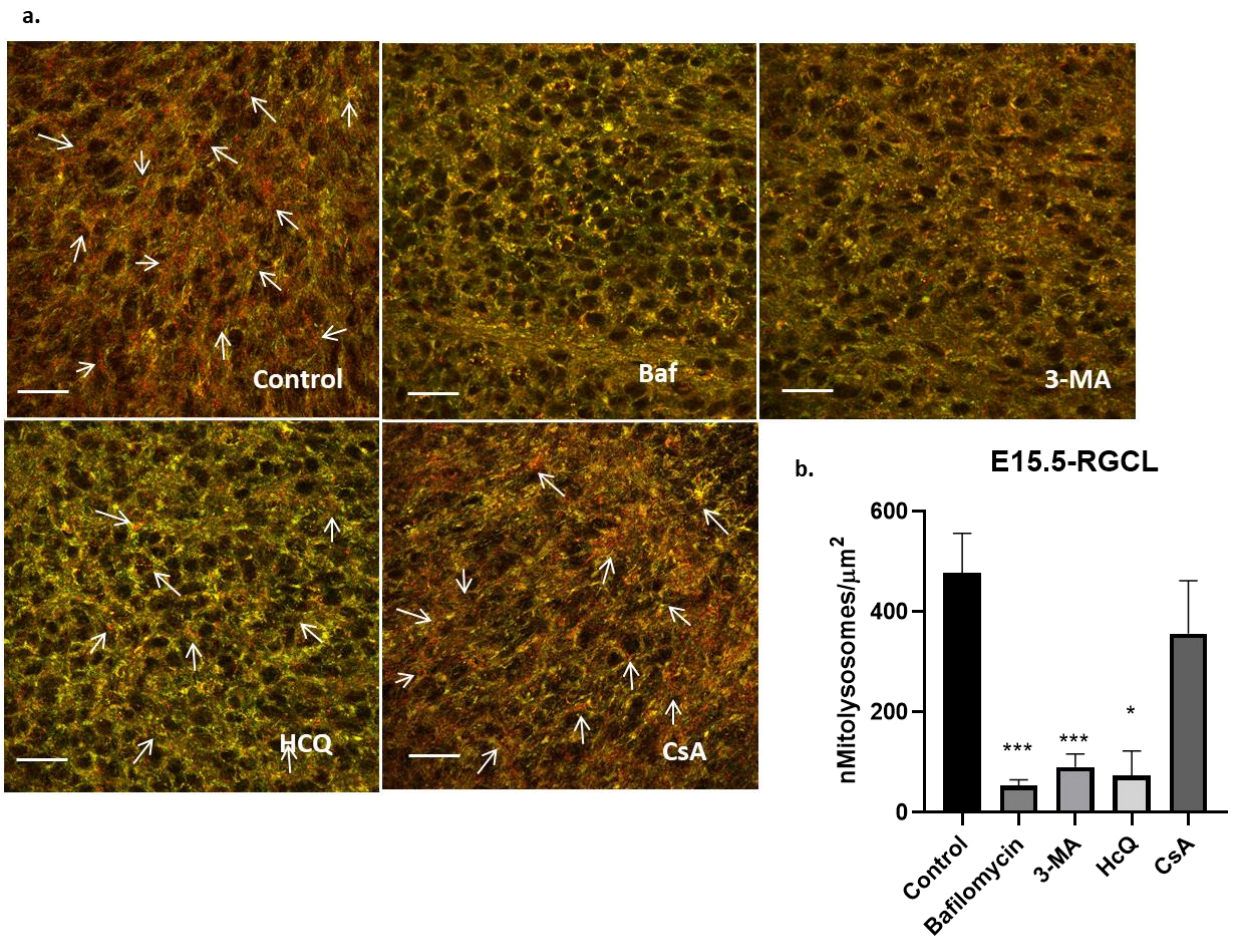

Figure 4.15. Bafilomycin, 3-MA and HcQ were able to significantly decrease the level of mitophagy in the retinal ganglion cell layer (RGCL) of the E15.5 retinal flatmounts. **a**. MitoQC reporter expression in RGCL of flatmounted retinas of E15.5 MitoQC mice with Baf, CsA, HcQ, treatments for 6 hours. **b**. Graphical presentation of mitophagy levels in RGCL of E15.5 retinas after 6 h of treatments *ex vivo*. Ordinary one-way ANOVA statistical tests. Scale bars 25 µm. (n=3).

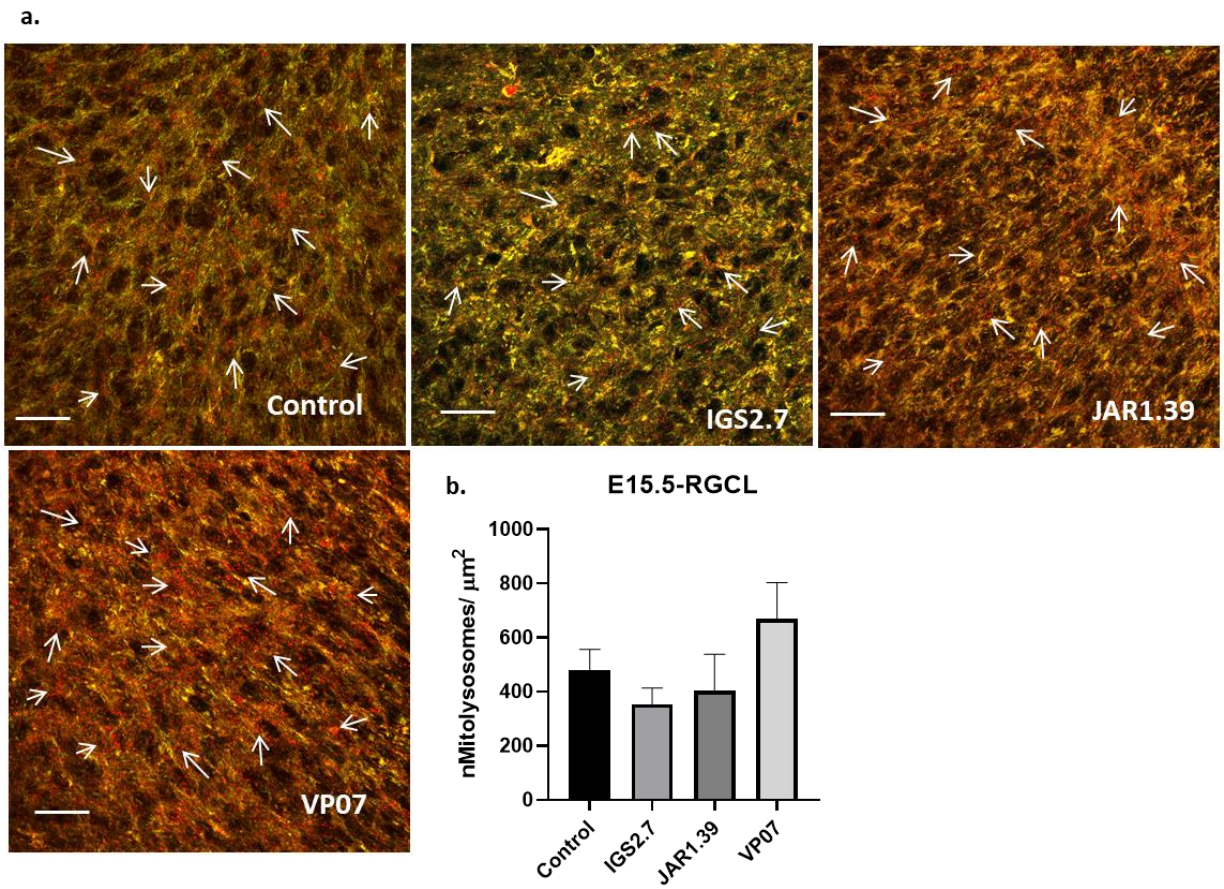

Figure 4.16. Modulation of mitophagy in the retinal ganglion cell layer (RGCL) of the E15.5 retinal flatmounts using compounds from the MBC chemical library. a. MitoQC reporter expression in RGCL of flatmounted retinas of E15.5 MitoQC mice with IGS2.7, JAR1.39 and VP07, treatments for 6 hours. **b**. Graphical presentation of mitophagy levels in RGCL of E15.5 retinas after 6 h of treatments *ex vivo*. Ordinary one-way ANOVA statistical tests. Scale bars 25 µm. (n=3).

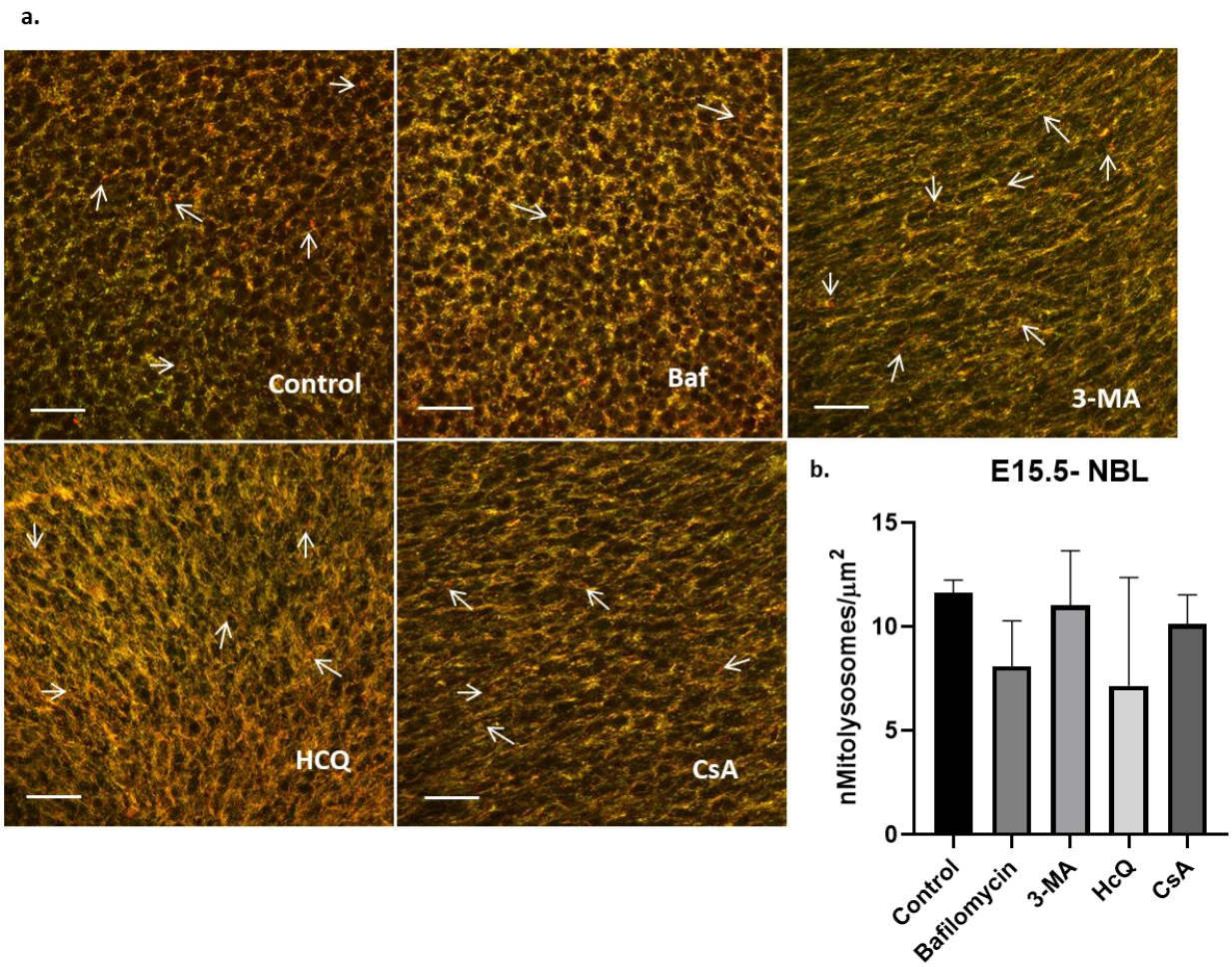

Figure 4.17. There is no change in the level of mitophagy in the neuroblast layer (NbL) of E15.5 MitoQC retinal flatmounts using autophagy inhibitors. **a.** MitoQC reporter expression in NbL of flatmounted retinas of E15.5 MitoQC mice with Bafilomycin (Baf), CsA, HcQ treatments for 6 hours. **b.** Graphical presentation of mitophagy levels in NbL of E15.5 retinas after 6 h of treatments *ex vivo*. Ordinary one-way ANOVA statistical tests. Scale bars 25 µm. (n=3).

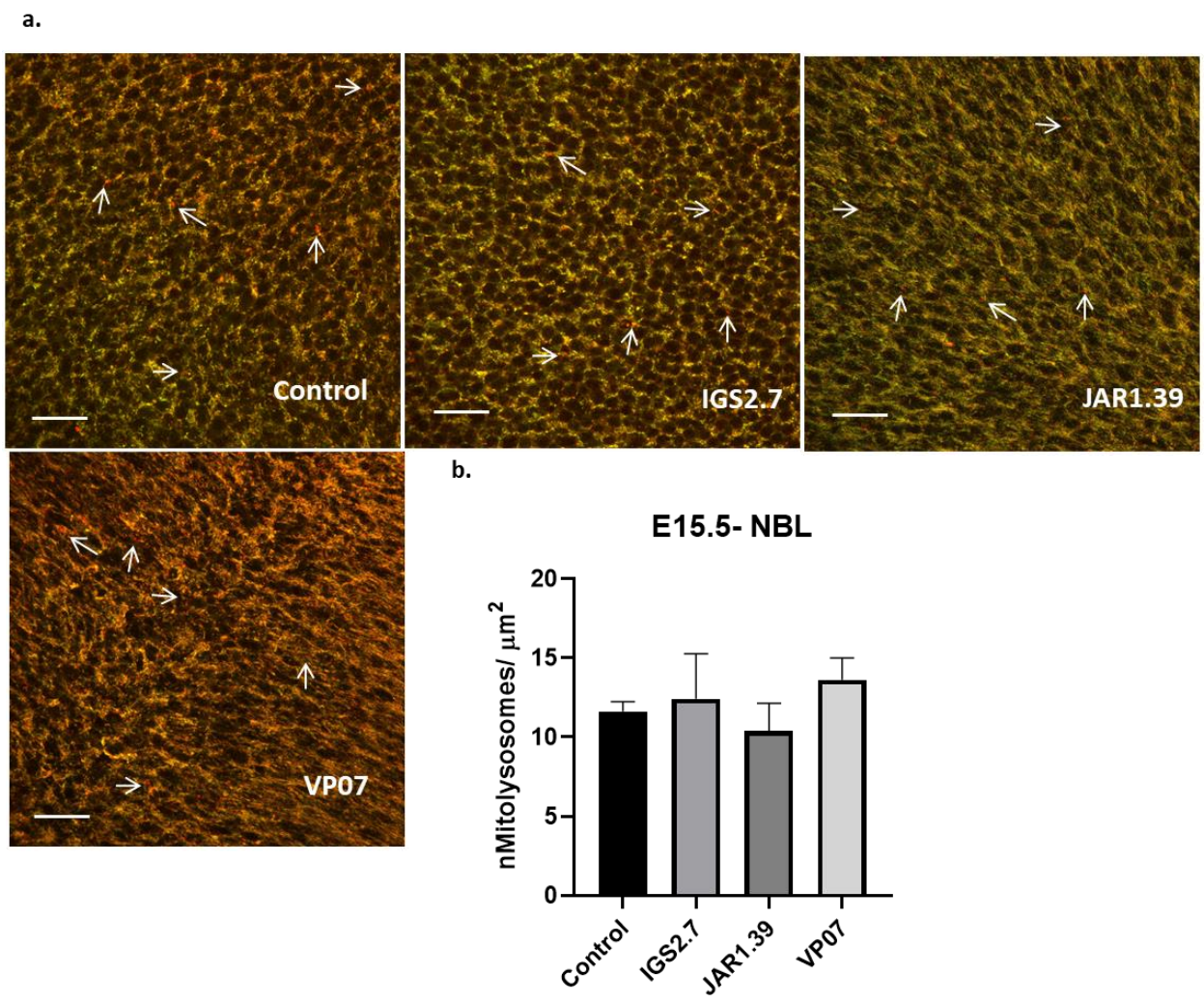

Figure 4.18. There is no change in the level of mitophagy in the neuroblast layer (NbL) of E15.5 MitoQC retinal flatmounts using compounds from the MBC chemical library. **a.** MitoQC reporter expression in NbL of flatmounted retinas of E15.5 MitoQC mice with JAR1.39, VP07 and IGS2.7 treatments for 6 hours. **b.** Graphical presentation of mitophagy levels in NbL of E15.5 retinas after 6 h of treatments *ex vivo*. Ordinary one-way ANOVA statistical tests. Scale bars 25 µm. (n=3).

4.2.4. Pharmacological modulation of mitophagy in P1

RGCs, horizontal cells, cone photoreceptors, and a subset of amacrine cells are born predominantly during the embryonic stages of retinal development (first wave of retinogenesis E11–E18), rod photoreceptors, bipolar interneurons, and Müller glial cells are born postnatally (second wave of retinogenesis P0–P7) (Heavner and Pevny 2012). Mouse RGCs at P1 cannot be categorized using the adult RGC classification criteria. They lack differentiation, and their dendrites stratify diffusely inside the IPL. At P3 (Stacy and Wong, 2003), the cholinergic stratification is detectable, and the morphology of RGCs is nearly identical to that of P1 RGCs, with the difference that the RGC stratification is tighter, albeit still diffuse in the IPL. From P0 through P3, RGCs are classified as simple or complex RGCs based on the complexity of the dendritic field. Dendritic motility is at its peak during P1 when the whole retina is still rudimentary. While amacrine and ganglion cells have developed (Cepko et al., 1996; Young, 1985), their morphologies are far from mature (Diao et al., 2004), i.e., they are tiny in size, their processes are dispersed across the IPL, and the retina is not yet ready to form synapses.

We utilized the same compounds for this age as we did for E15.5. Bafilomycin was shown to be the most effective mitophagy inhibitor in the whole retina, as well as the RGCL and NbL. CsA was also able to reduce the levels of mitophagy. CsA had a significant impact in the RGCL while having no effect in the NbL of the retina (Figure 4.19; Figure 4.21).

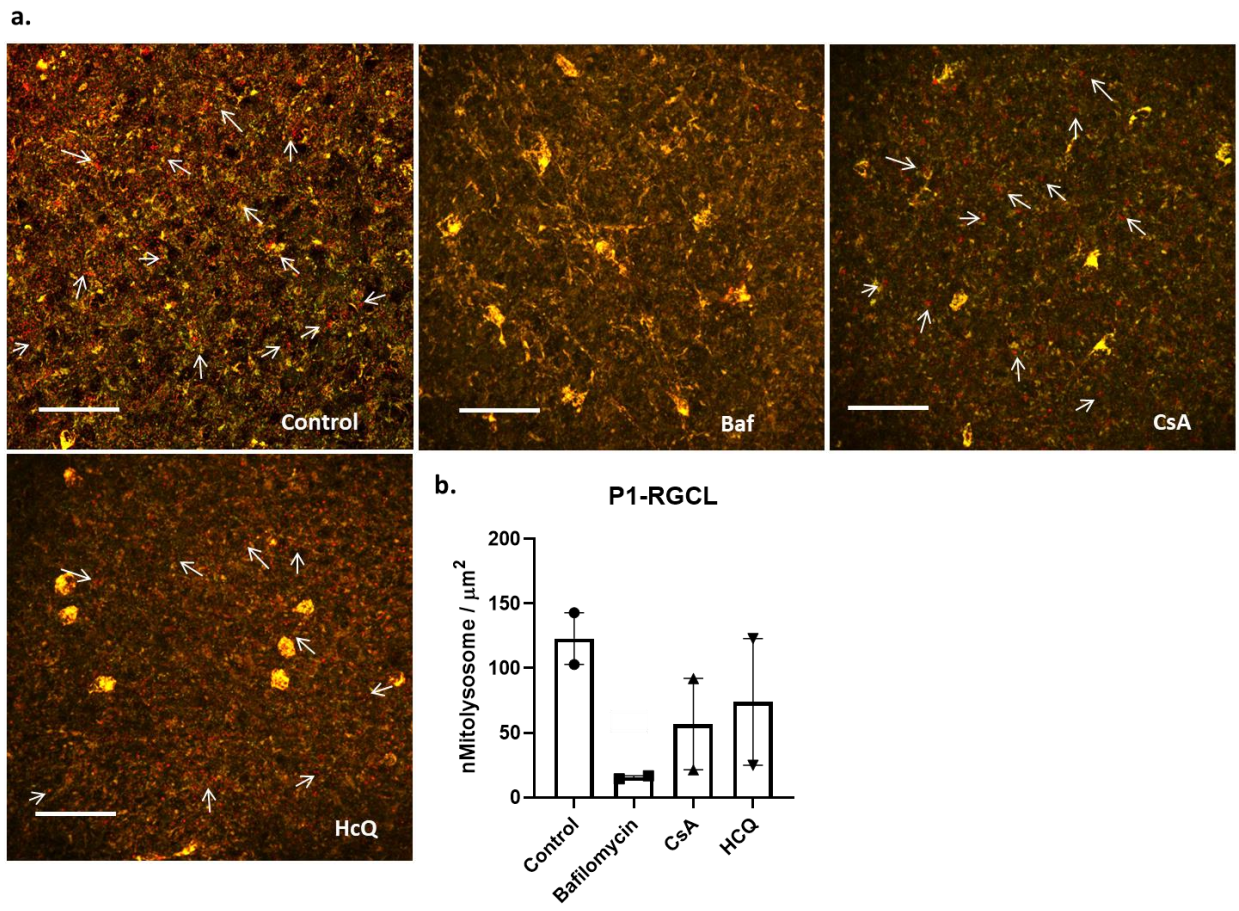

Figure 4.19. Bafilomycin is the inhibitor that decreases the levels of mitophagy in P1 retinas *ex vivo* the most. a. MitoQC reporter expression in retinal ganglion cell layer (RGCL) of flat-mounted retinas of P1 MitoQC mice with Baf, CsA, HcQ, treatments for 6 hours. **b.** Graphical presentation of mitophagy levels in entire P1 retinas after 6 h of treatments. Scale bars=25 µm. (n=2).

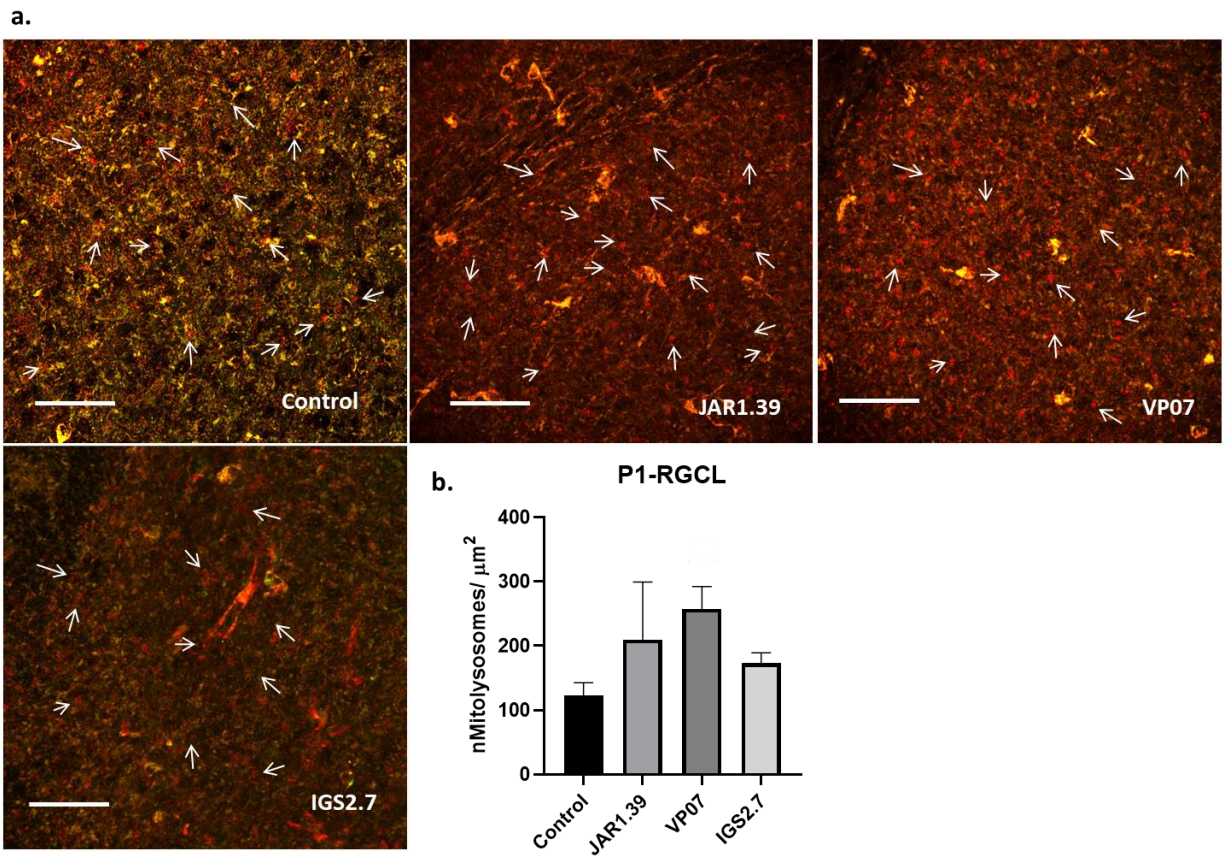

Figure 4.20. VP07 and JAR1.39 induce mitophagy levels in P1 retinal ganglion cell layer (RGCL) flatmounts. a. MitoQC reporter expression in RGCL of flat-mounted retinas of P1 MitoQC mice with JAR1.39, VP07 and IGS2.7 treatments for 6 hours. b**.** Graphical presentation of mitophagy levels in RGCL of P1 retinas after 6 h of treatments. Scale bars= 25 µm. (n=2).

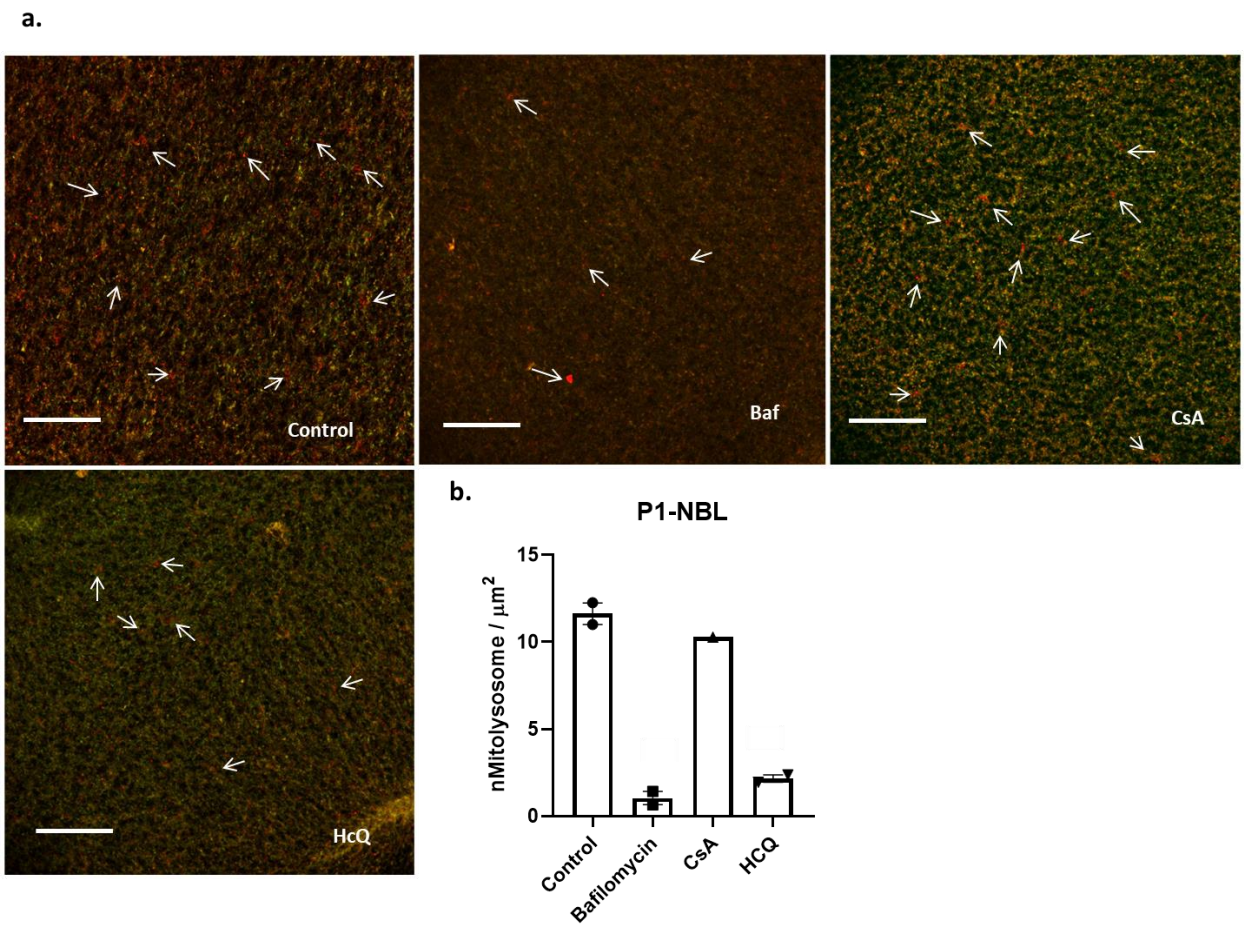

Figure 4.21. Bafilomycin is the most effective inhibitor of mitophagy in the P1 retina's neuroblast layer (NbL) *ex vivo*. a. MitoQC reporter expression in RGCL of flat-mounted retinas of P1 MitoQC mice with Baf, CsA, HcQ, treatments for 6 hours. b. Graphical presentation of mitophagy levels in NbL of P1 retinas after 6 h of treatments. Scale bars 25 µm. (n=2).

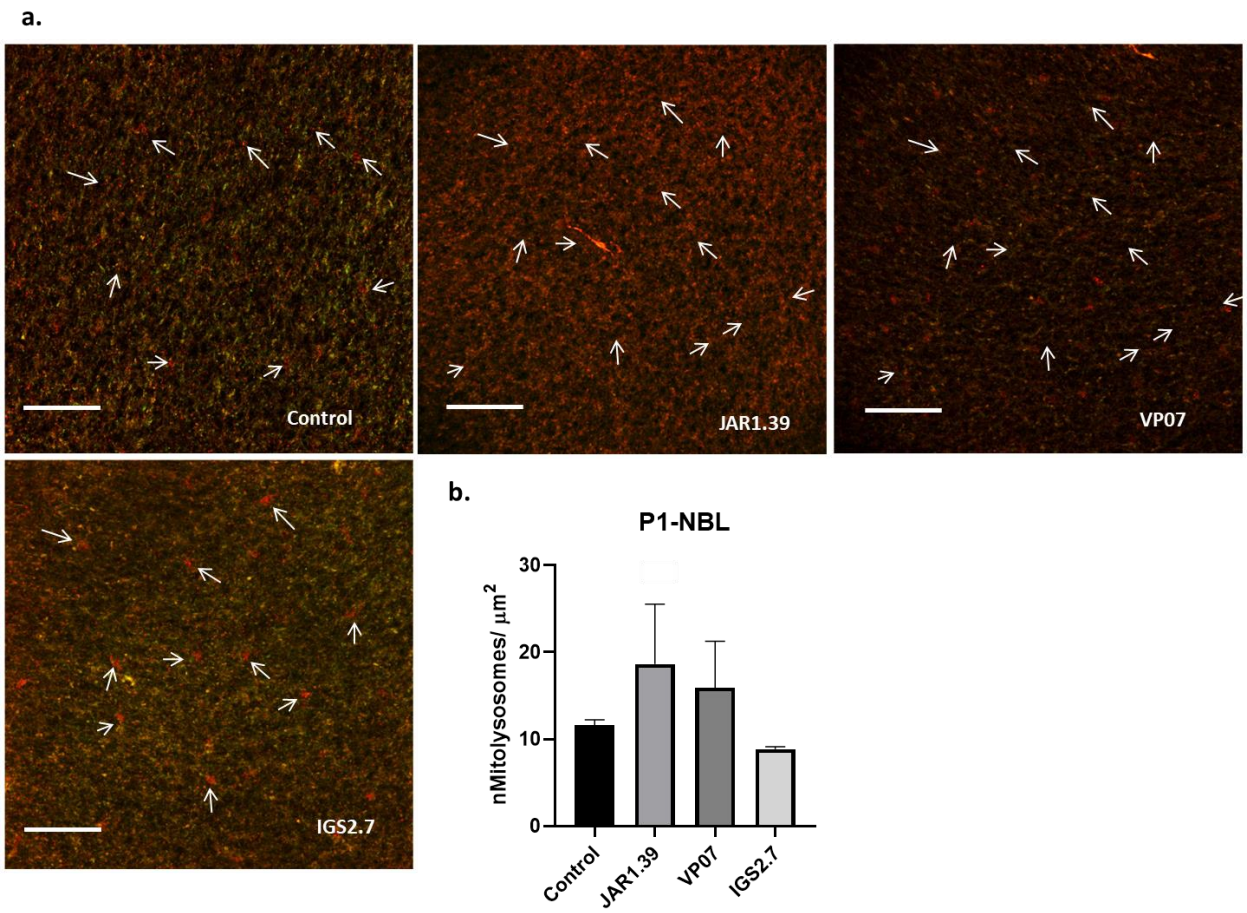

Figure 4.22. JAR1.39 increases mitophagy levels in P1 neuroblast layer (NbL) flatmounts. a. MitoQC reporter expression in NbL of flat-mounted retinas of P1 MitoQC mice with JAR1.39, VP07 and IGS2.7 treatments for 6 hours. **b.** Graphical presentation of mitophagy levels in NbL of P1 retinas after 6 h of treatments. Scale bars 25 µm. (n=2).

In contrast to CsA, HCQ had a greater effect on mitophagy inhibition in the NbL while having no effect in the RGCL. VP07 and JAR1.39, two compounds from MBC chemical library, surprisingly, promoted mitophagy in the whole retina (both RGCL and NbL) (Figure 4.20; Figure 4.22.). Our results indicate that bafilomycin has a significant inhibitory impact across the retina, while CsA inhibits mitophagy in the RGCL and HCQ inhibits NbL mitophagy.

In conclusion our data show that Bafilomycin has managed to significantly reduce the levels of mitophagy in both RGCL and NbL. On the other hand, HcQ had a stronger effect in the NbL and CsA in the RGCL. Interestingly VP07 and JAR1.39 were able to induce mitophagy to a certain degree in both layers.

4.3. Study of mitophagy in the zebrafish retina

4.3.1. Mitophagy in the retina and its relationship with cell death during embryonic development in zebrafish

The zebrafish eye's early development has already been detailed in detail (Schmitt and Dowling, 1994). Ganglion cells are the first neurons to be formed in the zebrafish retina, much as they are in other vertebrates (Nawrocki, 1985; reviewed by Altshuler et al., 1991). At 36 hpf, none of the neuronal cell layers can be identified (Figure 4.23.). The overwhelming majority of neurons in the central retina have already been born by 60 hpf and are arranged into three nuclear layers divided by two plexiform layers (Nawrocki, 1985). The zebrafish retina's photoreceptor cell layer includes five kinds of photoreceptors: rods, short single cones, long single cones, and long and short components of the double cone pair (Branchek and Bremiller, 1984). By 12 dpf, all photoreceptor types can be identified using morphological criteria (Branchek and Bremiller, 1984). Mitophagy reporter zebrafish offers the unique ability to illuminate and measure *in vivo* mitophagy trafficking and subcellular dynamics. In a recent study, they show widespread basal mitophagy in many organs during development, including the retina (Wrighton et al., 2021). However, the level of mitophagy in the retina was not studied in detail. In this study, we look at how the levels of mitophagy vary throughout the process of retinogenesis. In this thesis, we used a stable transgenic zebrafish (Danio rerio) line that expresses the mitophagy reporter cytochrome c oxidase subunit 8A (Cox8A)-GFP-mCherry in the same manner as the MitoQC (Jung Kim et al., 2008; Princely Abudu et al., 2019). We will refer to this line as MitoFish from here on.

As found in the mouse retina, very low levels of mitophagy were detected in the zebrafish at 24 hpf (Figure 4.24.). Interestingly, there is a peak in mitophagy at the ages of 36 hpf and 48 hpf (Figure 4.25.) this is the moment when the RGCL and INL are formed and the ONL begins to form, that is also the time point in which we have the highest BNIP3 protein expression (Figure 4.24.; Figure 4.29.). Mitophagy levels begin to decline at 72 hpf, when the retinal layers are fully formed (Figure 4.24.; Figure 4.25.). However, mitophagy increases again at 92 hpf and then decreases again at 120 hpf. Coincidentally,

the similar pattern can be seen in graphical representations of mitophagy activity in both NbL and RGCL, albeit the decreases are more pronounced (Figure 4.24.; Figure 4.25.).

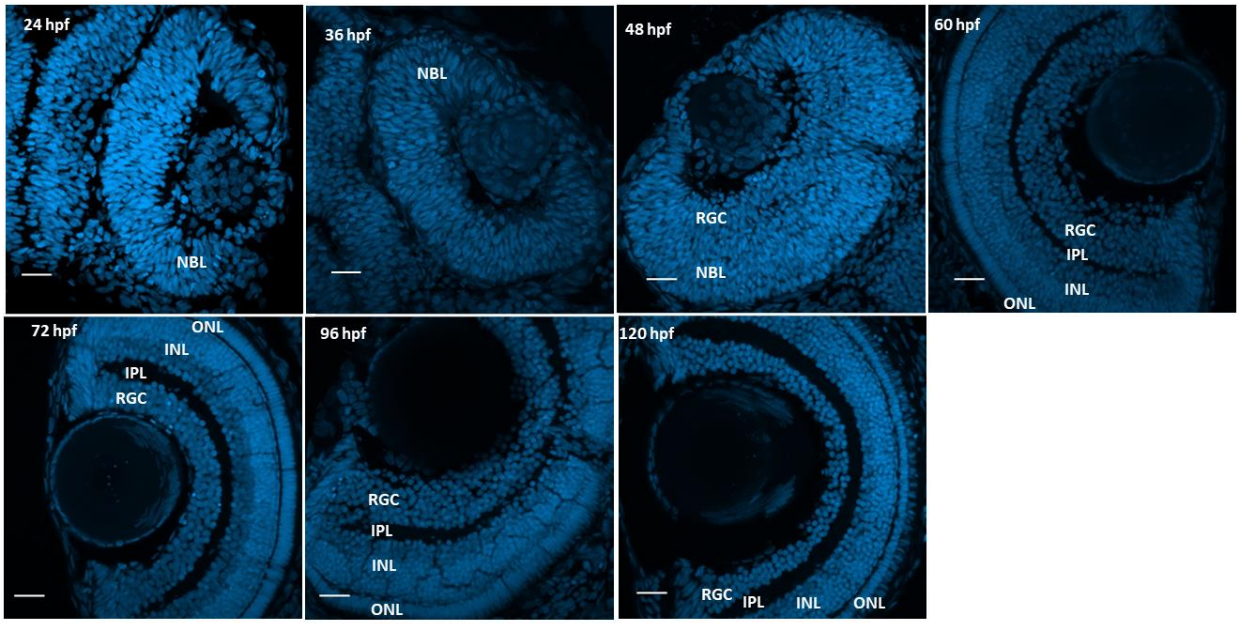

Figure 4.23. Development of wild-type zebrafish eye. At 24 hpf and 36 hpf retinal cells do not form distinct layers. Three nuclear and two plexiform layers are already visible at 60 hpf. At 72 hpf the retinal stratification is well developed. RGC, retinal ganglion cell layer; INL, inner nuclear layer; IPL, inner plexiform layer; OPL, outer plexiform layer; PCL, photoreceptor cell layer. This basic laminar pattern is preserved into adulthood. Scale bars 25 μm.

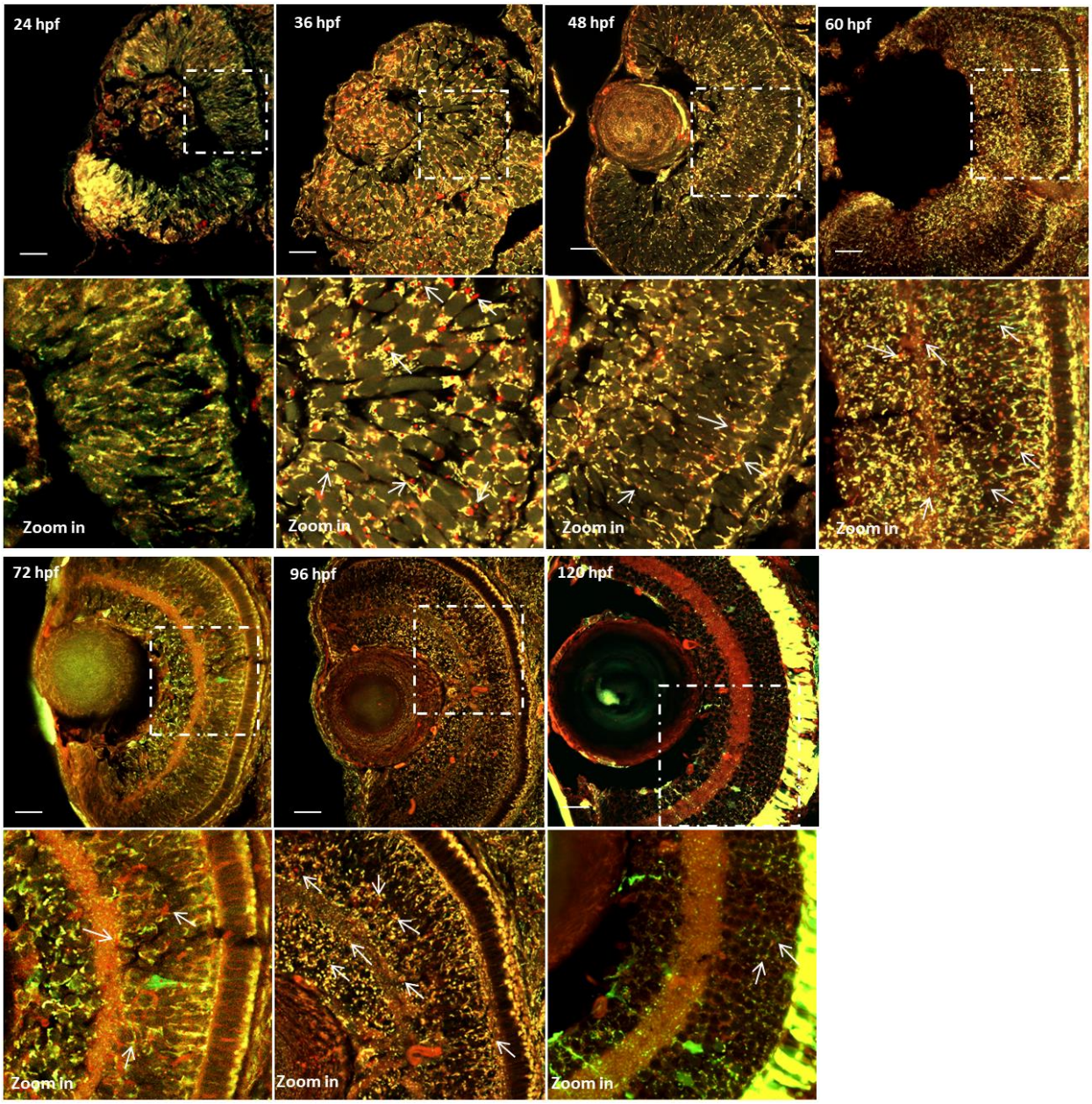

Figure 4.24. Basal mitophagy is widespread in developing zebrafish retinas. a. confocal images of Mitofish larvae at the indicated developmental time points, displaying developing retinas. Green indicates EGFP mitochondria, which are healthy, and red indicates mCherry puncta, representing mitolysosomes (mitophagy). Scale bars 25 μm. (n=4).

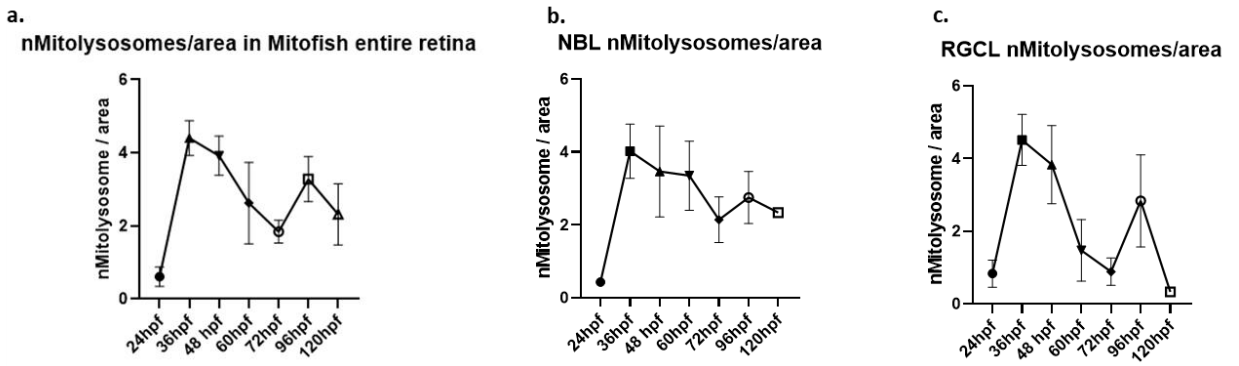

Figure 4.25. Graphical representation of mitophagy levels throughout Mitofish retina development **a.** Quantification of number of mitolysosomes all divided by the total tissue (ROI) volume. **b**. Quantification of number of mitolysosomes all divided by the total NbL (ROI) volume. **c.** Quantification of number of mitolysosomes all divided by the total RGCL (ROI) volume. Kruskal-Wallis Ordinary one-way ANOVA statistical test. (mean + SEM). (n=4).

In mammalian development, apoptosis spreads over the retina in consecutive waves and induces a remarkable amount of cell loss. As the zebrafish is of growing importance as a model for retinal development and for degenerative retinal diseases, we examined the onset and time course of apoptosis in the developing zebrafish retina and in adult fish. Previous research indicates that the start and time course of apoptosis in the RGCL and INL of the zebrafish is similar to those of other vertebrates.

In our study TUNEL-positive cells were detected in all retinal layers (GCL, INL, and ONL) at all developmental phases studied from 24 hpf to 120 hpf, but only in the ONL and GCL occasionally. At 2 dpf, the RGCL in the retina of larval zebrafish begins to separate from the neuroblast layer by the successively developing inner plexiform layer (IPL; Schmitt and Dowling 1999). As a result, the different retinal layers in retinal slices from embryonic stages anterior to 2 dpf cannot be recognized histologically. We found that apoptosis peaked in the entire retina in three developmental stages followed by a second, but clearly smaller wave at 6-7 dpf. Cell death was observed in all layers of the retina at 24 hpf (Figure 4.26.; Figure 4.27.), as well as on the subquential day, 48 hpf, when a peak in apoptosis was recorded (Figure 4.26.; Figure 4.27.). TUNEL- positive cells can be detected exclusively in the INL at 60 hpf, while cell death can be found in both the INL and the RGCL at 72 hpf (Figure 4.26.; Figure 4.27.). On 96 hpf TUNEL-positive cells are recorded in both INL and RGCL, at this age there is the third peak in

cell death and at this is the moment when both RGCL and INL have the greatest apoptosis percentage (Figure 4.26.; Figure 4.27.).

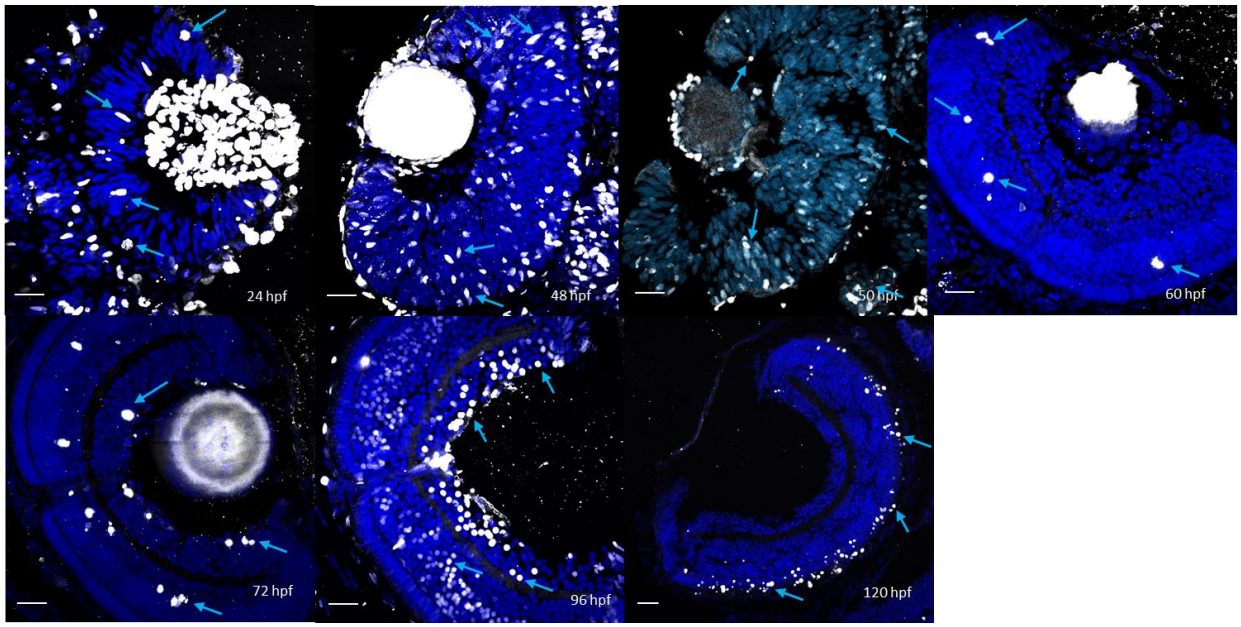

Figure 4.26. Progression of apoptosis in the developing zebrafish retina a. TUNEL labelling (white nuclei) of sections of larval zebrafish eyes at various developmental stages (dorsal up). Arrows in cyan indicate TUNEL positive cells. Scale bars 25 µm. (n=3).

a.

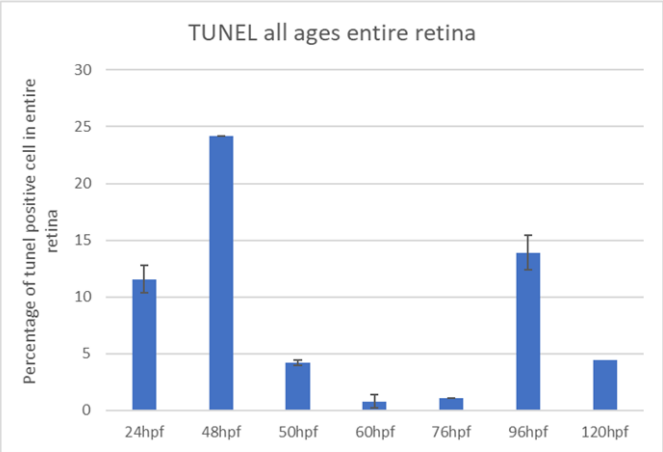

b.

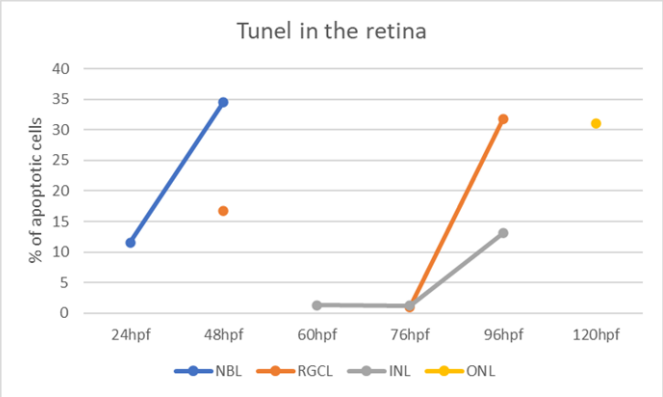

Figure 4.27. Apoptosis progression in the developing zebrafish retina. a. Changes in the number of apoptotic cells in the entire retina (bars total number of TUNEL-positive cells at the various developmental stages counted in 14-µm-thick sections) **b.** Rate of apoptosis in the neuroblast layer (NbL), outer nuclear (ONL), inner nuclear (INL) and ganglion cell layer (GCL) of the zebrafish retina at various developmental stages. Graphs show the percentage of TUNEL-positive cells. (mean + SEM). (n=3)

Apoptosis in the outer nuclear layer (ONL) started and peaked at 120 hpf. This late-onset high peak of apoptosis of photoreceptors is different from that of all other species examined to date. However, there was also cell death in the marginal zone of the INL and RGCL. It is worth noting that the mitophagy peaks coincide with the apoptosis peaks. At 48 hpf, we see a peak in mitophagy, which corresponds to cell death, followed by another peak in mitophagy at 96 hpf, which corresponds to cell death. At these two developmental stages, we demonstrated that the red punctae correspond to TUNEL-positive cells (Figure 4.28.). In conclusion, we see a peak in cell death at 48 hpf, predominantly in the NbL, followed by another peak at 96 hpf, in both INL and RGCL. Finally, at 120 hpf, we see cell death only in the ONL.

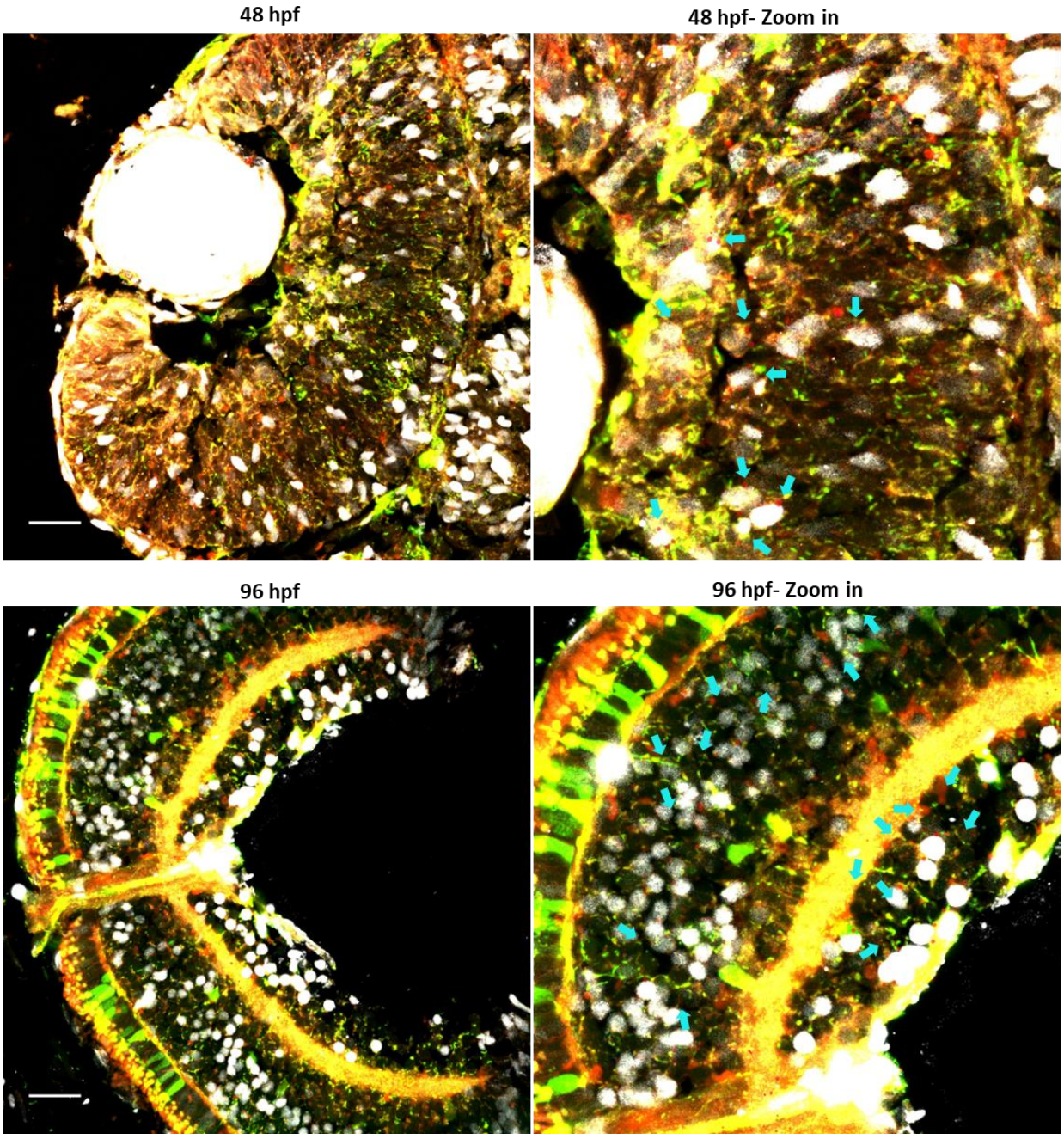

Figure 4.28. The role of mitophagy in regulating cell death in the developing zebrafish retina a. TUNEL labelling of sections of larval MitoQC zebrafish eyes at developmental stages with highest cell death percentage (dorsal up). Arrows in cyan indicate TUNEL positive cells with red punctae. Scale bars 25 μm.

To get a better understanding of how mitophagy evolves throughout zebrafish retinogenesis, we examined how the protein levels of mitophagy-related proteins vary. The proteins whose levels we tested were, COX IV, Component of cytochrome c oxidase,

the last enzyme in the mitochondrial electron transport chain responsible for oxidative phosphorylation. NIPSNAP1, a mitochondrial matrix protein that accumulates on the outer mitochondrial membrane after depolarization of the mitochondria, engaging autophagy receptors and adaptors, as well as human Atg8 (autophagy-related 8)-family proteins, to promote mitophagy. PRKCD (Protein Kinase C Delta) a regulator of Parkin-independent mitophagy which is not essential for Parkin-dependent mitophagy or starvation-induced autophagy. PRKCD kinase is present on mitochondria and its activity is needed for effective mitophagy *in vitro*. The translocase of the inner membrane23 (TIM23), a protein complex located in the inner mitochondrial membrane of the mitochondria that enables matrix-targeted protein translocation into the mitochondrial matrix. And finally, BNIP3, protein related to the BH3-only family, that regulates mitophagy in response to hypoxia. Western blot results show that Bnip3 and CoxIV levels decrease as the MitoQC Zebrafish grows (Figure 4.29.). We also observe an increase in Nipsnap and Prkcd concentrations (Figure 4.29.). This may imply that Parkin independent mitophagy is important throughout development and then changes for Parkin dependent mitophagy.

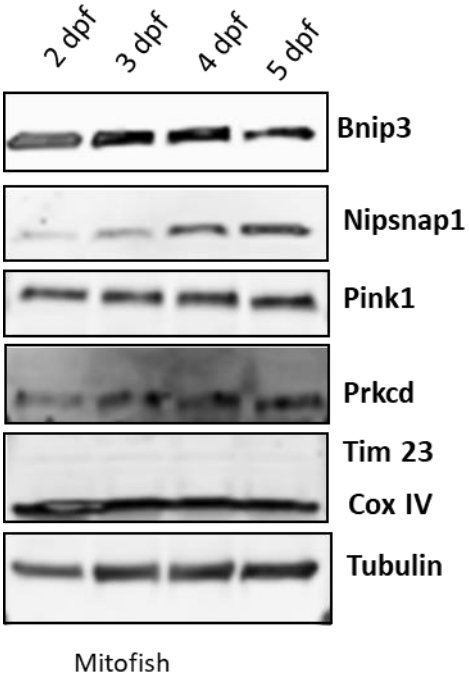

Figure 4.29. Changes of protein expression levels of Bnip3, Nipsnap1, Pink1, Prkcd, Tim23, CoxIV and Tubulin in the eye at various developmental days. Western blot assay showing protein expression in MitoQC zebrafish eyes.

We first investigated the transcriptional profile of several mitophagy regulators in the zebrafish eyes during development to get a better understanding of our results. Unlike the mouse, the zebrafish contains two homologues of the *nix* gene: *bnip3la (nix)* and *bnip3lb (nip3a)*. As the eye developed, the levels of both *bnip3la* and *bnip3lb* homologues increased. The *optn* and *pink1* genes exhibit the same trajectory. *Fundc1 and hif1* mRNA levels, on the other hand, decrease after 4 dpf (Figure 4.30.).

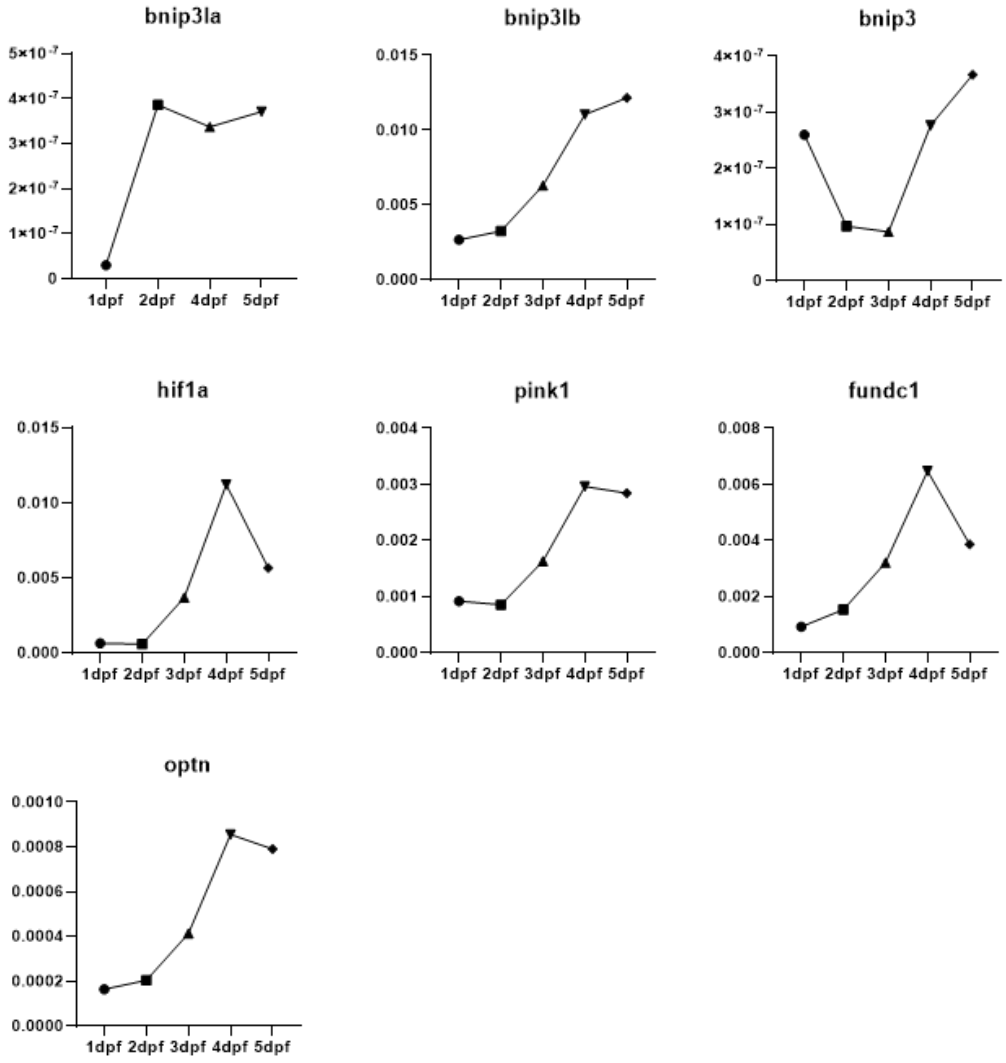

Figure 4.30. mRNA expression levels of mitophagy and mitochondria related genes was detected by real-time PCR. The levels of *bnip3la* and *bnip3lb* homologues increased with the development of the eye. The optn and pink1 genes acted similarly throughout retinal development. On the other hand, *fundc1* and *hif1* mRNA levels fall after 4 dpf**. (**n=1)

4.4. Parkinson´s disease mouse models to analyse mitophagy *in vivo* (MitoQC mice)

To create effective animal models of Parkinson's disease, dopaminergic neurons in the substantia nigra were injected with genes linked with the condition. AAV containing human WT α-syn cDNA causes progressive neurodegeneration and the appearance of α-syn inclusions in the substantia nigra (Lindgren, et al., 2012; Decressac, et al., 2012). Studies demonstrate some loss of TH and robust α-syn expression, that are critical for disease modelling which is why we decided to inject the AAV9-h-α-SYN-A53T into the SN of the MitoQC mouse as the PD model for our studies (results are shown in Sara Castro Sánchez doctorate thesis).

Additionally, the unilaterally lesioned 6-hyroxydopamine (6-OHDA) rat model of Parkinson's disease has been contributory in advancing our understanding of the mechanisms underlying parkinsonian symptoms, as it accurately reproduces the changes in basal ganglia circuitry and pharmacology observed in parkinsonian patients (Blum et al., 2001). This is the second PD model that we selected for our research.

4.4.1. Mitophagy in MitoQC mice injected with 6-OHDA

6-OHDA acts in two ways: it readily generates free radicals and inhibits the mitochondrial respiratory chain complexes I and IV. It also induces mitochondrial membrane permeabilization and causes mitochondrial fragmentation through a process involving the mitochondrial fission machinery, resulting in Drp1 translocation from the cytosol to the mitochondria (GomezLazaro et al., 2008). The connection between 6-OHDA and mitochondrial damage is still debatable, therefore we were eager to examine the results of our MitoQC mice Parkinson's disease model.

4.4.1.2. Mitophagy in dopaminergic neurons

6-OHDA is transported through the same catecholamine transporter as dopamine and accumulates in the cytosol, resulting in neurotoxicity (Luthman et al. 1989; Gonzalez-Hernandez et al. 2004). Because 6-OHDA does not pass the blood-brain barrier, it is possible to induce a toxic impact in the central nervous system through stereotaxic surgery. The animal was placed in the stereotaxic apparatus and bregma and lambda were identified. An injecting cannula was then loaded onto the holder of the stereotaxic

apparatus and placed over the specified target according to predetermined coordinates. Unilateral 6-OHDA lesions were made in the striatum (right hemisphere of the brain). To begin, we wanted to determine if the surgeries were effective and resulted in the death of dopaminergic neurons in the SN. Immunohistochemical labelling of injected MitoQC brain slices revealed a substantial reduction in dopaminergic cell mass on the injected (ipsilateral) side of the brain (Figure 4.31.). This indicates that the surgeries were successful, and we may now continue to monitor the mitophagy level in our PD model.

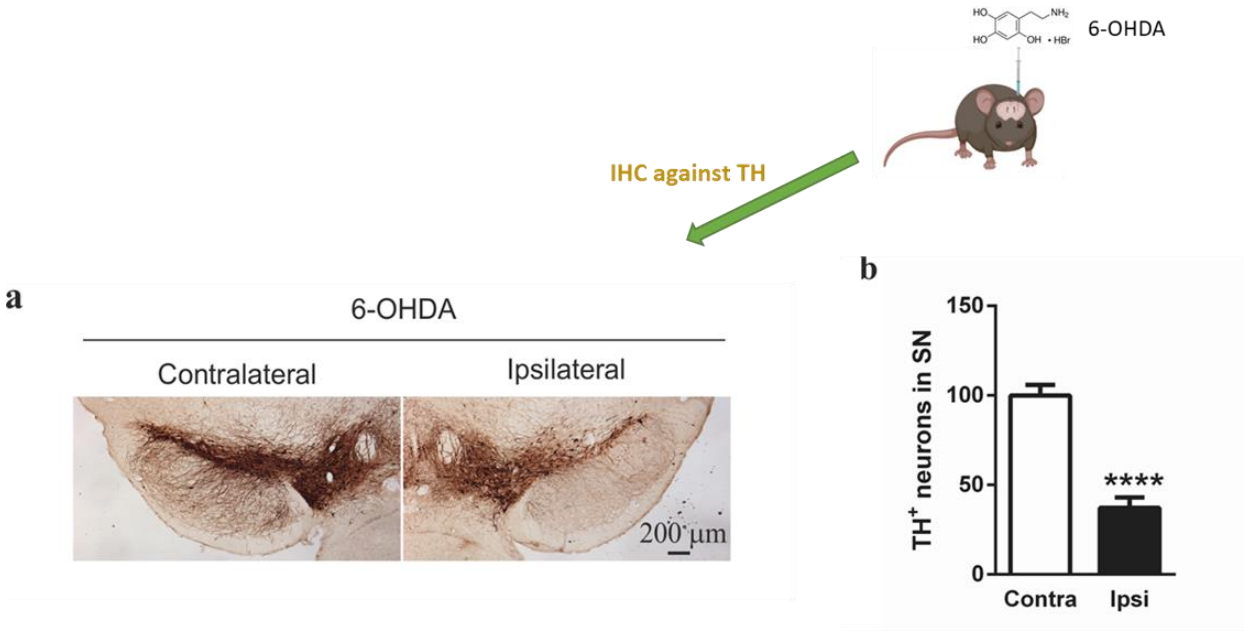

Figure 4.31. 6-OHDA administration in the SN causes neurodegeneration in the nigrostriatal tract. a. Immunohistochemical staining of the injected (ipsilateral), right SN for TH+ dopaminergic neurons and vehicle (contralateral), left SN for TH+ dopaminergic neurons. 2 weeks after administration of 6-OHDA into the SN a significant difference of TH+ dopaminergic neuronal cell number is visible comparing vehicle to 6-OHDA treated mice **b.** Analysis of degeneration of dopaminergic neurons in SN of MitoQC mice injected with 6-OHDA. 6-OHDA (black bar) induces a significant reduction of TH+ neurons as compared to vehicle mice (white bar). Mann-Whitney U Test. (mean ± SEM). (n=5).

We next imaged the SNPC and cuantified the number of red dtos indicative of mitohagy. Our data show that the effect of 6-OHDA on the mitophagy of dopaminergic neurons was significantly reduced (Figure 4.32.). Knowing that 6-OHDA has the same effect on mitophagy in dopaminergic neurons as A53T α- syn, we wanted to know what effect it had on the astrocytes of these mice.

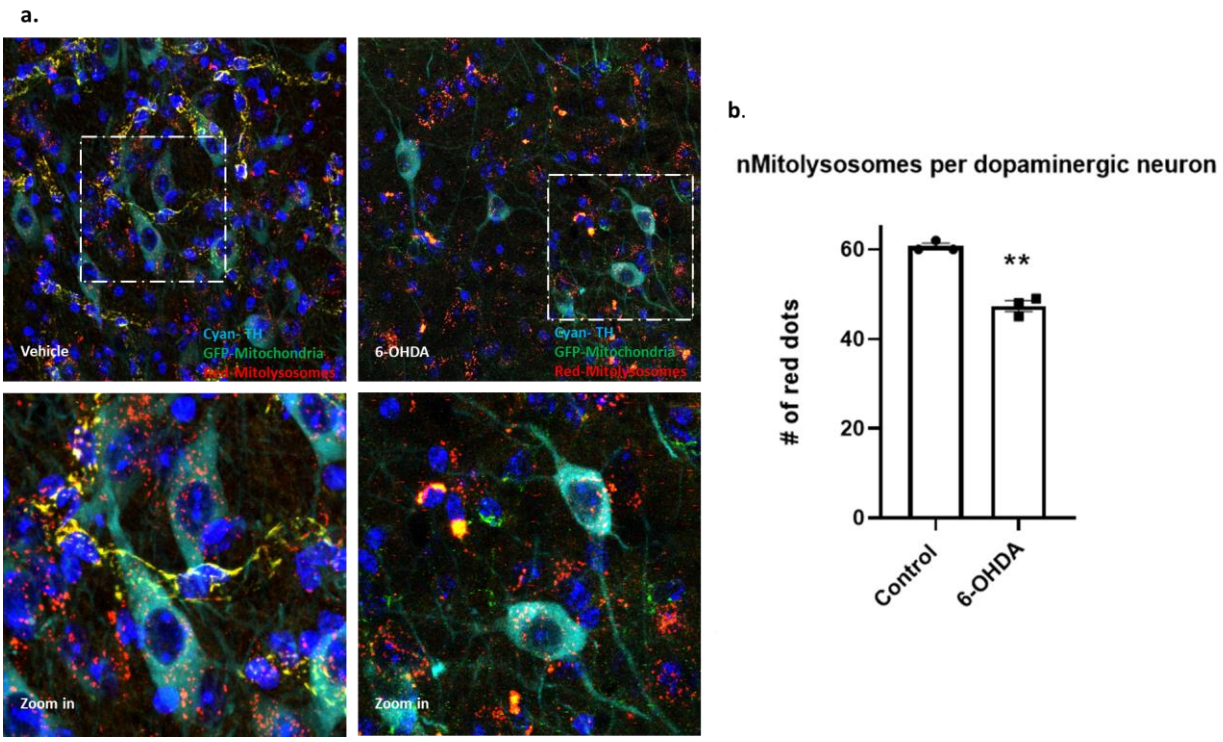

Figure 4.32. Mitophagy is decreased in TH+ neurons of SN after 6-OHDA injection in MitoQC mice. a. Immunofluorescence of TH in MitoQC SNpC sections, where red dots are indicative of mitophagy. On the right side are the images of the contralateral (control) side of the brain, and on the right side are the images of the ipsilateral (6-OHDA injected side of the brain. b. Graphical representation of 6-OHDA (right bar) decreases mitophagy levels significantly as compared to vehicle mice (left bar). Mann-Whitney U Test (mean ± SEM). (n=5).

4.4.1.3. Mitophagy in astrocytes

Astrocytes and astrocyte-related proteins play important roles in maintaining normal brain function, and also regulate pathological processes in brain diseases and injury. A recent study provided compelling evidence that transneuronal mitophagy occurs *in vivo* in Parkinson's disease models (Morales et al., 2020) and that astrocytes are the main cell type responsible for the clearance of damaged mitochondria. Remarkably, PINK1 activity was recently shown to be predominant in astrocytes but virtually non-existent in neurons (Barodia et al., 2019). With all of this research highlighting the significance of astrocytes, we were interested to investigate how mitophagy was affected in our PD model. Given the importance of brain processes that rely on proper astrocyte-neuron connections, certain pathological conditions are triggered by a malfunction or failure in this process at some level (Halliday and Stevens, 2011; Sathe et al., 2012). Because astrocytes play an important role in disease progression, we examined the degree of mitophagy in our 6-

OHDA MitoQC model. Mitophagy levels were found to be substantially higher in the astrocytes of the 6-OHDA MitoQC model (Figure 4.33.).

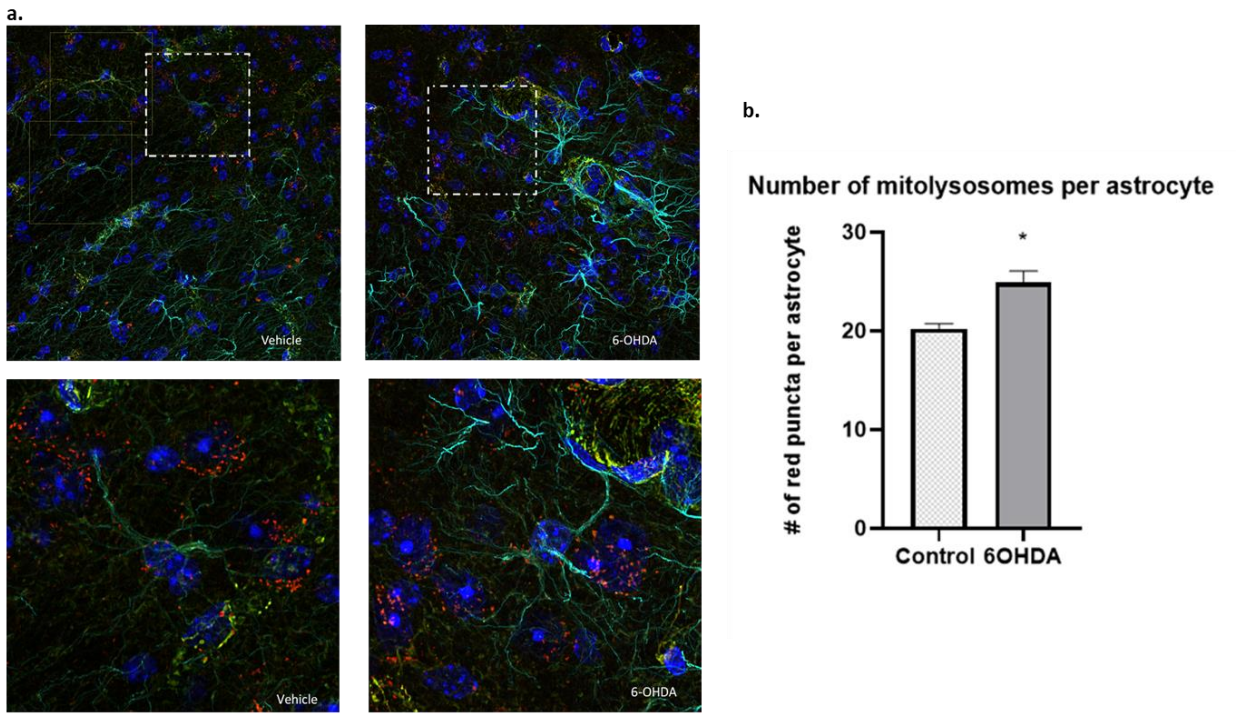

Figure 4.33. Mitophagy is increased in astrocytes of SN after 6-OHDA injection in MitoQC mice. a. Immunofluorescence of GFAP in MitoQC SNpC sections, where red dots are indicative of mitophagy. On the right side are the images of the contralateral (control) side of the brain, and on the right side are the images of the ipsilateral (6-OHDA injected side of the brain). **b.** Graphical representation of 6-OHDA (right bar) induces mitophagy significantly as compared to vehicle mice (left bar) (mean ± SEM). All images were taken at Leica SP8 with a 63x objective. Mann-Whitney U Test (mean ± SEM). (n=4).

Given that dopaminergic neurons and astrocytes reacted differentially to 6-OHDA injections, we examined the gene expression levels in the SNpC. Interestingly, *CoxIV* levels rose substantially in the 6-OHDA injected side of the brain whereas other mitochondria or mitophagy associated genes (*Nix, Bnip3, Pgc1α,* and *Tomm20*) remained unchanged (Figure 4.34.). This implies that, although mitophagy was affected in the same manner in both PD models, the molecular mechanisms underlying these two PD models are distinct.

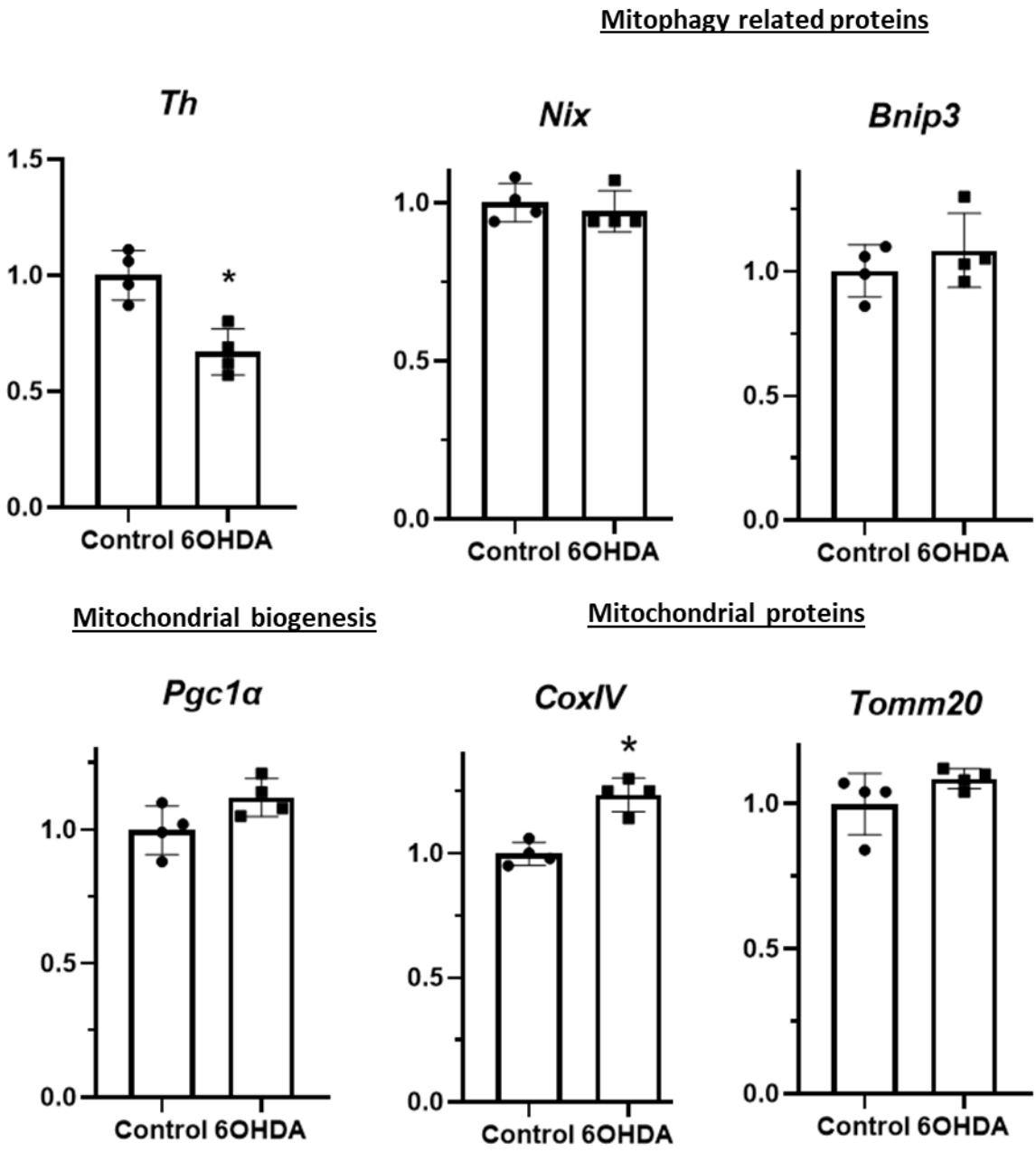

Figure 4.34. 6-OHDA increases the expression of cox IV mitochondrial protein in SN of MitoQC mice. **a.** The expression of th, pgc1α, coxIV, tomm20, nix and bnip3 in the SN after AAV9-h-α-SYN-A53T injection. (n = 4).

4.4.1.4. Mitophagy in microglia

Given that 6-OHDA had a distinct impact on dopaminergic neurons and astrocytes, we were curious to see how it affected microglia in the SNpC. Microglia are resident macrophages and main immune cells in the CNS and are dynamic, mobile, and watchful

observers of tissue injury or infection, and hence play a critical role in parenchymal homeostasis maintenance (Nimmerjahn et al., 2005). Microglia have received considerable attention in PD and other neurodegenerative illnesses due to their activities as immune mediators, particularly their propensity to trigger neuroinflammation in response to pro-inflammatory chemicals. Both neuroinflammation and mitochondrial dysfunction have been implicated in the etiology of Parkinson's disease.

Damaged or defective mitochondria may further prolong inflammatory reactions by producing ROS or releasing mitochondrial damage-associated molecular patterns (DAMPs). Thus, microglia may be predisposed to an inflammatory phenotype in the absence of normal mitochondrial activity (Nakahira et al., 2011; Zhong et al., 2016).

When brain tissue is injured, it triggers a local inflammatory response that includes microglial activation. The morphological shift of a microglia from a highly ramified to a less ramified or amoeboid cell shape reflects its activation level. As a result, microglial morphological alterations are routinely used to assess microglial activation and explore their participation in all brain illnesses. In our PD model, the morphological transition from inactivated (Vehicle; Figure 4.35. a) to activated (6-OHDA, Figure 4.35. b) state is clear proving there was in fact an inflammatory response in the 6-OHDA injected side of the brain. Not only did we observe that the microglia were activated but we also saw large red aggregates we have not seen in other cell types of the SNpC (Figure 4.35.). These aggregates could be due to the phagocytosis of the damaged DA neurons or due to horizontal transfer of mitochondria through TNTs, microtubule-based transport methods, and vesicles (Rodriguez et al., 2018).

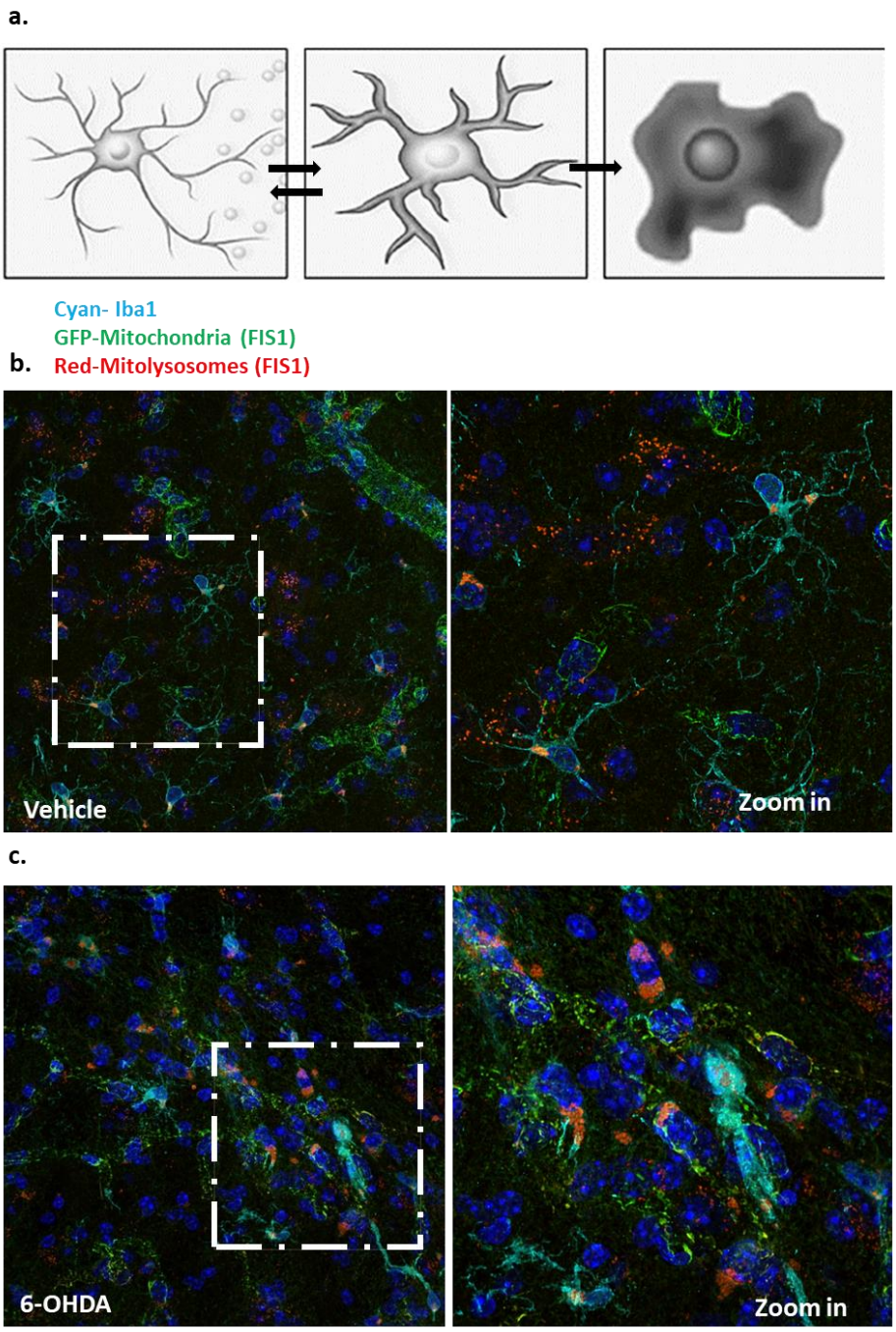

Figure 4.35. Mitophagy in microglia of SN after 6-OHDA injection in MitoQC mice. a. Microglia with activated morphology. Brain microglia schematics demonstrating the morphological phases of microglial activation. Ramified or B resting microglia have lengthy, ramified processes with relatively tiny cell bodies. Bushy morphology is characterized by swelling, shortened processes and expanded cell bodies and is associated with intermediate activation. Amoeboid or "phagocytic" microglia have a rounded macrophage-like shape with no or few processes and are linked with high levels of proinflammatory activity, oxidative free radicals, and microglial death (Kreutzberg 1996; Raivich et al. 1999). **b**. Immunofluorescence of Iba1 in MitoQC SNpC sections, where red dots are indicative of mitophagy. The upper images are of the contralateral (control) side of the brain, **c**. and the images bellow of the ipsilateral (6-OHDA injected side of the brain).

In conclusion 6-OHDA reduced the level of mitophagy in the dopaminergic neurons while increasing it in astrocytes. We see a considerable decrease in the number of dopaminergic neurons in the injected side of the brain's SNpC. All of these factors may contribute to the activation of microglia, as seen by their activated morphology.

4.5. Parkinson´s disease cell models to analyse mitophagy *in vitro*

To facilitate understanding of the molecular mechanisms behind our *in vivo* findings. We wanted to explore if we could find a suitable PD *in vitro* model to study mitophagy.

SH-SY5Y cells have been utilized to investigate the molecular and cellular processes behind the effects of certain PD-related toxins, as well as to conduct functional investigations on family PD genes and to evaluate potential protective agents for PD therapy. As a result, this cell line has proven a significant tool in unravelling the molecular complexity of Parkinson's disease. We wanted to see whether the MitoQC SH-SY5Y cell line would be an appropriate *in vitro* model for our study.

4.5.1. MitoQC SH-SY5Y

To the determine if the SH-SY5Y MitoQC cells are the ideal *in vitro* model for our experiments we wanted to see the effect of 6-OHDA as well as the transfection of α-syn on mitophagy. First, we had to determine the working concentrations of 6-OHDA in our PD model. SH-SY5Y cells were exposed to different concentrations of 6-OHDA (15–150 μM) during 24 h. 6-OHDA had a concentration-dependent impact on the viability of SH-SY5Y cells, as shown in the figure 4.36. The highest neurotoxicity effect was obtained at 200 μM with a cell viability reduction of more than 80%. We chose 15μM and 20μM as our PD model concentrations (Figure 4.36.).

Cells were then treated for 24 hours with two positive controls, DFP and CCCP, as well as different doses of 6-OHDA. Additionally, the cells were transfected with either pHM6-alphasynuclein-WT or pHM6-alphasynuclein-A53T. As expected, both DFP and CCCP managed to significantly induce mitophagy after 24-hour cell culture (Figure 4.37.). Compared to control cells, no change was detected in the mitophagy or mitochondrial network in cells transfected with the empty vector pHM6.

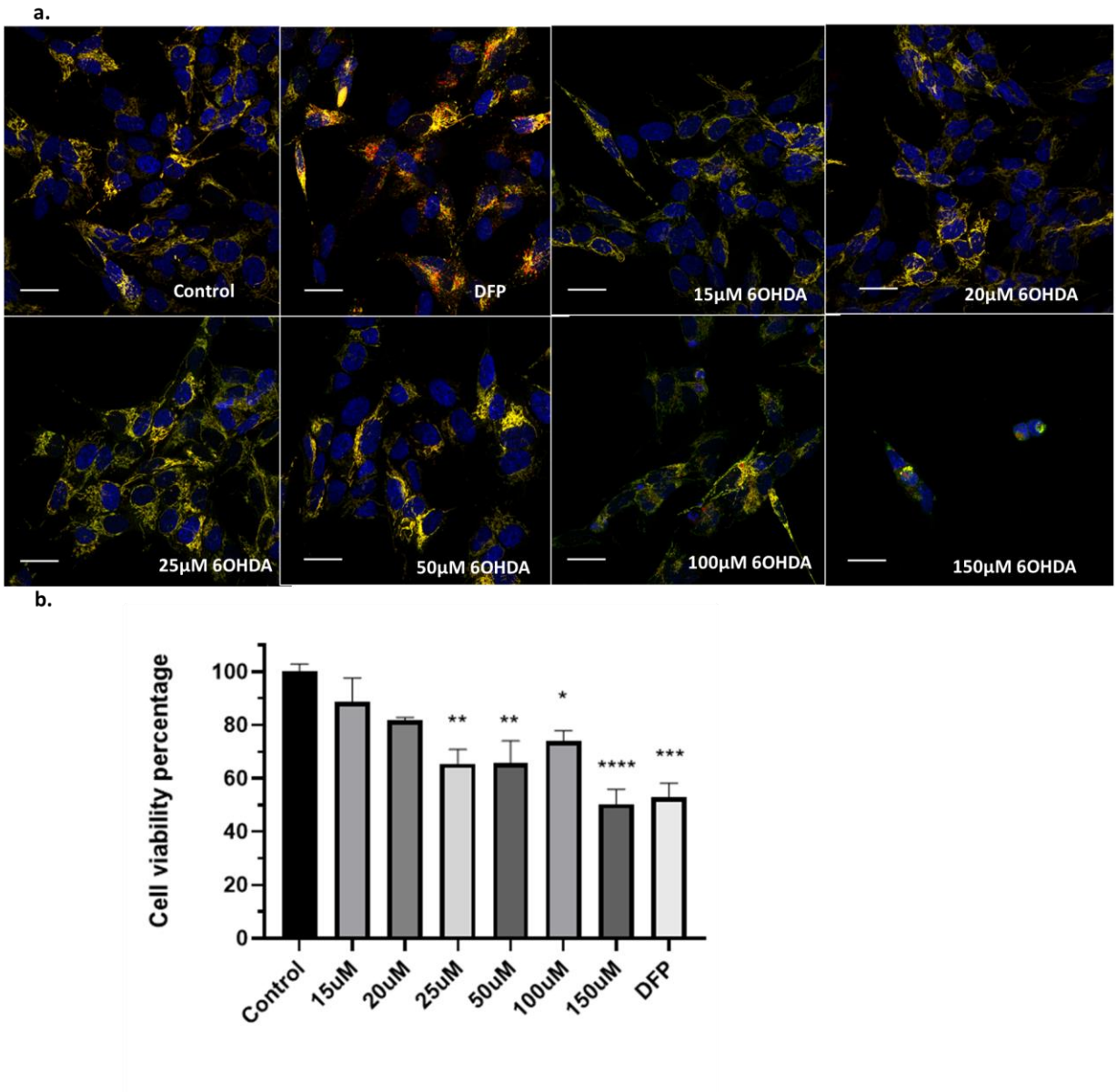

Figure 4.36. Viability assay on SH-SY5Y MitoQC cell lines treated with different concentrations of 6-OHDA. a. Confocal microscopy images showing the effect of increasing concentrations of 6-OHDA on the SH-SY5Y MitoQC cells. **b**. Graph of crystal violet assay after 24 h treatment of SH-SY5Y MitoQC cells and with various concentrations of 6-OHDA. Positive control shows SH-SY5Y MitoQC cells without the exposure to 6-OHDA. The cell viability is expressed as % cell viability in comparison to a positive control. Scale bar = 25µm. (mean ± SEM) (n=3).

Although there was no apparent difference between WT and A53T α-synuclein transfected cells, they did reduce mitophagy levels in comparison to the control (Figure 4.37.). Additionally, the mitochondrial network is obviously disturbed in transfected cells, and mitochondrial mass is lost (Figure 4.38.). Interestingly, 6-OHDA had no impact on

mitophagy levels (Figure 4.37.). With these findings, we were curious to determine if mitophagy is irreversibly impaired or whether it might be restored. To find out, we first transfected the cells with WT and A53T α-synuclein and then continued by treating them with either DFP or CCCP. Curiously, both CCCP and DFP managed to re-establish mitophagy in the transfected SH-SY5Y Mito QC cells, meaning the mitophagy pathway was not compromised when WT or mutated A53T are expressed.

Next, we examined the levels of expression of different mitophagy, and mitochondria associated genes to dig deeper and further explore the molecular pathways impacted by the treatments.

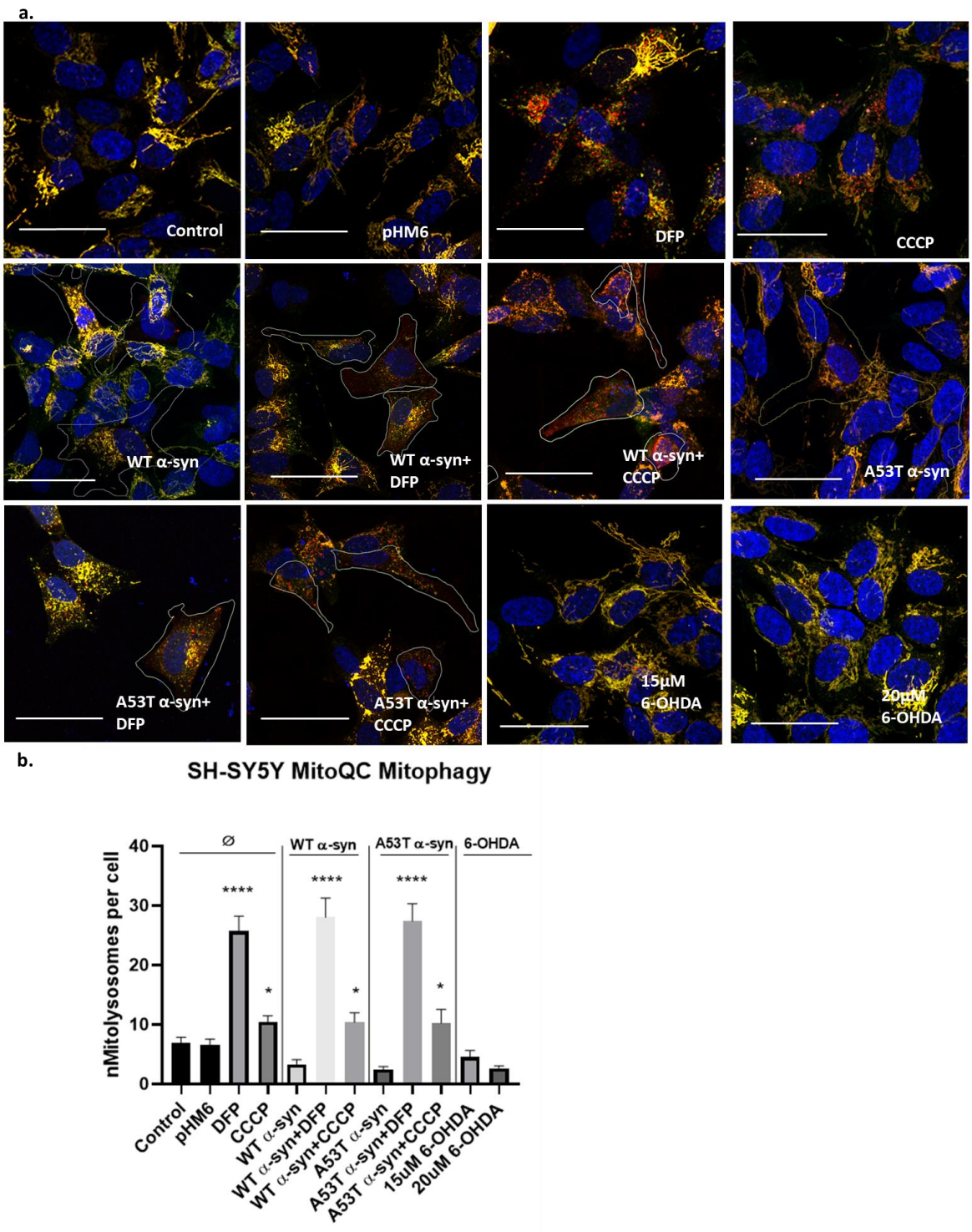

Figure 4.37. MitoQC SH-SY5Y cells treated with 6-OHDA and transfected with α-syn decrease the levels of mitophagy. a. Representative images of SHS Y5Y MitoQC cells after 24-hour treatment with DFP, CCCP or 6-OHDA or α-syn transfection, the nuclei were stained with DAPI. **b.** Graphical representation of the levels of mitophagy after 24-hour treatment with DFP, CCCP or 6-OHDA or α-syn transfection. Ordinary one-way ANOVA statistical tests. (mean ± SEM) Scale bar 25µm. (n=6)

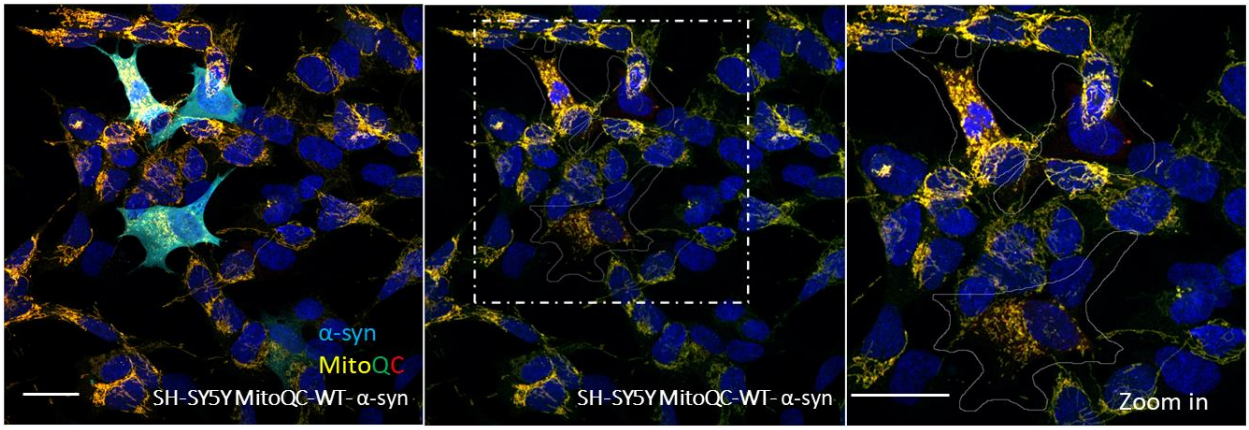

Figure 4.38. Transfected SH-SY5Y cells have clearly disrupted mitochondrial filaments. a. A representative image of the MitoQC SH-SY5Y cell transfected with wt α-syn demonstrates that the mitochondrial network is visibly disrupted and that there is a noticeable loss of mitochondrial mass. Scale bar = 25 µm.

α-syn levels were significantly increased in both wt and mutant A53T α-syn transfected cells, although the rise was not as dramatic in the mutant as in the wt. This may indicate that the mutant α-syn caused more cell death, resulting in less A53T transfected cells in the well. Also, the expression of *pgc1α*, which is a transcriptional coactivator that is a central inducer of mitochondrial biogenesis in cells, was significantly increased in both wt and mutant A53T α-syn transfected cells. As expected, DFP, an iron-chelator that induces mitophagy in response to HIF1-dependent upregulation of *Bnip3* and *Nix*, was able to raise both bnip3 and nix levels significantly (Figure 4.39.). *Mfn2*, *Lamp1*, and *Pink1* were all found to be significantly expressed in wells treated with 20µM 6-OHDA and CCCP. Yet, only CCCP, but not 6-OHDA, was able to increase *Prkn* gene expression, which may explain why we did not detect red dots in the SH-SY5Y MitoQC cells (Figure 4.39.). Mitochondrial protein genes levels, *Tomm20* and *CoxIV*, were not affected by neither of the treatments (Figure 4.39.). In brief, α-syn doesn't have an effect on mitophagy related genes which supports our previous observations. On the other hand, 6-OHDA, had a significant impact on *Mfn2* which supporst the reduced mitophagy and disrupted mitochondrial network. However, it induced the levels of *Lamp1 and Pink1*, but didn't increase the *Prkn* gene expression which could be the reason we dodn't see red punctae in the SH-SY5Y MitoQC cells.

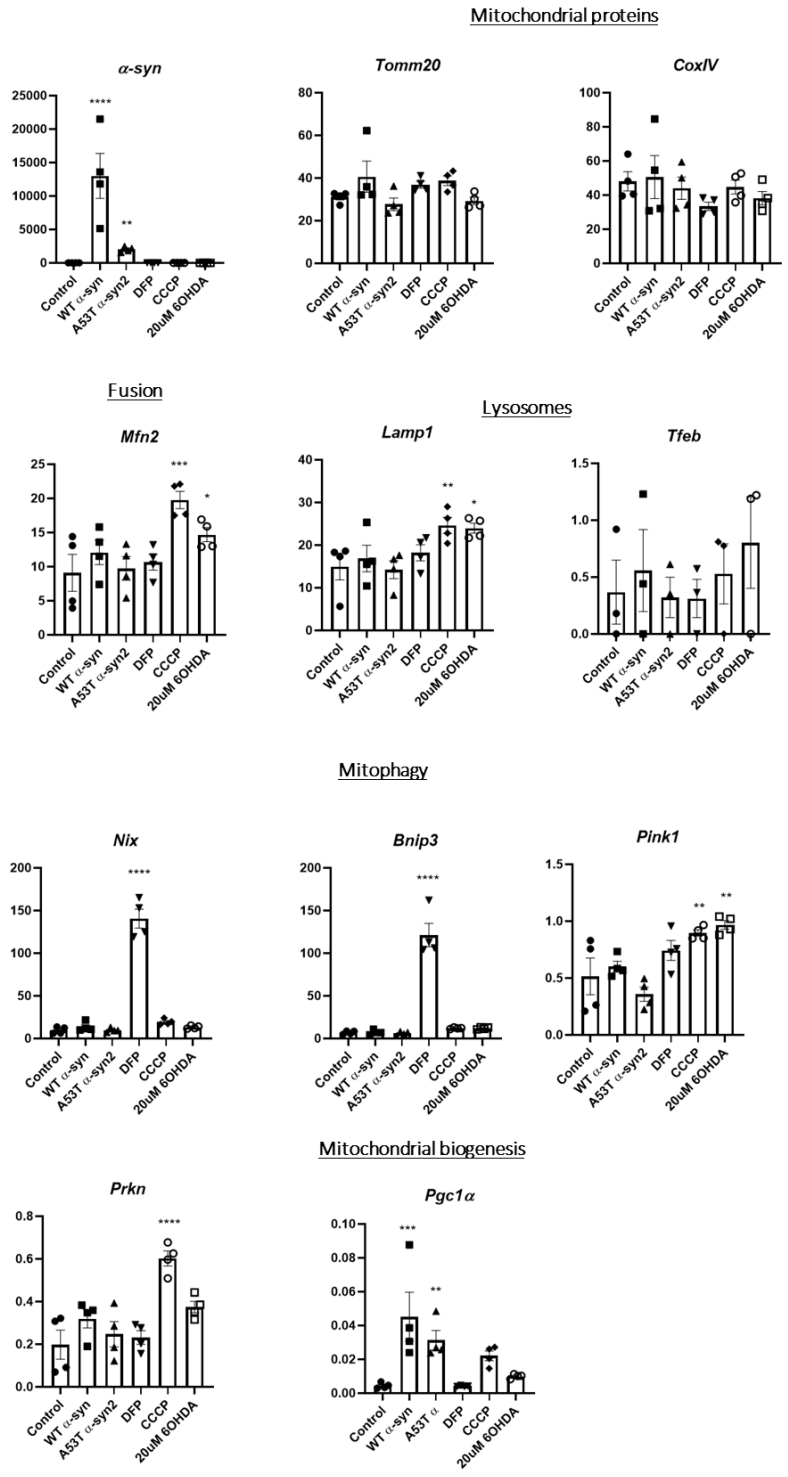

Figure 4.39. α-syn induces the expression of *Pgc1α*, while DFP increases the expression of *Bnip3 and Bnip3l* mitophagy protein genes in MitoQC SH-SY5Y cells. Both CCCP and 6-OHDA enhance mfn2, lamp1, and pink1 levels. a. The expression of *α-syn, Mfn2, Pgc1α, Coxiv, Tomm20, Tomm40, Tfeb, Lamp1, Nix, Bnip3, Pink1, Prkn* in the MitoQC primary astrocyte culture after 24-hour treatment with DFP, CCCP or 6-OHDA or α-syn transfection. Ordinary one-way ANOVA statistics. (mean ± SEM). (n = 4).

4.5.2. Primary astrocyte culture MitoQC

When the α-syn inclusions outnumber the degradation pathway's capacity to handle and eliminate excess α-syn, oxidative stress, mitochondrial damage, and ER stress are triggered (Xu et al., 2005). Despite the apparent significance of α-syn inclusions in astrocytes, most research have focused on dopaminergic neurons, and we now have only a limited grasp of the connection between α-syn and astrocytes. As a result, we investigated the effects of α-syn and 6-OHDA on mitophagy in primary MitoQC astrocytes.

After 24 hours of treatment with CCCP and DFP, MitoQC primary astrocytes exhibit substantially increased mitophagy (Figure 4.40.). Furthermore, when treated with 6-OHDA, they do not exhibit red dots, which indicate mitophagy, but higher concentrations disrupt the mitochondrial network (Figure 4.40.). In addition, cultured primary astrocytes transfected with α-syn exhibit an irregular morphology with long and rich processes and accumulate α-syn but lack mitophagy.

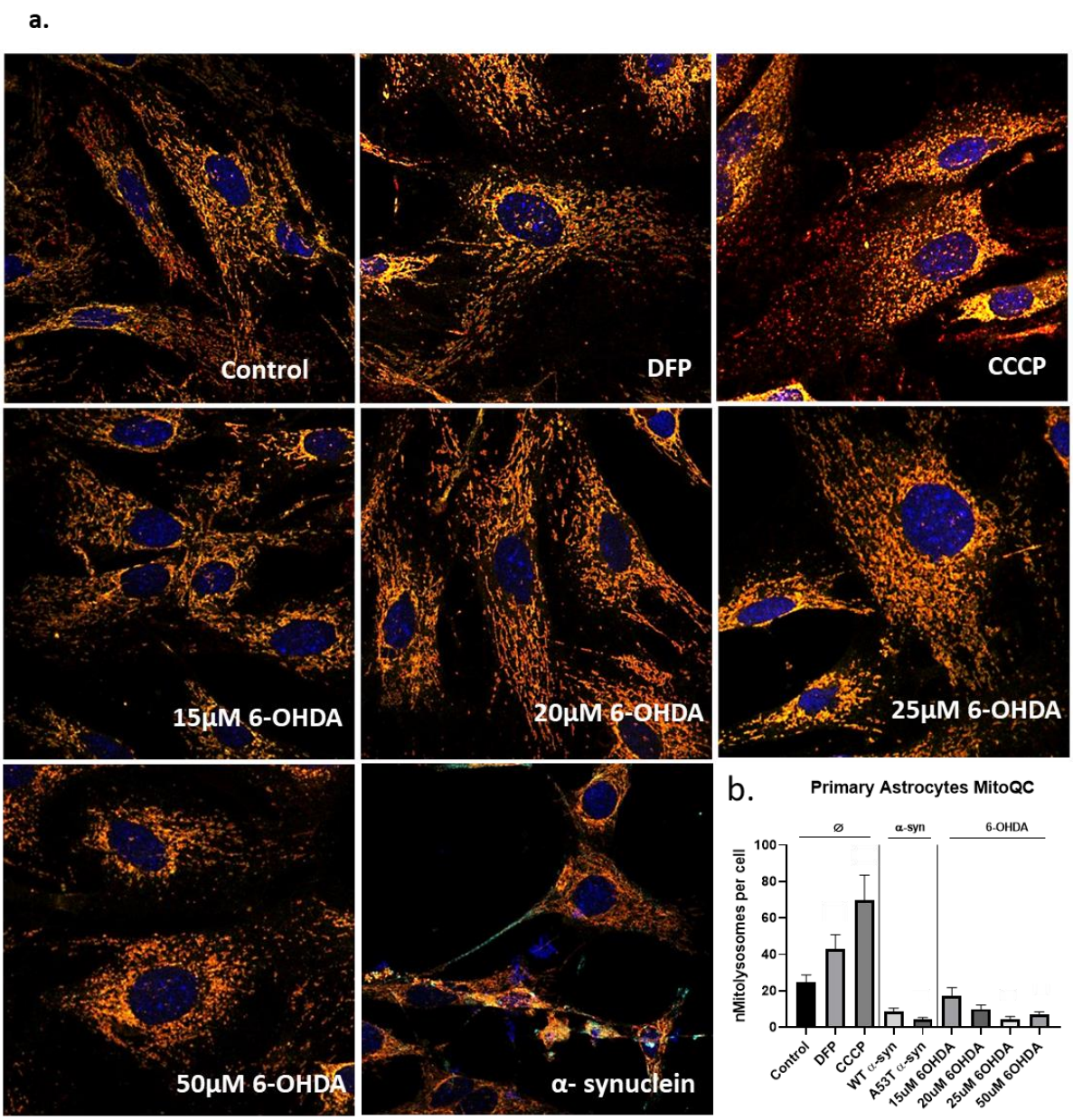

Figure 4.40. MitoQC astrocytes treated with 6-OHDA and transfected with α-syn decrease the levels of mitophagy. a. Representative images of MitoQC primary astrocytes after 24-hour treatment with DFP, CCCP or 6-OHDA or α-syn transfection, the nuclei were stained with DAPI. **b**. Graphical representation of the levels of mitophagy after 24-hour treatment with DFP, CCCP or 6-OHDA or α-syn transfection. (mean±SEM). (n=2).

To examine whether the primary astrocytes were affected by the overexpression of wild-type or mutant α-syn, immunofluorescence was used. We observed that the primary astrocytes transfected with either the wt or mutant α-syn displayed an irregular

shape with long and rich processes, as well as accumulations of α- synuclein (Figure 4.41.). In contrast to the SH-SY5Y transfection appearance, in which the α-syn antibody labelled the whole cytoplasm, the α-syn transfection was localized in clumps (Figure 4.41.).

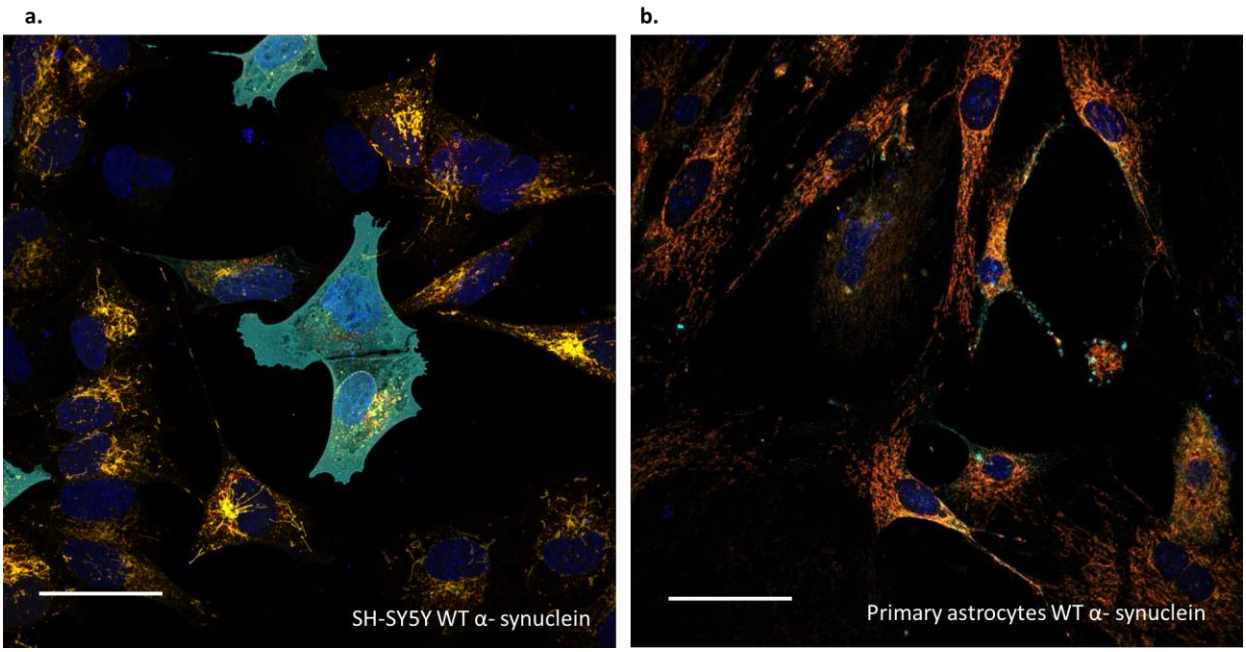

Figure 4.41. WT α-synuclein transfection comparison in MitoQC SH-SY5Y cells and primary astrocyte culture. **a**. In contrast to the SH-SY5Y transfection appearance, which showed the α-syn antibody labelling the whole cytoplasm, b. the primary astrocytes transfected with the wt α-syn exhibited an uneven shape with long and rich processes, as well as accumulations of α - synuclein.

Following that, we sought to look at the expression levels of various mitophagy and mitochondria related genes, so we performed a qPCR on primary astrocyte cultures that had been treated for 24 hours with either DFP, CCCP, 15 µM 6-OHDA, 20 µM 6-OHDA, or 50 µM 6-OHDA, or transfected with either the wild type or mutant α-syn. The positive control, α-syn, demonstrated that astrocytes transfected with either WT or mutant α-syn expressed significantly more *α-syn* (Figure 4.42.). Additionally, DFP was able to increase the levels of *Bnip3* and *Nix* in our primary astrocyte cultures (Figure 4.42.), suggesting that the experiments were successful. Having said that, there was no significant change in any of the other genes examined (Figure 4.42.).

Since we were not able to reproduce the *in vivo* data, we concluded that neither of the *in vitro* models is suitable for the purposes of our experiments.

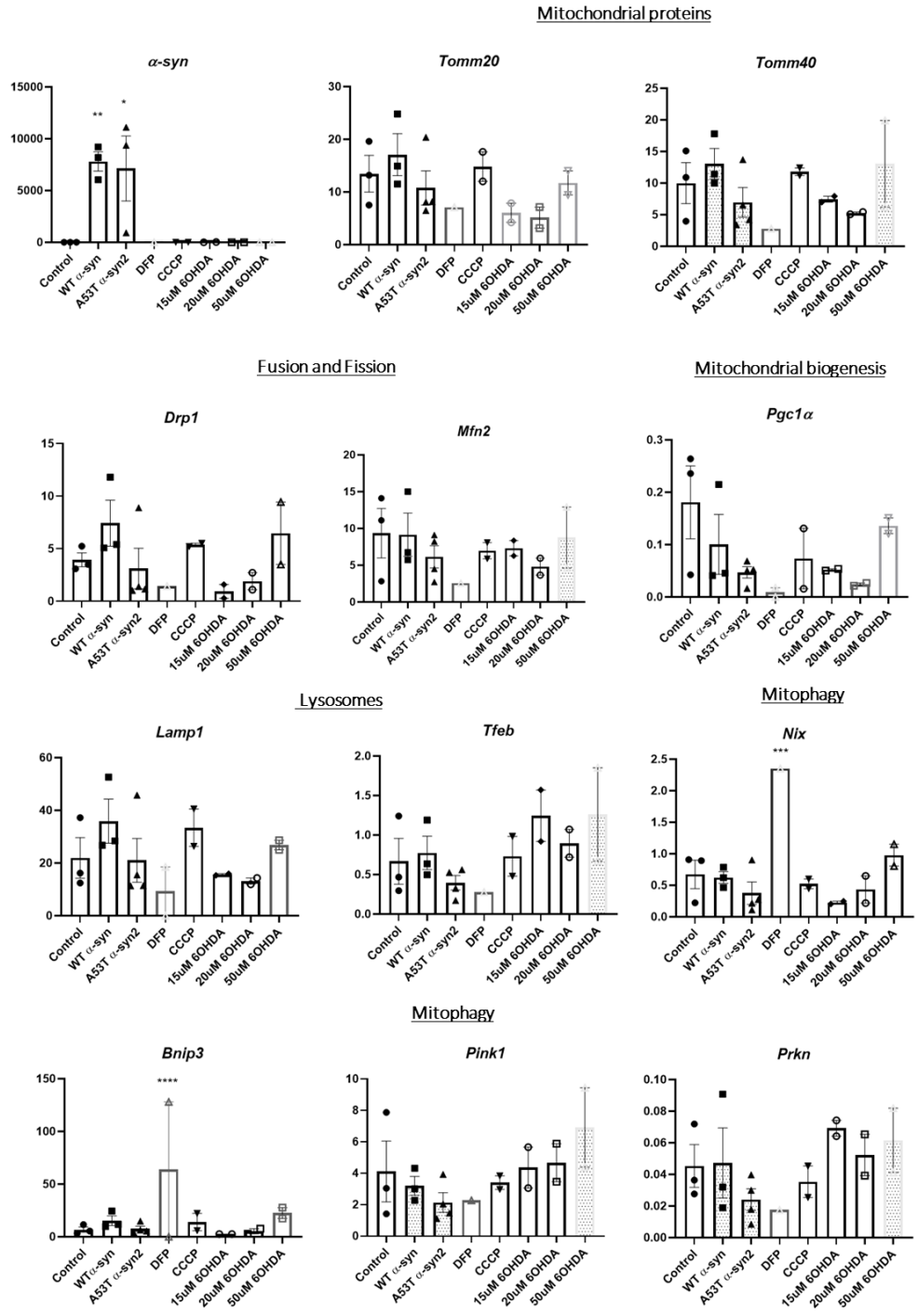

Figure 4.42. DFP increases the expression of bnip3 and bnip3l mitophagy genes in MitoQC primary astrocyte culture. a. The expression of *αsyn, Drp1, Mfn2, Pgc1α, Cox Iv, Tomm20, Tomm40, Tfeb, Lamp1, Nix and Bnip3, Pink1, Prkn* in the MitoQC primary astrocyte culture after 24-hour treatment with DFP, CCCP or 6-OHDA or α-syn transfection. Ordinary one-way ANOVA statistical test. (mean±SEM). (n = 3).

4.6. Mitophagy inducers with therapeutic potential for Parkinson's disease

We intended to expand our study and conduct further tests on the three earlier examined compounds. JAR1.39 and VP07 were previously synthesized and placed in the MBC library as part of a medicinal chemistry effort aimed at discovering allosteric brain permeable GSK3 inhibitors (Palomo et al., 2017). IGS2.7 is a CK-1delta inhibitor that has been found to preserve motor neurons and reduce astroglial and microglial reactivity in spinal cord samples from both (A315T) transgenic mice and a human cell-based model of ALS (Martínez-González et al., 2020). To determine whether the chemicals are capable of inducing mitophagy *in vivo*, MitoQC mice received a 5 mg/kg intraperitoneal injection and were sacrificed 8 hours later for tissue dissection and fixation. Excitingly, JAR1.39 was capable of significantly inducing mitophagy in TH-stained dopaminergic neurons (Figure 4.43.). This is interesting because the next stage will be to investigate whether it can promote mitophagy in PD model mice and, if so, if it has a neuroprotective properties (Maestro et al., 2021).

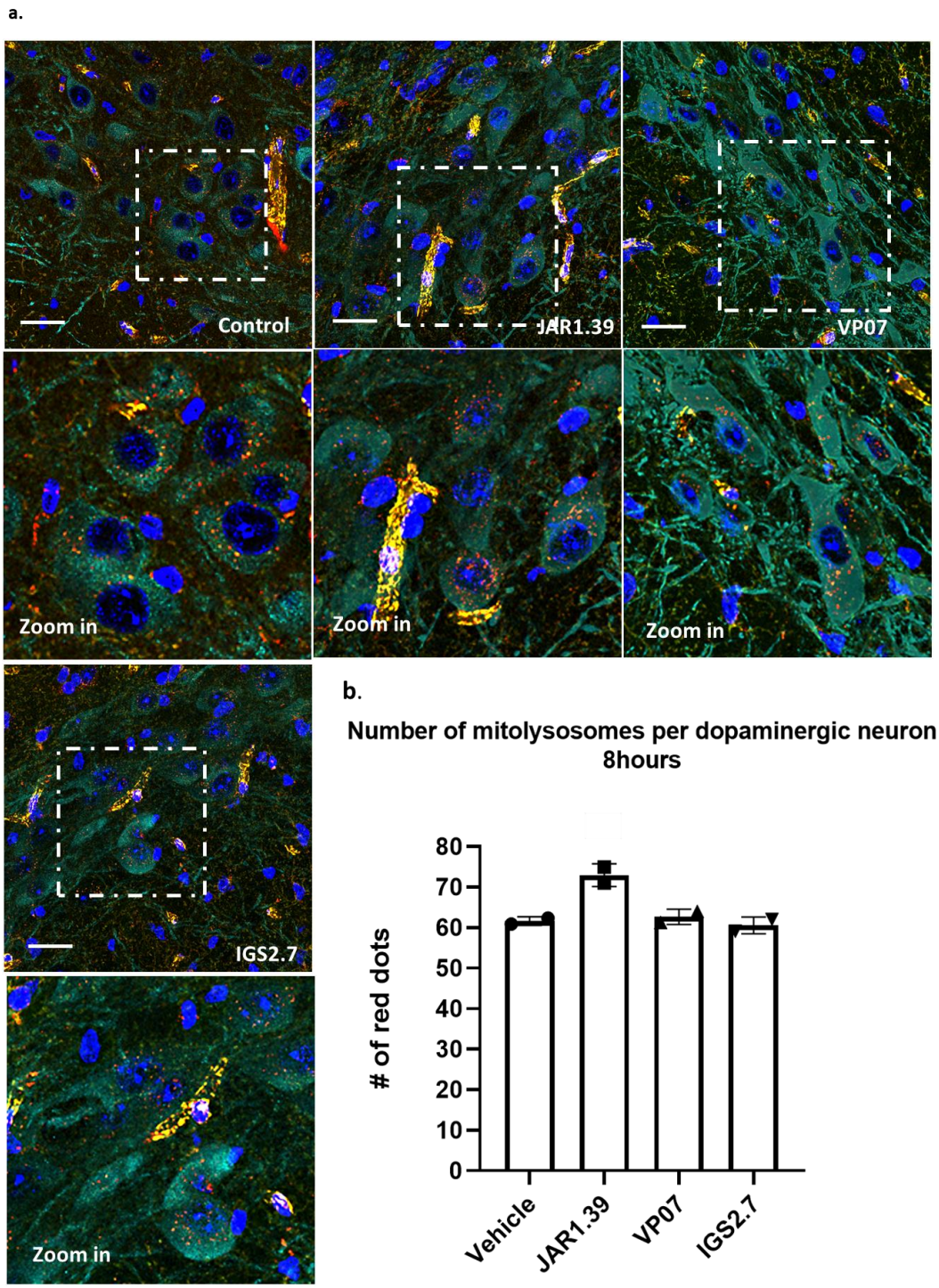

Figure 4.43. *In vivo* treatment with mitophagy inducers. a. Representative pictures of MitoQC reporter; mitochondria (yellow) and mitophagy (red); and **b.** red-only puncta quantification of brain explants from treated MitoQC mice. (mean±SEM). (n=2).

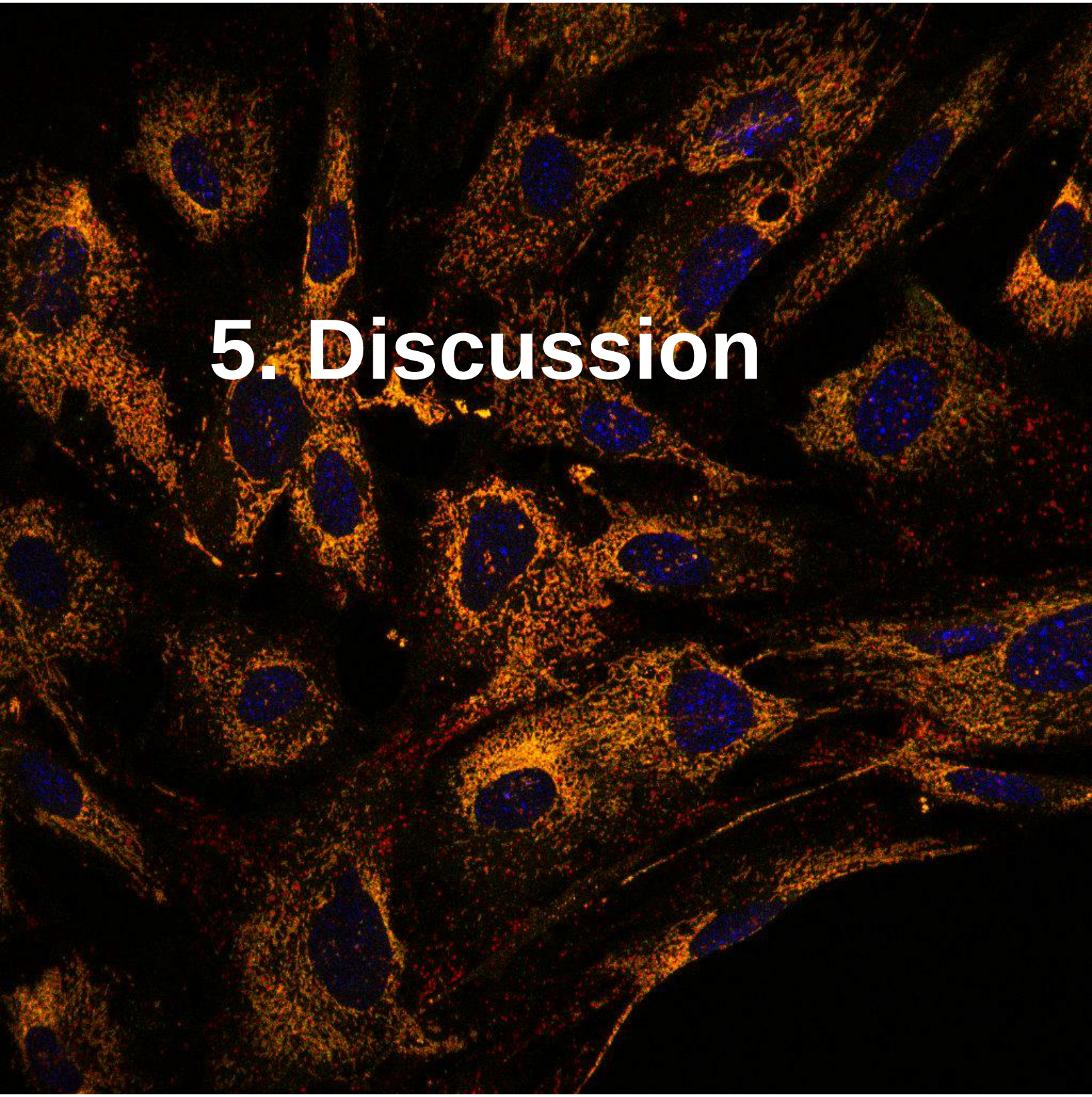

5. Discussion

5. Discussion

5.1. Mitophagy activity during mouse retinal development

In this Doctoral Thesis, we have demonstrated the activation of mitophagy in specific stages of the development of the mouse embryonic retina. We discovered no basal mitophagy at embryonic day E13.5, while at E14.5, we observed some red puncta at the RGCL-NbL border. The level of mitophagy in the same area increased in E15.5, with significant mitophagy in the RGCL as well, whereas just a few red dots can be seen in the ONbL. This was also evident at embryonic day E16.5, with a number of red dots on the border of RGCL and NbL, as well as red dots inside the RGCL and ONbL. On the final embryonic day in utero, E18.5, red spots may be observed in the IPL (on the border of the RGCL and INbL), but also in the NbL. After birth, on postnatal day P1, mitophagy levels increase in all five layers (ONbL, INbL, NbL, IPL, and RGCL), but red dots are visible in all layers, and large accumulations of red dots can be seen in the INL and IPL, which could be due to programmed cell death, which is highest at this age in the INL (Pequignot et al., 2003). The mice open their eyes at P9 and begin to see about P15, coinciding with the last phases of neuronal differentiation and retinal vascular development. On this postnatal day, P15, we found that the ONL had the greatest levels of mitophagy compared to the other layers (ONL, INL, IPL, and RGCL). Furthermore, in the adult retina, mitophagy is abundant in the ONL. This indicates that mitophagy levels are observed in different cells throughout the development of the embryonic retina as the cells differentiate. Also, the cells that are newly differentiated or are in the process are the ones with high degree of mitophagy. Across the whole retina, three peaks in mitophagy levels have been observed. The first peak occurs at E15.5 embryonic day, the second at P1, and the third around P15 postnatal day; curiously, these are the ages at which significant levels of programmed cell death are observed (Pequignot et al., 2003), suggesting that these processes are synchronized and might be regulated together.

We next wanted to study how and by which mechanisms mitophagy is controlled throughout retinogenesis. Previously, our lab has demonstrated that mitochondrial mass increase in E15.5 Atg5-deficient retinas and when autophagy and mitophagy are pharmacologically inhibited using 3-MA and CsA, respectively. Additionally, Esteban-

Martínez et al. demonstrated that while hypoxia and NIX have an effect on the mitophagy process during retinogenesis, the decrease in mitochondrial mass during embryonic retinal development is not due to a decrease in expression levels of mitochondrial biogenesis genes, highlighting the critical role of mitophagy in retinal mitochondrial homeostasis. NIX expression levels are generally low in most tissues, an increase in its expression levels has been associated with a decrease in mitochondrial mass during physiological processes such as the development of the lens of the eye (Costello et al, 2013; Brennan et al., 2020), the differentiation of erythrocytes (Kundu et al, 2008; Sandoval et al, 2008; Schweers et al, 2007) and the generation of memory NK cells (O'Sullivan, 2015). Therefore, the expression of NIX seems to be increased in situations where it plays a role in cellular differentiation. The fact that the expression of NIX increases at E15.5 during embryonic development of the mouse retina, whereas other known regulators of mitophagy do so primarily at the postnatal level, suggests that NIX may play a different role in regulating mitophagy during embryonic development of the mouse retina. HIF1 α seems to be an essential mechanism in the control of NIX levels under hypoxic circumstances, suggesting that the rise in NIX expression during retinal development may be regulated by hypoxia. Other researchers have linked HIF1 α levels in hypoxic circumstances to mTORC1. Rapamycin therapy reduces HIF1 α levels in several trials (Brugarolas et al, 2003; Land and Tee, 2007). Thus, our findings that rapamycin has no effect on mitophagy at E13.5 make perfect sense given that HIF1 α levels are decreased. As a result, it is conceivable that there exist oxygen constraints in the retina anterior to the peak of mitophagy, since the vascularization is still very low and not a lot of oxygen reaches the retina. Thus, promoting mitophagy with DFP is entirely reasonable at this stage, given the retina's extremely hypoxic environment. This correlates with elevated levels of ROS, but since the mitochondrial membrane potential is somewhat disturbed at this point, an increase in mitophagy may also be detected using CCCP.

Previously, Esteban-Martínez et al. found that mTORC1 is active in retinas at E15.5, when there is mitophagy, which may indicate that the induction of HIF1 α in retinas at that time is reliant on mTORC1. Furthermore, when E15.5 retinas are cultured in EBSS, treatment with rapamycin and fasting amino acids does not promote mitophagy, which

may be related to mTORC1 suppression (Esteban-Martínez, doctoral thesis). In addition, we have observed a decrease in ROS from E15.5 that is not due to the mitophagy process observed in this age, since the pharmacological inhibition of mitophagy with 3-MA does not alter ROS levels. In E15.5 retinas, mitophagy may be controlled by HIF1α. Taking this mTORC1-dependent control of HIF1 α into consideration, the induction of mitophagy across the retina by DFP administration at E13.5 supports this hypothesis; however, the fact that CCCP treatment also increases mitophagy suggests that other mechanisms may be involved in the regulation of mitophagy. In fact, protonophore compounds have been shown to induce Parkin relocalization to mitochondria and that Parkin translocation is PINK1-dependent (Vives-Bauza et al, 2010). Under hypoxic conditions, the ROS generated in complex III of the electronic transport chain are required for the activation of HIF1α (Chandel et al, 2000; Klimova and Chandel, 2008). Energy demands and the availability of metabolic substrates and oxygen are the central determinants of mitochondrial respiration under optimal conditions of mitochondrial functioning, so a change in substrate availability or a decrease in oxygen levels could alter mitochondrial function, increase ROS levels, and induce mitophagy. As a result, in the lack of oxygen, a variety of critical survival processes are triggered, such as an increase in the expression of HIF1α, which allows for a reduction in the number of mitochondria and the formation of new vasculature to improve oxygen availability (Klimova and Chandel, 2008).

These data, together with the decrease in mitochondrial membrane potential at E14.5, prior to the peak of mitophagy, indicate that there is a mitochondrial alteration that precedes the activation of mitophagy. At this stage of development, CCCP had a greater effect on mitophagy induction compared to DFP, which confirms the fact that there is a decrease in mitochondrial membrane potential. As mentioned above, ROS generated in the electronic transport chain are essential for hypoxia-dependent activation of HIF1α, so this mitochondrial alteration could trigger a pseudohypoxic response observed in retinas to E15.5 (Chandel et al, 2000; Klimova and Chandel, 2008). The transfer of electrons through the complexes of the electron transport chain in the inner mitochondrial membrane is essential for the maintenance of the mitochondrial membrane potential, so the loss of it already in retinas of E14.5 could be related to an alteration of the activity of

the electronic transport chain and therefore the induction of mitophagy with CCCP facilitated the process.

However, we have also observed an increase in the expression of other mitophagy regulators, such as PINK1, Parkin, Optineurin, FUNDC1, Smurf1 at ages in which the presence of mitophagy has been determined, so cooperation should not be ruled out of other mechanisms of regulation of mitophagy. There are different mechanisms of interrelation between the mitophagy pathways known to date. It has been described that NIX prepares mitochondria for degradation by mitophagy by controlling the mitochondrial localization of Parkin under mitochondrial depolarization and mitochondrial depolarization with CCCP restores mitophagy even in NIX-deficient reticulocytes, demonstrating the presence of NIX-independent compensation mechanisms to mediate mitophagy (Gao et al, 2015). On the other hand, the mechanism by which NIX and BNIP3 induce mitophagy is controversial, since it can degrade mitochondria through the LIR domain and can also promote mitochondrial depolarization, which is sufficient to induce mitophagy (Twig et al. al, 2008). Most of the mitophagy processes in which other regulators are involved, such as PINK1 and Parkin, are due to the need to eliminate mitochondria in the event of cellular damage (Lazarou et al, 2012; Lemasters, 2005; Narendra et al, 2008; Narendra et al, 2010; Pickrell and Youle, 2015; Vives-Bauza et al, 2010; Youle and Narendra, 2011). On the contrary, previous studies have shown that NIX is involved in processes of programmed mitophagy (Kundu et al, 2008; Sandoval et al, 2008; Schweers et al, 2007), so that NIX seems to be involved in processes of mitophagy during physiology of different cell types. Previous studies have described different functions of mitophagy during development, such as the selective degradation of mitochondria of paternal origin in fertilized oocytes, the maturation of erythrocytes, adipose tissue and the lens (Ashrafi and Schwarz, 2013) thus it is perfectly reasonable that mitophagy has an important role in the development of the retina as we have shown in this doctoral thesis.

Compounds from the MBC library, JAR1.39 and VP07, which were previously shown to induce mitophagy via Parkin-dependent pathway (Maestro et al., 2021), and IGS2.7, a CK-1delta inhibitor that has been found to preserve motor neurons and reduce astroglial and microglial reactivity in ALS models (Martínez-González et al., 2020) were

also tested to see if they have an effect on mitophagy levels in the developing retina. All of the compounds were shown to have an impact on mitophagy levels in the developing retina. However, the outcomes differed depending on the age. At age E13.5, JAR1.39 and VP07 significantly increased mitophagy levels in the retina (Figure 4.8 of the results section), with the increase occurring in the RGCL (Figure 4.10 of the results section) and not in the NbL (Figure 4.12. of the results section), indicating that the compounds had diverse effects depending on the cell type.

At the age of E14.5 we saw a significant increase in mitophagy after incubating the retinas with VP07 and JAR1.39 (Figure 4.12. of the results section). VP07 exhibited a larger impact at this age, which might be attributed to differences in gene expression and cell differentiation between the ages. It's interesting to note that at the ages of E15.5 and P1, VP07 was able to increase the mitophagy levels, but only in the RGCL and not in the NbL. This is more evidence that the compounds from the MBC library impact various cell types in distinct ways. To conclude, it was shown that VP07 was the most efficient mitophagy inducer in retinas of various ages cultured *ex vivo*.

5.2. Mitophagy and physiological cell death in the developing zebrafish retina

Kerr, Wyllie, and Currie published an article in 1972 defining apoptosis, a form of cell death separate from necrosis (Kerr et al., 1972.) This is the first time the concept of apoptosis has been introduced to the general public (D'Arcy, 2019; Kerr, 2002; Tang et al., 2019). Apoptosis is thought to be an essential component of many physiological processes, including proper cell replacement, development, and immune system function. Furthermore, apoptotic cells may be observed in pathological conditions (Elmore, 2007). In multicellular organisms, apoptosis is a kind of programmed cell death (PCD). It triggers a sequence of ongoing processes in the cell by activating different kinds of cysteine-aspartic proteases, which eventually leads to cell death. The production of apoptotic bodies is what distinguishes apoptosis in this process. Apoptotic bodies, which contain the contents of dead cells, may be swallowed by surrounding cells; therefore, the occurrence of apoptosis does not result in leaking of the contents and harm to adjacent cells (Hacker, 2000). Apoptosis has two pathways: intrinsic and extrinsic (Jin and El-Deiry, 2005). The intrinsic route is also known as the apoptosis mitochondrial pathway,

while the extrinsic pathway is known as the apoptosis death receptor pathway (D'Arcy, 2019). Numerous research on these two routes have been performed, and many important apoptotic proteins, such as caspase3, have been discovered. In our study TUNEL-positive cells were found in all retinal layers (GCL, INL, and ONL) throughout all developmental stages examined from 24 hpf to 120 hpf, but only in the ONL and GCL on rare occasions. The GCL in the retina of larval zebrafish starts to split from the neuroblast layer by the growing inner plexiform layer at 2dpf (IPL; Schmitt and Dowling 1999). As a consequence, histologically, the various retinal layers in retinal slices from embryonic stages prior to 2 dpf cannot be distinguished. We discovered that apoptosis peaked over the whole retina in three embryonic stages, followed by a second, although noticeably smaller, wave at 6-7 dpf. Cell death was seen in all layers of the retina at 24 hpf (Figure 4.26.; Figure 4.27. in Results), as well as on the subquential day, 48 hpf (Figure 4.26. in Results), when apoptosis was at its height (Figure 4.26.; Figure 4.27. in Results). TUNEL-positive cells are only observed in the INL at 60 hpf (Figure 4.26.; Figure 4.27. in Results), while cell death is found in both the INL and the RGCL at 72 hpf (Figure 4.26.; Figure 4.27. in Results). TUNEL-positive cells are seen in both INL and RGCL at 96 hpf (Figure 4.26.; Figure 4.27. in Results); at this age, the third peak in cell death (Figure 4.26.; Figure 4.27. in Results) occurs, and both RGCL and INL have the highest apoptosis percentage (Figure 4.26.; Figure 4.27. in Results). Apoptosis began and peaked in the outer nuclear layer (ONL) at 120 hpf. This late-onset high peak of photoreceptor apoptosis differs from all other species studied by far. However, there was cell death in the INL and RGCL peripheral zones. It is worth noticing that the mitophagy and apoptosis maxima overlap. We observe a peak in mitophagy at 48 hpf, which corresponds to cell death, followed by another peak at 96 hpf, which also correlates to cell death. This might suggest that these two biological processes are connected in some way, since both exhibit high expression levels at the same times.

Mitophagy allows cells to deal with mitochondrial stress until the damage becomes too severe, at which point apoptosis is activated (Redmann et al., 2014). When there is extensive mitochondrial damage, such as that seen after a myocardial infarction, apoptotic proteases are activated, which shuts off mitophagy and activates apoptosis to guarantee cell death (Kubli et al., 2015). Ham et al. discovered that the PINK1–Parkin

pathway regulates mitophagy and apoptosis by generating two kinds of ubiquitination on VDAC1. Parkin-mediated mitophagy is promoted by polyubiquitinated VDAC1, while monoubiquitinated VDAC1 reduces mitochondrial calcium uptake, thereby protecting cells from apoptosis (Ham et al., 2020). This demonstrates that mitophagy and apoptosis are interconnected in some way and even share a molecular pathway.

Furthermore, degradation of mitochondria may help avoid the build-up of ROS-generating mitochondria and cell death. An increase in mitophagy, in addition, may destroy functioning mitochondria, reducing their capacity to generate ATP and causing cell death (Figure 5.1.). This would explain the significant reduction in apoptosis at the same time we see a decrease in mitophagy throughout zebrafish retinogenesis (Figure 4.26.; Figure 4.27.; Figure 4.28 in Results). We don't know for certain if this mitophagy activation kills the cells or whether it acts as a survival mechanism. To further study this hypothesis, we could inhibit mitophagy at different stages and see the effect on cell death. Additionally, we may examine the degree of cell death in mitophagy gene knockout zebrafish. If we see a reduction in TUNEL after inactivation of mitophagy genes, this might provide more support for this idea.

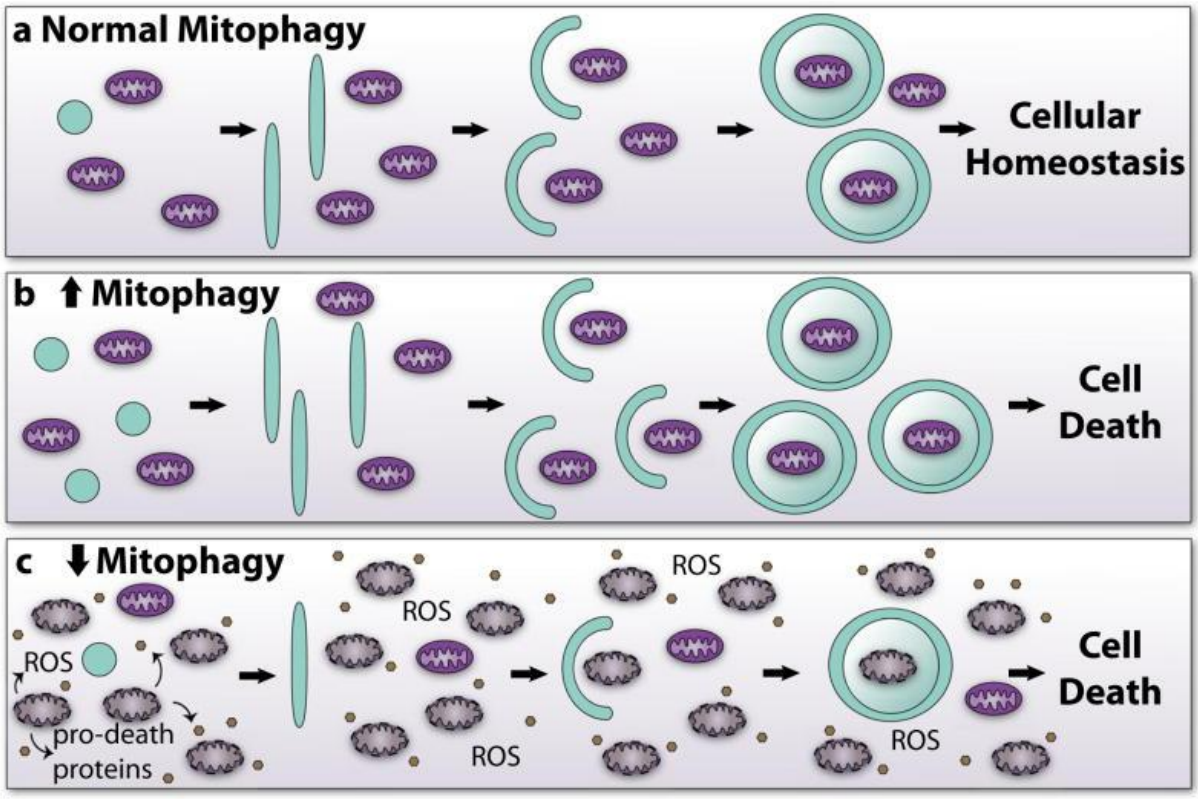

Figure 5.1. Interplay between mitophagy and apoptosis. a Normal mitophagy starts with the formation of a double-membraned autophagic vesicle and its extension. The vesicle subsequently engulfs and sequesters mitochondria for destruction. Mitophagy regulation leads to mitochondrial quality control and cellular homeostasis. **b** Increased mitophagy has the potential to significantly decrease the pool of functioning mitochondria. When a cell has too few mitochondria, it loses its capacity to generate enough energy and ultimately dies. **c** Mitophagy deficiency leads to the build-up of defective mitochondria. Excess ROS and pro-death proteins are released by defective mitochondria, resulting in fast cell death alteration of Parkin and suppression of mitophagy in the heart. (Shires and Gustafsson, 2015).

5.3. Mitophagy in the pathogenesis of Parkinson's disease

Due to mitochondria's critical role in energy production and metabolic control, increased focus has been devoted to the regulation of mitophagy in the preservation of cellular homeostasis and its function under pathological conditions. Neurodegenerative disorders such as Parkinson's disease, Alzheimer's disease, Huntington's disease, and amyotrophic lateral sclerosis, have been characterized by aberrant mitochondrial morphology (shape and size), mitochondrial dynamics (imbalance between fission and fusion), function (insufficient energy supply), mitophagy (deficient or excessive) as well as misfolded and abnormally accumulated proteins. Mutations in genes producing mitochondrial-associated proteins, such as PINK1, parkin, DJ-1, and CHCHD2, have

been demonstrated to produce Parkinson's disease in humans (Malpartida et al, 2021; Ryan et al; 2015), suggesting that mitochondrial malfunction alone may result in versions of this condition caused by specific mutations. Sporadic Parkinson's disease (cases with no identifiable single hereditary basis) may also be caused by mitochondrial dysfunction (Doric and Nakamura, 2021). Individuals with this version of the illness have lower than usual amounts of mitochondrial complex I in their substantia nigra dopamine neurons (Hattori, et al., 1991; Grünewaldet al. 2016). Additionally, two agents that block complex I, MPTP and rotenone, kill dopamine neurons preferentially in humans and rodents (Haddad and Nakamura, 2015). Furthermore, recently a genetically designed mouse that lacks the gene producing a complex I component termed NDUFS2 in dopamine neurons exhibits neurodegeneration providing a model of Parkinson's disease based on mitochondrial failure (labelled the MCI-Park model) (González-Rodríguez et al., 2021; Doric and Nakamura, 2021). Also, mitophagy is critical for the quality control system of mitochondria and for the elimination of misfolded and undesirable proteins accumulated in mitochondria. Although the precise processes behind these illnesses remain unknown, inducing mitophagy as a means of maintaining a healthy mitochondrial and proteinic level seems to be a good therapeutic strategy (Moors et al., 2017; East and Campanella, 2016). A recent study has shown that drugs that regulate mitophagy may help alleviate the pathology of these illnesses in mouse models. Additional research is needed to understand the processes behind mitophagy and to determine the exact function of mitophagy in neurodegenerative disorders (Georgakopoulos et al., 2017; Koentjoro et al., 2017; Park et al., 2017; Olszewska and Lynch, 2017).

Although the previously mentioned research on mitochondrial dysfunction has been done within neurons that have been extensively studied in PD, the prevalence and consequences of OXPHOS failure in astrocytes remain unknown. Chen et al. demonstrate for the first time that OXPHOS impairment exists among SN astrocytes of human patients with PD affecting all complexes (except complex III). Additionally, they observed alterations in the mitochondrial mass of PD astrocytes, which may have an effect on the function of these critical glia (Chen et al., 2021). Astrocytes' abilities to sustain neurons and their function are required for their survival. These changes demonstrate the critical role of astrocytic support for DNs in PD, which may contribute to

the neuronal loss seen in afflicted people (Chen et al., 2021). With this information in mind, we were keen to determine the degree of mitophagy in both cell types. In our Parkinson's disease models, we found that injected animals DAn had much lower mitophagy than control mice. In contrast, we found a substantial increase in mitophagy levels in the same mice's astrocytes when compared to the vehicle controls. Damaged mitochondria that cannot be transported to the DAn somata for breakdown may be discharged into the extracellular media, where they may trigger the neuro-inflammatory process that usually promotes DAn degeneration in Parkinson's disease (Maeda and Fadeel, 2014; Matheoud et al., 2016; Wilkins et al., 2017; Zhang et al., 2010). Morales et al. recently discovered that proteins from degenerating DAergic terminals concentrate in spheroids before migrating to striatal astrocytes (transautophagy) (Morales et al., 2020). Degenerating DAergic terminal mitochondria concentrate in spheroids and may be transported to striatal astrocytes for destruction (Morales et al., 2020). Intercellular transfer of healthy mitochondria has been observed between different cell types (horizontal transfer) (Jackson and Robinson, 2018), and astrocytes may serve as acceptors for damaged mitochondria of axons of retinal ganglion cells destined for degradation (transmitophagy) (Jackson and Robinson, 2018; Davis et al., 2014). This is a direct transfer between axonal protrusions containing mitochondria and apposed astrocytic processes, with no involvement of spheroids. Mitochondrial transfer may occur between DAn and striatal astrocytes (Morales et al., 2020) which could explain why we observe lower mitophagy in the Dan and higher in the astrocytes of the SNpC. This transfer may prevent the release of mitochondrial DAn into the extracellular medium and the subsequent activation of “professional” phagocytes (microglia and macrophages) in Parkinson's disease (Halliday and Stevens, 2011; Kreutzberg, 1996), thereby delaying the onset and progression of neuro-inflammation in the disease (Morales et al., 2020).

Recently, a similar connection between microglia was identified, as cells may communicate through long strands of membranes or filopodia that create membrane or tunnelling nanotubes (TNT). Scheiblich et al., 2021 studied the microglial response to toxic α-syn aggregation. Microglia can decrease the harmful potential and proliferation of α-syn fibrils by ingesting and degrading protein aggregates. Accumulation of α-syn in microglia causes endoplasmic reticulum stress, decreased mitochondrial function, and

enhanced inflammatory cytokine release. Cultured microglia loaded with α-syn produced TNTs, which facilitated the transfer of α-syn to "unloaded" acceptor microglia (Scheiblich et al., 2021). Notably, the transfer of α-syn from donor to acceptor cells was accompanied by the opposite direction passage of mitochondria. Due to the fact that α-syn attaches to mitochondria, causing mitochondrial malfunction and abnormal generation of ROS, receiving healthy mitochondria reduced the ROS load in α-syn donor cells (Chen and Colonna, 2021). The transcriptome profile of donor microglia co-cultured with acceptor microglia indicated that oxidative stress, apoptosis, and inflammatory cytokine production were reduced (Chen and Colonna, 2021). All of these studies demonstrate that a complex network of communication exists between cells in the SNpC in order to maintain homeostasis and a healthy environment. Therefore, all cell types in the SNpC should be taken into consideration while studying PD. In our Parkinson's disease animals we found highly activated microglia with large red aggregates, which might be attributed to an enhanced ROS environment caused by aberrant mitochondrial function as well as the previously mentioned TNT transfer of α-syn and mitochondria. It is important to keep in mind that the number of DAn cells has decreased significantly owing to the microglia phagocytosis of damaged DAn.

5.4. α-syn controls mitochondrial morphology

α-syn has been demonstrated to localize to mitochondria in a broad variety of experimental models, in addition to its presence in the cytosol and nucleus of neurons (Martin et al., 2006; Li et al., 2007; Devi et al., 2008; Cole et al., 2008; Shavali et al., 2008; Chinta et al., 2010; Kamp et al., 2010). Endogenous α-syn has been detected in mitochondria of mouse neurons (Li et al., 2007; Zhang et al., 2008). Furthermore, a research found that α-syn levels in mitochondrial fractions are comparable to those seen in other synaptic-derived membranes or vesicle fractions collected from mouse brains (Nakamura et al., 2008). Notably, mitochondria in the substantia nigra of post-mortem brains from individuals with Parkinson's disease were shown to be enriched for α-syn (Devi et al., 2008; Devi and Anandatheerthavarada, 2010). However, the precise location of α-syn inside mitochondria is unknown. α-syn has been found in the OMM (Cole et al., 2008; Kamp et al., 2010), both the OMM and the inner mitochondrial membrane (IMM) (Li et al., 2007; Devi et al., 2008), and the mitochondrial matrix (Zhang et al., 2008). The

authors found that α-syn localizes to the IMM in a study of PD post-mortem human brains in which the OMM was biochemically stripped (Devi et al., 2008). Because α-syn lacks a genuine mitochondrial localization signal, its internalization process is unknown. Overexpression of α-syn may increase its mitochondrial location, which is also affected by pathogenic mutations (Shavali et al., 2008; Kamp et al., 2010). Overall, there is strong evidence supporting α-syn localization to mitochondria; nevertheless, it remains unclear how various α-syn mutations affect its localization. Our data shows that overexpression of WT α-syn, as well as the A53T α-syn affect the mitochondrial network of both the SH-SY5Y cells as well as the primary astrocyte cultures. A disruption in mitochondrial dynamics may play a role in both familial and sporadic neurodegenerative disorders, including Parkinson's disease (Cho et al., 2010; Lees et al., 2009; Su et al., 2010; Thomans and Beal, 2007). There is evidence that an amplification of fission events may induce the development of human Parkinson's disease. It remains to be shown that α-syn directly controls mitochondrial morphology; however, we have shown that its overexpression leads to mitochondrial fragmentation in both SHSY5Y cells as well as in primary astrocyte cultures respectively. Some research suggests a connection between α-syn and the proteins involved in mitochondrial fusion and fission (Xie and Chung, 2012; Gui et al., 2012; Menges et al., 2017). Our data shows a slight increase in Drp1 expression when we overexpress WT α-syn and a decrease in Mfn2 expression when we transfect the primary astrocytes with A53T α-syn (Figure results). This supports the theory that α-syn is in some way involved in mitochondrial fusion and fission, but it is also implicated in mitophagy inhibition. This assertion is supported by a considerable decrease in red dots in α-syn transfected MitoQC cells.

In addition, Ryan et al. demonstrated that SNCA-mutant hPSCs and SNCA-transgenic mice have fragmented mitochondria and accumulate α-syn deposits that cluster to mitochondrial membranes in response to cardiolipin exposure on the mitochondrial surface. Additionally, exposed cardiolipin selectively binds to and aids refolding of α-syn fibrils, prolonged cardiolipin exposure in SNCA-mutants induces mitochondrial recruitment and mitophagy (Ryan et al., 2018). Furthermore, they also discovered that co-culture of SNCA-mutant neurons with their isogenic controls resulted in transmission of α-syn disease in control neurons, which coincides with the

mitochondrial pathology (Ryan et al., 2018). The mechanism that underlies the α-syn-mediated changes in mitochondrial morphology is not clear. Understanding the precise mechanism of the α-syn-mitochondria interaction is a crucial step toward developing a molecular model that explains how α-syn mutations or dose cause alterations in the mitochondria.

5.5. Therapeutic potential of mitophagy inducers

Although mitophagy is recognized to have an important function in mitochondrial quality control, which is essential for neuronal homeostasis, further research is required to understand its involvement in neurological disorders and suggest novel treatments for these unmet illnesses. Defects in mitochondrial dynamics, as is well documented, are one of the hallmarks of neurodegeneration (Moors et al., 2017). Defective mitophagy and autophagy, in particular, have been observed in post-mortem brains of Parkinson's disease patients, as well as in *in vitro* and *in vivo* models. This, together with mitophagy-related gene alterations in Parkinson's disease, highlights the importance of mitophagy enhancers in the therapy of this illness (Malpartida et al., 2021).

Ana Martinez's lab discovered two structurally similar compounds, JAR1.39 and VP07, based on hydrazine derivatives with a quinoline scaffold that triggered mitophagy *in vivo* and may be useful pharmacological probes for molecular investigations of mitophagy in physiology and disease. They postulated that the chemicals might operate as light chain 3 (LC3) interactors, comparable to cardiolipin or ceramide, activating mitophagy through PINK1/Parkin (Maestro et al., 2021). In our experiment, JAR1.39 was able to promote mitophagy in the dopaminergic neurons of SNpC in MitoQC mice and has shown a potential that should be further investigated. Additionally, in a new study, Maestro et al. utilized the human neuroblastoma cell line SH-SY5Y expressing the MitoQC reporter and treated it with paraquat (PQ) and 6-OHDA. PQ is a toxin that has been shown to produce oxidative stress and Parkinsonian lesions in various mouse strains and rats, as well as α-synuclein aggregation and neurodegeneration in mice. They discovered that treating SH-SY5Y cells with 6-OHDA enhanced the expression of PD-related genes like SNCA (α-synuclein) while decreasing the expression of mitophagy-related genes like PINK1 (Maestro et al., 2021). PQ dramatically decreased baseline mitophagy compared to the control, as predicted, indicating faulty mitophagy in this

model. Pre-treatment with VP07 reversed the reduction of mitophagy caused by PQ, and a similar trend was detected with 6-OHDA treatment, demonstrating the therapeutic promise of mitophagy inducers, and particularly the function of VP07 in the recovery of the impairments reported in PD (Maestro et al., 2021). Future research will determine the therapeutic potential of these mitophagy inducers, proving their significance for the treatment of PD and other neurodegenerative diseases.

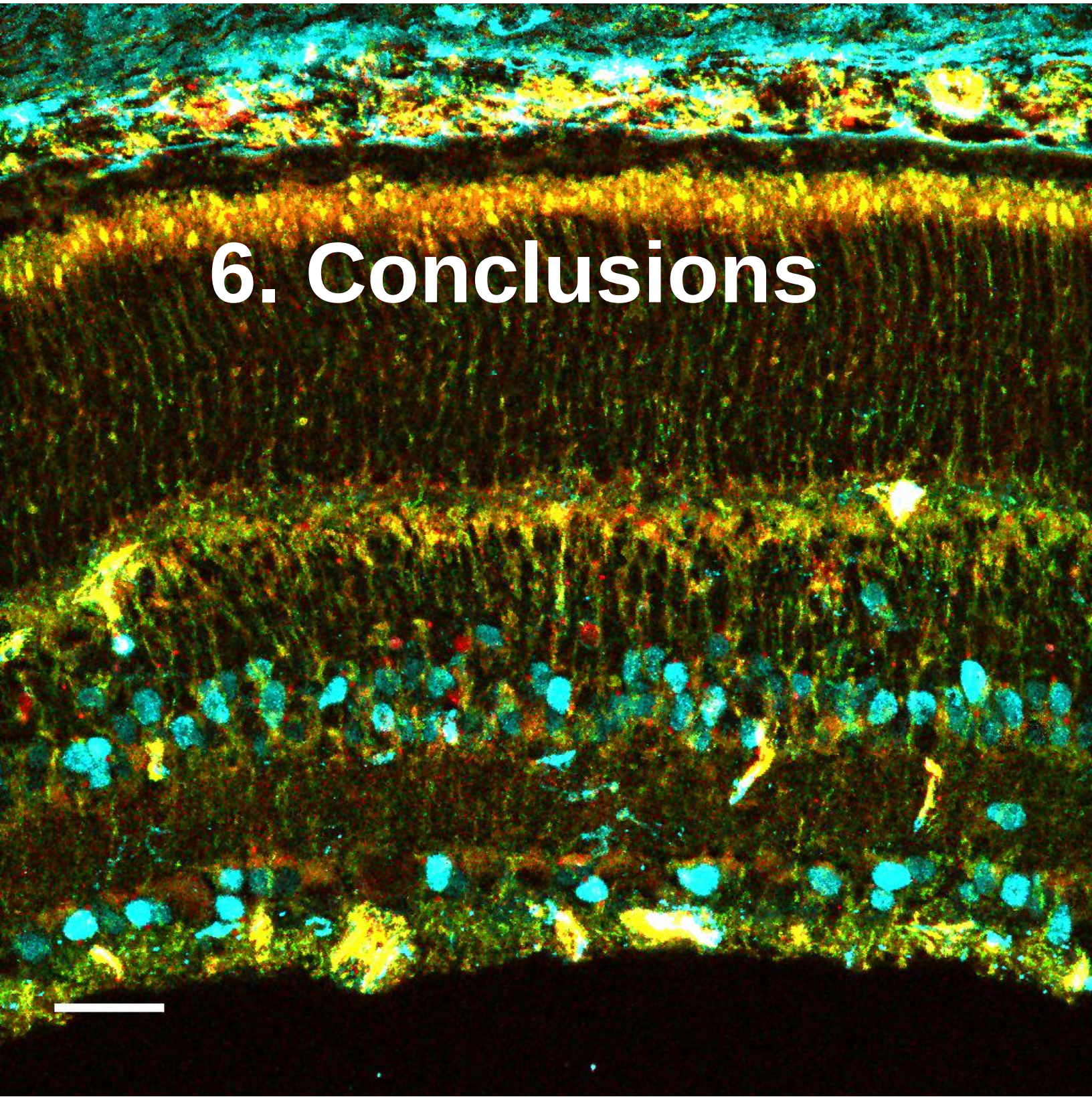

6. Conclusions

6. Conclusions

1. Mitophagy levels are modulated both spatially and temporally during retinal development in both mouse and zebrafish models.

2. DFP and CCCP induce mitophagy in the embryonic retina at E13.5 although to different extents. VP07 induces mitophagy in most of the ages studied.

3. Physiological cell death and mitophagy occur at the same developmental stages in the developing zebrafish retina.

4. In an *in vitro* model of Parkinson's disease α-syn overexpression induces mitochondrial morphological alterations including fission.

5. Mitophagy levels are decreased in the dopaminergic neurons of SNpc of mice injected with 6-OHDA while it is increased in the astrocytes of the same animals.

6. Compound JAR1.39 is able to stimulate mitophagy in the dopaminergic neurons of SNpC of MitoQC mice after injection.

Conclusiones

1. Los niveles de mitofagia se modulan tanto espacial como temporalmente durante el desarrollo de la retina en los modelos de ratón y pez cebra.

2. DFP y CCCP inducen mitofagia en la retina embrionaria en E13.5 aunque en diferentes grados. VP07 induce mitofagia en la mayoría de las edades estudiadas.

3. La muerte celular fisiológica y la mitofagia ocurren en las mismas etapas de desarrollo en la retina del pez cebra.

4. En un modelo in vitro de la enfermedad de Parkinson, la sobreexpresión de α-syn induce alteraciones morfológicas mitocondriales, incluida la fisión.

5. Los niveles de mitofagia están disminuidos en las neuronas dopaminérgicas de la SNpc de ratones inyectados con 6-OHDA mientras que están aumentados en los astrocitos de los mismos animales.

6. El compuesto JAR1.39 es capaz de estimular la mitofagia en las neuronas dopaminérgicas de SNpC de ratones MitoQC.

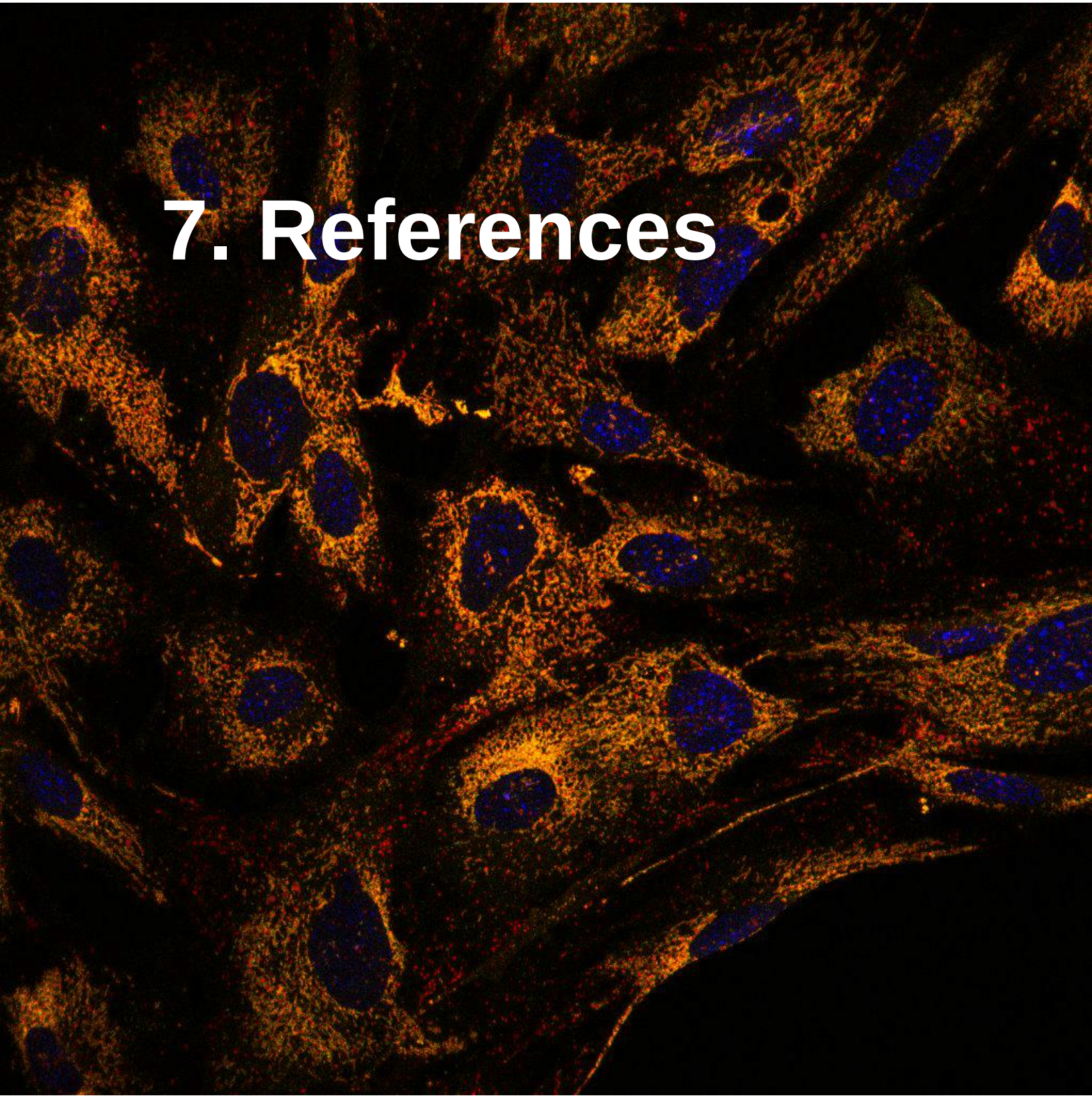

7. References

7. References

Allen, G. F. G., Toth, R., James, J., and Ganley, I. G. (2013). Loss of iron triggers PINK1/Parkin-independent mitophagy. *EMBO Reports*, *14*(12), 1127–1135. https://doi.org/10.1038/embor.2013.168

Alquezar, C., Salado, I. G., de la Encarnación, A., Pérez, D. I., Moreno, F., Gil, C., de Munain, A. L., Martínez, A., and Martín-Requero, Á. (2016). Targeting TDP-43 phosphorylation by Casein Kinase-1δ inhibitors: a novel strategy for the treatment of frontotemporal dementia. *Molecular Neurodegeneration*, *11*(1), 36. https://doi.org/10.1186/s13024-016-0102-7

Altshuler-Keylin, S., Shinoda, K., Hasegawa, Y., Ikeda, K., Hong, H., Kang, Q., Yang, Y., Perera, R. M., Debnath, J., and Kajimura, S. (2016). Beige Adipocyte Maintenance Is Regulated by Autophagy-Induced Mitochondrial Clearance. *Cell Metabolism*, *24*(3), 402–419. https://doi.org/10.1016/j.cmet.2016.08.002

Arias, E., and Cuervo, A. M. (2011). Chaperone-mediated autophagy in protein quality control. *Current Opinion in Cell Biology*, *23*(2), 184–189. https://doi.org/10.1016/j.ceb.2010.10.009

Ashrafi, G., and Schwarz, T. L. (2013). The pathways of mitophagy for quality control and clearance of mitochondria. *Cell Death and Differentiation*, *20*(1), 31–42. https://doi.org/10.1038/cdd.2012.81

Backer, J. M. (2008). The regulation and function of Class III PI3Ks: novel roles for Vps34. *Biochemical Journal*, *410*(1), 1–17. https://doi.org/10.1042/BJ20071427

Bantle, C. M., Hirst, W. D., Weihofen, A., & Shlevkov, E. (2021). Mitochondrial Dysfunction in Astrocytes: A Role in Parkinson's Disease? *Frontiers in Cell and Developmental Biology*, *8*. https://doi.org/10.3389/fcell.2020.608026

Barodia, S. K., McMeekin, L. J., Creed, R. B., Quinones, E. K., Cowell, R. M., and Goldberg, M. S. (2019). PINK1 phosphorylates ubiquitin predominantly in astrocytes. *Npj Parkinson's Disease*, *5*(1), 29. https://doi.org/10.1038/s41531-019-0101-9

Barth, S., Glick, D., and Macleod, K. F. (2010). Autophagy: assays and artifacts. *The Journal of Pathology*, *221*(2), 117–124. https://doi.org/10.1002/path.2694

Bassett, E. A., and Wallace, V. A. (2012). Cell fate determination in the vertebrate retina. *Trends in Neurosciences*, *35*(9), 565–573. https://doi.org/10.1016/j.tins.2012.05.004

Baye, L. M., and Link, B. A. (2007). Interkinetic Nuclear Migration and the Selection of Neurogenic Cell Divisions during Vertebrate Retinogenesis. *Journal of Neuroscience*, *27*(38), 10143–10152. https://doi.org/10.1523/JNEUROSCI.2754-07.2007

Bhujabal, Z., Birgisdottir, Å. B., Sjøttem, E., Brenne, H. B., Øvervatn, A., Habisov, S., Kirkin, V., Lamark, T., and Johansen, T. (2017). FKBP8 recruits LC3A to mediate Parkin-independent mitophagy. *EMBO Reports*, *18*(6), 947–961. https://doi.org/10.15252/embr.201643147

Bilotta, J., Saszik, S., and Sutherland, S. E. (2001). Rod contributions to the electroretinogram of the dark-adapted developing zebrafish. *Developmental Dynamics*, *222*(4), 564–570. https://doi.org/10.1002/dvdy.1188

Blackshaw, S., Harpavat, S., Trimarchi, J., Cai, L., Huang, H., Kuo, W. P., Weber, G., Lee, K., Fraioli, R. E., Cho, S.-H., Yung, R., Asch, E., Ohno-Machado, L., Wong, W. H., and Cepko, C. L. (2004). Genomic Analysis of Mouse Retinal Development. *PLoS Biology*, *2*(9), e247. https://doi.org/10.1371/journal.pbio.0020247

Blum, D., Torch, S., Lambeng, N., Nissou, M.-F., Benabid, A.-L., Sadoul, R., and Verna, J.-M. (2001). Molecular pathways involved in the neurotoxicity of 6-OHDA, dopamine and MPTP: contribution to the apoptotic theory in Parkinson's disease. *Progress in Neurobiology*, *65*(2), 135–172. https://doi.org/10.1016/S0301-0082(01)00003-X

Booth, H. D. E., Hirst, W. D., and Wade-Martins, R. (2017). The Role of Astrocyte Dysfunction in Parkinson's Disease Pathogenesis. *Trends in Neurosciences*, *40*(6), 358–370. https://doi.org/10.1016/j.tins.2017.04.001

Boya, P., and de la Rosa, E. J. (2005). Cell death in early neural life. *Birth Defects Research Part C: Embryo Today: Reviews*, *75*(4), 281–293. https://doi.org/10.1002/bdrc.20054

Boya, P., Esteban-Martínez, L., Serrano-Puebla, A., Gómez-Sintes, R., and Villarejo-Zori, B. (2016). Autophagy in the eye: Development, degeneration, and aging. *Progress in Retinal and Eye Research*, *55*, 206–245. https://doi.org/10.1016/j.preteyeres.2016.08.001

Boya, P., González-Polo, R.-A., Casares, N., Perfettini, J.-L., Dessen, P., Larochette, N., Métivier, D., Meley, D., Souquere, S., Yoshimori, T., Pierron, G., Codogno, P., and Kroemer, G. (2005). Inhibition of Macroautophagy Triggers Apoptosis. *Molecular and Cellular Biology*, *25*(3), 1025–1040. https://doi.org/10.1128/MCB.25.3.1025-1040.2005

Brennan, L., Disatham, J., and Kantorow, M. (2020). Hypoxia regulates the degradation of non-nuclear organelles during lens differentiation through activation of HIF1a. *Experimental Eye Research*, *198*, 108129. https://doi.org/10.1016/j.exer.2020.108129

Budovskaya, Y. v, Stephan, J. S., Reggiori, F., Klionsky, D. J., and Herman, P. K. (2004). The Ras/cAMP-dependent Protein Kinase Signaling Pathway Regulates an Early Step of the Autophagy Process in Saccharomyces cerevisiae. *Journal of Biological Chemistry*, *279*(20), 20663–20671. https://doi.org/10.1074/jbc.M400272200

Camara, A. K. S., Zhou, Y., Wen, P.-C., Tajkhorshid, E., and Kwok, W.-M. (2017). Mitochondrial VDAC1: A Key Gatekeeper as Potential Therapeutic Target. *Frontiers in Physiology*, *8*. https://doi.org/10.3389/fphys.2017.00460

Centanin, L., and Wittbrodt, J. (2014). Retinal neurogenesis. *Development*, *141*(2), 241–244. https://doi.org/10.1242/dev.083642

Cepko, C. L., Austin, C. P., Yang, X., Alexiades, M., and Ezzeddine, D. (1996). Cell fate determination in the vertebrate retina. *Proceedings of the National Academy of Sciences*, *93*(2), 589–595. https://doi.org/10.1073/pnas.93.2.589

Chen, C., Turnbull, D. M., and Reeve, A. K. (2019). Mitochondrial Dysfunction in Parkinson's Disease—Cause or Consequence? *Biology*, *8*(2), 38. https://doi.org/10.3390/biology8020038

Chen, Y., and Colonna, M. (2021). Microglia esprit de corps: Sharing the burden of eliminating toxic aggregates. *Cell*, *184*(20), 5082–5084. https://doi.org/10.1016/j.cell.2021.08.033

Chinnadurai, G., Vijayalingam, S., and Gibson, S. B. (2008). BNIP3 subfamily BH3-only proteins: mitochondrial stress sensors in normal and pathological functions. *Oncogene*, *27*(S1), S114–S127. https://doi.org/10.1038/onc.2009.49

Cho, D.-H., Nakamura, T., and Lipton, S. A. (2010). Mitochondrial dynamics in cell death and neurodegeneration. *Cellular and Molecular Life Sciences*, *67*(20), 3435–3447. https://doi.org/10.1007/s00018-010-0435-2

Chow, R. L., and Lang, R. A. (2001). Early Eye Development in Vertebrates. *Annual Review of Cell and Developmental Biology*, *17*(1), 255–296. https://doi.org/10.1146/annurev.cellbio.17.1.255

Chu, C. T., Ji, J., Dagda, R. K., Jiang, J. F., Tyurina, Y. Y., Kapralov, A. A., Tyurin, V. A., Yanamala, N., Shrivastava, I. H., Mohammadyani, D., Wang, K. Z. Q., Zhu, J., Klein-Seetharaman, J., Balasubramanian, K., Amoscato, A. A., Borisenko, G., Huang, Z., Gusdon, A. M., Cheikhi, A., … Kagan, V. E. (2013). Cardiolipin externalization to the outer mitochondrial membrane acts as an elimination signal for mitophagy in neuronal cells. *Nature Cell Biology*, *15*(10), 1197–1205. https://doi.org/10.1038/ncb2837

Chung, E., Choi, Y., Park, J., Nah, W., Park, J., Jung, Y., Lee, J., Lee, H., Park, S., Hwang, S., Kim, S., Lee, J., Min, D., Jo, J., Kang, S., Jung, M., Lee, P. H., Ruley, H. E., and Jo, D. (2020). Intracellular delivery of Parkin rescues neurons from accumulation of damaged mitochondria and pathological α-synuclein. *Science Advances*, *6*(18). https://doi.org/10.1126/sciadv.aba1193

Cuervo, A. M., Hildebrand, H., Bomhard, E. M., and Dice, J. F. (1999). Direct lysosomal uptake of α2-microglobulin contributes to chemically induced nephropathy. *Kidney International*, *55*(2), 529–545. https://doi.org/10.1046/j.1523-1755.1999.00268.x

Cuervo, A. M., Knecht, E., Terlecky, S. R., and Dice, J. F. (1995). Activation of a selective pathway of lysosomal proteolysis in rat liver by prolonged starvation. *American Journal of Physiology-Cell Physiology*, *269*(5), C1200–C1208. https://doi.org/10.1152/ajpcell.1995.269.5.C1200

D'Arcy, M. S. (2019). Cell death: a review of the major forms of apoptosis, necrosis and autophagy. *Cell Biology International*, *43*(6), 582–592. https://doi.org/10.1002/cbin.11137

Dagda, R. K., Zhu, J., Kulich, S. M., and Chu, C. T. (2008). Mitochondrially localized ERK2 regulates mitophagy and autophagic cell stress. *Autophagy*, *4*(6), 770–782. https://doi.org/10.4161/auto.6458

Davis, C. O., Kim, K.-Y., Bushong, E. A., Mills, E. A., Boassa, D., Shih, T., Kinebuchi, M., Phan, S., Zhou, Y., Bihlmeyer, N. A., Nguyen, J. v, Jin, Y., Ellisman, M. H., and Marsh-Armstrong, N. (2014). Transcellular degradation of axonal mitochondria. *Proceedings of the National Academy of Sciences*, *111*(26), 9633–9638. https://doi.org/10.1073/pnas.1404651111

Decressac, M., Mattsson, B., and Björklund, A. (2012). Comparison of the behavioural and histological characteristics of the 6-OHDA and α-synuclein rat models of Parkinson's disease. *Experimental Neurology*, *235*(1), 306–315. https://doi.org/10.1016/j.expneurol.2012.02.012

Decressac, M., Mattsson, B., Lundblad, M., Weikop, P., and Björklund, A. (2012). Progressive neurodegenerative and behavioural changes induced by AAV-mediated overexpression of α-synuclein in midbrain dopamine neurons. *Neurobiology of Disease*, *45*(3), 939–953. https://doi.org/10.1016/j.nbd.2011.12.013

Deter, R. L., and de Duve, C. (1967). Influence of glucagon, an inducer of cellular autophagy, on some physical properties of rat liver lysosomes. *Journal of Cell Biology*, *33*(2), 437–449. https://doi.org/10.1083/jcb.33.2.437

Devi, L., Raghavendran, V., Prabhu, B. M., Avadhani, N. G., and Anandatheerthavarada, H. K. (2008). Mitochondrial Import and Accumulation of α-Synuclein Impair Complex I in Human Dopaminergic Neuronal Cultures and Parkinson Disease Brain. *Journal of Biological Chemistry*, *283*(14), 9089–9100. https://doi.org/10.1074/jbc.M710012200

di Maio, R., Barrett, P. J., Hoffman, E. K., Barrett, C. W., Zharikov, A., Borah, A., Hu, X., McCoy, J., Chu, C. T., Burton, E. A., Hastings, T. G., and Greenamyre, J. T. (2016). α-Synuclein binds to TOM20 and inhibits mitochondrial protein import in Parkinson's disease. *Science Translational Medicine*, *8*(342). https://doi.org/10.1126/scitranslmed.aaf3634

Dikic, I., and Elazar, Z. (2018). Mechanism and medical implications of mammalian autophagy. *Nature Reviews Molecular Cell Biology*, *19*(6), 349–364. https://doi.org/10.1038/s41580-018-0003-4

Ding, Q., Xie, X.-L., Wang, M.-M., Yin, J., Tian, J.-M., Jiang, X.-Y., Zhang, D., Han, J., Bai, Y., Cui, Z.-J., and Jiang, H.-Q. (2019). The role of the apoptosis-related protein BCL-B in the regulation of mitophagy in hepatic stellate cells during the regression of liver fibrosis. *Experimental and Molecular Medicine*, *51*(1), 1–13. https://doi.org/10.1038/s12276-018-0199-6

Diwan, A., Koesters, A. G., Odley, A. M., Pushkaran, S., Baines, C. P., Spike, B. T., Daria, D., Jegga, A. G., Geiger, H., Aronow, B. J., Molkentin, J. D., Macleod, K. F., Kalfa, T. A., and Dorn, G. W. (2007). Unrestrained erythroblast development in Nix $^{-/-}$ mice reveals a mechanism for apoptotic modulation of erythropoiesis. *Proceedings of the National Academy of Sciences*, *104*(16), 6794–6799. https://doi.org/10.1073/pnas.0610666104

Doric, Z., and Nakamura, K. (2021). Mice with disrupted mitochondria used to model Parkinson's disease. *Nature*, *599*(7886), 558–560. https://doi.org/10.1038/d41586-021-02955-z

Drake, J. C., Laker, R. C., Wilson, R. J., Zhang, M., and Yan, Z. (2019). Exercise-induced mitophagy in skeletal muscle occurs in the absence of stabilization of Pink1 on mitochondria. *Cell Cycle*, *18*(1), 1–6. https://doi.org/10.1080/15384101.2018.1559556

Duguez, S., Féasson, L., Denis, C., and Freyssenet, D. (2002). Mitochondrial biogenesis during skeletal muscle regeneration. *American Journal of Physiology-Endocrinology and Metabolism*, *282*(4), E802–E809. https://doi.org/10.1152/ajpendo.00343.2001

Dumont, F. J., and Su, Q. (1996). Mechanism of action of the immunosuppressant rapamycin. *Life Sciences*, *58*(5), 373–395. https://doi.org/10.1016/0024-3205(95)02233-3

Dunn, W. A. (1990). Studies on the mechanisms of autophagy: maturation of the autophagic vacuole. *Journal of Cell Biology*, *110*(6), 1935–1945. https://doi.org/10.1083/jcb.110.6.1935

Dunn, W. A. (1994). Autophagy and related mechanisms of lysosome-mediated protein degradation. *Trends in Cell Biology*, *4*(4), 139–143. https://doi.org/10.1016/0962-8924(94)90069-8

Durcan, T. M., Tang, M. Y., Pérusse, J. R., Dashti, E. A., Aguileta, M. A., McLelland, G., Gros, P., Shaler, T. A., Faubert, D., Coulombe, B., and Fon, E. A. (2014). USP8 regulates mitophagy by removing K6-linked ubiquitin conjugates from parkin. *The EMBO Journal*, *33*(21), 2473–2491. https://doi.org/10.15252/embj.201489729

East, D. A., and Campanella, M. (2016). Mitophagy and the therapeutic clearance of damaged mitochondria for neuroprotection. *The International Journal of Biochemistry and Cell Biology*, *79*, 382–387. https://doi.org/10.1016/j.biocel.2016.08.019

East, D. A., Fagiani, F., Crosby, J., Georgakopoulos, N. D., Bertrand, H., Schaap, M., Fowkes, A., Wells, G., and Campanella, M. (2014). PMI: A ΔΨm Independent Pharmacological Regulator of Mitophagy. *Chemistry and Biology*, *21*(11), 1585–1596. https://doi.org/10.1016/j.chembiol.2014.09.019

Elmore, S. (2007). Apoptosis: A Review of Programmed Cell Death. *Toxicologic Pathology*, *35*(4), 495–516. https://doi.org/10.1080/01926230701320337

Eskelinen, E.-L., Reggiori, F., Baba, M., Kovács, A. L., & Seglen, P. O. (2011). Seeing is believing: The impact of electron microscopy on autophagy research. *Autophagy*, *7*(9), 935–956. https://doi.org/10.4161/auto.7.9.15760

Esteban-Martínez, L., Sierra-Filardi, E., McGreal, R. S., Salazar-Roa, M., Mariño, G., Seco, E., Durand, S., Enot, D., Graña, O., Malumbres, M., Cvekl, A., Cuervo, A. M., Kroemer, G., and Boya, P. (2017). Programmed mitophagy is essential for the glycolytic switch during cell differentiation. *The EMBO Journal*, *36*(12), 1688–1706. https://doi.org/10.15252/embj.201695916

Fadok, V. A., Voelker, D. R., Campbell, P. A., Cohen, J. J., Bratton, D. L., and Henson, P. M. (1992). Exposure of phosphatidylserine on the surface of apoptotic lymphocytes triggers specific recognition and removal by macrophages. *Journal of Immunology (Baltimore, Md. : 1950)*, *148*(7), 2207–2216.

Fu, M., St-Pierre, P., Shankar, J., Wang, P. T. C., Joshi, B., and Nabi, I. R. (2013). Regulation of mitophagy by the Gp78 E3 ubiquitin ligase. *Molecular Biology of the Cell*, *24*(8), 1153–1162. https://doi.org/10.1091/mbc.E12-08-0607

Funayama, M., Ohe, K., Amo, T., Furuya, N., Yamaguchi, J., Saiki, S., Li, Y., Ogaki, K., Ando, M., Yoshino, H., Tomiyama, H., Nishioka, K., Hasegawa, K., Saiki, H., Satake, W., Mogushi, K., Sasaki, R., Kokubo, Y., Kuzuhara, S., … Hattori, N. (2015). CHCHD2 mutations in autosomal dominant late-onset Parkinson's disease: a genome-wide linkage and sequencing study. *The Lancet Neurology*, *14*(3), 274–282. https://doi.org/10.1016/S1474-4422(14)70266-2

Gatica, D., Lahiri, V., and Klionsky, D. J. (2018). Cargo recognition and degradation by selective autophagy. *Nature Cell Biology*, *20*(3), 233–242. https://doi.org/10.1038/s41556-018-0037-z

Gatliff, J., East, D., Crosby, J., Abeti, R., Harvey, R., Craigen, W., Parker, P., and Campanella, M. (2014). TSPO interacts with VDAC1 and triggers a ROS-mediated inhibition of mitochondrial quality control. *Autophagy*, *10*(12), 2279–2296. https://doi.org/10.4161/15548627.2014.991665

Georgakopoulos, N. D., Wells, G., and Campanella, M. (2017). The pharmacological regulation of cellular mitophagy. *Nature Chemical Biology*, *13*(2), 136–146. https://doi.org/10.1038/nchembio.2287

Geula, S., Naveed, H., Liang, J., and Shoshan-Barmatz, V. (2012). Structure-based Analysis of VDAC1 Protein. *Journal of Biological Chemistry*, *287*(3), 2179–2190. https://doi.org/10.1074/jbc.M111.268920

Gomez-Lazaro, M., Bonekamp, N. A., Galindo, M. F., Jordán, J., and Schrader, M. (2008). 6-Hydroxydopamine (6-OHDA) induces Drp1-dependent mitochondrial fragmentation in SH-SY5Y cells. *Free Radical Biology and Medicine*, *44*(11), 1960–1969. https://doi.org/10.1016/j.freeradbiomed.2008.03.009

González-Rodríguez, P., Zampese, E., Stout, K. A., Guzman, J. N., Ilijic, E., Yang, B., Tkatch, T., Stavarache, M. A., Wokosin, D. L., Gao, L., Kaplitt, M. G., López-Barneo, J., Schumacker, P. T., and Surmeier, D. J. (2021). Disruption of mitochondrial complex I induces progressive parkinsonism. *Nature*, *599*(7886), 650–656. https://doi.org/10.1038/s41586-021-04059-0

Greene, A. W., Grenier, K., Aguileta, M. A., Muise, S., Farazifard, R., Haque, M. E., McBride, H. M., Park, D. S., and Fon, E. A. (2012). Mitochondrial processing peptidase regulates PINK1 processing, import and Parkin recruitment. *EMBO Reports*, *13*(4), 378–385. https://doi.org/10.1038/embor.2012.14

Haddad, D., and Nakamura, K. (2015). Understanding the susceptibility of dopamine neurons to mitochondrial stressors in Parkinson's disease. *FEBS Letters*, *589*(24 Pt A), 3702–3713. https://doi.org/10.1016/j.febslet.2015.10.021

Hailey, D. W., Rambold, A. S., Satpute-Krishnan, P., Mitra, K., Sougrat, R., Kim, P. K., and Lippincott-Schwartz, J. (2010). Mitochondria Supply Membranes for Autophagosome Biogenesis during Starvation. *Cell*, *141*(4), 656–667. https://doi.org/10.1016/j.cell.2010.04.009

Ham, S. J., Lee, D., Yoo, H., Jun, K., Shin, H., & Chung, J. (2020). Decision between mitophagy and apoptosis by Parkin via VDAC1 ubiquitination. *Proceedings of the National Academy of Sciences*, *117*(8), 4281–4291. https://doi.org/10.1073/pnas.1909814117

Hamacher-Brady, A., and Brady, N. R. (2016). Mitophagy programs: mechanisms and physiological implications of mitochondrial targeting by autophagy. *Cellular and Molecular Life Sciences*, *73*(4), 775–795. https://doi.org/10.1007/s00018-015-2087-8

Hamacher-Brady, A., Brady, N. R., Logue, S. E., Sayen, M. R., Jinno, M., Kirshenbaum, L. A., Gottlieb, R. A., and Gustafsson, Å. B. (2007). Response to myocardial ischemia/reperfusion injury involves Bnip3 and autophagy. *Cell Death and Differentiation*, *14*(1), 146–157. https://doi.org/10.1038/sj.cdd.4401936

Hamasaki, M., Furuta, N., Matsuda, A., Nezu, A., Yamamoto, A., Fujita, N., Oomori, H., Noda, T., Haraguchi, T., Hiraoka, Y., Amano, A., and Yoshimori, T. (2013). Autophagosomes form at ER–mitochondria contact sites. *Nature*, *495*(7441), 389–393. https://doi.org/10.1038/nature11910

Han, J., Pluhackova, K., and Böckmann, R. A. (2017). The Multifaceted Role of SNARE Proteins in Membrane Fusion. *Frontiers in Physiology*, *8*. https://doi.org/10.3389/fphys.2017.00005

Hara, Y., Yanatori, I., Tanaka, A., Kishi, F., Lemasters, J. J., Nishina, S., Sasaki, K., & Hino, K. (2020). Iron loss triggers mitophagy through induction of mitochondrial ferritin. *EMBO Reports*, *21*(11). https://doi.org/10.15252/embr.202050202

Harms, M., and Seale, P. (2013). Brown and beige fat: development, function and therapeutic potential. *Nature Medicine*, *19*(10), 1252–1263. https://doi.org/10.1038/nm.3361

Hasegawa, J., Iwamoto, R., Otomo, T., Nezu, A., Hamasaki, M., and Yoshimori, T. (2016). Autophagosome–lysosome fusion in neurons requires <scp>INPP</scp> 5E, a protein associated with Joubert syndrome. *The EMBO Journal*, *35*(17), 1853–1867. https://doi.org/10.15252/embj.201593148

Hattori, N., Tanaka, M., Ozawa, T., and Mizuno, Y. (1991). Immunohistochemical studies on complexes I, II, III, and IV of mitochondria in parkinson's disease. *Annals of Neurology*, *30*(4), 563–571. https://doi.org/10.1002/ana.410300409

Hayashi-Nishino, M., Fujita, N., Noda, T., Yamaguchi, A., Yoshimori, T., and Yamamoto, A. (2009). A subdomain of the endoplasmic reticulum forms a cradle for autophagosome formation. *Nature Cell Biology*, *11*(12), 1433–1437. https://doi.org/10.1038/ncb1991

He, C., and Klionsky, D. J. (2009). Regulation Mechanisms and Signaling Pathways of Autophagy. *Annual Review of Genetics*, *43*(1), 67–93. https://doi.org/10.1146/annurev-genet-102808-114910

He, J., Zhang, G., Almeida, A. D., Cayouette, M., Simons, B. D., and Harris, W. A. (2012). How Variable Clones Build an Invariant Retina. *Neuron*, *75*(5), 786–798. https://doi.org/10.1016/j.neuron.2012.06.033

Heavner, W., and Pevny, L. (2012). Eye Development and Retinogenesis. *Cold Spring Harbor Perspectives in Biology*, *4*(12), a008391–a008391. https://doi.org/10.1101/cshperspect.a008391

Henson, P. M., and Hume, D. A. (2006). Apoptotic cell removal in development and tissue homeostasis. *Trends in Immunology*, *27*(5), 244–250. https://doi.org/10.1016/j.it.2006.03.005

Hertz, N. T., Berthet, A., Sos, M. L., Thorn, K. S., Burlingame, A. L., Nakamura, K., and Shokat, K. M. (2013). A Neo-Substrate that Amplifies Catalytic Activity of Parkinson's-Disease-Related Kinase PINK1. *Cell*, *154*(4), 737–747. https://doi.org/10.1016/j.cell.2013.07.030

Ho, D. H., Lee, H., Son, I., and Seol, W. (2019). G2019s LRRK2 promotes mitochondrial fission and increases TNFα-mediated neuroinflammation responses. *Animal Cells and Systems*, *23*(2), 106–111. https://doi.org/10.1080/19768354.2019.1585948

Hoon, M., Okawa, H., della Santina, L., and Wong, R. O. L. (2014). Functional architecture of the retina: Development and disease. *Progress in Retinal and Eye Research*, *42*, 44–84. https://doi.org/10.1016/j.preteyeres.2014.06.003

Hsieh, Y.-W., and Yang, X.-J. (2009). Dynamic Pax6 expression during the neurogenic cell cycle influences proliferation and cell fate choices of retinal progenitors. *Neural Development*, *4*(1), 32. https://doi.org/10.1186/1749-8104-4-32

Hu, M., and Easter, S. S. (1999). Retinal Neurogenesis: The Formation of the Initial Central Patch of Postmitotic Cells. *Developmental Biology*, *207*(2), 309–321. https://doi.org/10.1006/dbio.1998.9031

Ichimura, Y., Kirisako, T., Takao, T., Satomi, Y., Shimonishi, Y., Ishihara, N., Mizushima, N., Tanida, I., Kominami, E., Ohsumi, M., Noda, T., and Ohsumi, Y. (2000). A ubiquitin-like system mediates protein lipidation. *Nature*, *408*(6811), 488–492. https://doi.org/10.1038/35044114

Imazu, T., Shimizu, S., Tagami, S., Matsushima, M., Nakamura, Y., Miki, T., Okuyama, A., and Tsujimoto, Y. (1999). Bcl-2/E1B 19 kDa-interacting protein 3-like protein (Bnip3L) interacts with Bcl-2/Bcl-xL and induces apoptosis by altering mitochondrial membrane permeability. *Oncogene*, *18*(32), 4523–4529. https://doi.org/10.1038/sj.onc.1202722

Inoki, K., Zhu, T., and Guan, K.-L. (2003). TSC2 Mediates Cellular Energy Response to Control Cell Growth and Survival. Cell, 115(5), 577–590. https://doi.org/10.1016/S0092-8674(03)00929-2

Jackson, J. G., & Robinson, M. B. (2018). Regulation of mitochondrial dynamics in astrocytes: Mechanisms, consequences, and unknowns. Glia, 66(6), 1213–1234. https://doi.org/10.1002/glia.23252

Jacobs, D., Hoogerheide, D. P., Rovini, A., Jiang, Z., Lee, J. C., Rostovtseva, T. K., and Bezrukov, S. M. (2019). Probing Membrane Association of α-Synuclein Domains with VDAC Nanopore Reveals Unexpected Binding Pattern. *Scientific Reports*, *9*(1), 4580. https://doi.org/10.1038/s41598-019-40979-8

Jang, S., Kang, H. T., and Hwang, E. S. (2012). Nicotinamide-induced Mitophagy. *Journal of Biological Chemistry*, *287*(23), 19304–19314. https://doi.org/10.1074/jbc.M112.363747

Jin, S. M., Lazarou, M., Wang, C., Kane, L. A., Narendra, D. P., and Youle, R. J. (2010). Mitochondrial membrane potential regulates PINK1 import and proteolytic destabilization by PARL. *Journal of Cell Biology*, *191*(5), 933–942. https://doi.org/10.1083/jcb.201008084

Jin, Z., and El-Deiry, W. S. (2005). Overview of cell death signaling pathways. *Cancer Biology and Therapy*, *4*(2), 147–171. https://doi.org/10.4161/cbt.4.2.1508

Johansen, T., and Lamark, T. (2011). Selective autophagy mediated by autophagic adapter proteins. *Autophagy*, *7*(3), 279–296. https://doi.org/10.4161/auto.7.3.14487

Johansen, T., and Lamark, T. (2020). Selective Autophagy: ATG8 Family Proteins, LIR Motifs and Cargo Receptors. *Journal of Molecular Biology*, *432*(1), 80–103. https://doi.org/10.1016/j.jmb.2019.07.016

Jung Kim, M., Ho Kang, K., Kim, C.-H., and Choi, S.-Y. (2008). Real-time imaging of mitochondria in transgenic zebrafish expressing mitochondrially targeted GFP. *BioTechniques*, *45*(3), 331–334. https://doi.org/10.2144/000112909

Kamp, F., Exner, N., Lutz, A. K., Wender, N., Hegermann, J., Brunner, B., Nuscher, B., Bartels, T., Giese, A., Beyer, K., Eimer, S., Winklhofer, K. F., and Haass, C. (2010). Inhibition of mitochondrial fusion by α-synuclein is rescued by PINK1, Parkin and DJ-1. *The EMBO Journal*, *29*(20), 3571–3589. https://doi.org/10.1038/emboj.2010.223

Kang, R., Zeh, H. J., Lotze, M. T., and Tang, D. (2011). The Beclin 1 network regulates autophagy and apoptosis. *Cell Death and Differentiation*, *18*(4), 571–580. https://doi.org/10.1038/cdd.2010.191

Katayama, H., Kogure, T., Mizushima, N., Yoshimori, T., and Miyawaki, A. (2011). A Sensitive and Quantitative Technique for Detecting Autophagic Events Based on Lysosomal Delivery. *Chemistry and Biology*, *18*(8), 1042–1052. https://doi.org/10.1016/j.chembiol.2011.05.013

Kerr, J. F. R. (2002). History of the events leading to the formulation of the apoptosis concept. *Toxicology*, *181–182*, 471–474. https://doi.org/10.1016/S0300-483X(02)00457-2

Kerr, J. F. R., Wyllie, A. H., & Currie, A. R. (1972). Apoptosis: A Basic Biological Phenomenon with Wideranging Implications in Tissue Kinetics. *British Journal of Cancer*, *26*(4), 239–257. https://doi.org/10.1038/bjc.1972.33

Kim, E. H., and Choi, K. S. (2008). A critical role of superoxide anion in selenite-induced mitophagic cell death. *Autophagy*, *4*(1), 76–78. https://doi.org/10.4161/auto.5119

Kim, Y. Y., Um, J., Yoon, J., Kim, H., Lee, D., Lee, Y. J., Jee, H. J., Kim, Y. M., Jang, J. S., Jang, Y., Chung, J., Park, H. T., Finkel, T., Koh, H., and Yun, J. (2019). Assessment of mitophagy in mt-Keima *Drosophila* revealed an essential role of the PINK1-Parkin pathway in mitophagy induction *in vivo*. *The FASEB Journal*, *33*(9), 9742–9751. https://doi.org/10.1096/fj.201900073R

Kirisako, T., Ichimura, Y., Okada, H., Kabeya, Y., Mizushima, N., Yoshimori, T., Ohsumi, M., Takao, T., Noda, T., and Ohsumi, Y. (2000). The Reversible Modification Regulates the Membrane-Binding State of Apg8/Aut7 Essential for Autophagy and the Cytoplasm to Vacuole Targeting Pathway. *Journal of Cell Biology*, *151*(2), 263–276. https://doi.org/10.1083/jcb.151.2.263

Kirkin, V., McEwan, D. G., Novak, I., and Dikic, I. (2009). A Role for Ubiquitin in Selective Autophagy. *Molecular Cell*, *34*(3), 259–269. https://doi.org/10.1016/j.molcel.2009.04.026

Klionsky, D. J. (2007). Autophagy: from phenomenology to molecular understanding in less than a decade. *Nature Reviews Molecular Cell Biology*, *8*(11), 931–937. https://doi.org/10.1038/nrm2245

Koentjoro, B., Park, J.-S., and Sue, C. M. (2017). Nix restores mitophagy and mitochondrial function to protect against PINK1/Parkin-related Parkinson's disease. *Scientific Reports*, *7*(1), 44373. https://doi.org/10.1038/srep44373

Kondapalli, C., Kazlauskaite, A., Zhang, N., Woodroof, H. I., Campbell, D. G., Gourlay, R., Burchell, L., Walden, H., Macartney, T. J., Deak, M., Knebel, A., Alessi, D. R., and Muqit, M. M. K. (2012). PINK1 is activated by mitochondrial membrane potential depolarization and stimulates Parkin E3 ligase activity by phosphorylating Serine 65. *Open Biology*, *2*(5), 120080. https://doi.org/10.1098/rsob.120080

Koso, H., Satoh, S., and Watanabe, S. (2007). c-kit marks late retinal progenitor cells and regulates their differentiation in developing mouse retina. *Developmental Biology*, *301*(1), 141–154. https://doi.org/10.1016/j.ydbio.2006.09.027

Koyano, F., Yamano, K., Kosako, H., Tanaka, K., and Matsuda, N. (2019). Parkin recruitment to impaired mitochondria for nonselective ubiquitylation is facilitated by MITOL. *Journal of Biological Chemistry*, *294*(26), 10300–10314. https://doi.org/10.1074/jbc.RA118.006302

Krock, B. L., and Perkins, B. D. (2014). The Par-PrkC Polarity Complex Is Required for Cilia Growth in Zebrafish Photoreceptors. *PLoS ONE*, *9*(8), e104661. https://doi.org/10.1371/journal.pone.0104661

Kubli, D. A., Cortez, M. Q., Moyzis, A. G., Najor, R. H., Lee, Y., and Gustafsson, Å. B. (2015). PINK1 Is Dispensable for Mitochondrial Recruitment of Parkin and Activation of Mitophagy in Cardiac Myocytes. *PLOS ONE*, *10*(6), e0130707. https://doi.org/10.1371/journal.pone.0130707

Kundu, M., Lindsten, T., Yang, C.-Y., Wu, J., Zhao, F., Zhang, J., Selak, M. A., Ney, P. A., and Thompson, C. B. (2008). Ulk1 plays a critical role in the autophagic clearance of mitochondria and ribosomes during reticulocyte maturation. *Blood*, *112*(4), 1493–1502. https://doi.org/10.1182/blood-2008-02-137398

Kuter, K., Nowak, P., Gołembiowska, K., and Ossowska, K. (2010). Increased Reactive Oxygen Species Production in the Brain After Repeated Low-Dose Pesticide Paraquat Exposure in Rats. A Comparison with Peripheral Tissues. *Neurochemical Research*, *35*(8), 1121–1130. https://doi.org/10.1007/s11064-010-0163-x

Kuter, K., Śmiałowska, M., Wierońska, J., Zięba, B., Wardas, J., Pietraszek, M., Nowak, P., Biedka, I., Roczniak, W., Konieczny, J., Wolfarth, S., and Ossowska, K. (2007). Toxic influence of subchronic paraquat administration on dopaminergic neurons in rats. *Brain Research*, *1155*, 196–207. https://doi.org/10.1016/j.brainres.2007.04.018

Lambourne, O. A., and Mehellou, Y. (2018). Chemical Strategies for Activating PINK1, a Protein Kinase Mutated in Parkinson's Disease. *ChemBioChem*, *19*(23), 2433–2437. https://doi.org/10.1002/cbic.201800497

Lazarou, M., Jin, S. M., Kane, L. A., and Youle, R. J. (2012). Role of PINK1 Binding to the TOM Complex and Alternate Intracellular Membranes in Recruitment and Activation of the E3 Ligase Parkin. *Developmental Cell*, *22*(2), 320–333. https://doi.org/10.1016/j.devcel.2011.12.014

Lazarou, M., Sliter, D. A., Kane, L. A., Sarraf, S. A., Wang, C., Burman, J. L., Sideris, D. P., Fogel, A. I., and Youle, R. J. (2015). The ubiquitin kinase PINK1 recruits autophagy receptors to induce mitophagy. *Nature*, *524*(7565), 309–314. https://doi.org/10.1038/nature14893

Lee, H. il, Jang, S.-Y., Kang, H. T., and Hwang, E. S. (2008). p53-, SIRT1-, and PARP-1-independent downregulation of p21WAF1 expression in nicotinamide-treated cells. *Biochemical and Biophysical Research Communications*, *368*(2), 298–304. https://doi.org/10.1016/j.bbrc.2008.01.082

Lees, A. J., Hardy, J., and Revesz, T. (2009). Parkinson's disease. *The Lancet*, *373*(9680), 2055–2066. https://doi.org/10.1016/S0140-6736(09)60492-X

Lemasters, J. J. (2005). Selective Mitochondrial Autophagy, or Mitophagy, as a Targeted Defense Against Oxidative Stress, Mitochondrial Dysfunction, and Aging. *Rejuvenation Research*, *8*(1), 3–5. https://doi.org/10.1089/rej.2005.8.3

Levine, B., and Kroemer, G. (2008). Autophagy in the Pathogenesis of Disease. *Cell*, *132*(1), 27–42. https://doi.org/10.1016/j.cell.2007.12.018

Levine, B., and Kroemer, G. (2019). Biological Functions of Autophagy Genes: A Disease Perspective. *Cell*, *176*(1–2), 11–42. https://doi.org/10.1016/j.cell.2018.09.048

Liberman, E. A., Topaly, V. P., Tsofina, L. M., Jasaitis, A. A., and Skulachev, V. P. (1969). Mechanism of Coupling of Oxidative Phosphorylation and the Membrane Potential of Mitochondria. *Nature*, *222*(5198), 1076–1078. https://doi.org/10.1038/2221076a0

Lindgren, H. S., Lelos, M. J., and Dunnett, S. B. (2012). Do alpha-synuclein vector injections provide a better model of Parkinson's disease than the classic 6-hydroxydopamine model? *Experimental Neurology*, *237*(1), 36–42. https://doi.org/10.1016/j.expneurol.2012.05.022

Liou, H.-H., Chen, R.-C., Tsai, Y.-F., Chen, W.-P., Chang, Y.-C., and Tsai, M.-C. (1996). Effects of Paraquat on the Substantia Nigra of the Wistar Rats: Neurochemical, Histological, and Behavioral Studies. *Toxicology and Applied Pharmacology*, *137*(1), 34–41. https://doi.org/10.1006/taap.1996.0054

Liu, Y., Ji, Y., Li, X., Tian, K., Yf Young, C., Lou, H., and Yuan, H. (2013). Retigeric acid B-induced mitophagy by oxidative stress attenuates cell death against prostate cancer cells in vitro. *Acta Pharmacologica Sinica*, *34*(9), 1183–1191. https://doi.org/10.1038/aps.2013.68

Lu, X., Altshuler-Keylin, S., Wang, Q., Chen, Y., Henrique Sponton, C., Ikeda, K., Maretich, P., Yoneshiro, T., and Kajimura, S. (2018). Mitophagy controls beige adipocyte maintenance through a Parkin-dependent and UCP1-independent mechanism. *Science Signaling*, *11*(527). https://doi.org/10.1126/scisignal.aap8526

Ludtmann, M. H. R., Angelova, P. R., Horrocks, M. H., Choi, M. L., Rodrigues, M., Baev, A. Y., Berezhnov, A. v, Yao, Z., Little, D., Banushi, B., Al-Menhali, A. S., Ranasinghe, R. T., Whiten, D. R., Yapom, R., Dolt, K. S., Devine, M. J., Gissen, P., Kunath, T., Jaganjac, M., … Gandhi, S. (2018). α-synuclein oligomers interact with ATP synthase and open the permeability transition pore in Parkinson's disease. *Nature Communications*, *9*(1), 2293. https://doi.org/10.1038/s41467-018-04422-2

Luthman, J., Fredriksson, A., Sundström, E., Jonsson, G., and Archer, T. (1989). Selective lesion of central dopamine or noradrenaline neuron systems in the neonatal rat: motor behavior and monoamine alterations at adult stage. *Behavioural Brain Research*, *33*(3), 267–277. https://doi.org/10.1016/S0166-4328(89)80121-4

Maestro, I., de la Ballina, L. R., Simonsen, A., Boya, P., and Martinez, A. (2021). Phenotypic Assay Leads to Discovery of Mitophagy Inducers with Therapeutic Potential for Parkinson's Disease. *ACS Chemical Neuroscience*, *12*(24), 4512–4523. https://doi.org/10.1021/acschemneuro.1c00529

Mahul-Mellier, A.-L., Burtscher, J., Maharjan, N., Weerens, L., Croisier, M., Kuttler, F., Leleu, M., Knott, G. W., and Lashuel, H. A. (2020). The process of Lewy body formation, rather than simply α-synuclein fibrillization, is one of the major drivers of neurodegeneration. *Proceedings of the National Academy of Sciences*, *117*(9), 4971–4982. https://doi.org/10.1073/pnas.1913904117

Maiuri, M. C., le Toumelin, G., Criollo, A., Rain, J.-C., Gautier, F., Juin, P., Tasdemir, E., Pierron, G., Troulinaki, K., Tavernarakis, N., Hickman, J. A., Geneste, O., and Kroemer, G. (2007). Functional and physical interaction between Bcl-XL and a BH3-like domain in Beclin-1. *The EMBO Journal*, *26*(10), 2527–2539. https://doi.org/10.1038/sj.emboj.7601689

Malpartida, A. B., Williamson, M., Narendra, D. P., Wade-Martins, R., and Ryan, B. J. (2021). Mitochondrial Dysfunction and Mitophagy in Parkinson's Disease: From Mechanism to Therapy. *Trends in Biochemical Sciences*, *46*(4), 329–343. https://doi.org/10.1016/j.tibs.2020.11.007

Maro, B., Marty, M. C., and Bornens, M. (1982). In vivo and in vitro effects of the mitochondrial uncoupler FCCP on microtubules. *The EMBO Journal*, *1*(11), 1347–1352.

Marquardt, T., Ashery-Padan, R., Andrejewski, N., Scardigli, R., Guillemot, F., and Gruss, P. (2001). Pax6 Is Required for the Multipotent State of Retinal Progenitor Cells. *Cell*, *105*(1), 43–55. https://doi.org/10.1016/S0092-8674(01)00295-1

Martínez-González, L., Rodríguez-Cueto, C., Cabezudo, D., Bartolomé, F., Andrés-Benito, P., Ferrer, I., Gil, C., Martín-Requero, Á., Fernández-Ruiz, J., Martínez, A., and de Lago, E. (2020). Motor neuron preservation and decrease of in vivo TDP-43 phosphorylation by protein CK-1δ kinase inhibitor treatment. *Scientific Reports*, *10*(1), 4449. https://doi.org/10.1038/s41598-020-61265-y

Mathai, B., Meijer, A., and Simonsen, A. (2017). Studying Autophagy in Zebrafish. *Cells*, *6*(3), 21. https://doi.org/10.3390/cells6030021

Mauro-Lizcano, M., Esteban-Martínez, L., Seco, E., Serrano-Puebla, A., Garcia-Ledo, L., Figueiredo-Pereira, C., Vieira, H. L., and Boya, P. (2015). New method to assess mitophagy flux by flow cytometry. Autophagy, 11(5), 833–843. https://doi.org/10.1080/15548627.2015.1034403

McCabe, K. L., Gunther, E. C., and Reh, T. A. (1999). The development of the pattern of retinal ganglion cells in the chick retina: mechanisms that control differentiation. *Development*, *126*(24), 5713–5724. https://doi.org/10.1242/dev.126.24.5713

McLelland, G.-L., Soubannier, V., Chen, C. X., McBride, H. M., and Fon, E. A. (2014). Parkin and PINK1 function in a vesicular trafficking pathway regulating mitochondrial quality control. *The EMBO Journal*, n/a-n/a. https://doi.org/10.1002/embj.201385902

McWilliams, T. G., Prescott, A. R., Allen, G. F. G., Tamjar, J., Munson, M. J., Thomson, C., Muqit, M. M. K., and Ganley, I. G. (2016). MitoQC illuminates mitophagy and mitochondrial architecture in vivo. *Journal of Cell Biology*, *214*(3), 333–345. https://doi.org/10.1083/jcb.201603039

McWilliams, T. G., Prescott, A. R., Montava-Garriga, L., Ball, G., Singh, F., Barini, E., Muqit, M. M. K., Brooks, S. P., and Ganley, I. G. (2018). Basal Mitophagy Occurs Independently of PINK1 in Mouse Tissues of High Metabolic Demand. *Cell Metabolism*, *27*(2), 439-449.e5. https://doi.org/10.1016/j.cmet.2017.12.008

McWilliams, T. G., Prescott, A. R., Villarejo-Zori, B., Ball, G., Boya, P., and Ganley, I. G. (2019). A comparative map of macroautophagy and mitophagy in the vertebrate eye. *Autophagy*, *15*(7), 1296–1308. https://doi.org/10.1080/15548627.2019.1580509

Michel, P. P., Hirsch, E. C., and Hunot, S. (2016). Understanding Dopaminergic Cell Death Pathways in Parkinson Disease. *Neuron*, *90*(4), 675–691. https://doi.org/10.1016/j.neuron.2016.03.038

Mijaljica, D., Prescott, M., and Devenish, R. J. (2012). The Intriguing Life of Autophagosomes. *International Journal of Molecular Sciences*, *13*(3), 3618–3635. https://doi.org/10.3390/ijms13033618

Mishra, J., Davani, A. J., Natarajan, G. K., Kwok, W.-M., Stowe, D. F., Camara, A. K. S. (2019). Cyclosporin A Increases Mitochondrial Buffering of Calcium: An Additional Mechanism in Delaying Mitochondrial Permeability Transition Pore Opening. Cells, 8(9), 1052. https://doi.org/10.3390/cells8091052

Mizushima, N. (2007). Autophagy: process and function. *Genes and Development*, *21*(22), 2861–2873. https://doi.org/10.1101/gad.1599207

Mizushima, N., and Klionsky, D. J. (2007). Protein Turnover Via Autophagy: Implications for Metabolism. *Annual Review of Nutrition*, *27*(1), 19–40. https://doi.org/10.1146/annurev.nutr.27.061406.093749

Mizushima, N., Noda, T., Yoshimori, T., Tanaka, Y., Ishii, T., George, M. D., Klionsky, D. J., Ohsumi, M., and Ohsumi, Y. (1998). A protein conjugation system essential for autophagy. *Nature*, *395*(6700), 395–398. https://doi.org/10.1038/26506

Moors, T. E., Hoozemans, J. J. M., Ingrassia, A., Beccari, T., Parnetti, L., Chartier-Harlin, M.-C., and van de Berg, W. D. J. (2017). Therapeutic potential of autophagy-enhancing agents in Parkinson's disease. *Molecular Neurodegeneration*, *12*(1), 11. https://doi.org/10.1186/s13024-017-0154-3

Morales, I., Sanchez, A., Puertas-Avendaño, R., Rodriguez-Sabate, C., Perez-Barreto, A., and Rodriguez, M. (2020). Neuroglial transmitophagy and Parkinson's disease. *Glia*. https://doi.org/10.1002/glia.23839

Nakatogawa, H., Suzuki, K., Kamada, Y., and Ohsumi, Y. (2009). Dynamics and diversity in autophagy mechanisms: lessons from yeast. *Nature Reviews Molecular Cell Biology*, *10*(7), 458–467. https://doi.org/10.1038/nrm2708

Narendra, D., Tanaka, A., Suen, D.-F., and Youle, R. J. (2008). Parkin is recruited selectively to impaired mitochondria and promotes their autophagy. *Journal of Cell Biology*, *183*(5), 795–803. https://doi.org/10.1083/jcb.200809125

Noda, N. N., Kumeta, H., Nakatogawa, H., Satoo, K., Adachi, W., Ishii, J., Fujioka, Y., Ohsumi, Y., and Inagaki, F. (2008). Structural basis of target recognition by Atg8/LC3 during selective autophagy. *Genes to Cells*, *13*(12), 1211–1218. https://doi.org/10.1111/j.1365-2443.2008.01238.x

Olszewska, D. A., and Lynch, T. (2017). Nature's Parkin experiment: Nix-a novel protective mechanism in Parkinson's disease. *Movement Disorders*, *32*(7), 992. https://doi.org/10.1002/mds.27015

Orsi, A., Polson, H. E. J., and Tooze, S. A. (2010). Membrane trafficking events that partake in autophagy. *Current Opinion in Cell Biology*, *22*(2), 150–156. https://doi.org/10.1016/j.ceb.2009.11.013

Padman, B. S., Bach, M., Lucarelli, G., Prescott, M., and Ramm, G. (2013). The protonophore CCCP interferes with lysosomal degradation of autophagic cargo in yeast and mammalian cells. *Autophagy*, *9*(11), 1862–1875. https://doi.org/10.4161/auto.26557

Park, K.-S., Jo, I., Pak, Y., Bae, S.-W., Rhim, H., Suh, S.-H., Park, S., Zhu, M., So, I., and Kim, K. (2002). FCCP depolarizes plasma membrane potential by activating proton and Na+ currents in bovine aortic endothelial cells. *Pflügers Archiv - European Journal of Physiology*, *443*(3), 344–352. https://doi.org/10.1007/s004240100703

Park, S. J., Shin, J. H., Kim, E. S., Jo, Y. K., Kim, J. H., Hwang, J. J., Kim, J. C., and Cho, D.-H. (2012). Mitochondrial fragmentation caused by phenanthroline promotes mitophagy. *FEBS Letters*, *586*(24), 4303–4310. https://doi.org/10.1016/j.febslet.2012.10.035

Pattingre, S., Tassa, A., Qu, X., Garuti, R., Liang, X. H., Mizushima, N., Packer, M., Schneider, M. D., and Levine, B. (2005). Bcl-2 Antiapoptotic Proteins Inhibit Beclin 1-Dependent Autophagy. *Cell*, *122*(6), 927–939. https://doi.org/10.1016/j.cell.2005.07.002

Pickrell, A. M., and Youle, R. J. (2015). The Roles of PINK1, Parkin, and Mitochondrial Fidelity in Parkinson's Disease. *Neuron*, *85*(2), 257–273. https://doi.org/10.1016/j.neuron.2014.12.007

Poggi, L., Vitorino, M., Masai, I., and Harris, W. A. (2005). Influences on neural lineage and mode of division in the zebrafish retina in vivo. *Journal of Cell Biology*, *171*(6), 991–999. https://doi.org/10.1083/jcb.200509098

Princely Abudu, Y., Pankiv, S., Mathai, B. J., Håkon Lystad, A., Bindesbøll, C., Brenne, H. B., Yoke Wui Ng, M., Thiede, B., Yamamoto, A., Mutugi Nthiga, T., Lamark, T., Esguerra, C. v, Johansen, T., and Simonsen, A. (2019). NIPSNAP1 and NIPSNAP2 Act as "Eat Me" Signals for Mitophagy. *Developmental Cell*, *49*(4), 509-525.e12. https://doi.org/10.1016/j.devcel.2019.03.013

Quinsay, M. N., Thomas, R. L., Lee, Y., and Gustafsson, Å. B. (2010). Bnip3-mediated mitochondrial autophagy is independent of the mitochondrial permeability transition pore. *Autophagy*, *6*(7), 855–862. https://doi.org/10.4161/auto.6.7.13005

Ray, R., Chen, G., vande Velde, C., Cizeau, J., Park, J. H., Reed, J. C., Gietz, R. D., and Greenberg, A. H. (2000). BNIP3 Heterodimerizes with Bcl-2/Bcl-XL and Induces Cell Death Independent of a Bcl-2 Homology 3 (BH3) Domain at Both Mitochondrial and Nonmitochondrial Sites. *Journal of Biological Chemistry*, *275*(2), 1439–1448. https://doi.org/10.1074/jbc.275.2.1439

Raymond, P. A., Barthel, L. K., and Curran, G. A. (1995). Developmental patterning of rod and cone photoreceptors in embryonic zebrafish. *The Journal of Comparative Neurology*, *359*(4), 537–550. https://doi.org/10.1002/cne.903590403

Redmann, M., Dodson, M., Boyer-Guittaut, M., Darley-Usmar, V., and Zhang, J. (2014). Mitophagy mechanisms and role in human diseases. *The International Journal of Biochemistry and Cell Biology*, *53*, 127–133. https://doi.org/10.1016/j.biocel.2014.05.010

Rocha, E. M., de Miranda, B. R., Castro, S., Drolet, R., Hatcher, N. G., Yao, L., Smith, S. M., Keeney, M. T., di Maio, R., Kofler, J., Hastings, T. G., and Greenamyre, J. T. (2020). LRRK2 inhibition prevents endolysosomal deficits seen in human Parkinson's disease. *Neurobiology of Disease*, *134*, 104626. https://doi.org/10.1016/j.nbd.2019.104626

Rogov, V. v, Stolz, A., Ravichandran, A. C., Rios-Szwed, D. O., Suzuki, H., Kniss, A., Löhr, F., Wakatsuki, S., Dötsch, V., Dikic, I., Dobson, R. C. J., and McEwan, D. G. (2017). Structural and functional analysis of the GABARAP interaction motif (GIM). *EMBO Reports*, *18*(8), 1382–1396. https://doi.org/10.15252/embr.201643587

Russo, I., Kaganovich, A., Ding, J., Landeck, N., Mamais, A., Varanita, T., Biosa, A., Tessari, I., Bubacco, L., Greggio, E., and Cookson, M. R. (2019). Transcriptome analysis of LRRK2 knock-out microglia cells reveals alterations of inflammatory- and oxidative stress-related pathways upon treatment with α-synuclein fibrils. *Neurobiology of Disease*, *129*, 67–78. https://doi.org/10.1016/j.nbd.2019.05.012

Ryan, B. J., Hoek, S., Fon, E. A., and Wade-Martins, R. (2015). Mitochondrial dysfunction and mitophagy in Parkinson's: from familial to sporadic disease. *Trends in Biochemical Sciences*, *40*(4), 200–210. https://doi.org/10.1016/j.tibs.2015.02.003

Ryan, T., Bamm, V. v, Stykel, M. G., Coackley, C. L., Humphries, K. M., Jamieson-Williams, R., Ambasudhan, R., Mosser, D. D., Lipton, S. A., Harauz, G., and Ryan, S. D. (2018). Cardiolipin exposure on the outer mitochondrial membrane modulates α-synuclein. *Nature Communications*, *9*(1), 817. https://doi.org/10.1038/s41467-018-03241-9

Saftig, P., Beertsen, W., and Eskelinen, E.-L. (2008). LAMP-2: A control step for phagosome and autophagosome maturation. *Autophagy*, *4*(4), 510–512. https://doi.org/10.4161/auto.5724

Sandoval, H., Thiagarajan, P., Dasgupta, S. K., Schumacher, A., Prchal, J. T., Chen, M., and Wang, J. (2008). Essential role for Nix in autophagic maturation of erythroid cells. *Nature*, *454*(7201), 232–235. https://doi.org/10.1038/nature07006

Schmelzle, T., Beck, T., Martin, D. E., and Hall, M. N. (2004). Activation of the RAS/Cyclic AMP Pathway Suppresses a TOR Deficiency in Yeast. *Molecular and Cellular Biology*, *24*(1), 338–351. https://doi.org/10.1128/MCB.24.1.338-351.2004

Schmitt, E. A., and Dowling, J. E. (1994). Early-eye morphogenesis in the zebrafish,Brachydanio rerio. *The Journal of Comparative Neurology*, *344*(4), 532–542. https://doi.org/10.1002/cne.903440404

Schweers, R. L., Zhang, J., Randall, M. S., Loyd, M. R., Li, W., Dorsey, F. C., Kundu, M., Opferman, J. T., Cleveland, J. L., Miller, J. L., and Ney, P. A. (2007). NIX is required for programmed mitochondrial clearance during reticulocyte maturation. *Proceedings of the National Academy of Sciences*, *104*(49), 19500–19505. https://doi.org/10.1073/pnas.0708818104

Sebastián-Pérez, V., Roca, C., Awale, M., Reymond, J.-L., Martinez, A., Gil, C., & Campillo, N. E. (2017). Medicinal and Biological Chemistry (MBC) Library: An Efficient Source of New Hits. *Journal of Chemical Information and Modeling*, *57*(9), 2143–2151. https://doi.org/10.1021/acs.jcim.7b00401

Shahmoradian, S. H., Lewis, A. J., Genoud, C., Hench, J., Moors, T. E., Navarro, P. P., Castaño-Díez, D., Schweighauser, G., Graff-Meyer, A., Goldie, K. N., Sütterlin, R., Huisman, E., Ingrassia, A., Gier, Y. de, Rozemuller, A. J. M., Wang, J., Paepe, A. de, Erny, J., Staempfli, A., … Lauer, M. E. (2019). Lewy pathology in Parkinson's disease consists of crowded organelles and lipid membranes. *Nature Neuroscience*, *22*(7), 1099–1109. https://doi.org/10.1038/s41593-019-0423-2

Shen, Q., Yamano, K., Head, B. P., Kawajiri, S., Cheung, J. T. M., Wang, C., Cho, J.-H., Hattori, N., Youle, R. J., and van der Bliek, A. M. (2014). Mutations in Fis1 disrupt orderly disposal of defective mitochondria. *Molecular Biology of the Cell*, *25*(1), 145–159. https://doi.org/10.1091/mbc.e13-09-0525

Shiba-Fukushima, K., Inoshita, T., Sano, O., Iwata, H., Ishikawa, K., Okano, H., Akamatsu, W., Imai, Y., and Hattori, N. (2020). A Cell-Based High-Throughput Screening Identified Two Compounds that Enhance PINK1-Parkin Signaling. *IScience*, *23*(5), 101048. https://doi.org/10.1016/j.isci.2020.101048

Shires, S. E., & Gustafsson, Å. B. (2015). Mitophagy and heart failure. *Journal of Molecular Medicine*, *93*(3), 253–262. https://doi.org/10.1007/s00109-015-1254-6

Sin, J., Andres, A. M., Taylor, D. J. R., Weston, T., Hiraumi, Y., Stotland, A., Kim, B. J., Huang, C., Doran, K. S., and Gottlieb, R. A. (2016). Mitophagy is required for mitochondrial biogenesis and myogenic differentiation of C2C12 myoblasts. *Autophagy*, *12*(2), 369–380. https://doi.org/10.1080/15548627.2015.1115172

Sofroniew, M. v, and Vinters, H. v. (2010). Astrocytes: biology and pathology. *Acta Neuropathologica*, *119*(1), 7–35. https://doi.org/10.1007/s00401-009-0619-8

Spinelli, J. B., and Haigis, M. C. (2018). The multifaceted contributions of mitochondria to cellular metabolism. *Nature Cell Biology*, *20*(7), 745–754. https://doi.org/10.1038/s41556-018-0124-1

Stacy, R. C., and Oi Lun Wong, R. (2003). Developmental relationship between cholinergic amacrine cell processes and ganglion cell dendrites of the mouse retina. *The Journal of Comparative Neurology*, *456*(2), 154–166. https://doi.org/10.1002/cne.10509

Stenkamp, D. L. (2015). *Development of the Vertebrate Eye and Retina* (pp. 397–414). https://doi.org/10.1016/bs.pmbts.2015.06.006

Su, B., Wang, X., Zheng, L., Perry, G., Smith, M. A., and Zhu, X. (2010). Abnormal mitochondrial dynamics and neurodegenerative diseases. *Biochimica et Biophysica Acta (BBA) - Molecular Basis of Disease*, *1802*(1), 135–142. https://doi.org/10.1016/j.bbadis.2009.09.013

Szargel, R., Shani, V., Abd Elghani, F., Mekies, L. N., Liani, E., Rott, R., and Engelender, S. (2016). The PINK1, synphilin-1 and SIAH-1 complex constitutes a novel mitophagy pathway. *Human Molecular Genetics*, *25*(16), 3476–3490. https://doi.org/10.1093/hmg/ddw189

Takano-Ohmuro, H., Mukaida, M., Kominami, E., and Morioka, K. (2000). Autophagy in embryonic erythroid cells: its role in maturation. *European Journal of Cell Biology*, *79*(10), 759–764. https://doi.org/10.1078/0171-9335-00096

Tanaka, Y., Guhde, G., Suter, A., Eskelinen, E.-L., Hartmann, D., Lüllmann-Rauch, R., Janssen, P. M. L., Blanz, J., von Figura, K.,; Saftig, P. (2000). Accumulation of autophagic vacuoles and cardiomyopathy in LAMP-2-deficient mice. Nature, 406(6798), 902–906. https://doi.org/10.1038/35022595

Tang, D., Kang, R., Berghe, T. vanden, Vandenabeele, P., and Kroemer, G. (2019). The molecular machinery of regulated cell death. *Cell Research*, *29*(5), 347–364. https://doi.org/10.1038/s41422-019-0164-5

Terešak, P., Lapao, A., Subic, N., Boya, P., Elazar, Z., and Simonsen, A. (2022). Regulation of PRKN-independent mitophagy. *Autophagy*, *18*(1), 24–39. https://doi.org/10.1080/15548627.2021.1888244

Tracy, K., Dibling, B. C., Spike, B. T., Knabb, J. R., Schumacker, P., and Macleod, K. F. (2007). *BNIP3* Is an RB/E2F Target Gene Required for Hypoxia-Induced Autophagy. *Molecular and Cellular Biology*, *27*(17), 6229–6242. https://doi.org/10.1128/MCB.02246-06

Tsukada, M., and Ohsumi, Y. (1993). Isolation and characterization of autophagy-defective mutants of *Saccharomyces cerevisiae*. *FEBS Letters*, *333*(1–2), 169–174. https://doi.org/10.1016/0014-5793(93)80398-E

Valenciano, A. I., Boya, P., & de la Rosa, E. J. (2009). Early neural cell death: numbers and cues from the developing neuroretina. *The International Journal of Developmental Biology*, *53*(8-9–10), 1515–1528. https://doi.org/10.1387/ijdb.072446av

Vecino, E., and Acera, A. (2015). Development and programed cell death in the mammalian eye. *The International Journal of Developmental Biology*, *59*(1-2–3), 63–71. https://doi.org/10.1387/ijdb.150070ev

Wager, K., and Russell, C. (2013). Mitophagy and neurodegeneration. *Autophagy*, *9*(11), 1693–1709. https://doi.org/10.4161/auto.25082

Wang, X., Becker, K., Levine, N., Zhang, M., Lieberman, A. P., Moore, D. J., and Ma, J. (2019). Pathogenic alpha-synuclein aggregates preferentially bind to mitochondria and affect cellular respiration. *Acta Neuropathologica Communications*, *7*(1), 41. https://doi.org/10.1186/s40478-019-0696-4

Wang, Y., Nartiss, Y., Steipe, B., McQuibban, G. A., and Kim, P. K. (2012). ROS-induced mitochondrial depolarization initiates PARK2/PARKIN-dependent mitochondrial degradation by autophagy. *Autophagy*, *8*(10), 1462–1476. https://doi.org/10.4161/auto.21211

Wauer, T., Simicek, M., Schubert, A., and Komander, D. (2015). Mechanism of phospho-ubiquitin-induced PARKIN activation. *Nature*, *524*(7565), 370–374. https://doi.org/10.1038/nature14879

Wong, Y. C., and Holzbaur, E. L. F. (2014). Optineurin is an autophagy receptor for damaged mitochondria in parkin-mediated mitophagy that is disrupted by an ALS-linked mutation. *Proceedings of the National Academy of Sciences*, *111*(42). https://doi.org/10.1073/pnas.1405752111

Wrighton, P. J., Shwartz, A., Heo, J.-M., Quenzer, E. D., LaBella, K. A., Harper, J. W., and Goessling, W. (2021). Quantitative intravital imaging in zebrafish reveals *in vivo* dynamics of physiological-stress-induced mitophagy. *Journal of Cell Science*, *134*(4). https://doi.org/10.1242/jcs.256255

Xie, Z., and Klionsky, D. J. (2007). Autophagosome formation: core machinery and adaptations. *Nature Cell Biology*, *9*(10), 1102–1109. https://doi.org/10.1038/ncb1007-1102

Xu, C. (2005). Endoplasmic reticulum stress: cell life and death decisions. *Journal of Clinical Investigation*, *115*(10), 2656–2664. https://doi.org/10.1172/JCI26373

Yang, Y., Hu, L., Zheng, H., Mao, C., Hu, W., Xiong, K., Wang, F., and Liu, C. (2013). Application and interpretation of current autophagy inhibitors and activators. *Acta Pharmacologica Sinica*, *34*(5), 625–635. https://doi.org/10.1038/aps.2013.5

Yue, M., Hinkle, K. M., Davies, P., Trushina, E., Fiesel, F. C., Christenson, T. A., Schroeder, A. S., Zhang, L., Bowles, E., Behrouz, B., Lincoln, S. J., Beevers, J. E., Milnerwood, A. J., Kurti, A., McLean, P. J., Fryer, J. D., Springer, W., Dickson, D. W., Farrer, M. J., and Melrose, H. L. (2015). Progressive dopaminergic alterations and mitochondrial abnormalities in LRRK2 G2019S knock-in mice. *Neurobiology of Disease*, *78*, 172–195. https://doi.org/10.1016/j.nbd.2015.02.031

Zaffagnini, G., and Martens, S. (2016). Mechanisms of Selective Autophagy. *Journal of Molecular Biology*, *428*(9 Pt A), 1714–1724. https://doi.org/10.1016/j.jmb.2016.02.004

Zagozewski, J. L., Zhang, Q., and Eisenstat, D. D. (2014). Genetic regulation of vertebrate eye development. *Clinical Genetics*, *86*(5), 453–460. https://doi.org/10.1111/cge.12493

Zambon, F., Cherubini, M., Fernandes, H. J. R., Lang, C., Ryan, B. J., Volpato, V., Bengoa-Vergniory, N., Vingill, S., Attar, M., Booth, H. D. E., Haenseler, W., Vowles, J., Bowden, R., Webber, C., Cowley, S. A., and Wade-Martins, R. (2019). Cellular α-synuclein pathology is associated with bioenergetic dysfunction in Parkinson's iPSC-derived dopamine neurons. *Human Molecular Genetics*, *28*(12), 2001–2013. https://doi.org/10.1093/hmg/ddz038

Zhang, J., and Ney, P. A. (2008). Role of BNIP3 and NIX in cell death, autophagy, and mitophagy. *Cell Death and Differentiation*, *16*(7), 939–946. https://doi.org/10.1038/cdd.2009.16

Zhang, T., Kho, A. M., & Srinivasan, V. J. (2021). In vivo Morphometry of Inner Plexiform Layer (IPL) Stratification in the Human Retina With Visible Light Optical Coherence Tomography. *Frontiers in Cellular Neuroscience*, *15*. https://doi.org/10.3389/fncel.2021.655096

Zhu, J. H., Gusdon, A. M., Cimen, H., van Houten, B., Koc, E., and Chu, C. T. (2012). Impaired mitochondrial biogenesis contributes to depletion of functional mitochondria in chronic MPP+ toxicity: dual roles for ERK1/2. *Cell Death and Disease*, *3*(5), e312–e312. https://doi.org/10.1038/cddis.2012.46

Zou, J., Wen, Y., Yang, X., and Wei, X. (2013). Spatial-temporal expressions of Crumbs and Nagie oko and their interdependence in zebrafish central nervous system during early development. *International Journal of Developmental Neuroscience*, *31*(8), 770–782. https://doi.org/10.1016/j.ijdevneu.2013.09.005